Synthetic and Structural Studies of Calix[4]pyrogallolarenes

Towards Biological Applications

Neil Bowley

A thesis submitted in partial fulfilment of the

Requirements of Nottingham Trent University

For the degree of Doctor of Philosophy

September 2008

Acknowledgements

Firstly I wish to thank my supervisor Dr. Gareth Cave for the help and advice he has provided during the three years of my Ph.D.

Thanks are due to the people who I have shared a lab with over the three years of my Ph.D. The numerous project students and fellow researchers that have passed through the synthetic chemistry lab ensured my time in the lab has been interesting and sometimes entertaining!

Thank you to Erasmus student Alex Massard for investigations into the solvent free preparation of calixarenes and acetals, and to M.Chem. project student Carl Rogers for synthesising bulk quantities of terpyridines. Thanks to M.Sc. students Winston Vetharoy and Kirsten Bostock under the supervision of Dr. Stéphanie. McArdle for performing cellular toxicity studies on the calixarenes.

Thank you to Dr. Patrick Huddlestone, for invaluable practical advice on a variety of organic chemistry problems.

Thank you to Prof. John Wallis for proofreading this thesis and many valuable contributions to my project throughout my time as a postgraduate student.

Thanks to Andrew Brooks whose friendship has been a constant support throughout my time at NTU. I couldn't have done it without you!

Thank you is simply not enough to Hannah and my Parents whose unswerving support has enabled me to achieve what I could only dream of.

Contents

List of figures

7

List of acronyms and abbreviations

ABV	-	Doxorubicin, Bleomycin and Vincristine
API	-	Active Pharmaceutical Ingredient
ASU	-	Asymmetric Unit
ATR	-	Attenuated Total Reflection
CCDb	-	Cambridge Crystallographic Database
CD	-	Cyclodextrin
COSY	-	Correlation Spectroscopy
CTV	-	Cyclotriveratrylene
DEPT	-	Distortionless Enhancement by Polarization Transfer
DLS	-	Dynamic Light Scattering
DMF	-	N,N'-Dimethylformamide
DMPK	-	Drug Metabolism and Pharmacokinetics
DMSO	-	Dimethylsulfoxide
DNA	-	Deoxyribonucleic Acid
DOSY	-	Diffusion Ordered Spectroscopy
DSC	-	Differential Scanning Caliometry
DSPE	-	Distearoyl Phosphatidyl Ethanolamine
EPR	-	Enhanced Permeability and retention
EPSRC	-	Engineering and Physical Sciences Research Council
ESI	-	Electrospray Ionisation
FDA	-	Food and Drug Administration
FRET	-	Fluorescence Resonance Energy Transfer
GCMS	-	Gas Chromatography / Mass Spectroscopy
HIV	-	Human Immunodeficiency Virus
HSA	-	Human Serum Albumin
LTP	-	Lipid Transfer Protein
MALDI	-	Matrix Assisted Laser Desorption Ionisation
mRNA	-	Messenger Ribonucleic Acid
MS	-	Mass Spectroscopy
NCE	-	New Chemical Entity
NMR	-	Nuclear Magnetic Resonance
PEG	-	Poly(ethylene glycol)
PBMC	-	Peripheral Blood Mononuclear Cell
PVC	-	Poly(vinyl chloride)
Rf	-	Retardation Factor
RNA	-	Ribonucleic Acid
SC-XRD	-	Single Crystal X-ray Diffraction
TFA	-	Trifluoroacetic Acid
TGA	-	Thermogravimetric Analysis
VT	-	Variable Temperature

Abstract

This work presented in this thesis details efforts towards understanding what factors control the formation of the myriad of architectures in calix[4]pyrogallolarenes, leading towards biological application. A variety of *C*-alkyl-calix[4]pyrogallolarenes have been synthesised and their solid-state and in-solution behaviour has been studied by diffusion NMR spectroscopy and single crystal X-ray diffraction.

It has been found that calix nano-capsules can be formed by calix[4]pyrogallolarenes in polar protic solvents when the alkyl chain is substituted with bromine at its terminus. This is speculated to be due to formation of a dipolar interaction between the bromine atoms of adjacent calix[4]pyrogallolarene molecules.

Calix[4]pyrogallolarenes with pendant chains bearing hydroxyl and cyano groups have been synthesised, and their behaviour in the solid state have been investigated by single crystal X-ray diffraction. They have been shown to form head-to-tail packing interactions in the solid state. As the hydroxyl functional group offers opportunity for further synthetic manipulations, in future investigations these molecules will provide a key intermediate in the synthesis of therapeutic delivery vectors.

Preliminary investigation of cellular toxicity of the calixarenes has also been performed and indicates that this class of molecules does not appear to possess a high degree of toxicity towards dendritic cells and peripheral blood mononuclear cells which are the envisioned target of this delivery vector.

Chapter 1 - Introduction

1   Supramolecular chemistry

Calixarenes are cup shaped molecules whose cavity can accommodate smaller guest molecules. There have been many calixarene derivatives synthesized with a diverse range of applications in mind. This includes their use as drug delivery vectors,[1] gas storage media,[2] memory for computing applications [3] and in catalysis.[4] This thesis focuses on the potential applications of functionalised calixarenes as drug delivery vectors, with details of work which will underpin the use of these molecules in a therapeutic setting.

The first section of the introduction gives an overview of the principles of supramolecular chemistry, which form the basis of the synthetic work carried out for this thesis.

Jean Marie Lehn, Donald J. Cram and Charles J. Pedersen shared the 1987 Nobel Prize in chemistry for their pioneering work on supramolecular chemistry. In his Nobel lecture, Lehn describes supramolecular chemistry as:

"The chemistry of the intermolecular bond, covering the structures and functions of the entities formed by association of two or more chemical species."

Jean Marie Lehn [5]

2 Inter- and intramolecular interactions

Chemists working in supramolecular science seek to design and control the formation of intermolecular bonds which Lehn refers to, in order to produce materials with novel structures and properties.

The intermolecular bond may take several different forms which are relevant to the construction of functional supramolecular species. In complex molecules there may be many different types of interaction which give rise to the molecular structure and therefore the bulk function. This interrelation between structure and function is best exemplified in nature by its ability to form functional macromolecules which catalyse chemical reactions. Urease (shown in Figure 1) is an enzyme which catalyses the hydrolysis of urea to ammonia and carbon dioxide, accelerating the reaction by 10^6 times.[6] The complex 3D structure shown below arises from multiple hydrogen bonds, hydrophobic interactions and metal to heteroatom bonds.[6]

Figure 1 - Cartoon of Urease enzyme structure

2.1 Hydrogen bonds

A hydrogen bond is an interaction (which may be inter or intra-molecular) between a hydrogen atom and another atom bearing an opposite partial charge. These dipoles arise as a result of differences in the Pauling electronegativity of the constituent atoms in a heteromeric covalent bond.[7]

"The nature of the hydrogen bond depends on the nature of the donor and acceptor groups"

Jeffrey [7]

Hydrogen bonds can have a wide variety of bond strengths (4 – 120 kJmol^{-1}) which in neutral molecules is proportional to the distance between the two interacting atoms (in the range of 1.2 Å to 3.2 Å).[8] Hydrogen bonds are directionally dependent, which means that the strongest hydrogen bonds are formed between atoms arranged at 180° to each other. From the strongest to the weakest, hydrogen bonds can have a range of bond angles from 180° to 90°. The deformation of hydrogen bonds is entropically favoured and compromises between the angle formed and other packing forces are often reached.[7]

Hydrogen bonding is one of the most important intermolecular interactions in nature; the genome of every living organism is contained in strands of DNA which are held together in its characteristic double helix by hydrogen bonding (Figure 2). The complementarity of hydrogen bonding between the base pairs allows faithful transcription and translation of the genetic code from DNA to produce proteins.
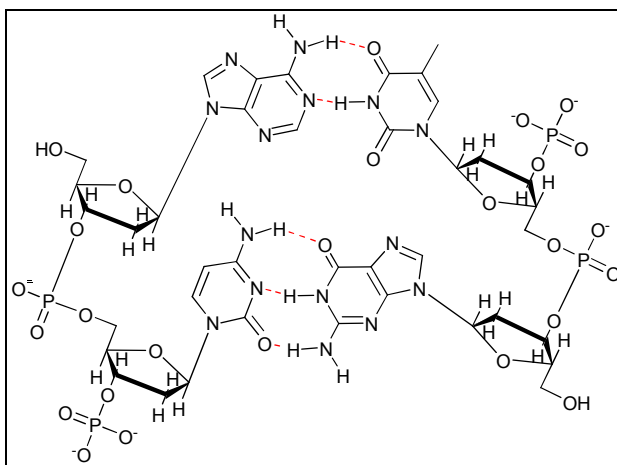
Figure 2 - Structure of DNA, showing hydrogen bonds between base pairs

2.2   Cation – π interactions

The interaction between a cation and the π electrons of an aromatic system are among some of the strongest non-covalent inter-molecular interactions found, having energies of interaction in the range of 160 kJmol^{-1} to 60 kJmol^{-1}.[9] The electrostatic model which describes the interaction between the cation and the cloud of electrons which reside above and below the plane of the aromatic ring has been validated.[10] However, inconsistencies between the standard model and reality do exist, for example the cation is treated of as a point charge 4 Å from the plane of the ring in the model, when in reality there are only the van der Waals radii of the atoms between the two interacting species.[11]

The concept of a cation to π interaction was developed after binding studies of cations with synthetic cyclophane hosts were carried out.[12] Cyclophanes, the general structure of which is shown below (Figure 3), are water soluble and monomeric between pH 7 and 9. The distance between the solubilising carboxyl groups and the binding cavity allowed electrostatic interactions between the carboxyl anion and any potential guest cation to be minimised in aqueous solution.[11] The hydrophobic effect may give a false positive of the binding of a cation by the cavity, therefore experiments using organic solvents have also been performed.[12-14]
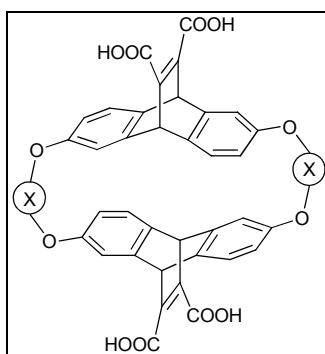
Figure 3 - Cyclophane host molecule (X = C_6H_4)

Cation to π interactions are important in nature because amino acids containing aromatic residues such as tryptophan, phenylalanine, and tyrosine (Figure 4) are able to interact with a variety of biologically significant cations.
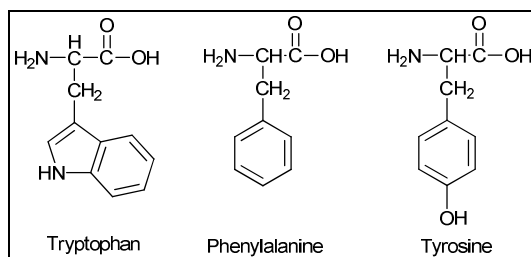
Figure 4 - Amino acids with aromatic side chains

Another illustration of the importance of cation to π interactions is the transmission of nerve impulses between neurons in vertebrates. For example, the active site of the enzyme acetylcholine esterase has been characterised by X-ray diffraction studies and shows a deep cavity with 14 aromatic amino acid residues in the active site.[15]
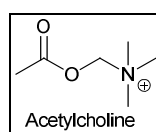
Figure 5 - Acetylcholine

The toxin from the green mamba (*Dendroaspis angusticeps*) blocks the hydrolysis of acetylcholine by strong inhibition of the acetylcholine esterase enzyme.[16] Inhibition of this enzyme prevents termination of a nerve impulse.[15] One of the toxins is a polypeptide of 61 amino acids, known as fasciculin.[17] This polypeptide is cationic overall due to the presence of many lysine and arginine residues. When these residues are functionalised there is a reduction of 70% in the inhibitory activity of fasciculin.[17] This is due to a blockage of the interaction between the lysine and arginine residues of the toxin and the aromatic amino acid residues of the active site. Therefore the strong binding between the toxin and the enzyme can be attributed to cation to π interactions.

2.3 Van der Waals interactions

Van der Waals interactions arise from the polarisation of an atom's cloud of electrons, but unlike hydrogen bonding they are non-directional and are a result of non-permanent polarisation.[18] This polarisation of a molecule's electron cloud may be the result of the proximity of another non-polar group. If the molecules are close enough the fluctuations may become synchronised and produce an attractive force which is strongly dependent on the intermolecular (or inter-atomic) distance. The strength of the interaction decreases as a function of distance to the negative 6th power. [8, 19]

Van der Waals interactions are important interactions between the alkyl chains in a wide variety of mesogens. The odd-even effect in calamitic liquid crystals is due to the disruption of the van der Waals interactions between long alkyl chain substituents. When there is an even number of carbon atoms in the chain the interactions are disrupted because the alkyl chains cannot come into close enough proximity for the van der Waals interactions to take place. This results in a destabilisation of the mesogenic phase.[20]

Another example of the importance of van der Waals interactions is that of the phospholipid membrane which surrounds cells and organelles in biological systems.[21] Biological membranes are not fully understood *in vivo* and are the subject of intense investigation.[22] The physical properties of the membrane (fluidity, thickness and lateral mobility of the constituent molecules) determine the conformation of proteins which are embedded in or pass through the membrane. This has important implications for drug delivery and anaesthesia which involve small lipophilic molecules causing changes in the cell membrane.[22, 23]

Pabst *et al.* modelled a lipid bilayer and demonstrated that it may be disrupted by the presence of ethanol.[24] Normally the lipid bilayer is twice the thickness of an individual phospholipid molecule.[21] However when ethanol is added, the hydroxyl group of the ethanol molecules coordinate to the polar phosphate head groups of the membrane, so the alkyl chain of the ethanol molecules reside in the more lipophilic area of the membrane. This inclusion of a guest into the bilayer causes the packing of the alkyl chains of the lipid to be disrupted, and to compensate for this and to prevent formation of a void in

the membrane, the chains begin to interdigitate to stabilise the membrane with increased van der Waals interactions.[24]

This interaction is put to use by geckos (*Gekko gecko*) which can climb a smooth glass surface at high speed.[25] This is possible because a gecko has approximately 500,000 keratinous hairs known as setae which measure 0.2-0.5 µm long, on the pad of each foot.[26] The van der Waals interactions between the setae and the surface on which the gecko is standing produce up to 20 N of adhesive force per foot.[27] The interaction can be rapidly applied and removed, allowing the gecko to quickly attach and detach its foot from a surface and move rapidly.[28] This is achieved because a small change in the angle between the hair and the surface allows the bond to be broken, since the interaction relies on intimate contact between the setae and the surface.[27]

2.4   The hydrophobic effect

The hydrophobic effect is an entropically driven phenomenon which causes non-polar groups to aggregate together in aqueous solution. The increase in entropy on formation of aggregates is due to the liberation of water molecules which would otherwise be rigidly associated around the non-polar groups. This liberation of water molecules is caused by a reduction in surface area when non-polar groups associate together. [29]

Lipid Transfer Proteins (LTP) transport hydrophobic molecules between membranes in plants. It has been discovered by Schramm *et al.* using X-ray diffraction data that oleic acid can interact with lipid transfer protein in two different ways.[30] The cavity of the LTP is smaller than oleic acid's molecular volume, therefore both the conformations of the bound guest which have been discovered possess non-staggered methylene interactions. These *gauche* interactions are thermodynamically unfavourable but this is compensated for by the hydrophobic effect, because when associated with lipid transfer proteins the oleic acid is shielded from the aqueous medium.[30]

In addition to natural systems, it has been shown by Trembleau *et al.* that the hydrophobic effect can negate energetically unfavourable interactions in synthetic systems.[31] When an alkene-based surfactant is introduced to a synthetic receptor molecule with a hydrophobic cavity in aqueous solution, a supramolecular complex is formed. If the guest in its linear form has a molecular volume greater than the cavity of the host, the complex will still form. This is because the entropic gain caused by the liberation of water molecules to the bulk solution will overcome the energetic cost of the unfavourable *gauche* interactions caused by folding the alkyl chain into a helix.[31]

3 Host-guest chemistry

Intermolecular interactions are the founding principle of supramolecular chemistry, and as shown above there are many different types of interaction possible. In order for a supramolecule to be formed, complementarity of these molecular interactions is required. This is achieved by manipulation of the molecular structure to effect changes in molecular shape. Complementarity of shape is as essential to formation of a supramolecule as the interactions themselves. This is because the strongest intermolecular interactions (ion-dipole, dipole-dipole and hydrogen bond) are directionally dependent and the forces which support the supermolecule (van der Waals forces and hydrophobic effect) rely on very close proximity of the interacting groups.

Perhaps the most elegant demonstration of complementarity has been provided by nature in the functioning of enzymes and metalloproteins. These molecules make life possible by accelerating physical and chemical processes, which are achieved by intricate combinations of inter- and intra-molecular interactions. That enzymes and their substrates fit together like a lock and key was first proposed by Emil Fischer in 1894.[32] This was further developed by Koshland *et al.* in 1960 by their suggestion that the protein can modify its shape to fit around its guest when the two are associated. This theory became known as the induced fit model.[33]

The induced fit model can be applied to one of the most closely studied metalloproteins, haemoglobin, which is responsible for the transport of oxygen in red blooded animals. Haemoglobin comprises four subunits, each responsible for transport of a single dioxygen molecule using their haem iron centre bound to a porphyrin macrocycle.[34] Haemoglobin demonstrates all of the interactions described in the section above in order to maintain its quaternary structure and therefore its function. [35]
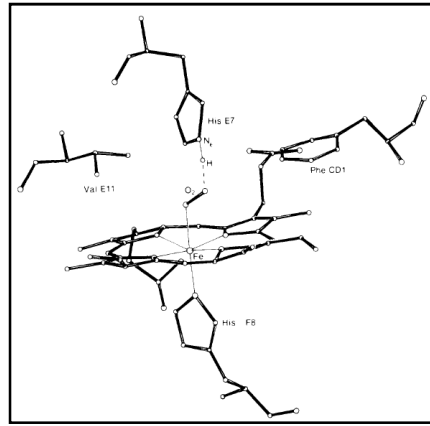
Figure 6 - Oxygen binding to haemoglobin

(taken from M. F. Perutz, Trends in Biochemical Sciences, 1989, 14, 42-44.)

When dioxygen binds to the haem iron, a conformational change takes place and the iron moves further towards the plain of the macrocycle.[36, 37] The position of the proximal imidazole ring of a histidine residue coordinating to the iron is also altered, causing a conformation change in the quaternary structure.[36] This conformation change on binding O_2 makes the haemoglobin convert to its 'relaxed' form and increases the affinity for further oxygen binding by the remaining sites.[35]

This cooperation between subunits allows oxygen to fully occupy haemoglobin's four binding sites when in a high oxygen environment (such as the lungs). When the oxygen concentration falls (*i.e.* in tissues) the removal of oxygen from an O_2 saturated haemoglobin molecule renders it in a "tense" state, where the binding of oxygen is energetically less favourable. Therefore haemoglobin readily unloads it remaining oxygen molecules and shows a sigmoid saturation curve illustrated by Figure 7.[38-40]
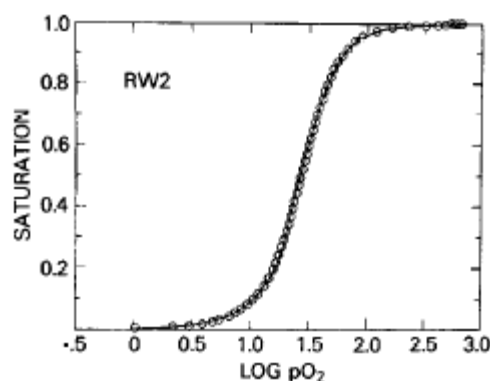
Figure 7 - Oxygen partial pressure *vs.* haemoglobin saturation

Taken from R. M. Winslow, M. L. Swenberg, R. L. Berger, R. I. Shrager, M. Luzzana, M. Samaja and

L. Rossi-Bernardi, *Journal of Biological Chemistry*, 1977, **252**, 2331-2337.

The affinity for oxygen by haemoglobin can be affected not only by cooperative binding but also its local environment. The Bohr Effect describes the pH dependence of haemoglobin's oxygen affinity, which is observed due to modification of the quaternary structure as a result of changes in inter- and intra-molecular interactions. The sigmoid curve moves to the left or right depending on the pH of the local environment. In the bloodstream an acidic environment is usually due to the presence of high concentrations of dissolved carbon dioxide characteristic of high metabolic activity. This low pH causes a decrease in the affinity of haemoglobin for binding oxygen, thus the oxygen cargo is delivered to tissues where it is most needed.[41]

"Evolution is a brilliant chemist"

Perutz [36]

3.1   Calixarenes

Calix[4]arenes are macrocyclic condensation products of 1,3-dihydroxybenzene (resorcinol) or 1,2,3-trihydroxybenzene (pyrogallol) with an aldehyde. Alternatively 4-*tert*-butylphenol may be reacted with formaldehyde to produce *t*-butyl-calix[*n*]arenes. Figure 8 below shows on the left calix[4]pyrogallolarene when X = OH and calix[4]resorcinarene when X = H. On the right of the Figure: *t*-butyl-calix[4]arene. There may be either alkyl or aryl substituents of the macrocycle denoted by R.
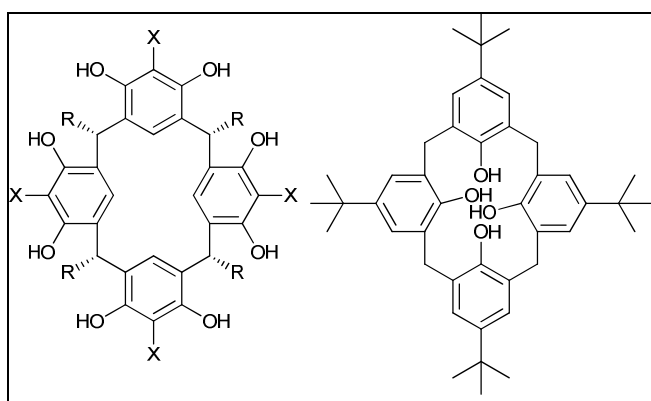
Figure 8 - Calix[4]arene molecules

The calix- prefix was applied to this class of molecules because *t*-butylcalix[4]arenes, which were the first to be synthesised, were found to have a shape resembling a cup.[42] The bowl shape is no longer a prerequisite for the *calix-* prefix (derived from the Greek: *calix* = cup) and all macrocyclic condensation products of aldehydes with resorcinol or pyrogallol are now included in this class. This expansion of the class of molecules given the prefix was necessary because *tert*-butylcalix[4]arenes were subsequently found to be conformationally flexible, and a large number of calixarene derivatives have been shown to have alternative conformations.[43]

In calix[4]pyrogallolarenes and resorcinarenes, the upper rim bearing the hydroxyl groups has a wider diameter than the lower rim (or annulus). The groups positioned axially at the macrocyclic methylene position are known as the pendant chains. These structural features are highlighted in the image generated from single crystal X-ray diffraction data in Figure 9 below.

←Upper Rim

←Lower Rim / Annulus

←Pendant Chains
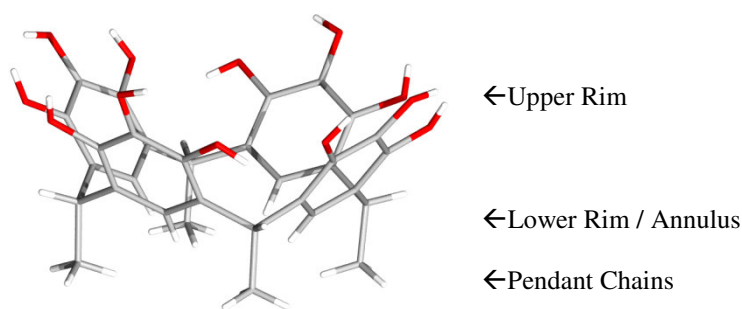
Figure 9 - Main structural features of calix[4]pyrogallolarenes

Calixarene molecules (pyrogallolarenes, resorcinarenes and *t*-butylcalixarenes) are cavitand molecules which can act as hosts to a surprising variety of guests. The cavity formed by a calixarene is hydrophobic, yet it has been proven that they can de-solvate a variety of alkali metal cations, as the aryl rings offer the potential to form a strong cation to π interaction. This interaction has been exploited in the use of calixarenes as simplified molecular models of complex biological systems such as sodium channels.[44] The coordination of a cation to a cavity of a calixarene inhibits the conformational flexibility exhibited by *t*-butylcalix[4]arenes. Coordination of a caesium ion to the cavity of the calixarene has been demonstrated in the solid state by X-ray crystallography and in the solution phase using NMR.[45, 46] The coordination of cations to calix[4]pyrogallolarenes has also been published by Ahman *et al.*[47]

The cation to π interactions have been shown to take different forms for the two calixarene species. When the *t*-butyl derivative is coordinated to the cation it holds the cation in the centre of its cavity.[45] The pyrogallolarene adopts a distorted boat-like conformation, allowing η^6 coordination to the cation by two equatorially positioned aromatic rings from neighbouring molecules. The distortion of the macrocycle allows the axial phenyl rings to come into close proximity and form π - π interactions.[47]

It is not only cations which can be bound to the cavity of the calixarenes, a wide variety of guest molecules have been coordinated to the interior of the cup, by either the hydrophobic effect or stacking interactions such as π - π stacking.

A variety of calix[n]arenes have a high affinity for buckminsterfullerenes. Atwood *et al.* and Suzuki *et al.* demonstrated that calix[8]arene selectively forms an inclusion complex with C_{60} Buckminsterfullerene.[48, 49] The supramolecular complex increased the solubility of C_{60} in a variety of organic solvents, allowing its separation from fullerene soot to a purity of 98%. It has subsequently been shown that other calix[*n*]arenes and cavitands form complexes with the fullerenes.[50-53]

Unfunctionalised calix[4]resorcinarenes have a wide cavity which allows rapid exchange of a range of guest molecules. However functionalisation of the upper rim creates deeper hydrophobic cavities, with the advantage that specificity for guests is increased and exchange rates are slowed. This extension of the cavity has allowed large steroid molecules to be encapsulated; a phenomenon driven by the hydrophobic effect.[54, 55] Cave *et al.* demonstrated that the cavity of calix[4]pyrogallolarenes can be extended by non covalent interactions of 4,4'-bipyridines to the upper rim.[56]

3.1.1   Conformations of calix[4]arenes

Calix[4]arenes possess four stereo-centres at the bridging points of the macrocycle. Different isomeric arrangements at these points produce a different conformation in the macrocycle. Figure 10 shows a cartoon of the possible conformations, with each square block representing a phenyl ring: A – cone, B – partial cone, C – 1,3-alternate, D – chair
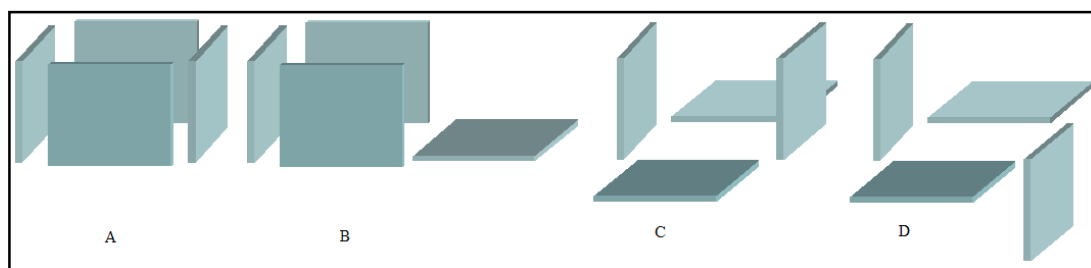
Figure 10 - Conformation of calix[4]arenes

Only *t*-butylphenyl-calix[*n*]arenes synthesised from formaldehyde and 4-*tert*-butylphenol have been reported in the literature.[43] There are no pendant chains attached to the bridging methylene position of the macrocycle present in these molecules. The macrocycle is therefore conformationally flexible and can convert between cone and chair *via* the intermediate forms. When the phenolic hydroxyl groups on the lower rim of the *t*-butylcalix[4]arenes are functionalised this locks the macrocycle in a single conformation.   Unlike   the   *t*-butylphenyl-calix[n]arenes,   calix[4]pyrogallolarenes   and calix[4]resorcinarenes are conformationally locked. The conformation interconversion is sterically impossible because the pendant chains are blocked passage through the annulus, therefore conversion of conformations is only possible by ring-opening and re-formation of the macrocycle.[57]

The conformation which predominates in a reaction mixture (during the synthesis of resorcinarenes and pyrogallolarenes) is dependent on the reaction conditions and the substituent on the pendant chains. The greater steric bulk at the α-position to the aldehyde, the greater yield of the chair conformation (D) is isolated; when benzyl aldehydes are used, the chair conformation is exclusively isolated.[58] It has been shown that cone conformation (A) has the greatest thermodynamic stability when alkyl calix[4]pyrogallolarenes are synthesised due to the greater number of intramolecular hydrogen bonds which can form.[59] Since much research has been undertaken on the cone conformation, syntheses have been optimised to yield higher quantities of this isomer.[57, 60]

3.1.2   Synthesis of calix[4]resorcinarenes and calix[4]pyrogallolarenes

Calixarenes are synthesised by the condensation of resorcinol or pyrogallol with an aldehyde under acidic catalysis as shown in Figure 11 below. There are currently three methods in use to access these molecules: reflux in mineral acid, transition metal catalysed condensations and grinding of the reactants are discussed in section 4.1.2.
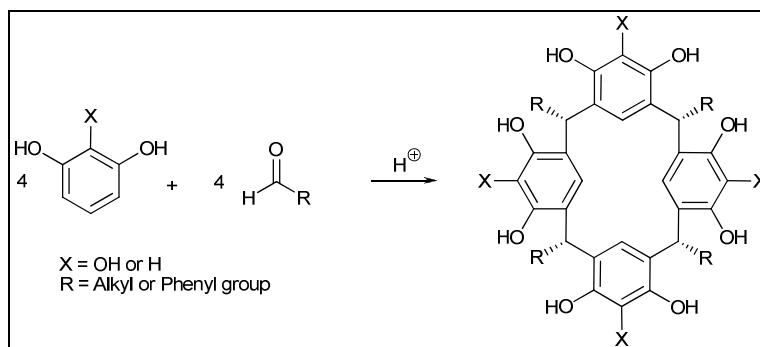
Figure 11 - General synthetic scheme for calix[4]arenes

Calix[4]resorcinarenes (see Figure 11 where X = H, R = CH_3) were first synthesised by Niederl and Vogel by the condensation of resorcinol and acetaldehyde in acidic solution.[61] However, it was a further 40 years before *C*-alkyl resorcinarenes were fully characterised by Högberg *et al.* [62]

The conditions of the synthesis determine which conformer and ring size product is formed.[63] Högberg extended the work of Niederl and Vogel to include *C*-alkyl-calix[4]resorcinarenes. He described the reflux of resorcinol with acetaldehyde in ethanol and hydrochloric acid, and found that changing the composition of the solvent and concentration of the hydrochloric acid produced varying amounts of the cone and chair isomers. The length of the alkyl chain also affects the solubility of the macrocycle and thus the distribution of products produced from the reaction.[57] This method became the standard technique which has been widely applied to the synthesis of *C*-alkyl-calix[4]resorcinarenes and *C*-alkyl-calix[4]pyrogallolarenes with minor adjustments made to the conditions to optimise the production of the desired product.[64-66]

3.1.2.1 Green methods for the synthesis of calix[4]pyrogallolarene derivatives

The technique of refluxing the reactants to prepare calixarenes is very time consuming and produces the product in only moderate yields.[64-66] As the cone conformation is often the desired product, long reaction times (up to 6 days) are used to exploit the low solubility of the thermodynamic product, causing its precipitation.[67] Coupled with the long reaction times the large solvent volumes required to synthesise calix[4]arenes prompted development of novel "green" techniques for their synthesis.

The use of microwave irradiation has been widely applied in synthetic chemistry in recent years to reduce reaction times, solvent volumes required and to increase the yield of a reaction.[68] This method of heating a reaction has been applied to the synthesise calix[4]resorcinarenes by Hedidi *et al.* and calix[4]pyrogallolarenes by Yan *et al.* [69, 70] It was reported in these articles that the use of microwave irradiation considerably shortened the reaction time and reduced the volume of solvent required to synthesise the macrocycles by up to 90%.

Hedidi *et al.* synthesised resorcinarenes as a single conformer, using microwave irradiation in 2-ethoxyethanol solution. 12-Tungstophosphoric acid (8 mol%) was used as catalyst, however this does not significantly increase the isolated yield over use of concentrated hydrochloric acid as the catalyst (HCl catalysed the synthesis of six of the nine compounds reported in the article in higher yield). There is no mention of recycling the tungsten catalyst or the isolation procedure which was used to separate the tungsten catalyst and the product. A claim in the article is that the technique is tolerated by a range of functional groups, yet the only functionality published aside from alkyl and benzyl groups was an aryl ether.[69]

Yan *et al*. employed the method developed by Hedidi *et al*. to synthesise a range of aryl pyrogallolarenes using a solution of concentrated hydrochloric acid. The range of functionality on the pendant phenyl rings which tolerate the conditions include aryl rings bearing ethers, halogens and esters, demonstrating an extension to the work of Hedidi. Due to the steric bulk at the alpha position below the macrocycle ring the chair conformation is formed exclusively.[70]

The 'green' methodology of using metal catalysis rather than mineral acids has been extended by the use of ytterbium (III) triflate as a Lewis acid catalyst in the reaction of resorcinol with a variety of aldehydes in ethanolic solution.[71] The catalyst was recovered from the reaction mixture and reused. This technique gives yields comparable to the standard reflux in mineral acid but is more atom efficient and therefore more environmentally friendly since there are only reactants, and the catalyst (which is recoverable and reusable) in absolute ethanol. [71]

Most recently a novel technique for synthesizing calix[4]pyrogallolarenes was developed by Antesberger *et al.*[72, 73] The reactants are mixed in equimolar amounts in the presence of a catalytic quantity of *para*-toluenesulfonic acid and ground together using a pestle and mortar. This process gave *C*-aryl and *C*-alkyl-calix[4]arenes in excellent yield. In contrast to the results of Högberg *et al.*[62] the equilibration between the cone and the chair isomer was not observed on prolonged standing. This supports the earlier theory that strong mineral acids and vigorous conditions are necessary for conformer interconversion.[63]

3.1.2.2   Green techniques for the synthesis of terpyridines

Terpyridines have been co-crystallised with calixarenes to form a variety of supramolecular systems. It was found by Cave and Raston that terpyridines can be synthesised by grinding together an aryl aldehyde and aryl acetates in the presence of sodium hydroxide to give Kröhnke type pyridines (2,4,6 substitution pattern). The reactants form a eutectic melt and undergo an aldol reaction followed by a Michael type condensation. The intermediate di-ketone is then reacted in acetic acid with ammonium acetate which cyclises the intermediate to a pyridine, as shown in Figure 12.
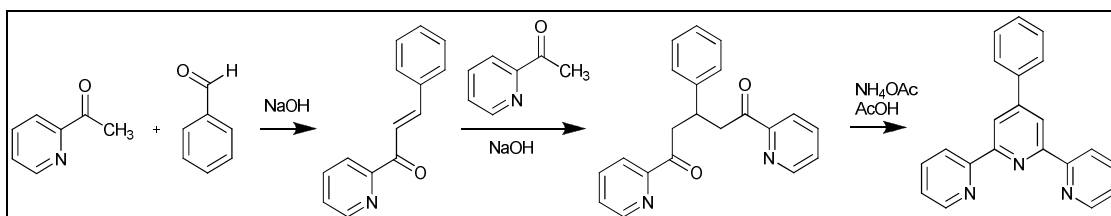
Figure 12 - Terpyridine synthesis

3.1.3   Capsules formed by calix[4]pyrogallolarenes and calix[4]resorcinarenes

Aoyama first postulated that calix[4]resorcinarenes self-assemble into aggregates in 1988. The mass spectra indicated a hexameric arrangement of calix[4]resorcinarene molecules in both chloroform and benzene solution but gave no indication of the nature of the structure that was formed.[74] It was a further nine years before MacGillivray and Atwood published an image generated from single crystal X-ray diffraction data showing the formation of a spherical hexameric molecular capsule in the solid state.[75] This *C*-methyl-calix[4]resorcinarene crystallised from nitrobenzene self-assembles into a nanometer scale-sphere with an external diameter of 24.3 Å, held together by 60 hydrogen bonds. Its central cavity was unprecedented in size (diameter = 17.7 Å) and volume (approximately 1375 $Å^3$) which was four and a half times larger than the capsule reported earlier that year by Kang and Rebek.[76]
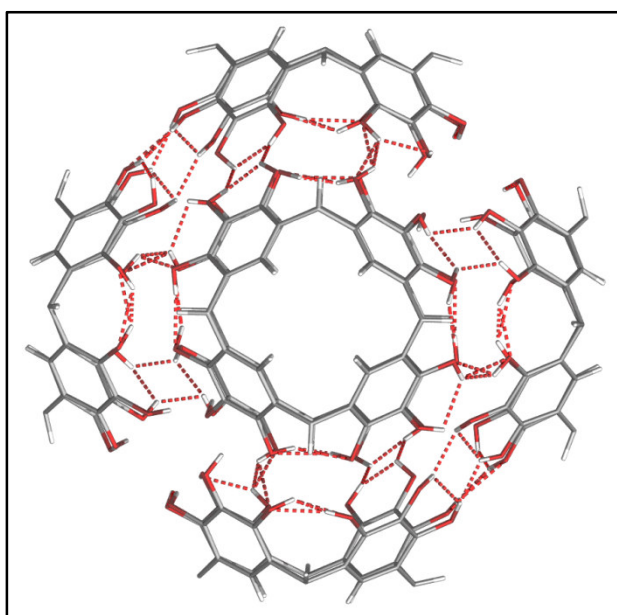
Figure 13 - Nanometer scale-capsule formed by *C*-alkyl-calix[4]pyrogallolarenes

A capsule formed by calix[4]pyrogallolarene was reported two years later by Gerkensmeier *et al.* who proposed that due to a lack of reproducibility of formation, the assembly of six calix[4]pyrogallolarene molecules was less stable than the previously reported resorcinarene capsule.[77] It has been subsequently shown that the pyrogallolarene capsule is in fact more stable due to the extra hydrogen bonding which the additional four phenolic hydroxyl groups allow.[78, 79]

The difficulty that Gerkensmeier had in reproducing the capsule formation was recently shown to be due to the acetonitrile solvent from which the crystals were grown. When crystallised from acetonitrile, *C*-alkyl-calix[4]pyrogallolarenes are capable of forming both bi-layers and dimeric or hexameric capsular packing motifs. The resulting packing arrangement is dependent on the degree of hydration of the solvent.[79]

The unequivocal determination of structure by single crystal X–ray crystallography allows the study of the interactions which lead to the formation of the various nanometer scale-architectures and packing motifs. From data gathered using this technique, it was found that the capsule formed by *C*-methyl-calix[4]resorcinarene is a spherical arrangement of six monomer molecules. The capsule is held together by 60 hydrogen bonds, 36 of which are intermolecular with each capsule having a seam of eight water molecules.[75] *C*-alkyl-calix[4]pyrogallolarenes have been shown to not require this belt of water molecules for capsule formation.[80] The nanometer scale-capsule itself can have different packing motifs in the solid state. The calix[4]pyrogallolarene molecules show varying degrees of interdigitation of pendant chains, with perturbation of the sphere observed in one of the polymorphs.[67, 79, 81] It has been recently shown by Dalgarno *et al.* that the formation of capsular architecture by calixarene derivatives is not limited to resorcinarene and pyrogallolarene molecules. An upper rim sulphonated and carboxyl functionalised calix[4]arene has been shown to enclose 700 $Å^3$ of space.[82] The symmetry that the carboxyl substituted calixarene possess in the 1,3-alternate conformation allows each calixarene to form the walls of two capsules.

3.1.3.1   Synthesis of capsules

Currently there are three techniques available for the synthesis of calixarene-derived nanometer scale-capsules. The technique used by MacGillivray of dissolution in a suitable solvent in the presence of an appropriate guest is still widely used for generating hydrogen bonded architectures. More recently it has been shown that the capsule can be held to together with metal to ion bonds and covalent bonds. For example, the capsule may be synthesised by dissolution of *C*-methyl-calix[4]resorcinarene in boiling nitrobenzene and slow evaporation of the resulting solution. This method of production exploited the self assembly of calix[4]resorcinarenes into hexameric spheres in solution when an appropriate guest molecule is present, and in this case the solvent proved to be a suitable guest for inclusion. The exact location of the guest molecules could not be determined by single crystal X-ray diffraction owing to their extensive disorder.[75]

In subsequent work, resorcinarene capsules have been shown to spontaneously self-assemble in chlorinated solvents saturated with water.[80] Dissolution of pyrogallolarenes and resorcinarenes in chloroform leads to spontaneous formation of nanometer scale-capsules which are stable enough to crystallise from solution when slow evaporation is allowed. If a methanolic solution is heated in a sealed tube within appropriate guest (to 150°C) and then allowed to slowly cool, crystals suitable for X-ray diffraction studies form.[83] The capsules have been shown to form *in-situ* during the macrocyclisation reaction when the grinding method is employed.[84] In order to speed capsule formation, solutions of calixarene may be sonicated in an ultrasonic bath which provides the additional energy required.

Calix[4]resorcinarene derived capsules may be held together by covalent linkers. This has been shown by Liu *et al.* who synthesised an imine link between resorcinarenes which had been functionalised with aldehyde groups on the upper rim of the molecule.[85] The 18 components of the reaction mixture came together to form a nanometer scale-sphere of unprecedented interior volume of approximately 1700 $Å^3$. In subsequent publications Liu *et al.* describe the synthesis of covalently bound dimeric and tetrameric capsules derived from upper rim substituted resorcinarenes.[86]

3.1.3.2 Metal fringed capsules

Orr *et al.* [87] showed that addition of a lanthanide salt and pyridine-N-oxide changed the molecular architecture formed by p-sulfonatocalix[4]arene from a bilayer to a sphere.[88] There are significant differences between the capsules formed by the resorcinarenes and pyrogallolarenes to those formed by *p*-sulfanatocalix[4]arenes. The capsules derived from *p*-sulfanatocalix[4]arenes are held together by a combination of van der Waals interactions, coordination to metals and the hydrophobic effect, while the resorcinarene capsules employ solely hydrogen bonding. Despite the greater number of constituent molecules which make up the *p*-sulfanatocalix[4]arene capsule (12 vs. 6), the molecular volume enclosed (1000 $\mathring{A}^3$) is smaller than that reported for the resorcinarene capsules (1300 $\mathring{A}^3$). The decrease in volume enclosed is due to the lower rim of the calixarene forming the interior surface of the capsule. The lower rim of these molecules bears four hydroxyl groups which offer coordination sites to the guest molecules, which causes ordering of the guest molecules. It is possible to determine the atomic positions of the guest molecules within the capsule by single crystal X-ray diffraction. This is not the case in the resorcinarene capsules because the interior of the capsule is formed by the cavity of the macrocycle. The upper rim hydroxyl groups are largely involved in hydrogen bonding to the other molecules which form the capsule, so the opportunity for coordination within the capsule is limited to cation to π interactions. This results in disorder of the guest molecules.[59] Perhaps most importantly the capsules are not discrete because the lanthanide ions which hold the capsules together are also coordinated to the capsule adjacent so each capsule is coordinated to 6 others which come into contact with it.[89]

It has been shown that the phenolic hydroxyl groups of the upper rim of calix[4]pyrogallolarenes offer a coordination site for a metal ion. Therefore capsules which were held together by hydrogen bonds can be synthesised by metal to oxygen bonds to form discrete metal bound nanometer scale-capsules.[90-92] A hexameric capsule formed by the coordination of copper (II) ions to six calix[4]pyrogallolarene molecules did not show significant changes in volume or shape compared to the hydrogen bonded structure.[93] The hexameric gadolinium capsule shows significant distortion of both the spherical arrangement of the capsule and of the individual calixarene molecules. Unusually for the pyrogallolarene capsule, four water molecules are included in the seam of the capsule. This inclusion of water is a result of the distortion providing a suitable gap in the hydrogen bonding network. The

distortion of the capsule and the larger ionic radius of gadolinium reduces the capsule volume to 1150Å^3.[94]

There are two possible capsular architectures when zinc (II) ions are coordinated to calix[4]pyrogallolarenes. Firstly a dimeric capsule forms when two calix[4]pyrogallolarene molecules are arranged with their upper rims coordinated to a belt of eight zinc ions.[91] Secondly, if the calixarene is manipulated by substituting a central hydroxyl group of the upper rim for a carboxyl group, this provides sites for coordination to metal ions. Single crystal X-ray diffraction data has been collected showing hexameric capsule formation with 16 zinc (II) ions coordinating to six calixarenes.[95]

Following the discovery that pyridines can coordinate to the upper rim of calix[4]resorcinarenes [96] and that therefore the dimensions of the cavity can be expanded, a nanometer scale capsule formed by the co-crystallisation of 4'-(4-octyloxyphenyl)-4,2':6',4''-terpyridine and *C*-methyl-calix[4]pyrogallolarene was published by Cave *et al.* [56, 97]

Kobayashi *et al.* combined covalent extension of the upper rim and the use of non-covalent interactions to form space enclosing architectures.[98] A hydrogen-bonded capsule forms when *C*-methyl-resorcinarene functionalised with carboxyl groups on the upper rim is co-crystallised with 2-aminopyrimidine. This capsular arrangement is stable in solution as well as the solid state because the amino-pyrimidine and carboxyl groups are complementary, and the capsule is held together by 16 hydrogen bonds.

3.1.3.3   The interior of the capsule

The interior of the capsule has been likened to a new phase of matter and therefore has been an area of interest for a variety of groups over the past 20 years since capsular arrangements of molecules were first discovered. [99, 100]

A study carried out by Mecozzi *et al.* led to the development of the 55% rule which states that the optimum volume of a host's cavity which a guest can occupy is 55% ± 9%. If the host capsule is tightly held together by hydrogen bonds the occupancy can rise to 70% however this degree of occupancy is infrequently observed. The remaining 45% of volume is required for thermal motion of the guest molecules. Constriction of these motions is thermodynamically unfavourable as it is effectively freezing the molecule out of solution. When solvent molecules are encapsulated (as in the sphere formed by pyrogallolarenes in chloroform) the concentration of solvent within the capsule is similar to the external concentration.[101] In synthetic systems it has been shown that it is possible for guest molecules to be contorted by intermolecular interactions into conformations which would be unfavourable in free solution, in order to compress its volume to occupy 55% of a cavity.[31]

The discovery of the 55% rule not only has implications for synthetic systems because it has been recently applied to enzymes and their active sites and the design of inhibitors which is of interest in the drug development process.[102] Zurcher *et al.* reported that a series of enzyme inhibitors were synthesised differing only in the alkyl chain length and that after modelling of the enzymes' active site they discovered that the most effective inhibitors occupied 55% of the volume of the active site.[102]

3.1.3.4   Capsules in solution

The spontaneous formation and stability in solution of capsules consisting of calix[4]arenes was independently proven by the groups of Cohen and Rebek within a few months of each other, using diffusion NMR spectroscopy to show both the large capsule and their encapsulated guests have the same diffusion coefficient. While robust, in solution the capsule is in dynamic equilibrium; individual calixarenes comprising the walls of the capsule can be exchanged and while the calixarenes are being exchanged the guests can enter and leave, without the complete destruction of the capsule.[78, 80, 103-109]

It has been recently shown that in the solution phase the resorcinarene capsule does not always have a seam of water molecules which is ubiquitous in the solid state structures.[75] The inclusion of water molecules into the structure of the sphere is dependent on the guest entrapped in the interior of the capsule. When solvent molecules or tetraalkylammonium halide salts are encapsulated the belt of water is present in agreement with the solid state structure published,[110] but if the counter ion of the tetraalkylammonium is changed to PF_6^- or BF_4^- the belt of water molecules is no longer observed.[111]

It has also been proven that in solution there is no formation of heteromeric capsules when calix[4]pyrogallolarenes and calix[4]resorcinarenes are mixed.[112] Cohen *et al.* discovered that *C*-alkyl-calix[4]resorcinarenes formed heteromeric capsules comprising of resorcinarene monomers with pendant chains of different lengths. The exchange between two discrete species and a mixture of capsules was shown to take seven days at ambient temperature or 2 hours at reflux.[78]

It has been shown that the calixarene molecules are capable of showing high degrees of self recognition in the formation of spheres. This capacity for self recognition has been tested by the synthesis of calixarenes containing both pyrogallol and resorcinol ring units. A statistical distribution of cyclic monomers precipitated from the reaction mixture containing equal quantities of pyrogallol and resorcinol. When dissolved in a non-polar solvent, homomeric nanometer scale capsules are formed. These contain a single heteromeric macrocycle which can be crystallised, showing extreme degrees of self recognition as the macrocycles differ only by a single hydroxyl group.[113]

To study the behaviour of nanometer scale capsules in solution at concentrations below the sensitivity limit of NMR, Fluorescence Resonance Energy Transfer (FRET) analysis was applied to the calixarene system by Barrett *et al.* FRET is the transfer of energy from one molecule to another by fluorescence. The fluorescence of the original molecule (donor) is absorbed and then re-fluoresced by another moiety (acceptor). The transfer of energy from donor to acceptor and re-fluorescence by the acceptor can be monitored by ultra-violet-visible spectroscopy. FRET can only be achieved by molecules which are in very close proximity, so if the donor and acceptor moieties are on different monomers which constitute the nanometer scale-sphere, FRET will only be observed in spherical arrangements of nanometer scale-capsules which hold donor and acceptor species together. FRET is achieved in calix[4]arene systems by mono-functionalisation of the pendant chain of calix[4]arene molecule with pyrene or perylene substituents. The FRET occurs between the pyrene moiety which absorbs light at 346 nm (the donor) and the perylene substituted calix[4]arene (the acceptor), causing its fluorescence. A reduction in the pyrene and increase in the perylene fluorescence is therefore observed only when the molecules are arranged in a nanometer scale capsule. The FRET studies have demonstrated high levels of self recognition in the formation of nanometer scale spheres, because mixtures of calix[4]pyrogallolarene and calix[4]resorcinarene monomers do not form. Also shown is the enhanced stability to polar protic solvents of the pyrogallolarene spheres over the resorcinol derived derivatives.[114, 115]

In contrast Ajami *et al.* used NMR to characterise a calix[4]resorcinarene which had been extended on its upper rim with an imido group forming a heteromeric dimer with a calix[4]resorcinarene.[116] This type of non-self recognition in calixarene systems was unprecedented, showing flexibility in the recognition which will lead to capsule formation. In solution there was equilibrium between the three capsular species; hexameric capsule of resorcinarene, heteromeric capsule of extended species and calixarene and dimeric capsule of extended calixarene. The heteromeric capsule was templated by the encapsulation of an appropriate guest. Different guests had different affinities for the capsules and the presence of 1,4-diethylbenzene shifted the equilibrium in favour of the hetero-capsule, while addition of 4,4'-dimethyl-trans-stilbene favoured the formation of the homomeric capsules.

3.1.3.5   Capsules in the gas phase

It has been shown in the literature that obtaining mass spectra of supramolecular capsules is possible for smaller assemblies such as Rebek's softball [117] and urea functionalised calixarenes.[118] Larger hexameric capsules have proven more troublesome to detect in the mass spectrum but recently it has been shown that the hexameric capsule formed by calix[4]pyrogallolarene is stable in the gas phase.[119] The presence of a cationic guest molecule of appropriate size to template the formation of the capsule is required to observe the hexamer. If smaller guest molecules are used (e.g. tetramethylammonium tetrafluoroborate) dimers and trimers are observed.

In contrast to the work of Cohen *et al.*[104] and Rebek *et al.*[112] Beyeh *et al.* found that mixed hexamers of pyrogallol and resorcinol derived calixarenes were formed in a near statistical distribution when a pseudo-octahedral ruthenium(II)tris(2,2'-bipyridine) complex (Figure 14) is the guest molecule. It was also found that when solutions of pyrogallolarenes and resorcinarenes were mixed an equilibration towards a statistical distribution of calixarene molecules comprising nano-spheres occurred rapidly (<30 seconds).[119]
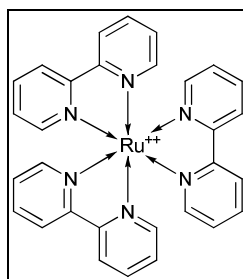
Figure 14 - Ruthenium(II)tris(2,2'-bipyridine) complex

Molecular modelling of the supramolecular nano-capsule shows that the di-cation is the correct size for the cavity of the sphere and that the deviation from octahedral geometry of the guest is tolerated. There may be a strong cation to π interaction driving the formation of the sphere but this is not considered by Beyeh. The discovery that capsules are stable in the gas phase and that heteromeric capsules can be formed if the association to the guest is favourable enough, indicates that the formation of a sphere is driven very strongly by the presence of a guest molecule and that the forces which control capsule formation can be manipulated with an appropriate guest.

4   Drug Delivery

4.1   Historical perspective

In the UK over the past 150 years modern healthcare has more than doubled life expectancy from 39 to 79 years, and in the past 50 years has reduced infant mortality by 80%.[120] Pharmaceuticals developed over the past 100 years are a significant weapon in the armoury of healthcare professionals, rendering treatable, diseases once considered fatal. The following discussion shows why pharmaceuticals are important, how they are developed and used and how this development and use can be improved by novel drug delivery techniques.

Treatments available from local apothecaries, unchanged for many hundreds of years, have been replaced relatively quickly by a pharmaceutical industry which in its early days was closely linked to companies specialising in petrochemicals. Today, pharmaceuticals are a multi-billion dollar industry.[120] This transformation began with the extraction of "active principles" from a variety of plants traditionally used in the treatment of illness. One of the earliest examples of this extraction and purification was morphine's extraction from opium in 1803. Once the active ingredient was isolated, the dosage could be controlled and treatment could be given in a precise, repeatable fashion.[121] This repeatability was improved by the invention of tablets which gave further control over the dosage of medicines. The industrial tablet compression machine was introduced in England in 1843 and gelatine capsules followed in 1875.[120]

The movement away from the use of plant extracts towards synthetic chemicals can be attributed to Paul Ehrlich, who can be described as the originator of antibacterial chemotherapy. While studying azo dyes produced by the chemical industry in Germany, Ehrlich noticed that certain dyes stained only bacteria. This led to the idea that bacteria could be selectively targeted with a chemical which was toxic only to the bacterium like a "magic bullet".

Methylene Blue, a dye which selectively stained the malaria protozoan was used by Ehrlich to successfully treat a malaria case in 1891, but due to its renal toxicity and difficulty in producing an animal model for malaria (the mosquito vector was unknown at the time) the treatment was not developed further. [120, 121]
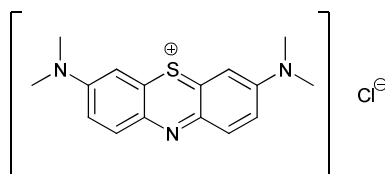
Figure 15 - Methylene Blue

Ehrlich continued to screen a variety of dyes and organometallic complexes for antibacterial activity. The bacterium which caused syphilis (*Treponema pallidum*) responded successfully to the 606th compound to be synthesised. This compound became known as Salvarsan, the first antibacterial chemotherapy available. While offering a cure for syphilis, Salvarsan did require a series of painful injections and due to a sulphur impurity from the synthesis, a variety of side effects were observed.[122] The molecular structure of Salvarsan was undetermined until 2005 when mass spectroscopy gave conclusive evidence to show that the drug was a mixture of a trimer and pentamer, as shown in Figure 16 below.[122]
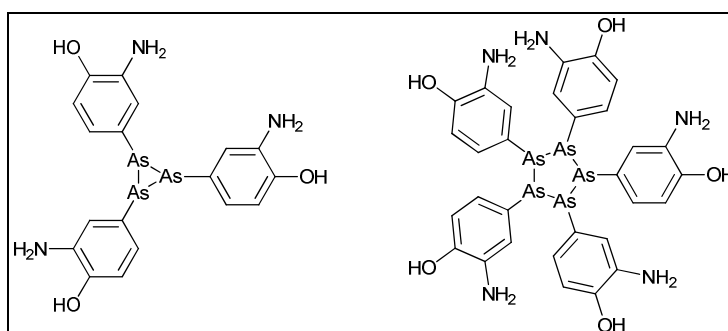
Figure 16 - Structures of Salvarsan

Those studying disease have refined the paradigm developed by Ehrlich by targeting specific receptor molecules rather than the whole cell. This advance has been made possible by the use of computers in the development of combinatorial chemistry and modelling of receptors which are the desired targets.[123]

This helps chemists design molecules with an appropriate molecular shape (*cf.* intermolecular forces discussed earlier) and size (*cf.* 55% rule above) which can interact appropriately with the receptor.[124]

The use of computers and receptor screening has helped to increase the number of New Chemical Entities (NCEs) synthesised, yet there still needs to be five thousand NCEs synthesised for each drug which makes it to market.[125]

Scientists involved in health research have made great progress in reducing mortality and morbidity using chemotherapy but great challenges remain, including; cancer, coronary heart disease, Human Immunodeficiency Virus (HIV) and malaria.

4.2 The drug development process

In order to facilitate the discussion of why new chemical entities fail to become drugs a very brief overview of the current method of drug development is required (Figure 17).
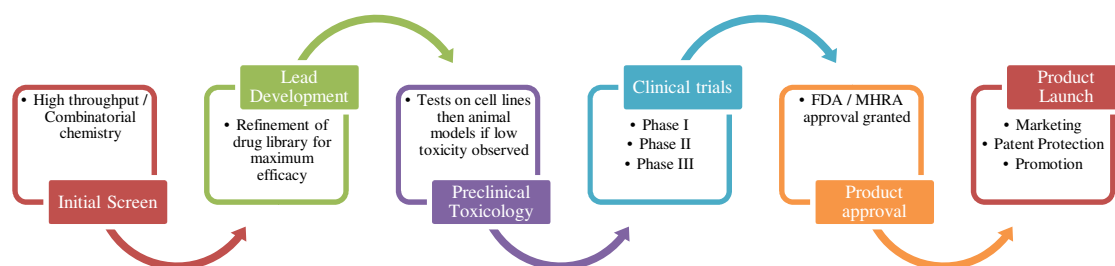
Figure 17 - Overview of drug development process

In a large pharmaceutical company an executive decision is made on which illness to treat. After this decision is made, a study of the available literature may suggest the mechanism of action of the disease and therefore targeting of which receptor (or gene) is likely to be most effective.[126] If possible the target receptor is modelled by computational chemists and protein crystallographers. This information allows design of a molecular structure that will be the starting point for testing activity against the desired receptor.

Medicinal and combinatorial chemists synthesise a series of molecules which are screened for activity at the desired receptor.[127] From this initial screening process a candidate having activity towards the receptor is taken forwards for further development.[128]

The toxicity of the candidate drug is tested on progressively more complex organisms requiring larger quantities of active ingredient. If the testing on animal models show no significant toxicity, the drug progresses onto double blind clinical trials.[129]

In the development of a new drug, clinical trials are the most time consuming and expensive phase for the company. Phase I trials are on healthy male volunteers and are designed to assess any side effects and determine the metabolism of a drug. [126] If Phase I is successful, the drug can pass on to Phase II and be tested on a small cohort of patients, to assess its efficacy and dosage against the current gold standard of treatment. If efficacy and potency is proven, a large cohort of patients is recruited for phase III trials and testing is undertaken. Only when large clinical trials are completed will the relevant agencies (Medicines and Healthcare Products Regulatory Agency (MHRA) in the UK and the Food and Drug Administration (FDA) in the USA) allow the drug to be marketed. If the number of eventually unsuccessful candidate drug molecules which make it clinical trial can be reduced, this will make the drug development process significantly quicker and cheaper.[121, 123, 124, 130 131, 132]

4.3   Why drugs fail

The process of bringing a new drug to market is both lengthy (taking up to 15 years) and costly (more than $800 million US dollars per drug[125]). The improvement of efficiency of this process would benefit both the company which develops the drug (in terms of cost reduction and an increase in the time which the drug can be marketed under patent protection) and patients, because more treatments may be available. In order to improve the efficiency of a process how it can fail must be understood. Below is a discussion of why drugs fail and what can be done to improve the process.

An analysis of the reasons for failure of candidate drugs which have undergone clinical trials between 1964 and 1988; Prentis *et al.* showed that adverse drug metabolism and pharmacokinetics were the main cause of failure to progress (89.9%). The remaining 11.1% of candidates failed to meet commercial interests.[133] Since this report was published, the pharmaceutical industry has undergone massive

changes, with the introduction of automation and computational elements to the drug development process. The integration of disciplines has also been helpful in reducing the failures from lack of commercial interest by improving communication between the departments.[132]

A more recent analysis of why candidate drugs fail was undertaken by Schuster *et al.*[125] Their analysis showed that between 1992 and 2002, a drug's potential efficacy and toxicity could not be determined in pre-clinical phases. This is because toxicity and lack of efficacy remain the major reasons for drug withdrawal once clinical trials have begun. Their data is in greater detail than that of Prentis *et al.*[133] and gives a phase by phase breakdown on the reasons for withdrawal. In Phase I the major reason for withdrawal was toxicity, this is because this is the first time that a new chemical entity is given to man, and animal models can not predict exact toxicity in man. In Phases II and III the major reason for withdrawal was a lack of efficacy. Since these Phases include administration of a candidate drug to patients with the targeted condition, accurate measurements of the effect of the drug are possible. The proportion of drugs which are discontinued due to toxicity increases from phase II to phase III, this has been reasoned to be due to the increased number of patients receiving the drug, allowing rare side effects to be observed.

Pharmaceutical companies are making major investments into *in vitro* and *in silico* methods to determine a candidate drug's efficiency and toxicity before it is brought to clinical trial, in the hope of reducing the number of costly animal and human trials which result in failure.[125, 129]

4.4 Pharmacology and Formulation

Bioavailability is critically important to the efficacy of a drug. Bioavailability is defined as:

"The rate and extent to which the active drug ingredient or therapeutic moiety is absorbed from a drug product and becomes available at the site of action." [134]

Pharmacologists and medicinal chemists jointly design a drug with an appropriate drug delivery system. A drug delivery system may involve chemical or physical manipulation of the active principle to control the bioavailability and prevention of premature drug excretion, inactivation and the Active Pharmaceutical Ingredient (API) inducing an immune response.

The provision of accurate, reproducible dosage by the selected route of administration is critical: it is known that identical drugs in different formulations give different plasma concentrations.[130] The plasma concentration which a drug achieves after administration is important because the therapeutic index shown below is variable between drugs. Some drugs have small therapeutic indexes therefore making control of the plasma concentration of the drug is critical.[135]

$$Therapeutic\ Index = \frac{Maximum\ non-toxic\ dose}{Minimum\ effective\ dose}$$

In order for the drug to reach the site of action (and cause an effect) the drug can be administered via the following routes: [135]

- Oral
- Sublingual
- Rectal
- Application to epithelial surfaces
- Inhalation
- Injection – subcutaneous, intramuscular, intravenous, intrathecal

With the exception of intravenous injection, the majority of drugs must be taken from the site of administration into the bloodstream. This process of transporting a drug to its site of action offers challenge for both the pharmacologist and medicinal chemist.

Small, hydrophobic drugs may enter the bloodstream by the trans-cellular route which means passing through the cell membrane. This transport may be active (involving carrier proteins or endocytosis) or passive (directly through the lipid membrane). The transport of drugs is partially dependent on its partition coefficient and therefore its solubility in water and organic solvents. Solubility of the API is of critical importance it has been estimated by Fahr *et al.* that approximately 40% of drugs on the market are poorly water soluble.[136]

Current techniques employed in the pharmaceutical industry for dealing with low solubility APIs are :

- Micronisation – grinding the drug so the final particle size is between 100 – 200 nm

- Crystal engineering – changing particle size / (pseudo)polymorphic forms

- Co-crystals can be formed by slow evaporation of mixtures, growth from melts, sublimation, and slurry preparation.

- Use of different counter ions which affect the solubility

- Solublisation of drugs in co-solvents

- Use of micelle / liposome systems.

- Use of cyclodextrins

- Use of carrier proteins

Physical methods for drug delivery such as acid resistant tablet coatings and transcutaneous routes, will not be covered in further detail in this review, which will concentrate on methods of encapsulation. Physical methods such as the micronisation and dispersible tablets rely on increasing the rate of dissolution and not increasing the solubility of a drug.[136]

4.5   Pro-drugs, Early Antibiotics and Nitrogen Mustards

One of the earliest techniques for improving the pharmacokinetics of a drug was to functionalise the molecule with a biodegradable group which renders it inactive, but when metabolised releases the active drug known as pro-drug formation. Addition of the biodegradable group can improve solubility, add specificity to the localisation of a molecule in the body,[130] prevent metabolism [124] or allow controlled release of the drug over a long period of time.[130]

Pro-drugs may be inadvertently discovered, a good example being the discovery of Prontosil Rubrum in 1932 by Domagk from the screening of a range of azo dyes. When further investigations into the mechanism of Prontosil Rubrum's bacteriostatic action took place in 1935 by Forneau, they showed that *in vivo* the azo bond was hydrolysed and the 4-aminobenzenesulfonamide was the product had the same bacteriostatic action as Prontosil Rubrum, and therefore must be responsible for the efficacy of the administered drug. [120, 121]
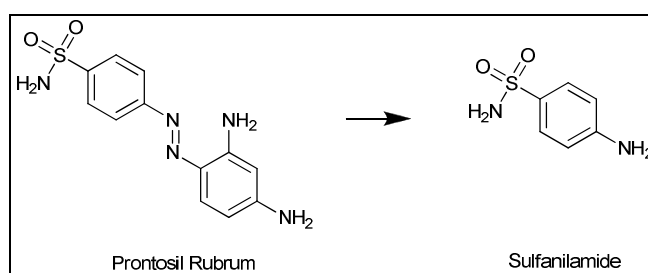
Figure 18 - Metabolism of Prontosil Rubrum

This was revolutionary because systemic bacterial infections were generally regarded as untreatable so only supportive measures could be taken for a patient. This prompted further derivatives to be synthesised and in 1938 Sulfacetamide was synthesised. The greater acidity which the acetyl group gave to the nitrogen of the sulphonamide meant that the drug was rapidly excreted through the kidneys to the bladder, where it would exert a bacteriostatic action. This side effect is particularly useful in patients with urinary tract infections.

The use of pro-drugs is exemplified by early DNA alkylating agents used in antineoplastic chemotherapy. It was known that nitrogen and sulphur mustard gas used during the First World War

damaged the bone marrow, however they were too toxic to be administered directly as they had a strong vesicant effect.[120] When the molecular structure was modified, their toxicity was reduced and on administration to patients suffering from non-Hodgkin's lymphoma dramatic remissions were observed.[124]

Nitrogen mustards work by alkylating DNA and therefore preventing cell division, their general structure is shown by the first structure of Figure 19. There are two delivery systems at work in this treatment; firstly the pro-drug (formation of the active agent within the cancerous cells) and secondly the variation of the R group. The general form of a nitrogen mustard is shown in the Figure below. Variation of the R group allows tuning of the reactivity of the molecule due to the biologically active component of the mustard is an aziridinium cation which the N-7 of guanine is reactive to. It is formed by the nucleophilic substitution of a chlorine atom with the lone pair of the nitrogen. The R group can exert an effect on the availability of the lone pair of the nitrogen and therefore the rate at which the aziridinium ion is formed.
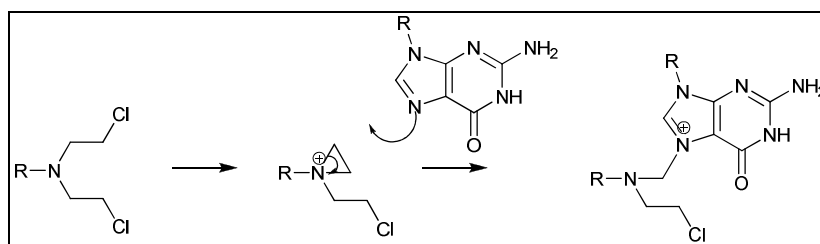
Figure 19 - Mechanism of action for nitrogen mustards

In an example of rational pro-drug design phosphoramidases were found to be over produced in tumour cells, and so a phosphoramide containing mustard was synthesised (Endoxana) in order to boost the reactivity of the nitrogen mustard in the tumour cell. The increase in reactivity is due to the increased availability of the lone pair of the nitrogen atom once hydrolysed. Endoxana was found to have improved pharmacological properties over mustine $R = CH_3$. [130]
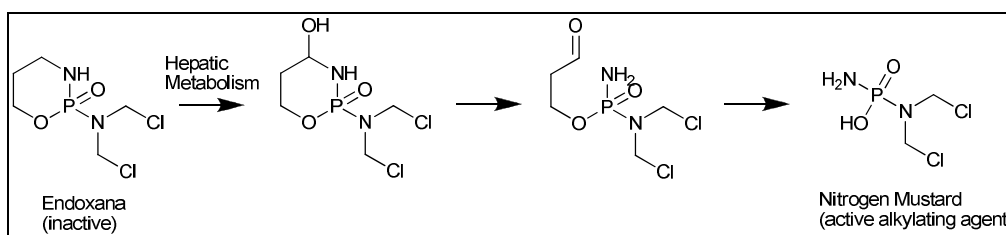
Figure 20 - Endoxana metabolism

4.6   Microemulsions, Protein Carriers and Taxol

Taxol is an antineoplastic drug approved for use in 1992 by the FDA to treat advanced metastatic breast and ovarian cancer.[137] The active ingredient was found in the bark of the Pacific yew tree (*Taxus brevifolia*) with yields for its extraction at 0.04% wt/wt meaning a single cycle of treatment would necessitate the sacrifice of 4 fully grown trees.[137] The drug can now be prepared semi-synthetically from the needles of the more common English yew tree (*Taxus Baccata*). Despite its high tumour response rates (51% in metastatic breast cancer [138]) Taxol has very low aqueous solubility (0.34 µg/ml) which makes both formulation and administration problematic.[137]
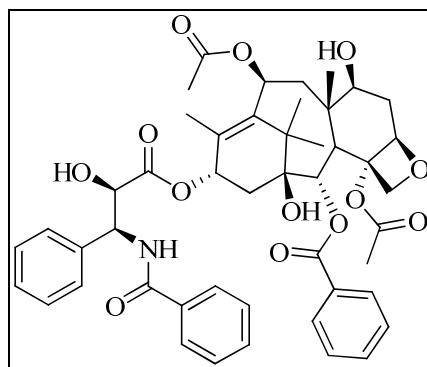
Figure 21 - Taxol

Currently Taxol is administered as a Cremophor® / ethanol microemulsion, in order to solubilise sufficient quantities of the drug. Cremophor® is a derivative of castor oil which has been developed to form micro-emulsions. Unfortunately there are problems associated with the formulation, as micelle formation in the bloodstream leads to non-linear dose – anti-tumour activity. It has been shown that the delivery method may cause a severe hypersensitivity reaction in 20 – 30% of patients.[139] In addition significant side effects are nephrotoxicity, neurotoxicity and leaching of Poly(vinyl chloride) (PVC) from the infusion apparatus, which may be caused by the delivery method. The majority of the side effects can be managed by pre-medication with corticosteriods and antihistamines before each cycle of treatment. [140]

Taxol has been found to be tightly bound(>90%) to serum proteins *in-vivo*. These proteins are the natural carriers of hydrophobic molecules around the body.[137] A formulation was subsequently developed in 2002 [139] formulating taxol with Human Serum Albumin (HSA) in order to overcome the

difficulties in using taxol. A phase III clinical trial (454 patients) found that HSA formulated taxol has significantly benefits over the Cremophor® formulation. A higher maximum tolerated dose was found to be possible and therefore a higher response rate to treatment was observed. The formulation was diluted in a saline or dextrose solution allowing a shorter administration time (30 minutes versus 3 hours) preventing leaching of the plasticisers from the administration kit removing the requirement for pre-medication.[141]

4.7   Liposomes and Doxorubicin

Liposomes are nanometer sized spherical assemblies of amphiphilic molecules which self assemble into a lipid bilayer in the solution phase. They can thereby entrap guest molecules, either within the central aqueous cavity (shown in blue in Figure 22) or the lipophilic inter-membrane zone (shown in yellow below). This method of drug delivery has been an area of intense scientific endeavour since the mid 1970's.[142, 143]

Liposomal drug delivery is not without problems: their primary method of excretion is by reticuloendothelial cells scavenging the vesicles and transporting them to the liver and the spleen for metabolism and excretion. This obviously leads to an accumulation of liposomes (and their cargo) in these organs.[144] As a result there may be hepatotoxicity observed due to increased concentrations of both drug and carrier molecules.[145] Short shelf life,[146] limited drug capacity, use of aggressive conditions for their preparation and problems with sterilisation are other problems which it has been necessary to overcome.[147] Therefore it is only recently (2005) that liposomes have been available in pharmaceutical formulations.[148]
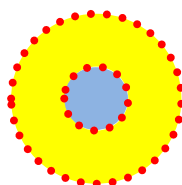
Figure 22 - Schematic representation of a mono-lamellar liposome

The FDA granted approval for the first formulation to use liposomes as a carrier system in November 2005. It consisted of mono-lamellar vesicles ≤100 nm diameter containing doxorubicin.[149] Doxorubicin is an anthracycline antibiotic which is used for treating a variety of solid malignant tumours.[150] The total maximum cumulative dosage of doxorubicin is limited to 450 mgm^{-2} due to its severe cardiotoxicity which can cause congestive heart failure.[151]
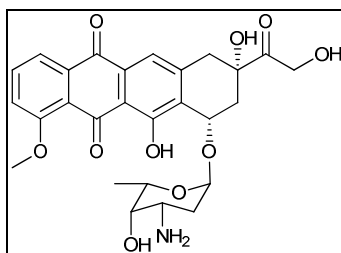
Figure 23 – Doxorubicin

It has recently been shown that doxorubicin is cytotoxic *in vitro* to glioma (a tumour of the non-nervous cells in the nervous system [152]) but the free drug has poor blood-brain barrier penetration, preventing its use in treatment of brain tumours. A recent clinical trial has shown that PEG-ylated liposomal doxorubicin can cause stabilisation of disease in 50% of patients with glioma.[148]

Other clinical trials have shown that encapsulation of doxorubicin in liposomes increases the concentration of drug in the tumour (by up to 10 times in advanced Kaposi's sarcoma) and also increases the drug's half life, allowing penetration of the blood-brain barrier and reduction in the drug's toxicity over the free molecule. These combined improvements in the pharmacology have been shown to result in improvement in the overall survival times for ovarian cancer patients in comparison to those receiving platinum based chemotherapy. Patients suffering from Kaposi's sarcoma are shown to have a longer mean survival rate and an increase in health-related quality of life than those on the standard ABV (Bleomycin, Vincristine & Doxorubicin) regimen.[153]

The improvement in pharmacological properties of the liposomal formulation has been attributed to the increase in time spent within the body's circulation over the un-encapsulated drug. The extension to half life is thought to be caused by the PEG reducing the attachment of plasma proteins to the liposome which would otherwise result in clearance from the circulation.[154] The increased circulation time allows increased concentration of the drug in solid tumours. This is due to the enhanced permeability and

retention effect (EPR effect) in solid tumours. A tumour has different pathophysiological characteristics from normal tissue.[130] This includes leaky vasculature within tumours which allows the tumour cells access to sufficient oxygen and other nutrients. This leaky vasculature allows drug delivery systems to leave the general circulation and become concentrated in the tumour.[155]

4.8   Cyclodextrins and Itraconazole

Cyclodextrins are cyclic oligosaccharides discovered in 1891,[156] whose arrangement of hydroxyl groups means that the interior of the torus shape is less polar than the exterior.[136] This difference in polarity of the interior and exterior allows the water molecules coordinated within the cyclodextrin to be liberated and replaced by lipophilic guest molecules.[157]
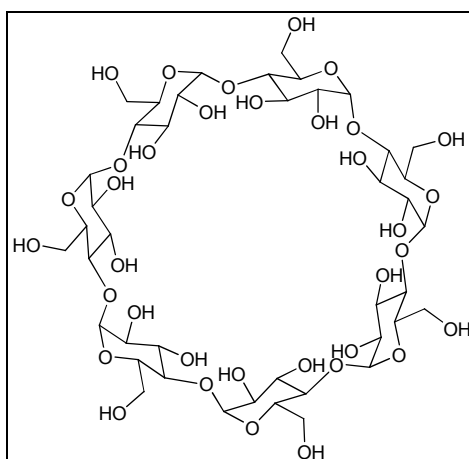
Figure 24 - β-Cyclodextrin

Cyclodextrins have been investigated for drug delivery applications and have been shown to increase solubility of lipophilic drugs without changing their molecular structure.[147] In 1976 the first cyclodextrin drug formulation was approved for use in Japan.[158] Currently cyclodextrins are marketed in over 30 pharmaceutical products.[157]

Due to their high hydrophilicity cyclodextrins show poor penetration of biological membranes and therefore act by increasing the concentration at a membrane surface.[159] When a drug is encapsulated, it is masked from the external environment, so cyclodextrins have found use in reducing local drug-induced irritation.[158, 160]

Itraconazole is a wide spectrum antifungal agent which is used to treat infections caused by organisms resistant to the standard treatment of fluconazole. Unfortunately it has a very low aqueous solubility (1 µgml^{-1}) which limits its clinical utility. It has been formulated with PEG but recently a cyclodextrin formulation for oral administration has been approved by the FDA.[161] It has been determined that the drug is released when the complex comes into contact with the gastric lumen, and once released follows the same pharmacokinetics as the un-encapsulated preparation. The cyclodextrin is not absorbed in large quantities (0.5% excreted intact in urine), but the majority of the undesirable side effects can be attributed to the cyclodextrin rather than Itraconazole.[161] The major advantage of the cyclodextrin formulation over the PEG capsule is the increased serum concentration achieved, which in clinical trials leads to a higher efficacy of treatment.[161]
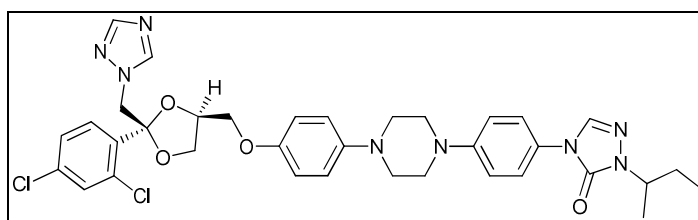
Figure 25 - Itraconazole

While there are significant advantages to the use of cyclodextrins in pharmaceutical formulation there remain some significant disadvantages. For example, β-cyclodextrin shows low water solubility and nephrotoxicity [161] and so is unsuitable for intravenous injection. and also the rate of formation / dissociation is very close to the diffusion limit so the guest molecules are only weakly held within the cavity.[158]

4.9   Summary of drug delivery

The recent progress in improving the pharmacokinetics of doxorubicin has confirmed that there is great potential in the field of drug delivery to improve existing treatments and potentially make viable chemical entities which were previously too harmful for therapeutic use. These recent developments demonstrate that significant progress being made to improve the treatments already available on the market by using novel drug delivery systems.

Ideally a new drug delivery system must be cheap to synthesise, be applicable to a variety of therapeutic agents, have good stability and improve the pharmacokinetics and efficacy of the drug it carries. Most importantly it must be non-toxic and have no major side effects. These are the stringent requirements which must be met in order for the drug to be approved by the MHRA and FDA, and therefore be used in a clinical setting.

5   Analytical Techniques

5.1   Single crystal X-ray Diffraction

The diffraction of X-rays by single crystals and powders is a technique widely used to determine unequivocally the arrangements of atoms in space and therefore the inter-molecule interactions which contribute to the packing motif formed. Several books and monographs have been published detailing the techniques currently in use for data collection and solution.[162-164]

X-ray diffraction techniques are limited somewhat because hydrogen atoms have $1/50^{th}$ of the X-ray scattering power of carbon atoms, therefore their position is difficult to determine.[7] If higher precision of the positions of hydrogen atoms is required, neutron diffraction can be performed. The significant limitations of this technique include the requirement for much larger crystals ($1mm^3$) than for standard X-ray diffraction experiments (therefore limiting the samples which can be run), neutron sources are limited and data collection times are much longer, which may contribute to decomposition of the sample before analysis is complete.[165]

X-rays generated by a synchrotron source allow data to be collected from crystals which would be unsuitable for analysis by standard lab based instruments. Data collection using a standard in-laboratory molybdenum or copper source can fail for several reasons, but most commonly small crystal size and weak diffraction are to blame. Crystals with a shortest dimension <0.01 mm or which show only low angle diffraction are often referred to national synchrotron sources for data collection. Successful analysis of smaller and flawed crystals is possible due to the shorter wavelength and increased intensity of the synchrotron radiation.[162-164]

5.2 Diffusion NMR spectroscopy

Diffusion NMR uses a conventional NMR instrument to perform non-destructive investigation into the shape and size of a species in solution. This technique is becoming widely used in medical sciences and more recently is becoming important in drug discovery, allowing probing of interactions between a larger host molecule and a smaller guest molecule.[108]

The work of Cohen *et al.* (discussed above in section 4.1.3.4) shows that formation of a supramolecular species can be monitored by diffusion NMR. It is possible to monitor the encapsulation of guest molecules because as the supramolecular assembly moves as a single entity the diffusion coefficient of an encapsulated molecule will be the same as the larger host molecule.[78, 80, 103, 105-108, 111, 166]

The diffusion coefficient of a spherical species through a solution can be determined using the Stokes-Einstein equation:[29]

$$D = \frac{k_b T}{6\pi\eta r_h}$$

Where D is the diffusion coefficient, k_b is the Boltzmann constant, T the absolute temperature η is the viscosity of the solution and r_h is the hydrodynamic radius of the species. For non-spherical species the Einstein-Smoluchowski equation can be used:

$$D = \frac{RT}{Nf}$$

Where N is Avogadro's number and f is the frictional coefficient which is dependent on the shape of the molecule. The diffusion coefficient of a species is proportional to the signal intensity which is proportional to the magnetic field gradient across the length of the NMR coil.

The diffusion NMR experiment is limited to systems which are at equilibrium with no concentration gradients across the sample as diffusion and convection will adversely affect any results. Most diffusion experiments are conducted using the PGSE pulse sequence. From the PGSE pulse sequence using an extra degree of data analysis a DOSY analysis can be performed. The DOSY experiment allows the separation of mixtures by their diffusion coefficients.[108]

Chapter 2 - Synthesis and molecular structures

of *C*-alkyl-calix[4]arenes

1 Synthesis

In order to study the molecular interactions which govern the nanometer scale architectures of *C*-alkyl-calix[4]pyrogallolarenes and *C*-alkyl-calix[4]resorcinarenes, a library of these compounds was synthesised and crystals grown from a variety of solvents. The crystals were then analysed by single crystal X-ray diffraction crystallography (SCXRD) and mass spectroscopy (MS).
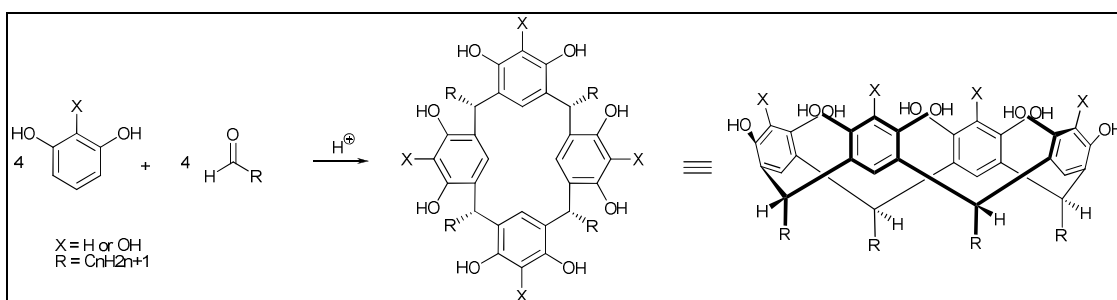
Figure 26 - General calixarene synthesis

The library of compounds was synthesised by optimisation of the procedure detailed by Gibb *et al*. for the maximum yield of the cone conformation.[167] In the article, Gibb details conditions for the synthesis of *C*-(butanol)-calix[4]resorcinarene by the slow addition of 2,3-dihydropyran to a solution of resorcinol in methanol hydrochloric acid, and subsequent heating for 5 days at 60°C. In the literature, other authors do not advocate slow addition of aldehydes or long reaction times for alkyl / aryl calix[4](resorcin/pyrogallol)arenes and favour rapid addition followed by reflux for up to 8 hours.[42, 43, 115]

Both 'green' and 'conventional' approaches were investigated and were found to give the desired product in moderate to high yields. It was found that longer reaction times gave materials which were easier to purify and therefore isolated yields were increased.

The reaction products which were produced were routinely analysed by ^{1}H and ^{13}C NMR with resonances diagnostic of formation of a macrocyclic product detected. These characteristic resonances can be attributed to the hydrogen bonded to the bridging carbon atom of the macrocycle in the ^{1}H spectra. There is also only a single aryl proton detectable by ^{1}H NMR which indicates an identical environment for the constituent protons therefore this excludes higher homologues of the calixarenes because the larger macrocycle size allows conformational flexibility which would result in a disruption of the NMR signals attributable to the proton of the aromatic rings. In the ^{13}C{^{1}H} NMR spectrum, there is a characteristic decrease in the intensity of the signal of the carbon atoms of the aryl ring (carbon atoms 4 and 6 of 1,2,3-trihydroxybenzene) which become bound to the macrocycle and therefore have their protons substituted.

It has been shown in the literature that during the calixarene synthesis the macrocyclisation reaction is reversible under the conditions. It has been determined that the cone conformation is the thermodynamic product, the intramolecular hydrogen bonds between phenolic hydroxyl groups give this conformation greater thermodynamic stability. This conformation also has lower solubility in the reaction mixtures than the other conformational isomers.[59, 63] Therefore a long, low temperature reaction was chosen for the synthesis of calix[4]pyrogallolarenes over the relatively short reaction at reflux favoured in the synthesis of *t*-butyl derived calix[4]arenes.[43] Figure 2 shows the conformations which a calix[4]arene can adopt, A – cone, B – partial cone, C – pinched cone, D – chair. The cone isomer is the only conformation to possess a structure suitable for nano-sphere formation, therefore it is the desired isomer in the work of this thesis.
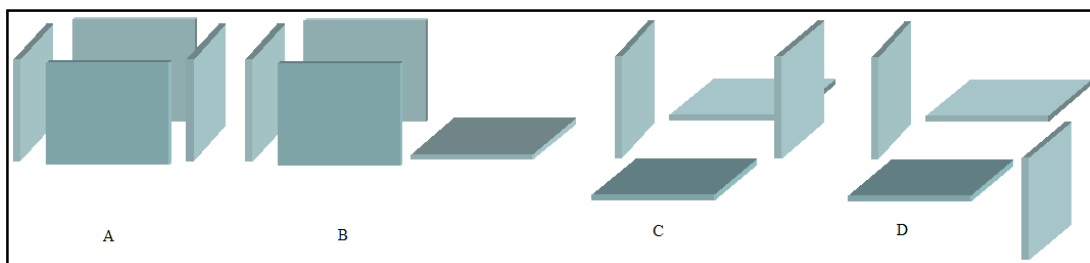
Figure 27 - Conformations of calix[4]resorcinarenes and calix[4]pyrogallolarenes

The solubility of the desired cone conformation is sufficiently low in the reaction mixture to allow its precipitation under the conditions, performance of the reaction under thermodynamic control therefore

allows the cone conformation to be the sole product of the reaction. The product was isolated by filtration of the precipitate which formed on cooling of the reaction mixture. The product was purified further by recrystallisation from a variety of solvents, with acetonitrile being used in preference for the initial isolation of product due to its rapid precipitation of the desired product when cooled.

During the synthesis of the library of compounds, it was found that the rate of addition of the aldehyde to the acidic solution of pyrogallol was critical to the yield of calixarene isolated. This was particularly evident when performing ring opening of 2,3-dihydrofuran and 2,3-dihydropyran. Rapid addition of an aldehyde to an acidic pyrogallol mixture gave low yields. The addition of acid to a mixture of pyrogallol and aldehyde was found to yield low amounts of the desired calixarenes.

This finding can be rationalised if the condensation reaction with pyrogallol or resorcinol was less rapid than the self condensation reaction which generates aldol products. This self condensation of enolisable aldehydes under the reaction conditions would be uncontrolled and therefore give a wide variety of products. This is exemplified in Figure 3 below.
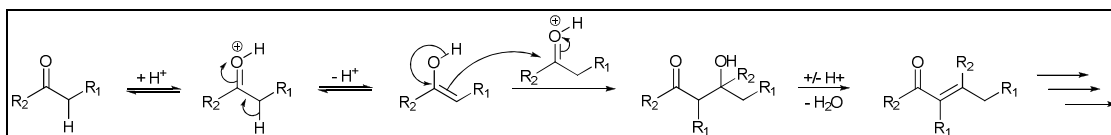
Figure 28 - Aldol condensation R_1 = alkyl / aryl R_2 = alkyl / aryl / hydrogen

In the past, pyrogallol was used in the laboratory as an indicator of the presence of oxygen, because it is easily oxidised, forming a black solution when exposed to oxygen. This high colouration is due to the formation of purpurogallin and related oligomers.[168] Therefore, in order to improve the yield of product, the calixarene syntheses were heated under a nitrogen atmosphere to prevent oxidation.
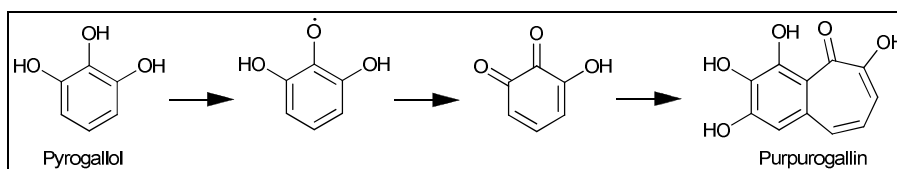
Figure 29 - Oxidation of pyrogallol to Purpurogallin

For clarity and ease of reading, the calixarene molecules have been given their own shortened nomenclature system; for example *C*-methyl-calix[4]pyrogallolarene will be noted as C1Pg. The number represents the number of carbon atoms in the pendant chain and the Pg or Rs suffix denotes the pyrogallolarenes and resorcinarenes respectively. This nomenclature system is demonstrated in Figure 5 below.
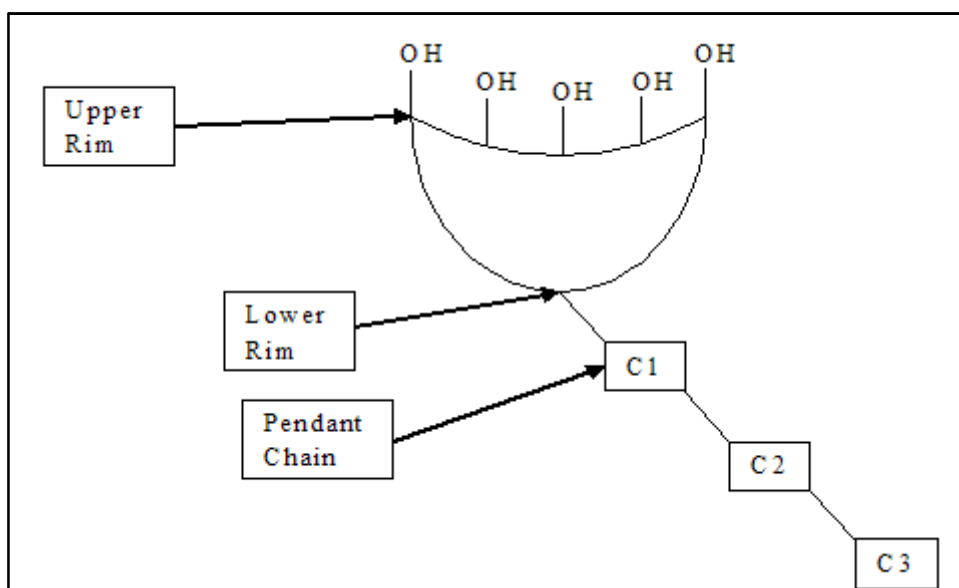
Figure 30 - Cartoon demonstrating calix[4]arene nomenclature system

Crystals were grown by slow evaporation of the pure product from the desired solvent. Where this method failed, diffusion methods of growing crystals were attempted. The calixarene was dissolved in a solvent and the solution was placed in a vial within a sealed container which contained a second, more volatile solvent in which the calixarene had low solubility. As the counter-solvent slowly diffuses into the calixarene solution, this causes crystallisation to occur, producing materials which were suitable for single crystal X-ray diffraction analysis.

The single crystal X-ray structures reported in this thesis were collected at three sources, Daresbury synchrotron, the EPSRC crystallography service at Southampton University and Heriot Watt University. At the non-synchrotron sources Mo$K\alpha$ radiation was used and in order to minimise the inter-atomic movement the crystals were cooled to 120 K. Structures were solved by direct methods using SHELX-97 *via* the X-SEED interface.[169-171] Molecular geometries and inter-atomic distances were calculated using X-SEED or Mercury programmes, X-ray coordinates have been deposited with the CCDC.[172] Volumes of cavities or solvent filled voids were calculated using the MCAVITY programme.[173] Where a hydrogen atom is geometrically generated using the AFIX command, hydrogen bond distances are quoted as the inter-heteroatom distance in addition to the hydrogen – heteroatom distance.

Table 1 - Crystallisation matrix of C-alkyl-calix[4]arenes

☺ = Crystal formation X = no crystal growth

Solvent	C1Pg	C2Pg	C2Rs	C3Pg	C4Pg	C5Pg	C6Pg	C7Pg	C8Pg	C9Pg	C10Pg
Acetonitrile	☺	☺	☺	☺	☺	☺	☺	☺	☺	X	☺
Acetone	X	X	X	☺	X	X	X	X	X	X	X
Diethyl Ether	☺	X	X	☺	☺	X	X	☺	X	☺	X
Ethanol	X	X	X	☺	X	X	X	☺	X	X	☺
Ethyl Acetate	X	X	X	☺	X	X	X	☺	X	X	☺

2 Molecular structures of *C*-alkyl-calix[4]arenes

2.1 *C*-Methyl-calix[4]pyrogallolarene

C-Methyl-calix[4]pyrogallolarene was successfully synthesised in the cone conformation using methods which required solvent and the solvent free technique. Crystals of the material were grown by slow evaporation of a saturated solution of calixarene in diethyl ether and acetonitrile.

The acetonitrile solvate ($C_{32}H_{32}O_{12}\cdot3(CH_3CN)$) crystallises in the space group *P2/n* and shows a head-to-tail arrangement of the calixarene molecules. A single acetonitrile molecule resides within the cavity which is formed between the pendant chains of one calixarene and the upper rim of the calixarene below. The acetonitrile is aligned vertically with respect to the cavity of the calixarene, with its methyl group pointing towards the cavity and a hydrogen bonding interaction between the nitrogen of the cyano group and the hydrogen atoms of the lower rim of the calixarene above. These hydrogen bonds interactions are N(1) ⋯ H(9) = 2.601 Å and N(1) ⋯ H(1A) = 2.60 Å in length are within the expected limits for this type of interaction (2.2 – 3.2 Å) as reported by Jeffrey (N(1) ⋯ C(1) = 3.53 Å and N(1) ⋯ C(9) = 3.53(6) Å).[7]
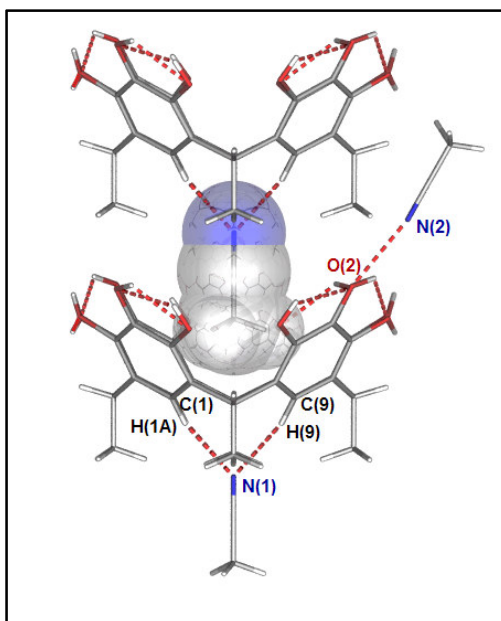
Figure 31 - *C*-Methyl-calix[4]pyrogallolarene acetonitrile clathrate

The volume of the cavity formed between the upper rim of one calixarene and including the pendant methyl groups and the lower rim of the calixarene molecule above was calculated using MCAVITY. The cavity was found to be approximately 85 $Å^3$ in volume and the volume of the guest acetonitrile (shown in a space filling representation in Figure 8 above) was calculated with X-SEED to be 47.3 $Å^3$. This represents 56% occupancy of the total volume of the cavity comparing favourably with Mecozzi's 55±9% solution for synthetic receptors.[101]

The very small difference in distances of the hydrogen bonds between the protons and the guest acetonitrile molecule show that the acetonitrile is centrally arranged and that there is very little distortion of the macrocycle in the solid state. This lack of distortion can be quantitatively assessed by generating centroids ((1)(2)(3)(4)) in the constituent aromatic rings of the calixarene and measuring the distance between opposite rings and comparing the difference between the two possible distances as shown in Figure 32 below.
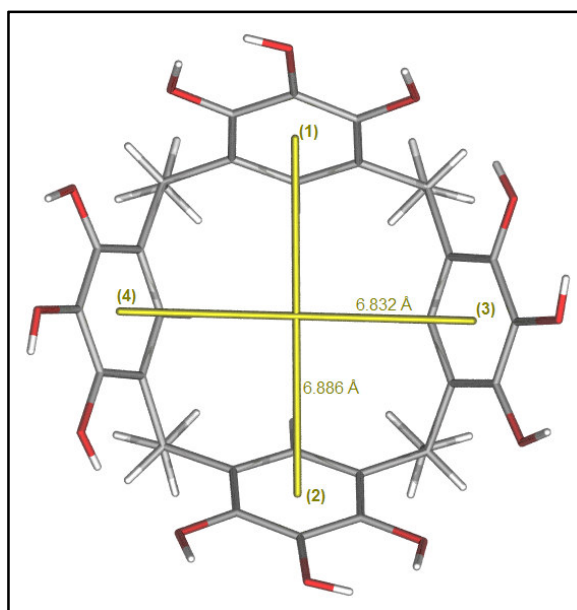
Figure 32 - Distortion factor calculation

This gives the distortion factor, which in this case is 0.99 indicating near perfect symmetrical arrangement of the aryl rings.

$$Distortion\ Factor = \frac{Shortest\ inter-phenyl\ ring\ distance}{Longest\ inter-phenyl\ ring\ distance}$$

A second acetonitrile molecule is found in the crystal lattice forming a hydrogen bond to the upper rim of the calixarene molecule (N(2) $\cdots$ H(2A) = 1.86 Å (N(2) $\cdots$ O(2) = 2.71 (6) Å)); however, this causes no perturbation of the macrocycle or packing arrangement because the calixarene above is perfectly superimposed onto the original. This means that an infinite 2D chain of calixarene molecules are formed because the neighbours in the other plane are arranged in the same way so there are chains of oppositely arranged calixarene molecules this is shown in Figure 33 below.
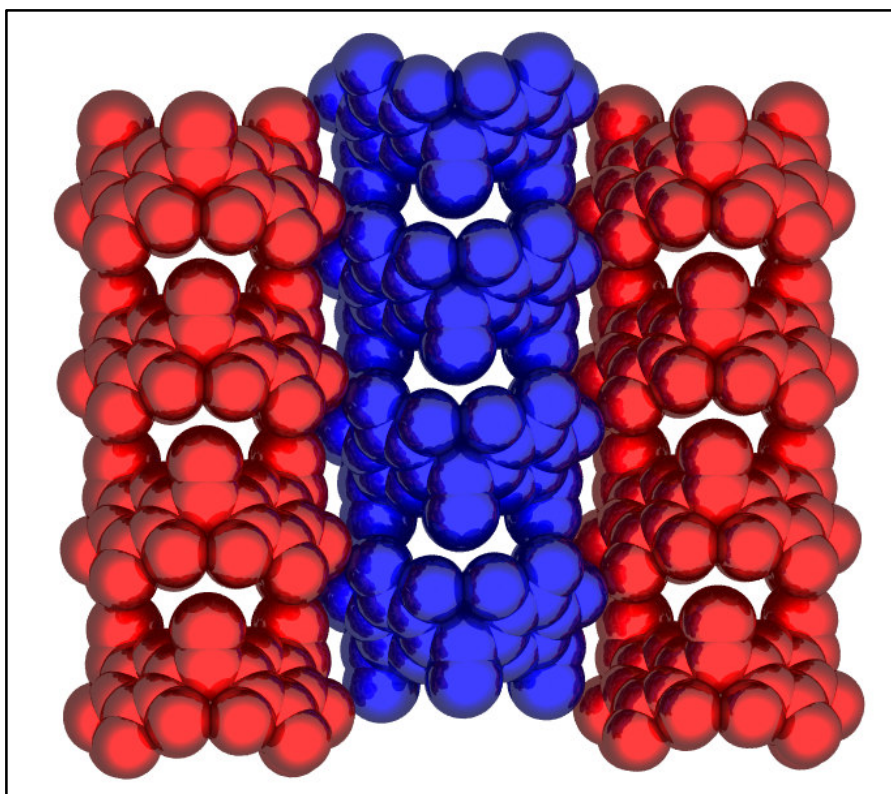
Figure 33 - Packing diagram of *C*-methyl-calix[4]pyrogallolarene acetonitrile clathrate (solvent molecules and hydrogen atoms removed for clarity)

A solid state molecular structure of the diethyl ether clathrate ($C_{32}H_{32}O_{12}\cdot3(CH_3CH_2OCH_2CH_3)$) was solved from data collected on crystals formed by slow evaporation of a solution of C1Pg in ether which had been sonicated for 20 minutes. The structure which forms is markedly different to that of the acetonitrile solvate. It is in space group *C*2/*c* with molecules arranged in a head-to-head packing

motif. The calculated density of the diethyl ether solvate is significantly lower (1.21 g cm^{-3}) than that of the acetonitrile solvate (1.35 g cm^{-3}). This may be due to the greater volume occupied by the three solvent molecules present in the lattice in the diethyl ether clathrate over the two acetonitrile molecules present in the previous structure.
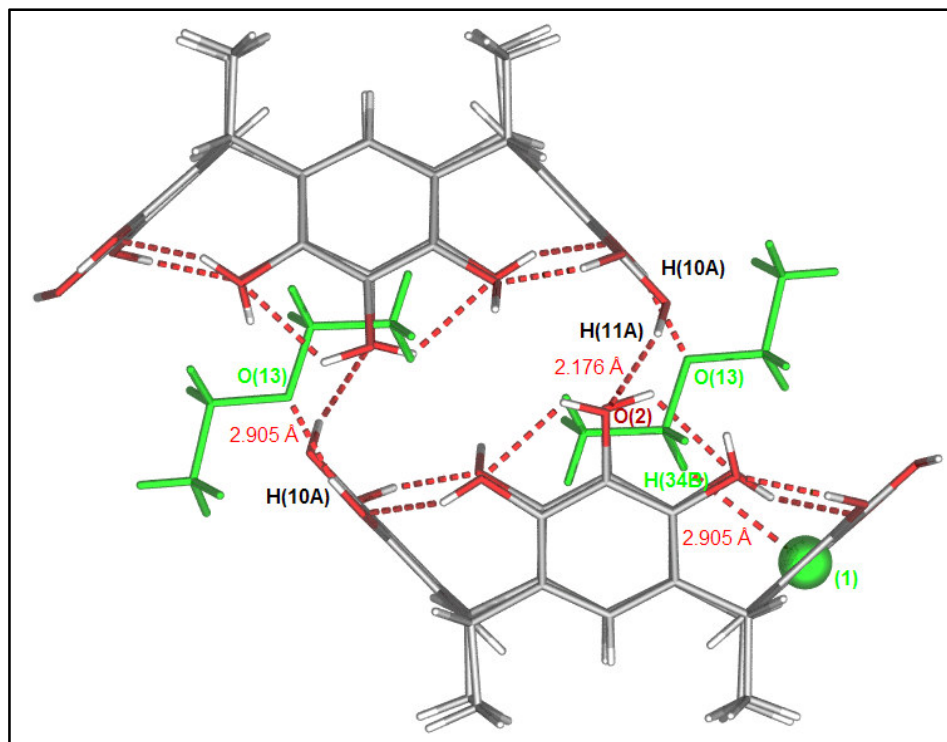
Figure 34 - *C*-Methyl-calix[4]arene diethyl ether solvate (*exo* solvent molecules removed for clarity)

Three solvent molecules are included in the asymmetric unit, the first of which partially resides within the cavity of the calixarene. One of the guest's ethyl groups resides in the cavity forming CH − π interactions (H(34B) ⋯ (1) = 2.91 Å and C(34) ⋯ (1) = 3.56 Å). The ethereal oxygen forms a hydrogen bond (O(13) ⋯ H(10A) = 1.86 Å and O(13) ⋯ O(10) = 2.61(6) Å) to the upper rim of the calixarene which is arranged in a head-to-head fashion with the first calixarene. This interaction causes a misalignment in the head-to-head arrangement and only approximately one third of the cavity's opening is covered by a single calixarene molecule above.

The remaining two solvent molecules reside outside the calixarene's cavity but form hydrogen bonds to the upper rim of the first calixarene molecule (O(15) ⋯ H(2A) = 1.98 Å and O(14) ⋯ H(5A) = 1.63 Å (O(15) ⋯ O(2) = 2.754 Å and O(14) ⋯ O(5) = 2.746(6) Å). One of these *exo* solvent molecules has

its alkyl chains disordered over two positions (shown as blue and red chains in the Figure below). Disorder is not seen in the *endo* solvent molecule, which indicates there is a greater freedom of movement in the exterior solvent molecules.
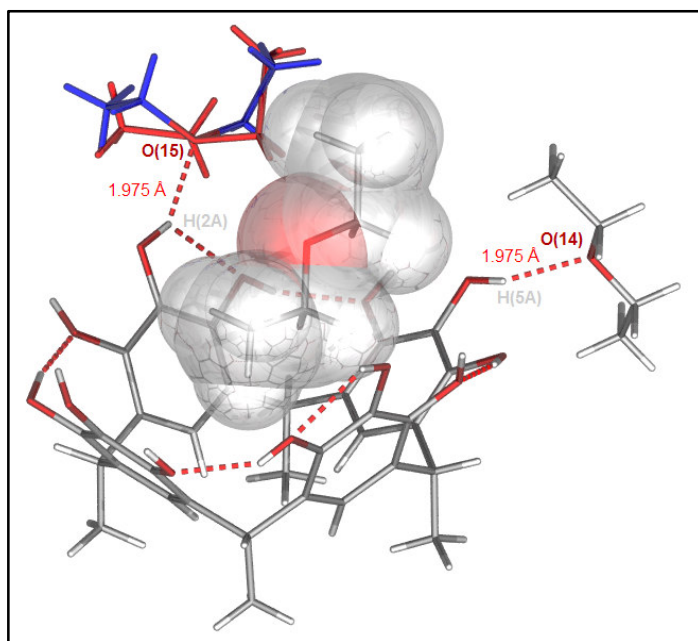
Figure 35 - *C*-Methyl-calix[4]arene diethyl ether solvate
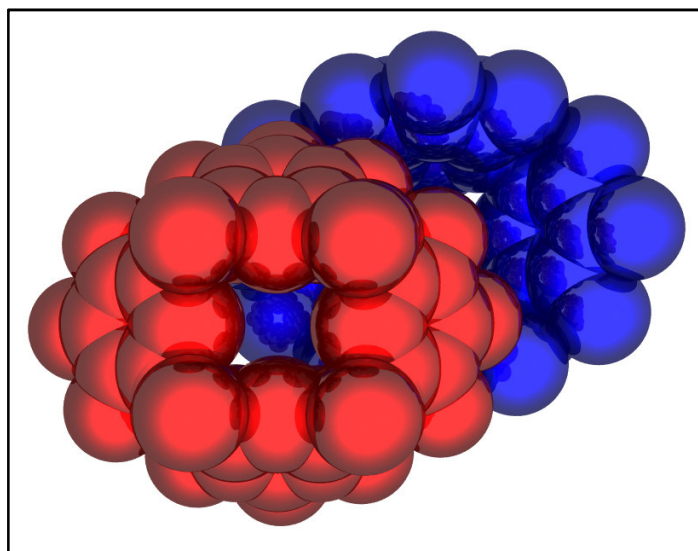
Figure 36 - Misalignment of head-to-head arrangement (solvent molecules and hydrogen atoms removed for clarity)

2.2   *C*-Ethyl-calix[4]pyrogallolarene

C-Ethyl-calix[4]pyrogallolarene was synthesised in the cone conformation by both the method requiring use of solvent and the grinding method. It was found that a significant proportion of the material generated by the grinding process was in the chair conformation which can be separated from the cone conformation by recrystallisation from acetonitrile. As the cone isomer is less soluble in organic solvents it is easily isolated by filtration.

Crystals were grown by the slow evaporation of an acetonitrile solution. This gave a structure which was dramatically different to that shown by the C1Pg acetonitrile clathrate ($C_{36}H_{40}O_{12} \cdot 5(CH_3CN)$). The molecule crystallises with one calixarene and five acetonitrile in its asymmetric unit and the unit cell is filled by symmetry operations of the space group $P2_1/c$, and as a result of the 2_1 screw axis a mixture of both head-to-head interactions and also head-to-tail interactions is found.
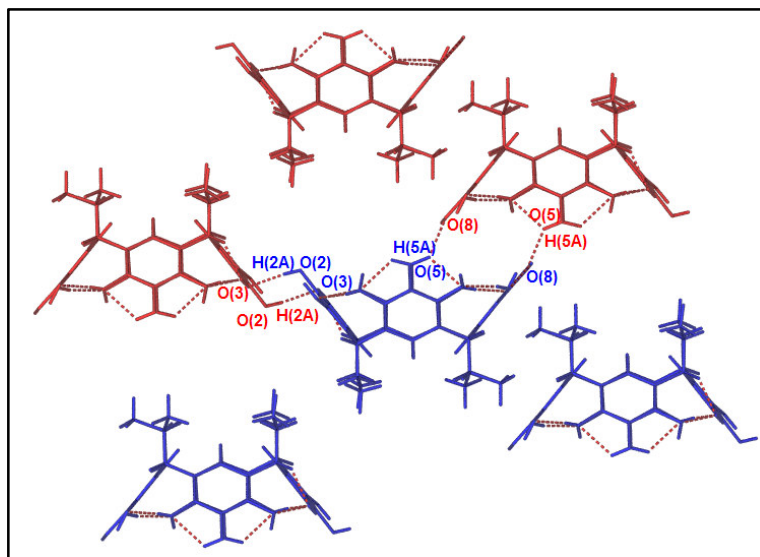
Figure 37 - Packing motif in *C*-ethyl-calix[4]pyrogallolarene acetonitrile clathrate (solvent molecules removed for clarity)

There are two crystallographically unique hydrogen bonds between the upper rims of calixarenes which have been rotated and translated: H(2A) $\cdots$ O(3) = 1.89 Å (O(2) $\cdots$ O(3) = 2.70 Å) and H(5A) $\cdots$ O(8) = 2.07(7) Å (O(5) $\cdots$ O(8) = 2.73(5) Å).

The head-to-tail interaction covers approximately one quarter of the surface area of the upper rim of each calixarene. Approximately half this area again is taken up by a head-to-tail interaction, with the remaining area being filled by three well defined solvent molecules.

One of the crystallographically unique acetonitrile molecules resides within the cavity of the calixarene but in contrast to the C1Pg case is tilted at an angle of 54° from the central plane of the calixarene, and does not interact with a lower rim of the above calixarene. This molecule instead interacts with the upper rim of a calixarene which has been inverted N(1) ⋯ H(7B) = 2.13 Å (N(1) ⋯ O(7) = 2.86 Å). A crystallographically unique acetonitrile coordinates to the lower rim of each calixarene molecule and is well aligned with the plane of the ring (shown as the red line in Figure 39) and is tilted 37.5° from the calixarene normal (shown as blue line in Figure 39) and forms a hydrogen bond to the lower rim of the annulus 2.69 Å long.
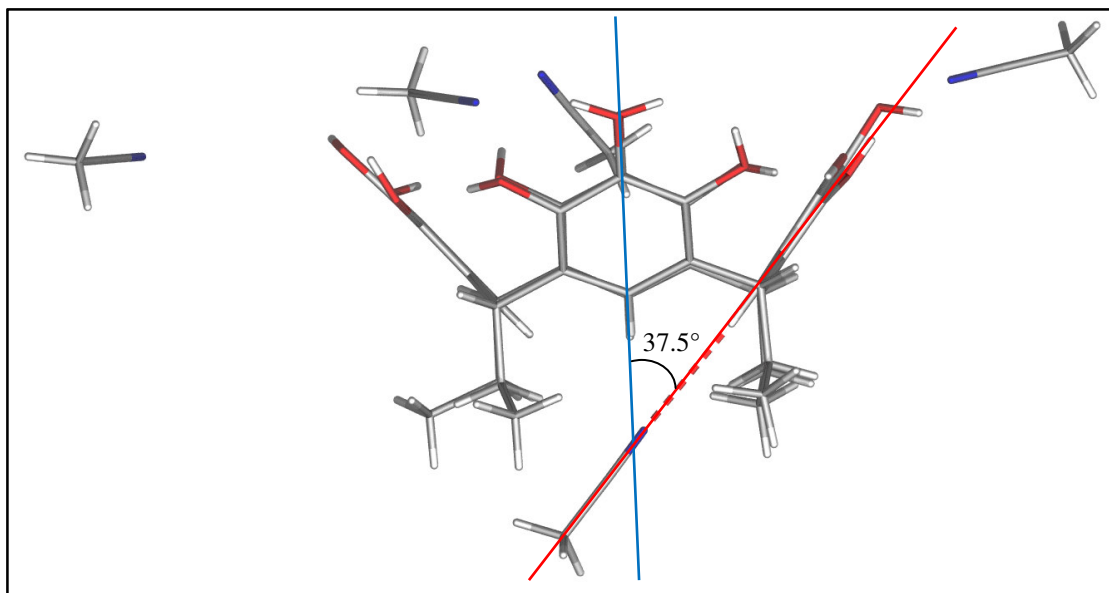
Figure 38 - *C*-Ethyl-calix[4]pyrogallolarene acetonitrile solvate

The hydrogen bonding interaction between an acetonitrile molecule and the lower rim of a calixarene is shown to be important to the formation of different packing architectures. This effect can be clearly observed in the packing motif of calixarenes which have pendant chains functionalised with nitrile groups, which will be discussed in later sections.

2.3   *C*-Ethyl-calix[4]resorcinarene

C-Ethyl-calix[4]resorcinarene was synthesised by a slow drop-wise addition of propanal to an acidic solution of resorcinol. The reaction was heated to 70°C for 4 days and upon cooling the desired product precipitated from solution. Recrystallisation of the material from ethanol gave the product in moderate yield. Crystals were grown by the slow evaporation of solvent from an acetonitrile solution.
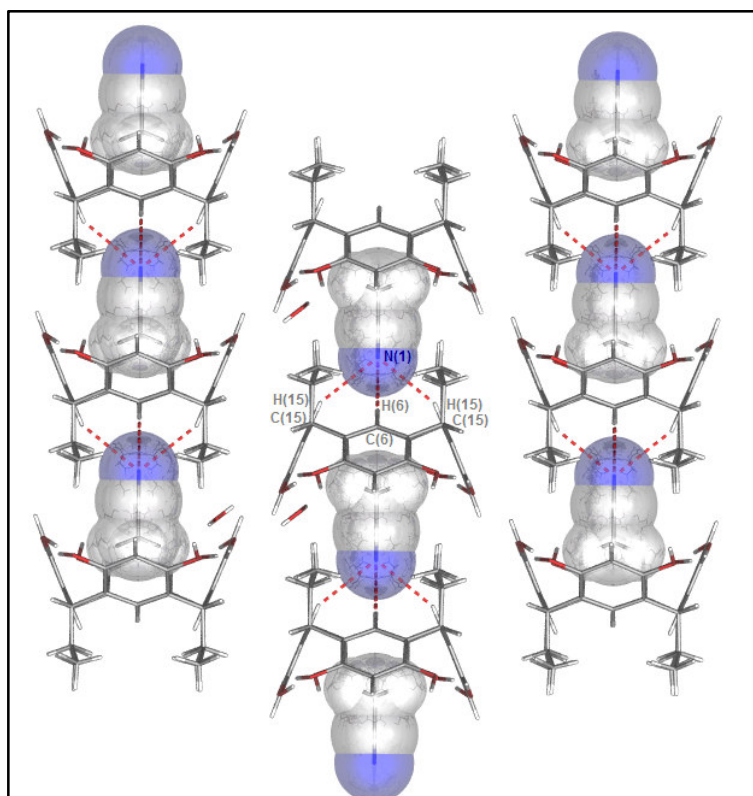
Figure 39 - *C*-Ethyl-calix[4]resorcinarene acetonitrile water clathrate (*exo* solvent molecules removed for clarity)

The packing motif and molecular structure ($C_{36}H_{40}O_8$·(CH_3CN)(H_2O)) which is revealed on solution of the data is strikingly different to that of *C*-ethyl-calix[4]pyrogallolarene acetonitrile water clathrate and bears a closer resemblance to the molecular structure of *C*-methyl-calix[4]pyrogallolarene acetonitrile clathrate. Firstly, the calixarene molecules are arranged in a head-to-tail packing motif which *P*2/*n* symmetry converts into an alternating infinite vertical sheet architecture, which is seen in C1Pg acetonitrile clathrate.

Secondly the position of the acetonitrile is remarkably different to that seen in the *C*-ethyl-calix[4]pyrogallolarene analogue, with the acetonitrile molecule being in parallel alignment with the calixarene and forming a hydrogen bond to the annulus of the calixarene above (N(1) $\cdots$ H(6) = 2.82 Å (N(1) $\cdots$ C(6) = 3.77(6) Å) and N(1) $\cdots$ H(15) = 2.85 Å (N(1) $\cdots$ C(15) = 3.72(6) Å)).

A water molecule resides *exo* to the cavity, and forms an intra-sheet bridge between calixarene molecules, This bridge runs from H(1A) of the upper rim to the oxygen of the water O(5) and is 1.85 Å long (O(1) $\cdots$ O(5) = 2.68(6) Å). The water molecule then forms a hydrogen bonds from one of its hydrogen atoms (H(5C)) to the upper rim of the adjacent calixarene (O(2)) which is 2.12 Å long (O(5) – O(2) = 2.79(6) Å).

2.4   *C*-Propyl-calix[4]pyrogallolarene

C-Propyl-calix[4]pyrogallolarene was produced by conventional and 'green' methods in high yield. This molecule was amenable to crystallisation and crystals were grown from saturated solutions of acetone, acetonitrile, diethyl ether, and ethanol to give four distinct phases.

In the ethanol clathrate the expected bilayer structure is formed ($C_{40}H_{48}O_{12} \cdot 3C_2H_5OH \cdot 2H_2O$). This bilayer is formed by the interdigitation of the pendant chains of calixarenes which are arranged in a head-to-head packing motif. The closest approach of the pendant chains to the annulus is H(20A,B&C) – plane generated from H(1,11,21,31) = 2.905 Å (C(20) – Plane (C(1,11,21,31)) = 4.045 Å) The asymmetric unit (ASU) contains one complete calixarene, three ethanol and two water molecules. The structure is in space group $P\bar{1}$ which converts the ASU into a bilayer as shown in the Figure below.
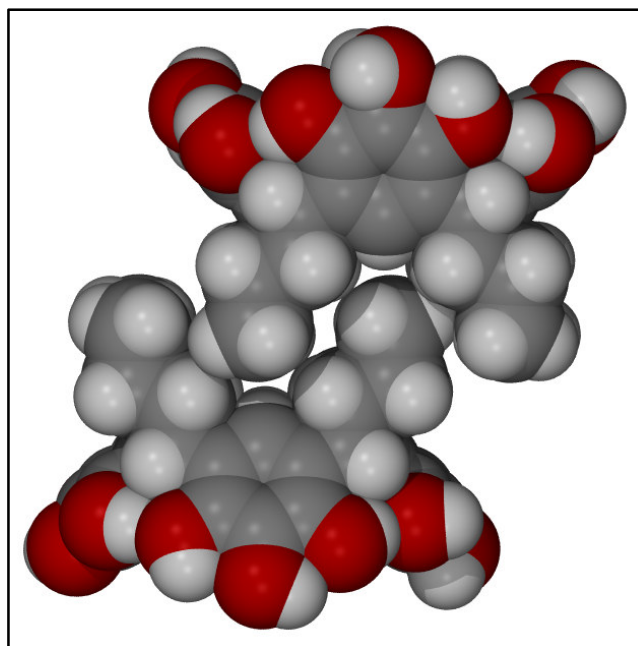
Figure 40 - Interdigitation of pendant chains in *C*-propyl-calix[4]pyrogallolarene ethanol water clathrate

Each face of the bilayer is formed by the square packing of calixarene molecules with alternating absences. These absences are filled with solvent molecules (two ethanol and two water molecules).

The solvent molecules form hydrogen bonds to the upper rims of the adjacent calixarenes (O(16) ⋯ H(4) = 1.83 Å (O(16) ⋯ O(2) = 2.65(5) Å), H(50) ⋯ O(11) = 2.19 Å (O(16) ⋯ O(11) = 2.83(5) Å), H(34) ⋯ O(17) = 1.84 Å (O(11) ⋯ O(17) = 2.71(6) Å)) which hold the layer in place. All four phenyl rings of each calixarene are involved in the hydrogen bonding to the solvent pool. The solvent filled void does not penetrate the full length of the bilayer and is capped by the pendant chains of a calixarene from the interdigitating layer. Above the plane of the bilayer the voids are capped by the presence of the cavity of a calixarene. This inclusion of ethanol into the bilayer is reminiscent of the disruption by ethanol to lipid bilayers in biological systems which is proposed by Pabst *et al.*[24]

An ethanol molecule resides within the cavity which forms a hydrogen bond to the upper rim of a calixarene of the next bilayer (O(13) ⋯ H(25) = 1.91 Å (O(13) ⋯ O(9) = 2.72(5) Å)).
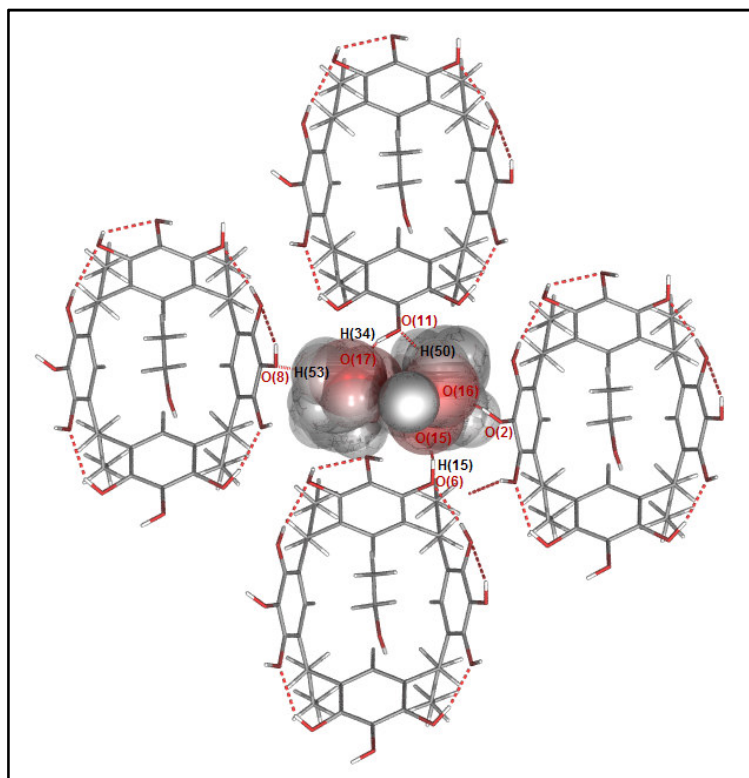
Figure 41 - Plan view of surface of bilayer formed by *C*-propyl-calix[4]pyrogallolarene ethanol water clathrate

The acetone clathrate ($C_{40}H_{48}O_{12} \cdot 3(CH_3C(O)CH_3)$) includes four molecules in its asymmetric unit (one calixarene and three acetone molecules). With *P2/c* symmetry a bilayer is formed. The first acetone resides outside the cavity of the calixarene and in a similar manner to C3OHPg (see Chapter 5 section 3.1) a hydrogen bond is formed from the oxygen of the acetone to the lower rim of the calixarene (O(9) ⋯ H(20) = 2.82 Å (O(9) ⋯ C(1) = 3.82(6) Å), O(9) ⋯ H(21) = 2.87 Å (O(9) ⋯ C(16) 3.79(6) Å)).
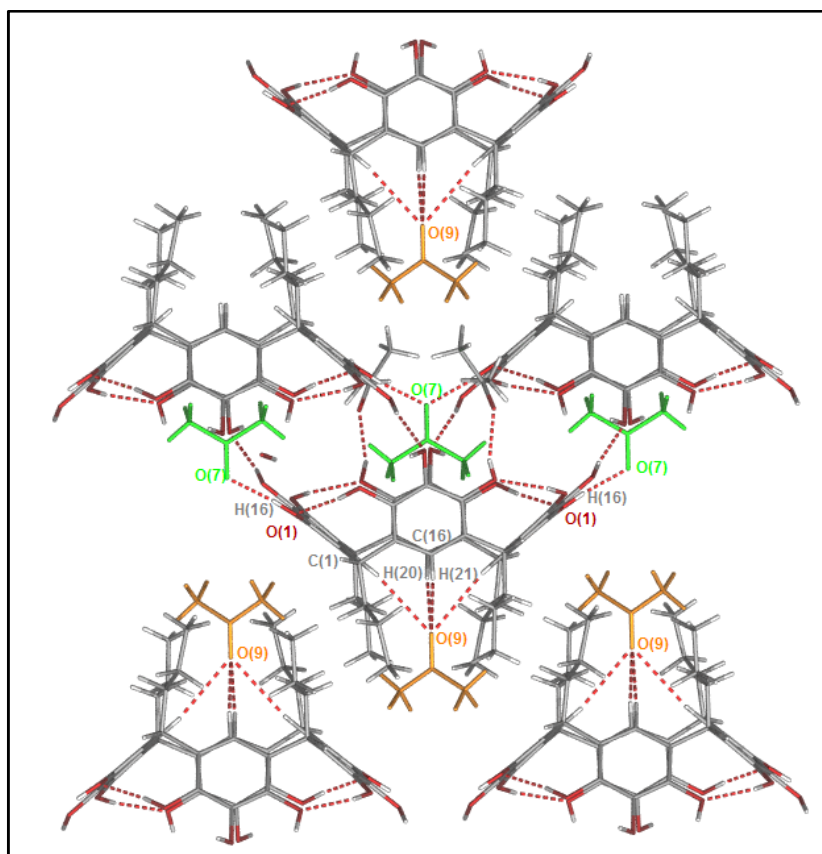
Figure 42 - Packing in *C*-propyl-calix[4]pyrogallolarene acetone clathrate

The second acetone forms a hydrogen bond to the upper rim of the calixarene (O(8) ⋯ H(17) = 1.83 Å (O(5) ⋯ O(8) = 2.76(5) Å)). The third acetone molecule resides within the cavity and coordinates to the upper rim of the next layer with one crystallographically unique hydrogen bond (O(7) ⋯ H(16) = 1.91 Å (O(7) ⋯ O(1) = 2.75(4) Å)).

Crystals rapidly formed when a solution of C3Pg in diethyl ether was left to slowly evaporate $(C_{40}H_{48}O_{12}\cdot(CH_3CH_2OCH_2CH3)\,(H_2O))$. The molecular structure which is revealed shows a bilayer arrangement of the calixarene molecules formed of two crystallographically unique calixarene molecules, two diethyl ether and one water molecule.

The architecture which is formed is interesting because there is no interdigitation of the pendant chains which is a formation commonly observed in the calixarenes bilayer. This is shown in Figure 43 below with each unique type of calixarene highlighted in a different colour.
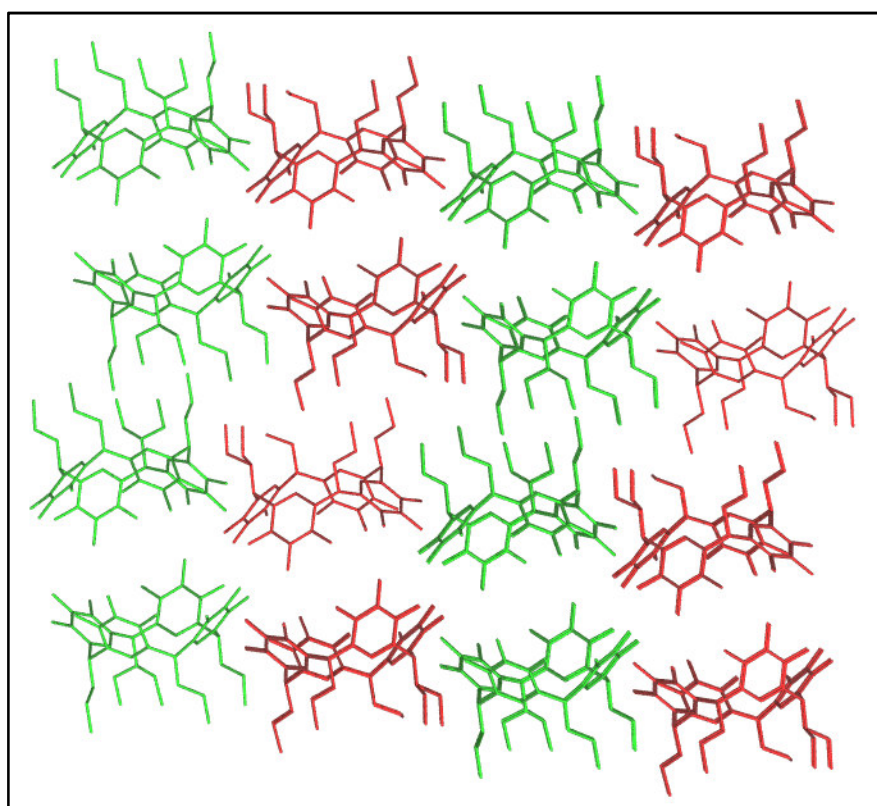
Figure 43 - Bilayer arrangement of *C*-propyl-calix[4]pyrogallolarene diethyl ether water clathrate (solvent molecules and hydrogen atoms removed for clarity)

Each crystallographically unique calixarene is tilted at an angle of 20.7° to each of other. Due to the tilting of each sheet of calixarenes, direct calixarene – calixarene inter layer hydrogen bonding is possible. H(25) ⋯ O(17) = 1.97 Å (O(25) ⋯ O(17) = 2.78(15) Å), H(15) ⋯ O(9) = 2.18 Å (O(15) ⋯ O(9) = 2.96(7) Å), H(14) ⋯ O(8) = 1.94 Å (O(14) ⋯ O(8) = 2.77(10) Å), H(10) ⋯ O(17) = 2.10 Å (O(10) ⋯ O(17) = 2.91(8) Å), H(25) ⋯ O(17) = 1.97 Å (O(11) ⋯ O(17) = 2.80(10) Å).

In addition to the bilayer packing, there is an additional symmetry in the packing of the calixarene, which is expressed by $P2_1/c$ symmetry. This can be seen in the formation of two sheet-like planes composed of one crystallographically unique calixarene molecule per sheet. These sheets are arranged perpendicular to the plane of the bilayer and extend in two dimensions throughout the structure. This can also be seen in Figure 43 above. There are intra-layer, inter-sheet hydrogen bonds formed between the upper rims of the calixarenes: $H(22) \cdots O(7) = 2.03$ Å $(O(22) \cdots O(7) = 2.73(6)$ Å$)$, $H(3) \cdots O(18) = 2.02$ Å $(O(3) \cdots O(18) = 2.70(6)$ Å$)$. The ether molecules which reside within the cavity forms an inter layer, intra-sheet hydrogen bond: $O(25) \cdots H(13) = 1.88$ Å $(O(25) \cdots O(13) = 2.67(15)$ Å$)$ and $O(26) \cdots H(12) = 1.86$ Å $(O(26) \cdots O(12) = 2.64(23)$ Å$)$. The shape and positioning of the diethyl ether molecules determines the architecture which is formed. Both ether molecule reside centrally within the respective cavities which gives the opportunity to form hydrogen bonds to the ethereal oxygen atoms by the next layer. This causes an offsetting of the packing of the calixarene molecules from central alignment as seen in earlier examples.

Both unique calixarenes within the structure have one of their pendant chains disordered over two positions from the α position to the macrocycle (disordered positions C(39), C(40) and C(49), C(50)). One of the calixarenes has one of its pendant chains projecting perpendicularly to the cavity (so that it is parallel to the plane of the bilayer). This is the first example of this projection of the pendant chains in the homologous series of C-alkyl-calix[4]pyrogallolarenes. The projection is intra sheet and therefore the projection of the pendant chain runs parallel to the plane of the bilayer in one plane but within the sheet. The calixarenes are tilted with respect to the plane of the bilayer and therefore in order to fill the space which is created between the calixarenes the projection fills any void which would otherwise form due to the tilted arrangement.

The molecular structure of the acetonitrile clathrate $(4(C_{40}H_{48}O_{12}) \cdot 6(CH_3CN) \cdot 3(H_2O))$ revealed a large unit cell (volume 4034 Å^3) with an unusually large number of molecules within the unit cell (4 calixarenes, 6 acetonitrile and 3 water molecules). The crystal is packed according to $P\bar{1}$ symmetry; no higher symmetry could be determined using PLATON's ADDSYM programme. The calixarene molecules once packed form a bilayer motif in a similar manner to that formed by the ethyl acetate, with each calixarene holding a single acetonitrile molecule within its cavity
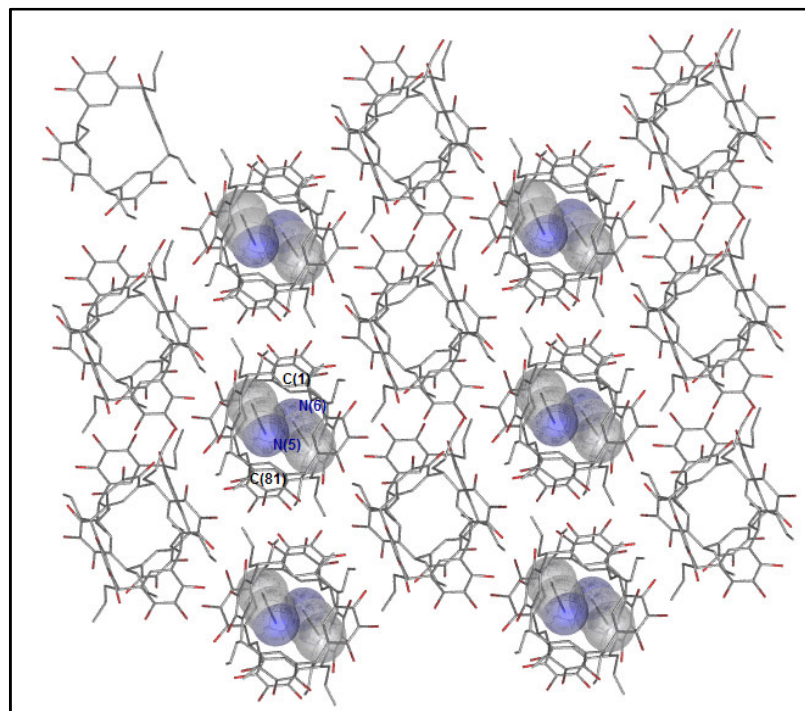
Figure 44 - Packing in *C*-propyl-calix[4]pyrogallolarene acetonitrile water clathrate

In a significant departure from the ethyl acetate derivative and the acetonitrile clathrates reported in shorter alkyl chain derivatives, the two crystallographically unique acetonitrile which are not bound by the cavity of the calixarenes are entrapped between the pendant chains of two calixarenes. The position of the solvent inclusion alternates over the *a* axis (1,0,0), This packing motif extends perpendicularly to the plane of the bilayer, therefore forming sheets of solvent including and excluding calixarenes which is reminiscent of C3Pg diethyl ether clathrate. This packing architecture can be seen in Figure 44 above and the individual detail of a solvent molecule including and excluding dimer can be seen below in Figures 45 and 46 respectively.

Unlike the C2Pg MeCN clathrate, the *exo* acetonitrile molecules are not aligned along the plane of the phenyl rings of the pyrogallolarene. Therefore the distance between the annulus and the nitrogen of the acetonitrile (N(6) – H(1A) = 2.93 Å (N(6) – C(1) = 3.872(6) Å and N) is greater than previously seen. The anti-parallel arrangement of the acetonitrile molecules is similar to that shown by C5Pg MeCN clathrate.
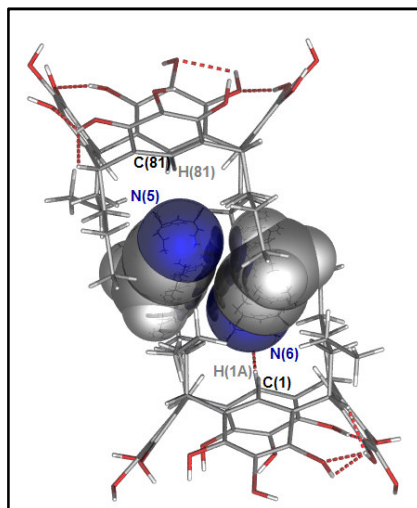
Figure 45 - Detail of structural repeating unit in solvent including sheet of *C*-propyl-

calix[4]pyrogallolarene

Unusually the water molecule which is present within the lattice resides close to the lower rim of the pendant chain and does not form a hydrogen bond to the upper rim of the any calixarenes. The calixarenes in the non-solvent including show strong interdigitation of the pendant chains in order to prevent void formation.
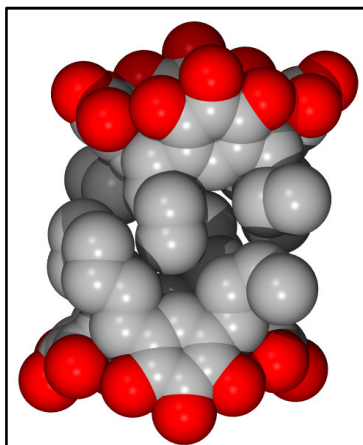
Figure 46 - Detail of non- solvent including sheet motif of *C*-propyl-calix[4]pyrogallolarene

acetonitrile clathrate (hydrogen atoms removed for clarity)

2.5 *C*-Butyl-calix[4]pyrogallolarene

C-Butyl-calix[4]pyrogallolarene solvates were grown from ether and acetonitrile. Both structures show dramatically different packing architectures whose origin can be attributed to the structure of the guest molecule which is present within the crystal lattice.

The diethyl ether clathrate ($C_{44}H_{56}O_{12}\cdot(CH_3CH_2OCH_2CH_3)\cdot3(H_2O)$) contains five molecules in its asymmetric unit (three water, one diethyl ether and one calixarene molecule) which fills its unit cell with $P2_1/c$ symmetry.
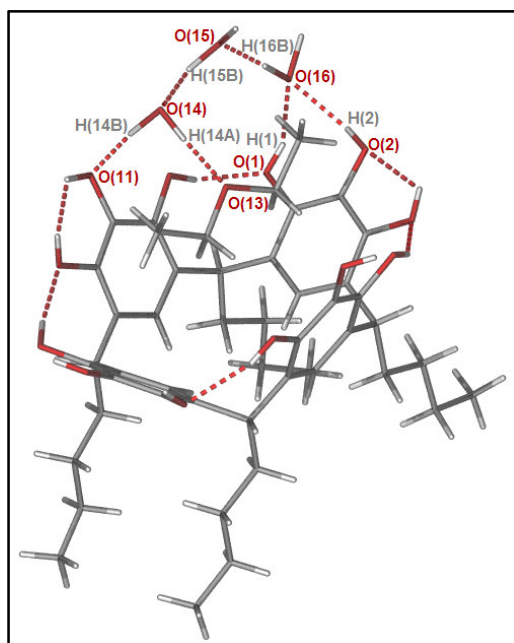
Figure 47 - Asymmetric unit of *C*-butyl-calix[4]pyrogallolarene diethyl ether water clathrate

As with previously reported examples of the diethyl ether clathrates of *C*-alkyl-calix[4]pyrogallolarenes, a bilayer architecture results. What separates this structure from the C1Pg and C3Pg clathrates is the interdigitation of the pendant chains, within the lipophilic region of the bilayer. Like the previously reported examples there is close proximity of the upper rims in opposite faces of the bilayers because there is a hydrogen bond between the solvent molecule and the upper rim of the facing calixarene. Therefore the bilayer does not form a contiguous solvent filled void across the lattice. Three water molecules are entrapped between the layers and form a hydrogen bonded network which links the polar upper rims of two facing bilayers.

O(13) ⋯ H(7) = 2.01 Å (O(13) ⋯ O(7) = 2.79(6) Å), O(14) ⋯ H(10) = 1.97 Å (O(14) ⋯ O(10) = 2.77(7) Å), O(14) ⋯ H(15B) = 1.75 Å (O(14) ⋯ O(15) = 2.76(8) Å), H(14B) ⋯ O(11) = 1.64 Å (O(14) ⋯ O(11) = 2.76(7) Å), H(14A) ⋯ O(13) = 1.82 Å (O(14) ⋯ O(13) = 2.82(7) Å), O(15) ⋯ H(5) = 1.84 Å (O(15) ⋯ O(5) = 2.65(7) Å), O(15) ⋯ H(16B) = 1.51 Å (O(15) ⋯ O(16) = 2.65(8) Å), H(15A) ⋯ O(6) = 1.95 Å (O(15) ⋯ O(6) = 2.80(6) Å), O(16) ⋯ H(2) = 2.10 Å (O(16) ⋯ O(2) = 2.72(7) Å), O(16) ⋯ H(1) = 1.91 Å (O(16) ⋯ O(1) = 2.62(7) Å), H(16A) ⋯ O(9) = 1.59 Å (O(16) ⋯ O(9) = 2.73(7) Å)

When crystallised from acetonitrile $C_{44}H_{56}O_{12} \cdot 5(CH_3CN)(H_2O)$, molecules within the crystal were found to pack into a hexameric nano-sphere formation. When the volume was calculated using MCAVITY the six *C*-butyl-calix[4]pyrogallolarene molecules enclose 1274 Å^3 of space.

The asymmetric unit consists of four acetonitrile molecules, one water and one calixarene molecule, as shown in Figure 48 below. Two of the acetonitrile and one water molecule reside *exo* to the capsule while the remaining two unique acetonitrile molecules are encapsulated within the nano-sphere.
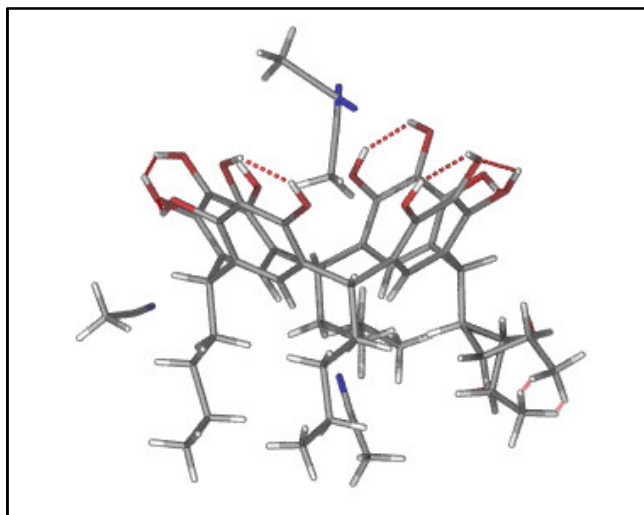
Figure 48 - Asymmetric unit of *C*-butyl-calix[4]pyrogallolarene acetonitrile water clathrate

The identity and position of twelve acetonitrile guest molecules encapsulated within the sphere can be conclusively determined. Location of the guest molecules within calixarene spheres is highly unusual; previously reported spheres have been formed from relatively non polar solvents (chloroform and ethyl acetate), which do not form strong interactions with the walls or seam of the capsule. The movement of these solvent molecules which do not interact with the walls of a sphere is unrestricted, therefore the guests may act as a liquid within the sphere and diffraction of X-rays is not possible. In the acetonitrile clathrate there has been sufficient ordering of the solvent molecules within the capsule to allow their determination (the specific interactions will be discussed later). There is however remaining unassigned electron density within the capsule, from which the structure of a guest molecule could not conclusively be determined and was therefore modelled as diffuse electron density. There is sufficient space within the capsule to accommodate a further six acetonitrile molecules (one extra MeCN per ASU[1]). This would be acceptable under the $55 \pm 9\%$ rule proposed by Mecozzi *et al.* as 62% of the available volume would be occupied by the eighteen acetonitrile molecules, rather than 41% with twelve acetonitrile molecules encapsulated.[101]

There are four crystallographically unique faces which the sphere forms are highlighted with different colours in Figure 49 below. Each face demonstrates a different set of Inter- and intra-molecular interactions and architectures. The nano-sphere is formed by $R\bar{3}$ symmetry operation on the crystallographically unique calixarene molecule, therefore any perturbation of the walls of the sphere must originate from the individual macrocycle. This highlights the importance of understanding how the inclusion of guest molecules affects the structure of the macrocycle.

---

[1] (The average volume of an acetonitrile molecule is calculated (using XSEED) to be 43.85 $Å^3$)
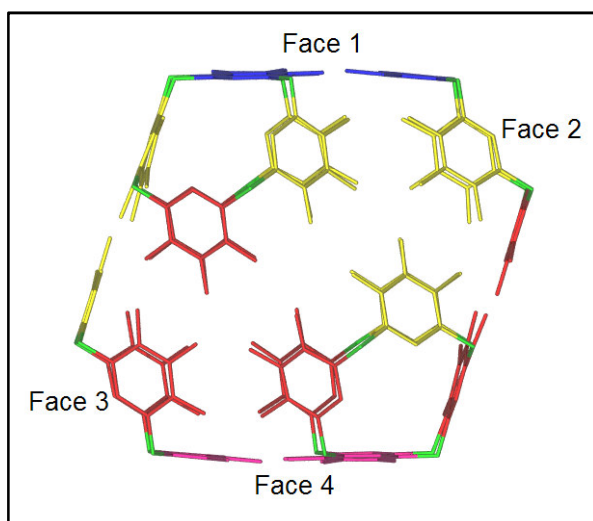
Figure 49 - Image showing unique faces of the nano-sphere formed by *C*-butyl-calix[4]pyrogallolarene acetonitrile clathrate (pendant chains, hydrogen atoms and solvent molecules removed for clarity)

Face 1 (shown in blue) and Face 4 (shown in pink) are enantiomers, as are Faces 2 and 3. The capsules are stacked along the *c* axis (0,0,1) with Face 4 being stacked against Face 1, the separation of the faces is 6.224 Å. Within a capsule Face 4 has its phenyl rings rotated through 60° relative to Face 1; therefore because the capsule is not rotated when stacked, the phenyl rings of Faces 1 and 4 are not directly aligned directly above each other.
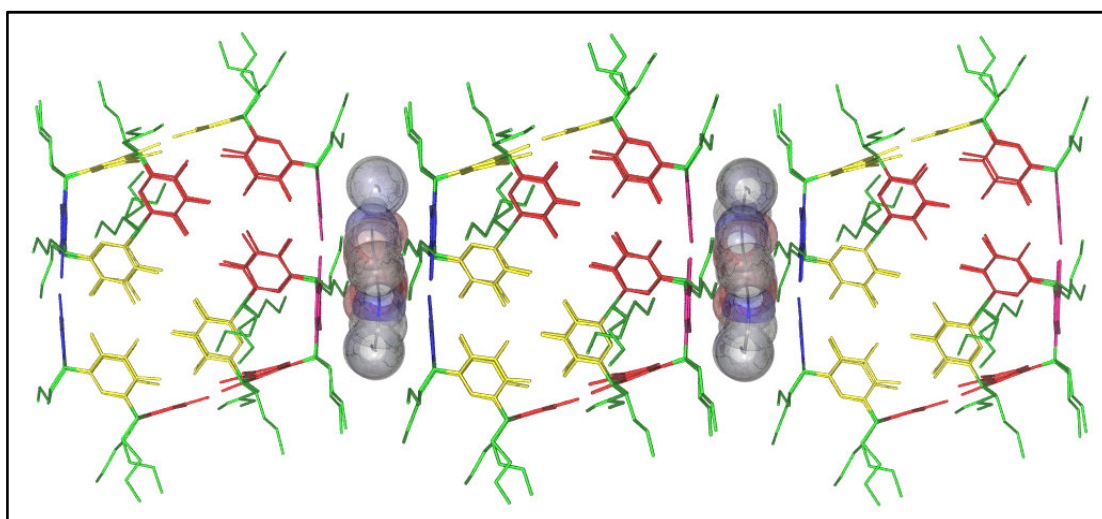
Figure 50 - Stack of nano-capsules *C*-butyl-calix[4]pyrogallolarene acetonitrile clathrate (*endo* solvent molecules removed for clarity)

The faces are separated by a channel of solvent molecules which are entrapped between Faces 1 and 4 and enclosed on all sides by the pendant chains of adjacent stacks of nano-spheres. The six acetonitrile molecules and six water molecules which reside within the channel are arranged into a torus shape with the acetonitrile molecules forming the exterior of the torus by a head-to-tail interaction and the six water molecules residing within the centre of the ring formed by the acetonitrile molecules. This is shown in Figure 51 below.
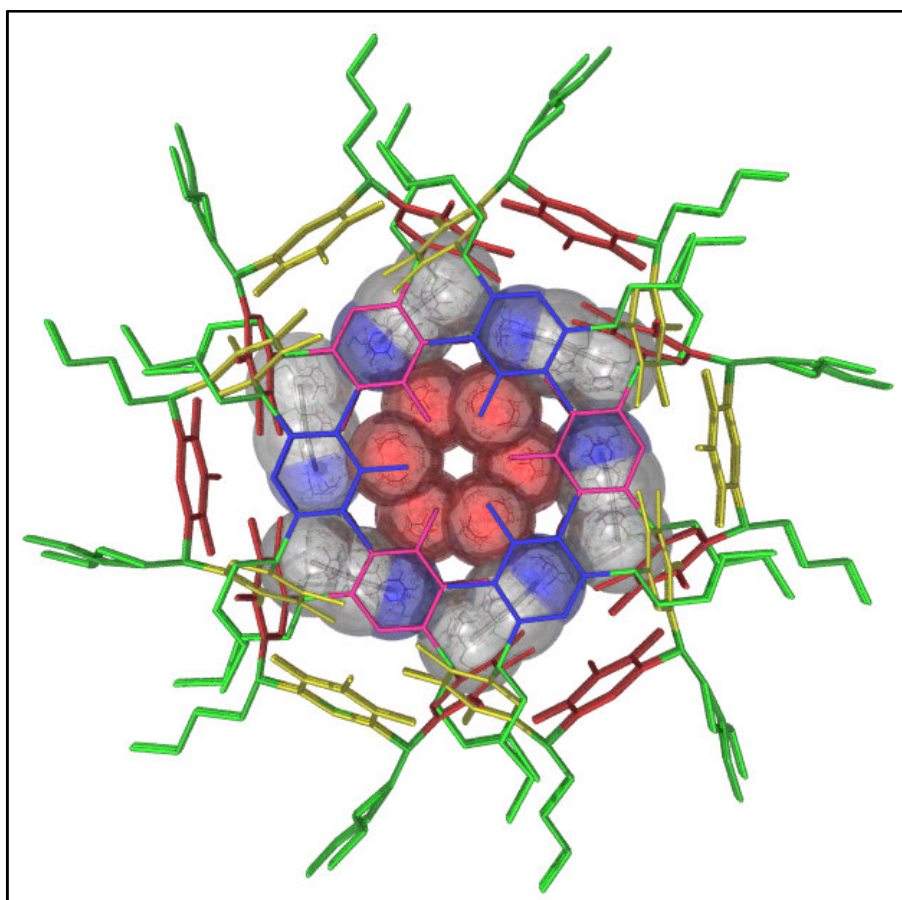
Figure 51 - Plan view of stack of nano-capsules showing *exo* solvent molecules in space-filling representation (hydrogen atoms removed for clarity)

The pendant chains of adjacent stacks of nano-spheres interpenetrates the gap between Faces 1 and 4 this allows the stacks of nano-capsules are offset along the *c* axis, therefore the nano-spheres form a hexagonal close packing arrangement.

2.6   *C*-Pentyl-calix[4]pyrogallolarene

C-Pentyl-calix[4]pyrogallolarene was synthesised by the solvent and solvent free methods in the cone conformation. A molecular structure was obtained by growing crystals from a solution of acetonitrile.

The first structure to be solved was that of *C*-pentyl-calix[4]pyrogallolarene acetonitrile water clathrate $C_{48}H_{64}O_{12} \cdot (CH_3CN)(H_2O)$. This structure has three molecules in its asymmetric unit (1 calixarene, 1 water molecule and one acetonitrile. On packing the unit cell a capsular arrangement arises from the $P2_1/c$ symmetry operations applied to the asymmetric unit. Two acetonitrile molecules are completely encapsulated by the head-to-head arrangement of the calixarene molecules. Two water molecules (both symmetrically identical) fringe the capsule. The distance between upper rims (2.26 Å) (planes generated from average O2, O5, O8, O11) combined with the offset of the capsules from perfect alignment (by 1.71 Å when viewed along crystallographic axis *b* and 1.54 Å when viewed along crystallographic axis *c* (0,0,1)) mean that direct calixarene – calixarene hydrogen bonding between layers is impossible.
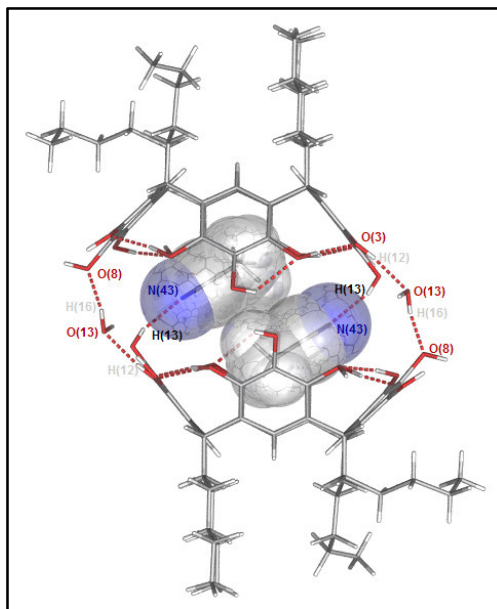
Figure 52 – *C*-Pentyl-calix[4]pyrogallolarene acetonitrile water clathrate

The acetonitrile guest is held in place by a hydrogen bond from the central hydroxyl group of a phenyl ring (H(13) $\cdots$ N(43) = 2.04 Å and N(43) $\cdots$ O(2) = 2.76 Å). The water molecule which is included in the crystal lattice forms four hydrogen bonds linking the calixarene capsule to three other capsules *via* bonds within layers and between layers. H(16) $\cdots$ O(8) = 1.88 Å (O(13) $\cdots$ O(8) = 2.73(6) Å), H(2) $\cdots$ O(12) = 1.91 Å (O(13) $\cdots$ O(12) = 2.77(6) Å), H(9) $\cdots$ O(13) = 1.84 Å (O(7) $\cdots$ O(13) = 2.75(6) Å), O(13) $\cdots$ H(12) = 1.88 Å (O(3) $\cdots$ O(13) = 2.63(6) Å). Dimeric capsules have been reported in the literature but with shorter chain lengths and the guests were simple alkylammonium salts.[110] On calculating the molecular volume of each acetonitrile guest species in X-SEED (44 Å^3) and comparing it to the volume of the cavity as calculated by MCAVITY (Test sphere radius = 1.56 Å, Resolution = 0.5 Å, limiting sphere radius = 0.5 Å) (155 Å^3), 56% of the available volume of the cavity is occupied by the two acetonitrile guests. This is a favourable when compared to the optimal 55% occupancy of synthetic receptors proposed by Mecozzi *et al*.[101]
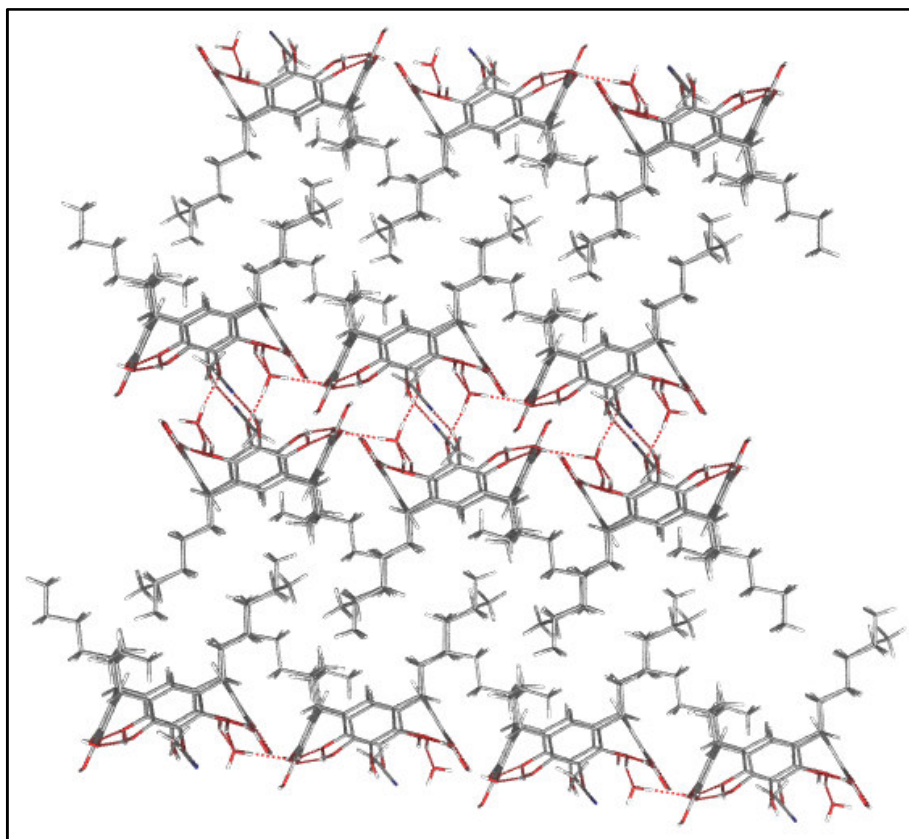
Figure 53 - Interdigitation of pendant chains in *C*-pentyl-calix[4]pyrogallolarene acetonitrile water clathrate

2.7 *C*-Hexyl-calix[4]pyrogallolarene

C-Hexyl-calix[4]pyrogallolarene hydrochloride acetonitrile clathrate ($C_{52}H_{72}O_{12} \cdot (CH_3CN)(H_3OCl)$) was synthesised by dissolving the crude material isolated from the calixarene synthesis reaction in acetonitrile. The solution was allowed to slowly evaporate and after 1 week crystals suitable for SCXRD studies were formed. On solution of the data, a structure is revealed which contains three species in its ASU; a calixarene, one chloride ion (the source is the hydrochloric acid used in the synthesis), one acetonitrile and one water molecule.

In a manner similar to enzymes, the cavity of the calixarene modifies its shape to accommodate its acetonitrile guest. The guest is tilted and the inter phenyl centroid distance is shortest along the longest edge of the acetonitrile molecule (centroid C(40)-C(45) to centroid C(14)-C(19) is shorter than the other inter phenyl distance.). This causes distortion of the macrocycle and the D*f* for this species is 0.87.
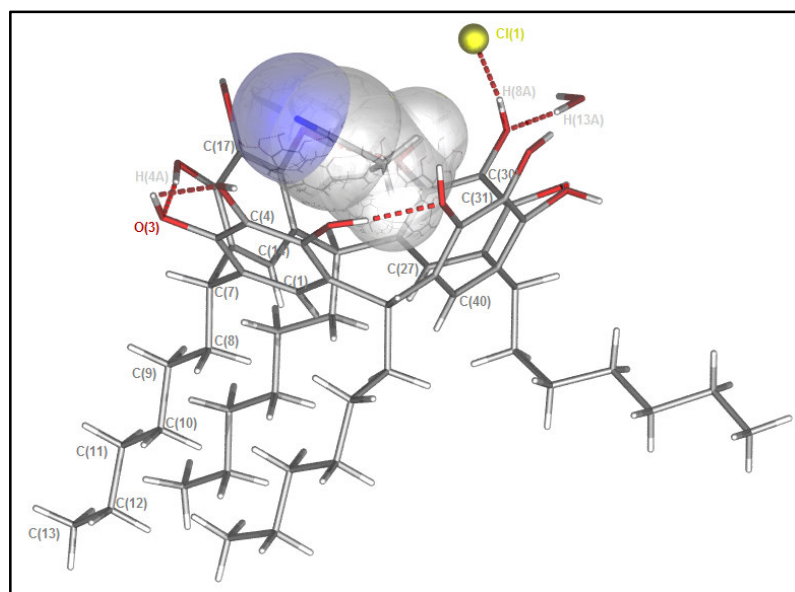
Figure 54 - *C*-Hexyl-calix[4]pyrogallolarene hydrochloride acetonitrile clathrate

The $P\bar{1}$ symmetry generates a head-to-head packing motif with the pendant chains formed into two groups, the first containing three chains and the second only one. This grouping of the pendant chains allows their interdigitation. The closest approach to the calixarene below is by H(26D) whose closest contact is 2.620 Å but the average separation from the hydrogen atoms of the annulus is 3.18 Å.

The lipophilic layer created by the pendant chains allows a separation of cavities of 8.58 Å (inter plane distance where the plane is calculated from the mean positions of H(1), H(14), H(27) and H(40)). The average through space distance from methine carbon to the terminal hydrogen atom e.g. C(7) – H(13C) is 7.94 Å and the average along bond distance is 10.09 Å. This is accounted for by twisting of the chain but if either of these figures is added to the mean separation between the terminal hydrogen and the annulus this gives a distance which is larger than that seen between layers. This means that the layers are tilted at 42° from the plane which is calculated from the average positions of C(1), C(4), C(27) and C(30) (shown by the red lines in Figure 55).
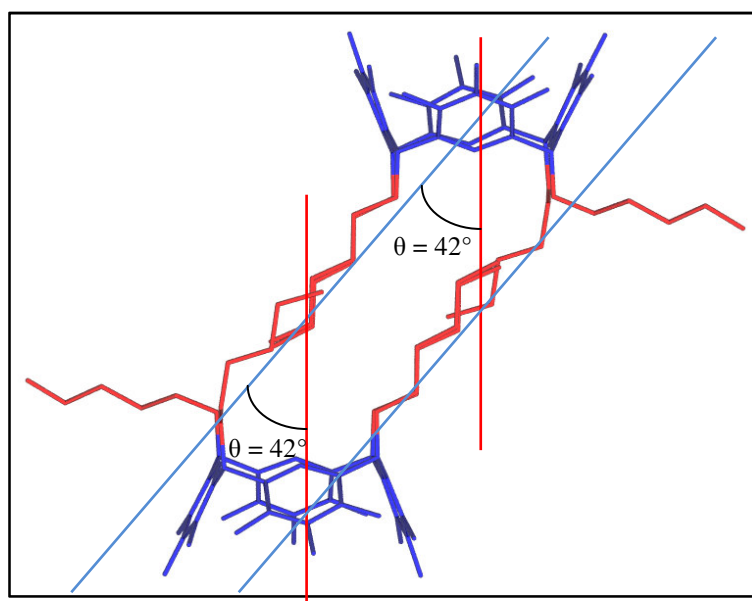
Figure 55 - Tilting of pendant chains in *C*-hexyl-calix[4]pyrogallolarene hydrochloride acetonitrile clathrate (solvent molecules and hydrogen atoms removed for clarity)

The strong inter-phenyl hydrogen bonding observed around the upper rim of each calixarene in this structure demonstrates why the cone isomer is thermodynamically favoured (H(1A) ⋯ O12 = 1.87 Å (O(1) ⋯ O(12) = 2.82(5) Å), H(4A) ⋯ O(3) = 1.87 Å (O(4) ⋯ O(3) = 2.71(5) Å), H(6A) ⋯ O(7) = 1.89 Å (O(6) ⋯ O(7) = 2.72(5) Å), H(9A) ⋯ O(10) = 1.82 Å (O(9) ⋯ O(10) = 2.66(5) Å)). The central hydroxyl in each pyrogallol group forms intra-molecular hydrogen bonds, H(8A) forms a hydrogen bond to the chloride in the lattice (H(8A) ⋯ Cl(1) = 2.19(7) Å) and the oxygen bearing this hydroxyl group is hydrogen bonded to the water in the lattice (O(8) ⋯ H(13A) = 1.77 Å (O(8) ⋯ O(13) = 2.88(7) Å)).
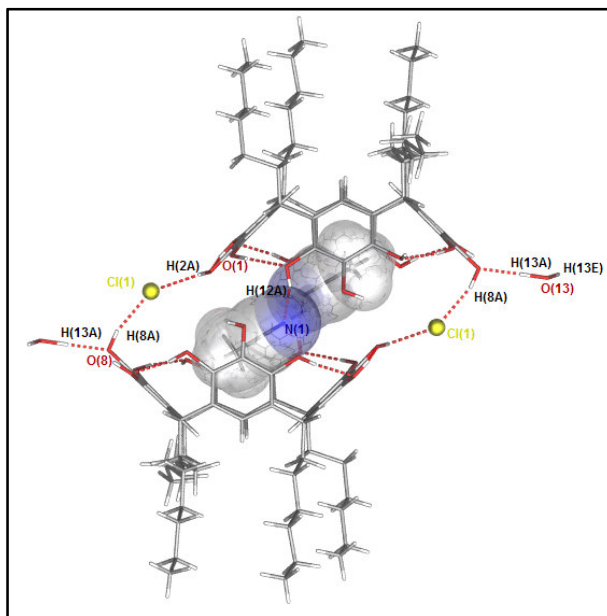
Figure 56 - *C*-Hexyl-calix[4]pyrogallolarene hydrochloride acetonitrile clathrate

There is an unusual arrangement of hydrogen bonding in the crystal structure; Firstly no inter-layer calixarene hydrogen bonds are observed, the bilayer is held together by hydrophobic interactions of the pendant chains and the bridge which is formed by the chloride ion. Secondly only a single hydrogen bond holds the acetonitrile within the cavity (H(12A) – N(1) = 1.92 Å) this causes the guest molecule to become 'twisted' within the cavity (i.e. directed towards H(3A) rather than H(2A)). This twisting of the guest molecule can be attributed to the presence of the chloride ion which bridges two calixarene molecules. Hydrogen bonds are formed between H(2A) and the Cl(1) and H(8A) and Cl(1) (H(2A) ⋯ Cl(1) = 2.33 Å (O(2) ⋯ Cl(1) = 3.06(6) Å)) rather than directed inwards towards N(1) (compare with *C*-pentane-calix[4]pyrogallolarene acetonitrile clathrate). The water molecule only bridges intra-layer calixarene molecules forming hydrogen bond from H(13E) to O(1) = 2.08 Å in addition to the H(13A) ⋯ O(8) bond described earlier.

This structure is very similar to the molecular structure of *C*-pentyl-calix[4]pyrogallolarene acetonitrile water clathrate reported earlier, but differs significantly because while it forms a highly overlapped head-to-head arrangement, the two acetonitrile guest molecules are not completely isolated from the exterior medium. This is due to the offset of the two calixarenes, which is a result of the coordination to the upper rims of the chloride ion.

2.8   *C*-Heptyl-calix[4]pyrogallolarene

Crystals of *C*-heptyl-calix[4]pyrogallolarene were grown from acetonitrile, diethyl ether, ethyl acetate and ethanol. In line with previous findings, different molecular architectures were formed according to which guests were present within the crystal lattice.

C-Heptyl-calix[4]pyrogallolarene ethyl acetate clathrate $C_{56}H_{80}O_{12} \cdot 2(CH_3CH_2OC(O)CH_3)$ is arranged by $R\bar{3}$ symmetry into a capsular architecture. The sphere which is formed shows both similarities and differences to the *C*-butyl-calix[4]pyrogallolarene acetonitrile clathrate sphere previously presented (See Chapter 1, Section 2.5).
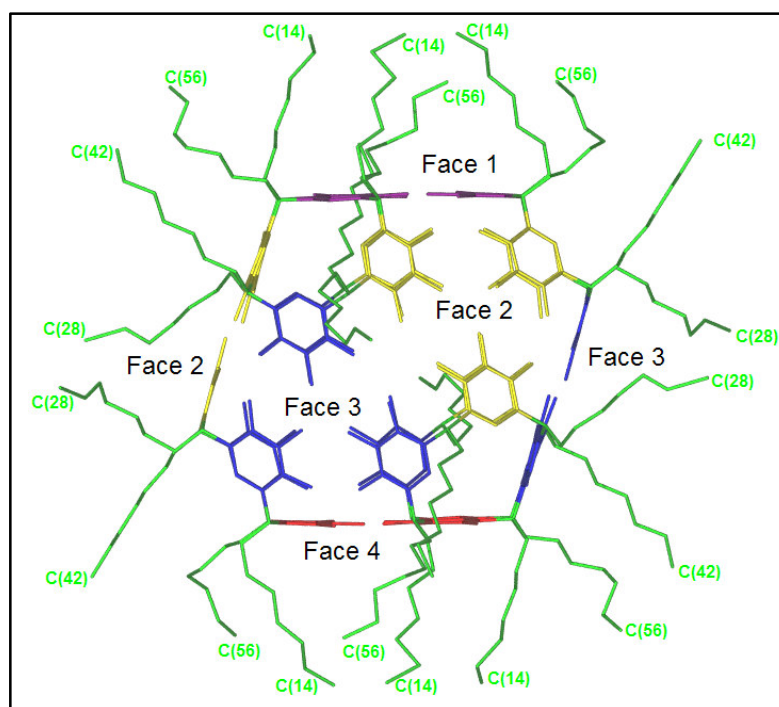
Figure 57 - Nano-capsule formed by *C*-heptyl-calix[4]pyrogallolarene ethyl acetate clathrate

The volume of the ethyl acetate sphere (calculated by MCAVITY) is smaller (~1249.5 Å^3) than that of the acetonitrile sphere which has two of its faces (1 & 4) bulging outwards (~1274 Å^3). This change in the distortion of the sphere parallels the change in the shape of the monomeric macrocycle when different guests are present within the cavity.

There is extensive disorder of guests within the capsule, due to their lack of permanent interactions with the capsule interior surface or its seam. Therefore the molecules within the capsule had to be modelled as diffuse electron density. Taking into consideration Mecozzi's 55±9% packing rule and the molecular volume of the *exo* ethyl acetate molecule calculated using XSEED (87.4 Å^3), there is potential for between seven and nine ethyl acetate molecules to be encapsulated within the sphere. Cave *et al.* performed a TGA-gas phase IR study on ethyl acetate containing nano-capsules which revealed that six ethyl acetate and one water molecule can reside within a calix[4]pyrogallolarene derived nano-sphere.[67]

In a major difference between the capsules, the ethyl acetate capsule has its pendant chains radiating out around the full sphere in three dimensions, whereas the acetonitrile sphere has its pendant chains directed only in two directions (perpendicularly to the stack of nano-capsules). This difference in packing architecture is due to the larger molecular volume of the *exo* guest molecule which coordinates to the lower rim *via* its carbonyl oxygen (O(14) ⋯ H(15A) = 3.05 Å (O(14 ⋯ C(15) = 3.98(19) Å) and O(14) ⋯ H(43A) = 3.10 Å (O(14) ⋯ C(43) = 4.05(18) Å)).
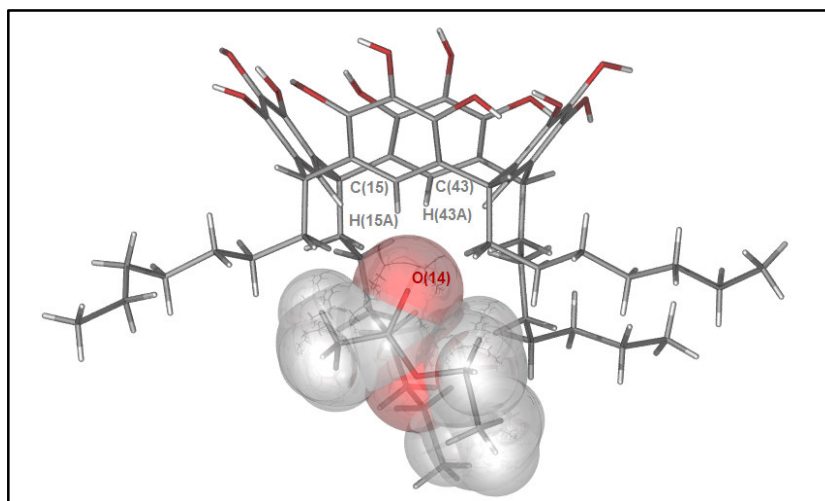
Figure 58 - Asymmetric unit of *C*-heptyl-calix[4]pyrogallolarene ethyl acetate clathrate

The sphere has four crystallographically unique faces consisting of two pairs of enantiomers (Face 1 is a mirror image of 4 and likewise for Faces 2 and 3) therefore rendering the sphere racemic (like the acetonitrile sphere). This can easily be determined by viewing each face along the plane of its phenyl rings and noting the arrangement of the pendant chains (as seen in Figure 57). Face 1 and 4 are each

comprised of three identical phenyl rings (C(1)-C(6)) whereas each of the other two faces (2 & 3) are comprised of a three non-identical phenyl rings.

The positioning (and increased length) of the pendant chains causes a difference in the packing arrangement of the nano-spheres. Unlike the acetonitrile sphere which forms stacks of nano spheres with Faces 1 & 4 arranged parallel to each other, interdigitation of the pendant chains dominates the packing and prevents nano spheres coming into close contact, and a hexagonal close packed arrangement of the spheres results.

Although the diethyl ether clathrate $(C_{56}H_{80}O_{12}\cdot2(CH_3CH_2OCH_2CH_3))$ of *C*-heptyl-calix[4]pyrogallolarene forms a bilayer in a similar manner to previously described examples, the structure shows a significant departure from the previously described ether clathrates. This difference is due to a combination of the increased length of the pendant chains and the positioning of a diethyl ether molecule *exo* to the cavity of the calixarene.
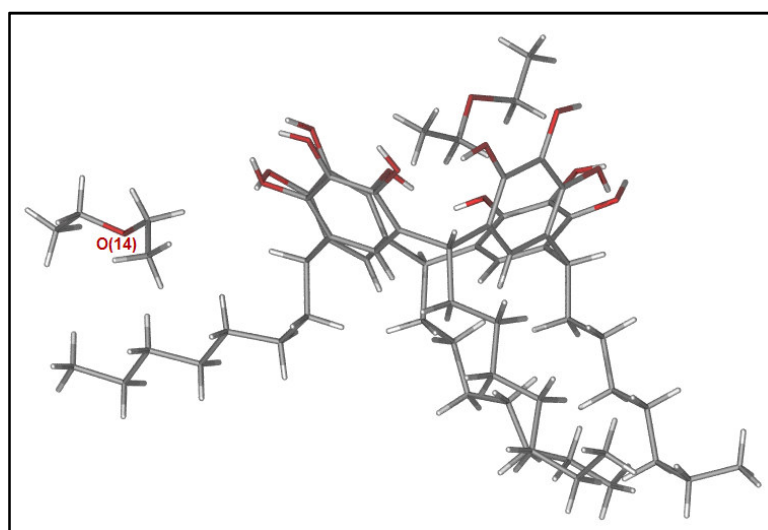
Figure 59 - Asymmetric unit of *C*-heptyl-calix[4]pyrogallolarene diethyl ether water clathrate

There is a three to one split in the alignment of the pendant chains of the calixarene. This allows interpenetration of the pendant chains by the lower layer. There is a close approach of the pendant chain of the acetonitrile methyl group of one calixarene to the annulus of the calixarene on the opposite face of a bilayer. Interestingly it is not the methyl group of the pendant chain which makes

the closest approach to the annulus, it is the penultimate methylene (CH$_2$) group which comes into closest contact with the lower rim. (H(9A) ··· H(23) = 2.90 Å (C(9) ··· C(23) = 4.77(8) Å))

The *exo* solvent molecule causes a disruption of the bilayer packing arrangement with an alternate solvent filled channel which is highlighted in the figure below. The alignment of the *endo* cavity solvent molecules (shown in blue in Figure 60 above) shows that there is a 90° rotation between the faces of each subsequent bilayer, is allowed to come into close contact with the subsequent bilayer because the *endo* solvent molecule's ethyl group which resides above the plane of the upper rim, penetrates the solvent filled channel. The solvent filled channel has a defined base which is formed by the extension of one of the pendant chains of the calixarene molecule
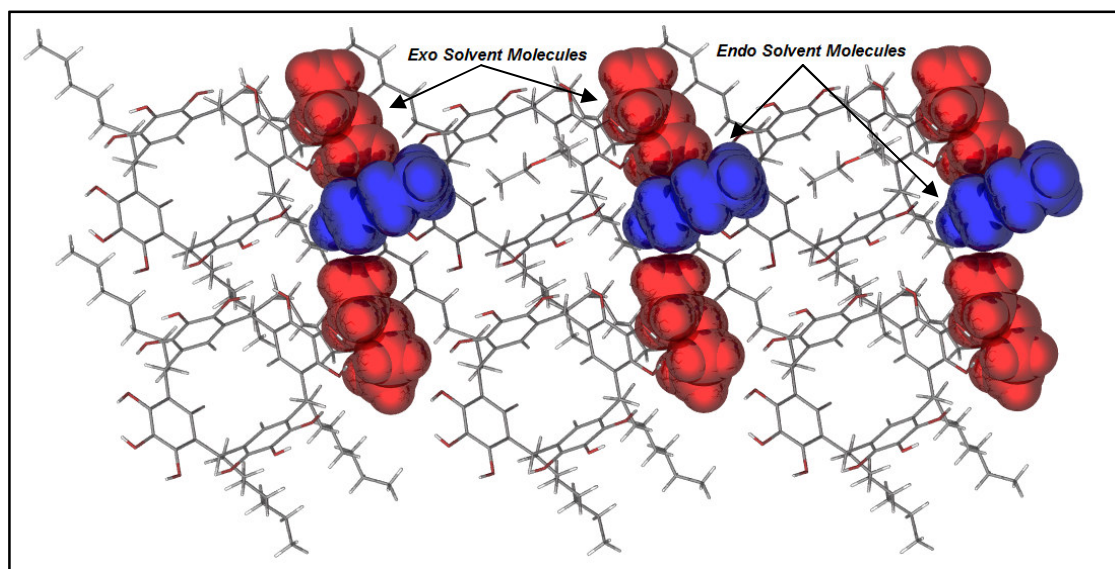
Figure 60 – Packing diagram highlighting the solvent filled channel in *C*-heptyl-

calix[4]pyrogallolarene diethyl ether water clathrate

This crystal structure shows an excellent mimic of the postulated disruption seen in biological membranes when polar anaesthetic molecules interact with the bilayer. This causes a contraction of the bilayer to less than twice the molecular length of the individual molecules. In the calixarene system, interdigitation is present in the majority of the bilayer architectures, however it is usually the terminal methyl group which makes the closest approach to the lower rim of the calixarene on the opposite face of the bilayer.

The separation between the upper rim of the bilayers from planes generated (using Mercury) from oxygen atoms (3), (5), (9) and (13) = 16.88 Å. The molecular length of an individual calixarene molecule from the upper rim oxygen atoms to the terminal carbon atoms of the trimer of pendant chains (C(11), C(41), C(46), C(55) = 9.25 Å). This shows a significant contraction of the thickness of the bilayer. It has been postulated in the biological model that the contraction has allows an increased number of van der Waals interactions between the pendant chains to form. This compensates for the decrease in the number of hydrogen bonds which are formed between the upper rims of the calixarene molecules.

The ethanol clathrate ($2(C_{56}H_{80}O_{12})\cdot5(CH_3CH_2OH)3(H_2O)$) has ten molecules in its asymmetric unit. In a similar fashion to the diethyl ether clathrate, there is a single solvent molecule included within the bilayer, disrupting the packing of the calixarene molecules into a face of the bilayer. Contraction of the bilayer is observed but not to the same extent as the diethyl ether clathrate as the distance between upper rims is 17.654 Å. One of the asymmetric calixarene molecules has two of its pendant chains directed parallel to the plane of the bilayer. In a similar manner to the ether clathrate, the pendant chains form the base to the solvent filled pocket in the face of the bilayer.

The *exo* solvent molecules (one ethanol and one water molecule) of one layer coordinates to the *endo* molecule of the next face of the structure, this means that the solvent filled pocket contains three solvent molecules. This is shown in the figure below which shows the calixarene which forms the base of the void in blue and the unperturbed calixarene in red.
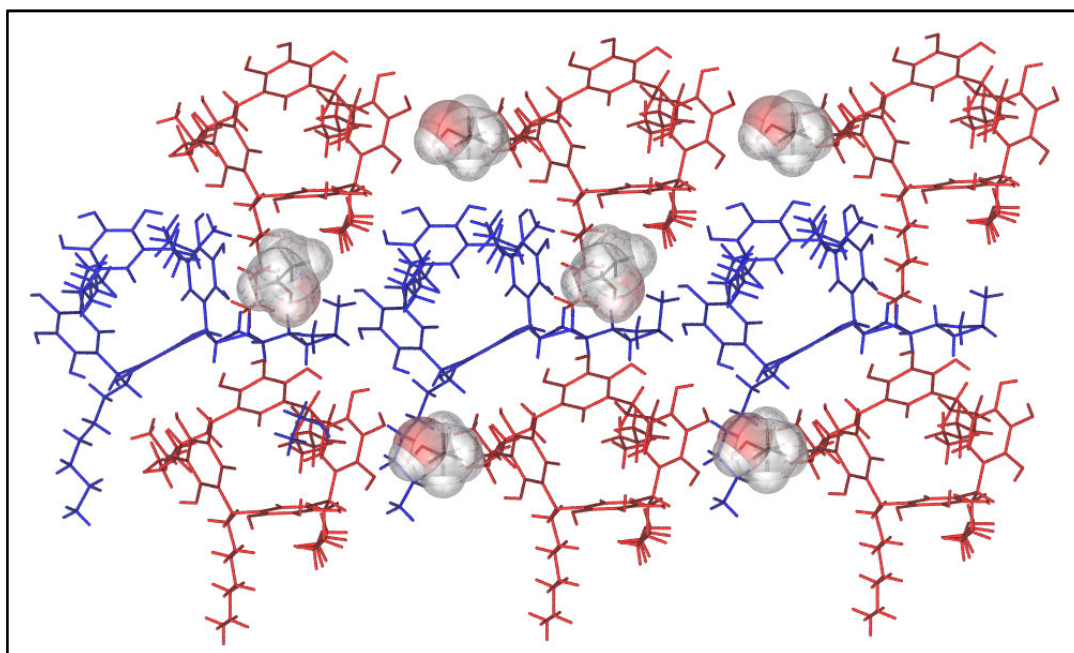
Figure 61 - Plan view of bilayer face showing *exo* solvent molecules creating voids within the bilayer structure

The material obtained directly from the 'boil' reaction was recrystallised from acetonitrile, the crystals which grew were suitable for single crystal X-ray diffraction studies ($C_{56}H_{80}O_{12} \cdot CH_3CN \cdot H_2O$). While the interdigitated bilayer which is formed is similar to the bilayers of the ethanol and diethyl ether clathrates there is a significant difference because there are only *endo* solvent molecules present within the crystal lattice. This means that the calixarenes are formed into a hexagonal arrangement within the faces of the bilayer.

As with the previous structures of the C7Pg discussed, there is a 3:1 split of the pendant chains with one of the pendant chains being directed parallel to the plane of the bilayer. This can be justified for two reasons; firstly, the pendant chain fills a void which forms due to the upper rim of the calixarene being wider than that of the lower rim (diameter of the upper rim C(8) – C(46) = 9.24(14) Å diameter of lower rim C(31) – C(26) = 5.23(11) Å) This is illustrated in the figure below which shows the chain filling the void in red and the two calixarenes which surround the chain in blue.
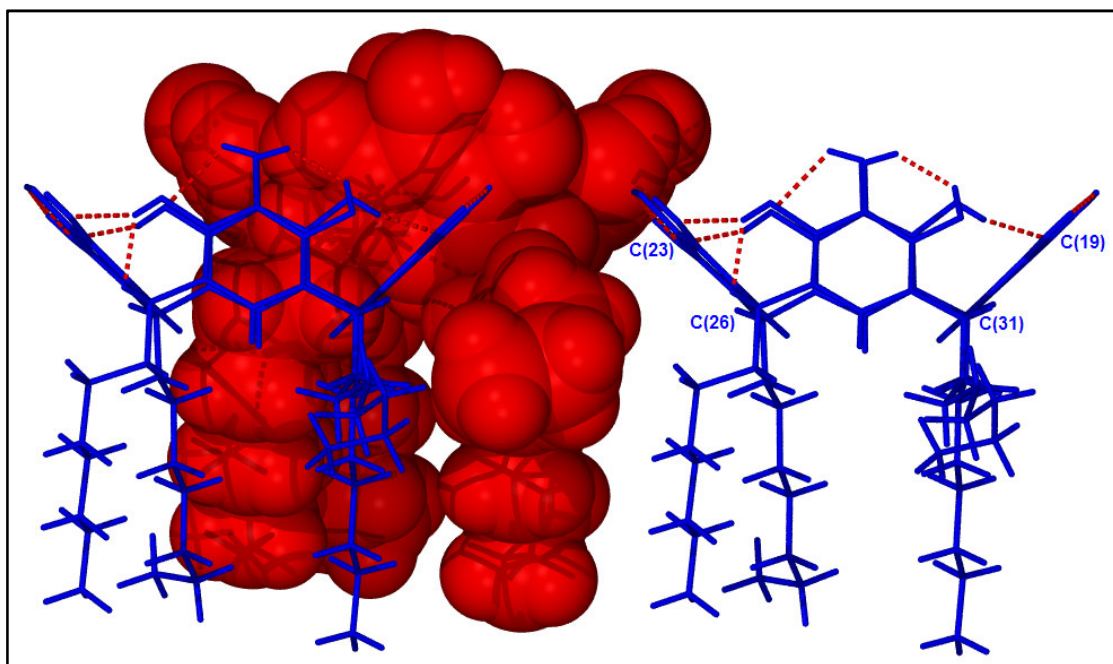
Figure 62 - Packing of pendant chains in *C*-heptyl-calix[4]pyrogallolarene hydrochloride acetonitrile clathrate

Secondly there is insufficient space between the calixarenes to have a completely interdigitated bilayer when all four pendant chains are directed vertically away from the annulus. Therefore the structure which results is a compromise between the formation of van der Waals interactions between the pendant chains on interdigitation and the packing efficiency gained by the horizontal projection of the pendant chain. This projection allows maximum interdigitation, and fills a void that would otherwise form. This also allows coordination of an appropriate guest molecule to the upper rim of the calixarene while residing in a non polar region (typical of guests which contain polar and non polar elements such as ethanol or diethyl ether).

2.9   *C*-Octyl-calix[4]pyrogallolarene

C-Octyl-calix[4]pyrogallolarene was synthesised by solvent and solvent-less methods. The crude filtrate from the reaction was taken up into acetonitrile, heated to boiling and then allowed to cool and slowly evaporate at room temperature. Crystals were produced which were suitable for single crystal X-ray diffraction studies ($C_{60}H_{88}O_{12} \cdot CH_3CN \cdot H_2O \cdot HCl$). The acetonitrile clathrate includes chloride ions which remain from the hydrochloric acid catalyst.
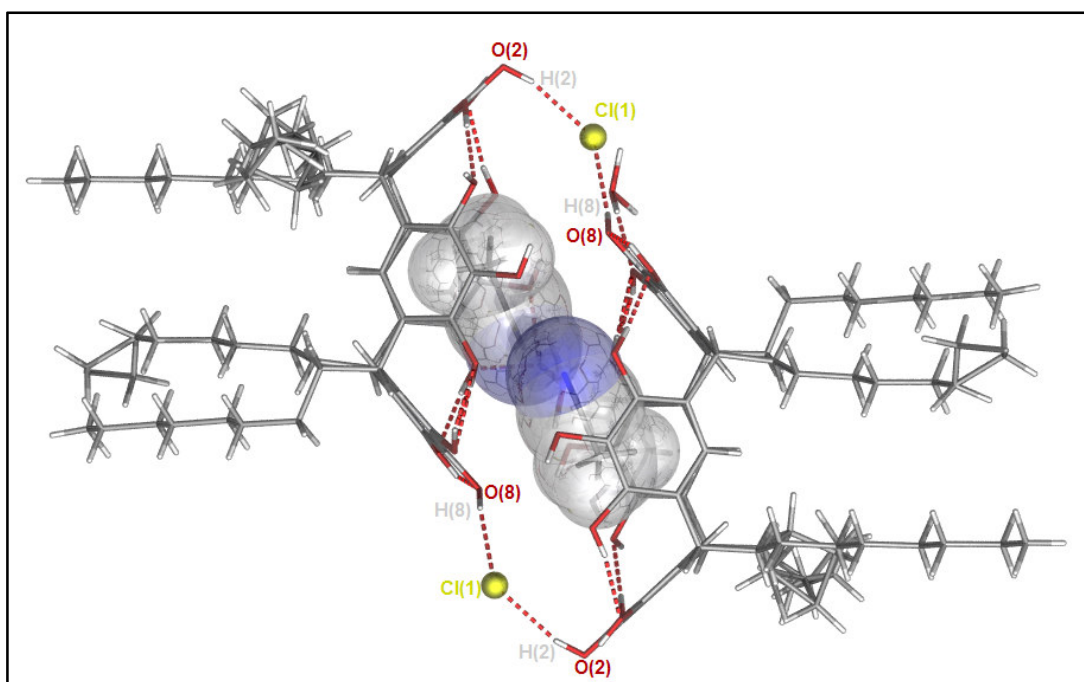
Figure 63 - Molecular structure of *C*-octyl-calix[4]pyrogallolarene hydrochloride acetonitrile clathrate

The molecular structure which is revealed shows the formation of an architecture closely related to *C*-hexyl-calix[4]pyrogallolarene hydrochloride acetonitrile clathrate; that is a bilayer which has calixarene molecules in facing layers are offset from perfect head-to-head alignment to allow hydrogen bonding from the upper rim of the calixarene to the chloride ion which is present in the lattice. (H(2) ⋯ Cl(1) = 2.21 Å (O(2) ⋯ Cl(1) = 3.02(6) Å) and H(8) ⋯ Cl(1) = 2.31 Å (O(8) ⋯ Cl(1) = 3.06(6) Å)). The angle at which the pendant chains are tilted relative to the cavity of the calixarene is reduced over the hexyl homologue to 34.5° (rather than 42°).

A similarity in the two hydrochloride analogues presented is the shape of the cavity. The cavity of the calixarenes are distorted in two ways; firstly by compression of one of the phenyl rings towards the centre of the macrocycle. In the octyl derivative the phenyl ring of C(16-21) is closer to the centre of the macrocycle (centroid 1) than the opposite ring (C(46-51)) ((1) ··· (2) = 3.13 Å and (1) – (3) = 3.27 Å).
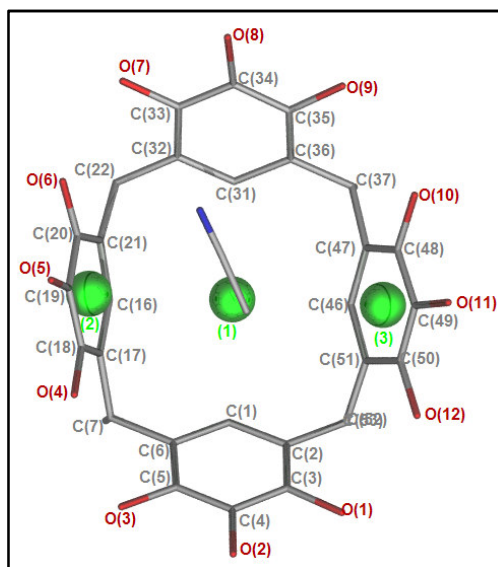
Figure 64 - Distortion of macrocycle in *C*-octyl-calix[4]pyrogallolarene hydrochloride acetonitrile clathrate

The second form which the distortion takes is the splaying outwards of one of the phenyl rings (C(31)-(36)). This is at its most extreme at C(33) which is furthest from the centre of the macrocycle (C(33) ··· (1) = 4.34 Å and C(35) ··· (1) = 4.29 Å). Both cases of distortion may be attributed to the presence of the acetonitrile guest molecule which is orientated diagonally across the cavity. The phenyl ring bent inwards is furthest from the methyl group and therefore its distortion will minimise the void which is formed. The phenyl ring which is distorted outwards is due to the electrostatic repulsion between the nitrogen of the acetonitrile group and the upper rim (N(1) and O(7)).

Chapter 3 - Host-guest chemistry of *C*-alkyl-calix[4]pyrogallolarenes

1 Introduction

Co-crystallisations of pyrogallol and other molecules were attempted to study the possible supramolecular interactions which calix[4]pyrogallolarenes form. Crystallisations were attempted using *ortho*-carborane and buckminsterfullerenes (C_{60}) under a variety of conditions (solvent calixarene pendant chain length, concentration and crystallisation technique) but none of the attempted combinations gave crystals which showed co-crystallised material.

It can be speculated that the systems are too electron rich to enter the cavity which has a hydroxyl fringed upper rim. Also the fullerene may be too large to be accommodated. In the literature several covalently bound calix[4]arene-fullerene species have been reported but it is only in the higher calix[n]arenes (n = 6, 8) that non-covalent coordination is observed.[48, 51] A notable exception is the coordination of C_{60} by cyclotriveratrylene (CTV) whose cavity walls are at a sufficiently large angle to accommodate the large spherical guest.[53]

Following the work of Cave *et al.* co-crystallisation of calixarene derivatives with terpyridines was carried out.[54, 56] A variety of terpyridines were synthesised using the green synthetic method developed by Cave *et al.*[174]
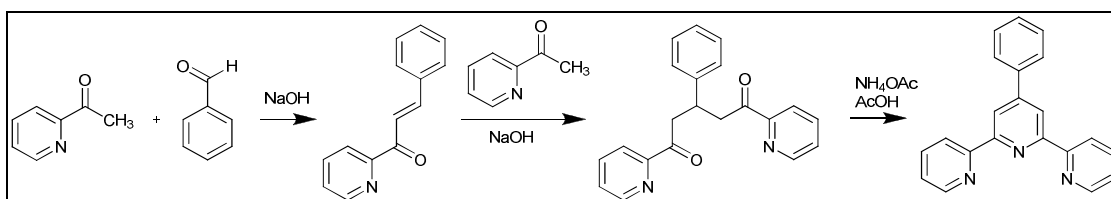
Figure 65 - Terpyridine synthesis

It was attempted to synthesise a phenanthrene substituted pyridine in order to probe the nature of the cavity formed by calix[4]arenes,
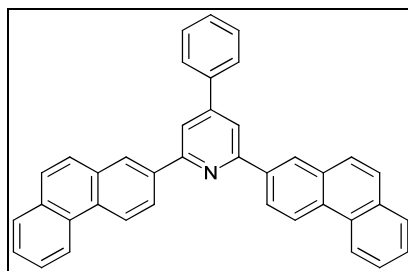
Figure 66 - 2,6-(2'-phenanthrene)-4-phenyl-pyridine

It was desired that the phenanthrene moiety could interact with the hydrophobic cavity while the pyridine could hydrogen bond with the upper rim of the cavitand. Unfortunately, the synthesis failed and material which had undergone the aldol reaction and subsequently dehydrated could be the only product isolated from the reaction mixture. This may be due to steric constraints at the 3 position of the 2,3-unsaturated carbonyl compound (C(35) and C(39)) (labelled in Figure 68), meaning that extended reaction times are required for 1,6-dicarbonyl compound formation.

2   Single crystal X-ray diffraction studies

Crystals of sufficient quality to undergo SCXRD investigations were obtained by recrystallising the solid from glacial acetic acid.
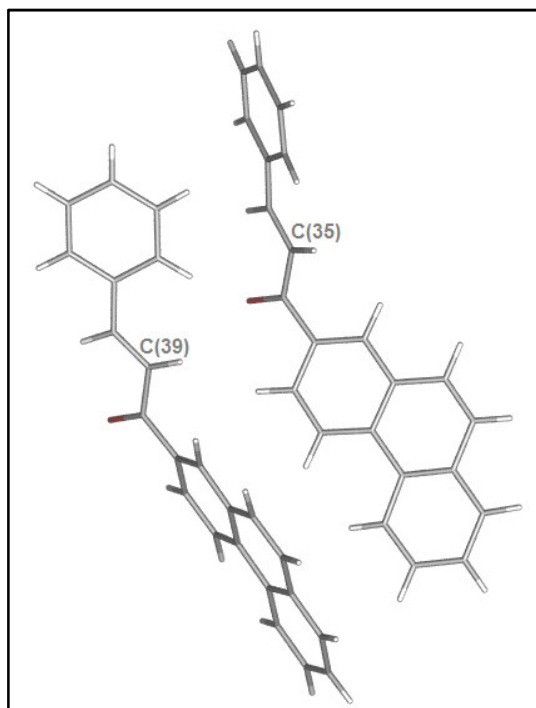
Figure 67 – SCXRD image of Phenanthren-2-yl-3-phenyl-propenone

The herringbone type packing of aromatic groups is observed for this species; however, the packing of this is somewhat unusual when compared to simple aromatic species such as benzene.[8] The structure shows very little overlap of the aromatic groups and also no CH – π interactions, due to a significant offset between the layers.

A variety of solvent / terpyridines / calix[4]arene combinations were mixed and allowed to slowly evaporate after sonication. Only a single combination of 2,6-(2-pyridyl)-4-phenylpyridine and *C*-heptane-calix[4]pyrogallolarene in methanol gave crystals suitable for single crystal X-ray diffractions studies.

The synthesis of this supramolecular species was achieved by addition of the terpyridine to a solution of calixarene, sonication for 10 minutes and then leaving the resulting solution to slowly evaporate. The product $(C_{56}H_{80}O_{12} \cdot C_{21}H_{15}N_3 \cdot 2(CH_3OH)(HCl))$ crystallised from solution and the crystals were found to be suitable for single crystal X-ray diffraction studies, with a synchrotron source as the crystals were weakly diffracting.
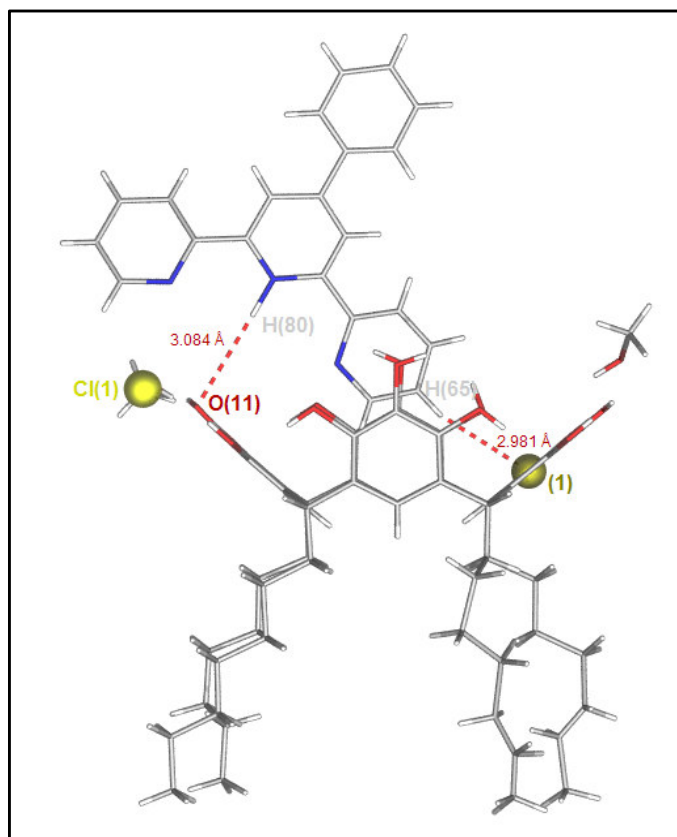
Figure 68 - *C*-Heptyl-calix[4]pyrogallolarene terpyridine complex

A hydrogen bond is formed between an aromatic hydrogen in the 3-position of the peripheral pyridine ring (H(65)) and the π-system of the interior face of the cavity (centroid 1). The closest contact is 2.85 Å (C(65) ⋯ (1) = 3.90 Å). This is reminiscent of the herringbone architecture formed by a large number of planar aromatic systems when crystallised.[8]

The closest contact is between the terpyridine and the calixarene is between the centre of the terpyridine nucleus and the upper rim of the calixarene H(80) ⋯ O(11) = 3.08 Å. The presence of chloride ion close by indicates protonation of the terpyridine and therefore this suggests a hydrogen

103

bond between the protonated terpyridine and the upper rim of the pyrogallolarene. This is in contrast to Cave *et al.* who show coordination of unprotonated terpyridines which bridge the gap between two resorcinarenes.[97]
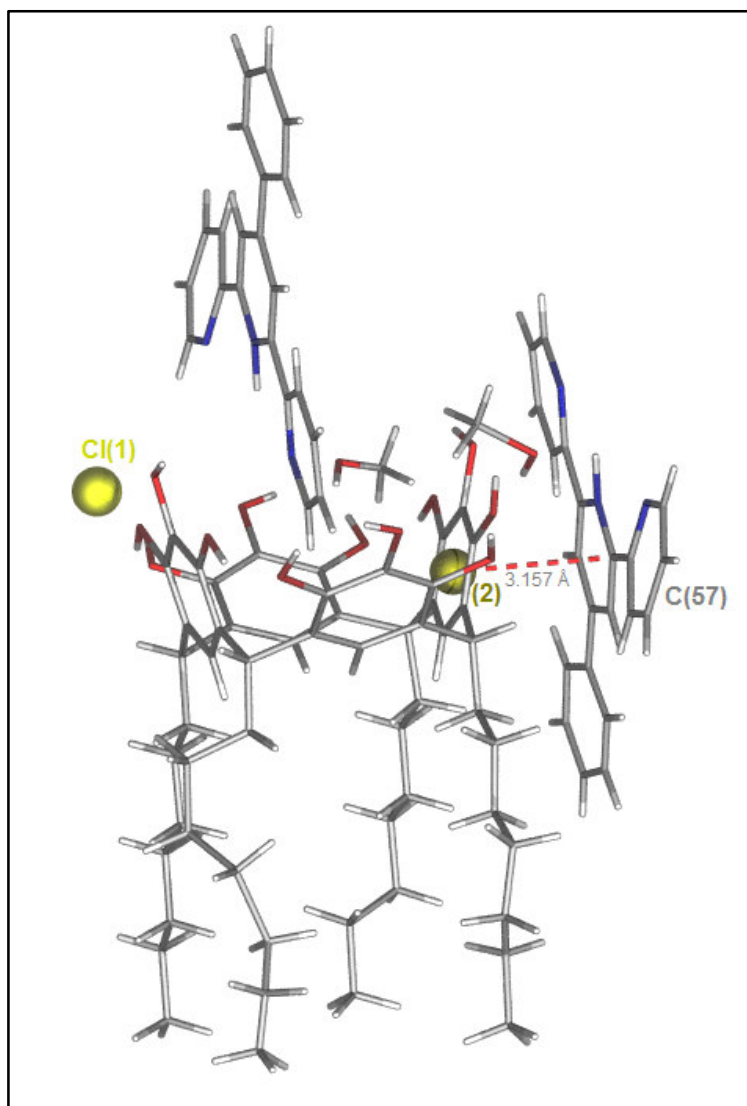
Figure 69 - *C*-Heptyl-calix[4]pyrogallolarene terpyridine complex showing π-π interactions

The structure shows a fascinating variety of intermolecular interactions. There are π stacking interactions between the external face of the calixarene with the terpyridine. The closest contact between the two species is centroid (2) – C(57) = 3.157 Å. This is significantly shorter distance than the only other reported instance of exo-coordination by a calixarene discovered by Messina *et al.* who discovered that *per*-halobenzenes can interact with bis-pyridylmethyl-tetra-*tert*-butylcalix[4]arene.[175]

These interactions were in the range 3.4 – 3.8 Å. Other π stacking interactions discovered involving endo coordination of phenanthroline ligated metals to calixarenes are in the range of 3.50 – 3.59 Å.[176]

The distortion factor of the macrocyle is 0.79 compared to crystal structures of C7Pg with small molecules as guests datas is: 0.86 - Et$_2$O, 0.98 - EtOAc, 0.92 - EtOH, 0.87 - MeCN. This shows that if the guest are in the cavity then the cup can distort to a certain extent to accommodate the guest molecule. This has been shown in the case of strong cation – π interactions to distort the macrocycle into a pinched cone conformation.[47] Taking the evidence from this structure it is possible to maipulate the structure of the macrocycle with significantly weaker interactions. Similar structure interconversions have been modelled by Mattay *et al.* in the conformation changes which take blace between *C*-methyl-resorcin[4]arene in its solvated and desolvated form.[177, 178]

Chapter 4 - Green chemistry

In order to rapidly generate the materials required for the structural studies of calix[4]pyrogallolarenes green chemistry methods were employed.[73, 84] When pyrogallol, *para*-toluene sulphonic acid and an appropriate aldehyde were ground together in a mortar and pestle, it was found that the macrocyclisation reaction was rapid, but the chair conformation was a significant by-product.

Calixarene	Green chemistry (Total Yield by NMR) %	Chair Conformation (By NMR) %	Standard Method (isolated yield) %
C1Pg	82	0	99
C2Pg	86	0	50
C3Pg	72	0	77
C4Pg	80	0	51
C5Pg	61	53	49
C6Pg	91	55	72
C7Pg	60	3	71
C8Pg	83	15	85
C9Pg	92	2	95
C10Pg	80	4	99

Table 2 - Green Chemistry Results

This conclusion was arrived at by inspection of the ^{1}H NMR spectra. The data shows a splitting of the aromatic proton resonance from a single signal at 7.2ppm to two individual signals at 7.3 and 7.1ppm. This is indicative to the chair isomer as it possesses two aromatic environments which would cause the splitting. (for a detailed discussion of conformational analysis of calix[4]arenes by NMR see *C*-(4-nitrophenyl)-calix[4]pyrogallolarene in Chapter 5 Section 4).

Separation of the conformational isomers was achieved by repeated recrystallisation from either diethyl ether or acetonitrile depending on the length of the pendant chain (as this has a significant effect on the solubility of the calixarene in organic solvents). This technique exploits the difference in solubility of the chair and cone conformers in organic solvents, the chair conformation is considerably more soluble in polar organic solvents than the cone conformation, and therefore can be separated by filtration and recrystallisation.

The use of automated grinding techniques was attempted to speed the synthesis of calix[4]pyrogallolarenes. Firstly a Fritsche Pulverisette # 6 ball mill was used. This instrument grinds the sample in a stainless steel bowl containing ball bearings which rapidly spin round the bowl when it is subjected to eccentric rotation within the instrument. The second piece of apparatus to be used was the Pulverisette # 2, which is an automatic pestle and mortar. The sample is placed in a ceramic bowl which rotates and the sample is ground by a pestle that can be positioned to affect the intensity of the grinding. Both pieces of apparatus are shown in Figure 70 below.

Figure 70 - Fritsche Pulverisette # 6 ball mill (left) and Fritsche Pulverisette # 2 automatic pestle and mortar (right)

When the calix[4]pyrogallolarenes were ground using the ball mill the reaction did not progress further than the eutectic melt stage and un-cyclised intermediates were isolated. It was speculated that due to the sealed nature of the system the water liberated by the condensation reaction could not escape and thereby prevent the reaction from progressing to completion. A series of experiments

where activated molecular sieves were added to the grinding bowl to absorb the water liberated during the reaction failed to yield the desired product and only oligomers could be isolated.

When the calixarene synthesis was attempted using the automated pestle and mortar, the desired product was obtained in yields identical to those gained with the hand held pestle and mortar. However, the temperature of the bowl had to be carefully monitored; if the bowl became too hot, and prolonged grinding took place (>1 hour) decomposition of the product was observed.

It can therefore be concluded that a ball mill is unsuitable for the synthesis of calix[4]pyrogallolarenes. This can be speculated that the failure of the reaction to progress to completion is due to the grinding being too energetic rather than the sealed nature of the system failing to allow water to be liberated. The automated pestle and mortar can be used to synthesise calix[4]pyrogallolarenes in a solvent free manner, but the conditions must be carefully monitored in order to maximise the yield of the desired product.

When the approach of functionalising the pendant chains of a calixarene was found to be impractical, the synthesis of functionalised aldehyde derivatives became necessary. However in doing this it became necessary to protect the aldehyde group during the synthesis of the additional functional groups.

Protecting aldehydes as cyclic acetals is a commonly used technique in synthetic organic chemistry.[179] These protecting groups are relatively easy to form yet are resistant to a wide variety of organic, organometallic and basic reagents. They are easily cleaved with a dilute solution of aqueous acid, a scheme showing their synthesis is shown in Figure 71 below:
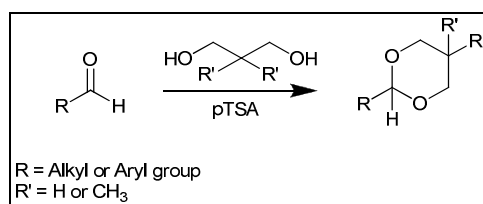
Figure 71 - Acetal formation

Traditionally the acetal group is prepared by reaction of the aldehyde with a 1,3-diol under *para*-toluenesulphonic acid catalysis. The reaction is typically performed in a toluene solution using a Dean-Stark apparatus to remove the water generated by the condensation reaction. This technique involves relatively large solvent volumes and lengthy reaction times.[179] It is possible to perform a wide variety of organic reactions under microwave irradiation.[68] An unmodified domestic microwave was used to perform the synthesis of an acetal group without the use of solvents and with minimal catalyst present. A typical procedure is as follows:

Acetaldehyde (0.17 ml, 3 mmol), 2,2-dimethyl-1,3-propanediol (0.312 g, 3 mmol) and *para*-toluenesulfonic acid (0.02 g, 0.105 mmol) were mixed in a vial. The mixture was heated for 120 seconds in a domestic microwave (ONN, Model OM010, 800 W). The reaction was allowed to cool, an NMR was taken of the resulting colourless solid showing product (>99 % yield).

This procedure has been shown to be successful in producing protected aldehydes with 1,3-propane-diol, 2-methyl-1,3-propane-diol and 2,2-dimethyl-1,3-propane diol. These findings are summarised in the table below which show the yields obtained for reaction of linear aliphatic aldehydes with ,2,2-dimethyl-1,3-propane diol.

Aldehyde	Yield by NMR %
CH_3CHO	99
C_2H_5CHO	97
C_3H_7CHO	99
C_4H_8CHO	98
$C_5H_{11}CHO$	99
$C_6H_{13}CHO$	99
$C_7H_{15}CHO$	99
$C_8H_{17}CHO$	98
$C_9H_{19}CHO$	99
$C_{10}H_{21}CHO$	99
$C_{11}H_{23}CHO$	99

Table 3 - Yields of acetals formed by microwave irradiation

This shows that lengthy reaction times, and large solvent volumes are unnecessary for the synthesis of acetals. The *p*TSA can be removed from an ethereal solution of the reaction mixture by liquid –liquid extraction using an aqueous base to yield the pure product.

Chapter 5 - Synthesis of functionalised calixarene derivatives

1 Introduction

The use of a calix[4]pyrogallolarene nanometer scale spheres as a drug delivery vectors relies on the decoration of the exterior of the capsule with functionality to enable targeting of the sphere to a specific tissue. This requires understanding of the factors which govern the host-guest interactions which guide capsule formation which was in part achieved by the preliminary investigations into the alkyl calixarenes and their interactions with solvent molecules.

The nano-capsule has 24 sites for potential functionalisation (these are highlighted in green in Figure 72 below). The purpose of the functionalisation is to allow delivery of the nano-capsule to dendritic cells. The nano-capsule may be decorated with peptide sequences which have been found exclusively on the surface of cancerous cells. This may lead to a novel form of antineoplastic immunotherapy.
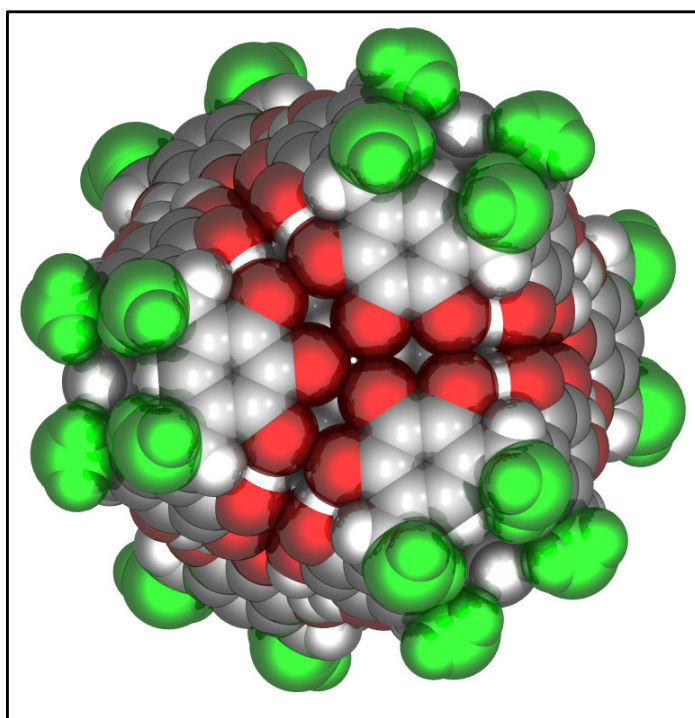
Figure 72 - Nano-capsule with potential functionalisation points highlighted in green

In cancer, due to mutation of cancerous cell's genetic code, peptide sequences unique to the cancer are presented on the surface of the cell. The genetic mutation may cause disruption of the protein's primary structure, and therefore could be recognised by the immune system as 'non self'. If

recognised as 'non-self' an immune response may be produced against the cell which carries the mutated peptide, and therefore regression of the tumour.[180] In order for the immune response to be activated the antigen must first be processed by an antigen presenting cell, which are usually dendritic cells. Dendritic cells present the metabolised peptide to T-cells which can then begin the response to the antigen in the body.[181] It is therefore essential to design a delivery system with high selectivity and low toxicity to dendritic cells.

Initial investigations were focused on the functionalisation of calix[4]arene derivatives. This was because the calixarene synthesis uses very harsh conditions (concentrated hydrochloric acid / methanol) and long reaction times (up to 6 days) which would destroy a large variety of functional groups. Secondly, the calixarene synthesis has widely variable yields (from 20 – 100% reported) which strategically is potentially very wasteful. Therefore the *C*-(dec-10-ene)-calix[4]pyrogallolarene (C10enePg) was synthesized.
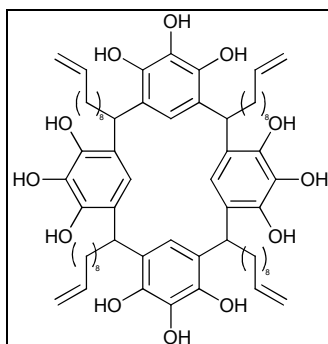
Figure 73 – *C*-(Dec-10-ene)-calix[4]pyrogallolarene

The boiling method which has proven successful for the library of aliphatic calixarenes was shown to be unsuccessful, possibly due to the hydro-chlorination of the alkene and subsequent nucleophilic substitution reactions with pyrogallol. The molecule was eventually synthesized by following the grinding technique developed by Antesberger *et al.*[73] Grinding pyrogallol and a catalytic amount of *para*-toluenesulfonic acid to a fine powder followed by drop-wise addition of undecyleneic aldehyde and further grinding and recrystallisation using ethyl acetate gave the desired product in high yield.

2   *C*-(Dec-10-ene)-calix[4]pyrogallolarene

When a solution of *C*-(dec-10-ene)-calix[4]pyrogallolarene in ethyl acetate is a allowed to slowly evaporate, crystals grow which are suitable for single crystal X-ray diffraction studies $((C_{68}H_{96}O_{12}\cdot(CH_3CH_2OC(O)CH_3))$. The data shows a capsular arrangement of molecules in the solid state. There is a single calixarene and a disordered ethyl acetate molecule in the asymmetric unit of the structure, which is transposed into a large unit cell (a = 37.22 Å, b = 37.22 Å, c = 26.03 Å) and spherical architecture by $R\bar{3}$ symmetry. The figure below shows the nano-capsule which has been formed with the pendant chains and encapsulated solvent molecules removed for clarity.
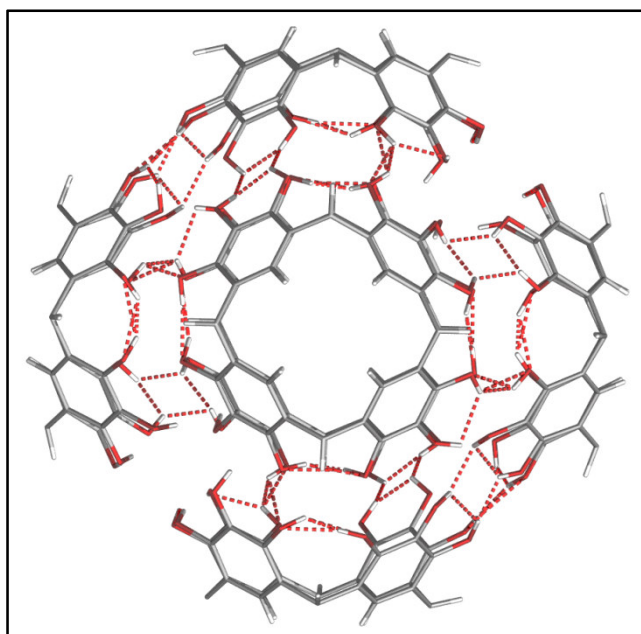
Figure 74 - Nano-capsule formed by *C*-(dec-10-ene)-calix[4]pyrogallolarene (pendant chains removed for clarity)

The exact location of the encapsulated guests could not be determined due to extensive disorder within the capsule. Therefore the contents of the nano-capsule were modelled as diffuse electron density. This disorder is due to a lack of interaction between the guest and the walls of the cavity making the contents fluid. Earlier gas-phase-infra-red-thermogravimetric analysis by Cave *et al.* showed that six ethyl acetate molecules are encapsulated within the sphere.[67] In the shorter chain capsules reported to date, [67] there are solvent molecules included in the lattice *exo* to the capsule, and

the extension of the chain length by 4 carbon atoms means that the lipophilic domain created by the pendant chains is sufficient to stabilise the nano-spheres without the inclusion of extra solvent molecules.

Each calixarene interacts with its pendant chains two faces of an adjacent sphere in a CH – π interaction (C(15) ⋯ centroid (11) = 2.97 Å and C(64) ⋯ centroid (10) = 2.86 Å). These interactions lead to a short inter-sphere distance. This inter-sphere distance is calculated by generating a centroid at centre of each macrocycle. A final centroid is generated from the position of the six monomers' centroid which gives the location of the centre of the capsule. This also gives the internal diameter of the nano-sphere to be 17.83 Å. The inter-capsule between centres of the capsule is 23.17 Å.
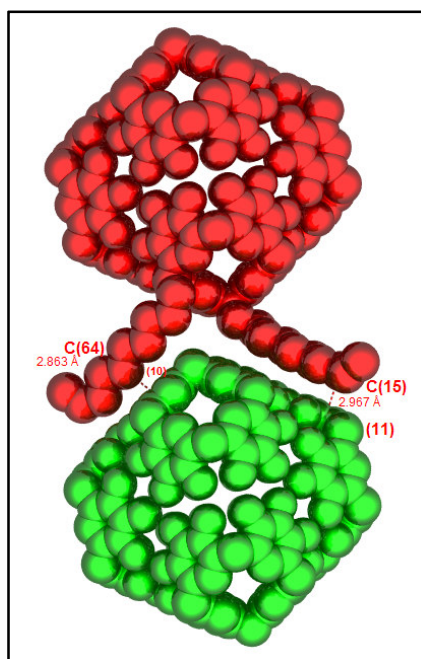
Figure 75 - Interactions between capsules (pendant chains and hydrogen atoms removed for clarity)

The lack of permanent interactions between the capsule and its contents and low distortion of the pendant chains means that the macrocycle is not perturbed significantly in conformation (Df = 0.97). The capsule is a result of $R\bar{3}$ symmetry and this lack of distortion of the macrocycle leads to the capsule that is formed showing little perturbation of the walls and a good alignment of the phenyl rings which make up the walls. This is in contrast to the "nano-rods" formed by C6Pg ethyl acetate capsules forming inter-capsule hydrogen bonds.[67]

The molecular structure of the capsule also demonstrates clearly why three individual signals in the ^{1}H NMR spectra are observed when in the capsule formation and only two are seen while in the monomer. There are three possible environments (square planar, trigonal or uncoordinated) for the hydrogen atoms, which is identical to the arrangement of hydrogen atoms in the metal fringed capsules reported in the literature.[93]

2.1   Synthetic manipulations of *C*-(dec-10-ene)-calix[4]pyrogallolarene (C10enePg)

With the C10enePg in hand, efforts to functionalise the pendant chains were pursued with a view to forming an attachment point on the terminus of the pendant chains for a peptide sequence.

It has been reported in the literature that the pendant chains of an alkene substituted resorcinarene can be thiolated by a photolytic mechanism. The thiol group was targeted because the group would give some degree of water solubility by increasing the polarity of the pendant chains, and secondly if a disulfide link to a cysteine amino acid this would form an ideal biodegradable link to a peptide chain which could be metabolised within a dendritic cell. Despite several attempts using different reaction conditions including; varying intensity and wavelength of ultraviolet light, different batches of starting material and reagents, solvent and reaction time, this reaction could not be repeated on the pyrogallolarene system and only starting materials were recovered.
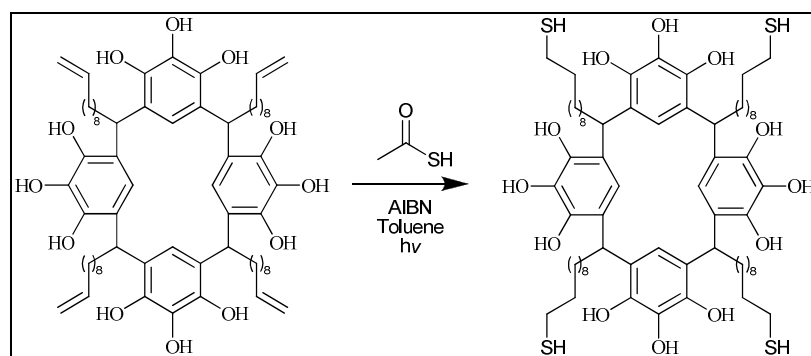
Figure 76 - Thioloation of *C*-(dec-10-ene)-calix[4]pyrogallolarene

In addition to thiolation, efforts to brominate the macrocycle were undertaken. Under a variety of conditions (NBS & AIBN, HBr, Br$_2$ Et$_3$N/pyridine, 9-BBN) the eventual result of the reaction was a black intractable solid. For the strongly acidic hydrobromic acid it would be reasonable to suggest that the macrocycle was destroyed during this reaction by protodealkylative ring opening and subsequent oxidation of the pyrogallol residues. If the bromination was partially complete it was speculated that oligomers of the calixarene have formed by nucleophilic substitution of the bromine by a phenolic hydroxyl group. When solids isolated from the reaction were analysed by ^{1}H NMR, residual alkene peaks were visible, indicating the reaction was incomplete. This lends further support to the suggestion that the calixarene has formed a cross linked ether polymer.
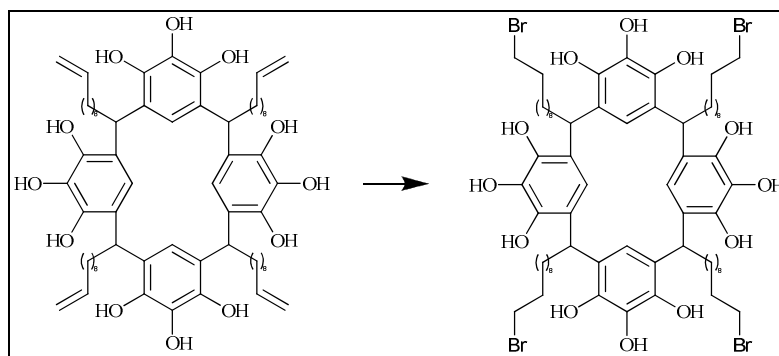
Figure 77 - Bromination of *C*-(dec-10-ene)-calix[4]pyrogallolarene

In order to attach peptide sequences to the nano-sphere amino or carboxyl substituted pendant chains were targeted. With the experience gained in the efforts to functionalise and protect the alkene substituted calixarene of bases turning the calixarene solution black and eventually forming an intractable resinous mixture, it was decided that the carboxyl group rather than the basic amino groups would prove simpler for further development as a synthetic target.

3 Hydroxyl footed calix[4]arenes

Hydroxyl footed calix[4]arenes were synthesised by following the method of Gibb *et al.*.[167] This involves the acid catalysed ring opening of unsaturated pyran or furans to yield an enol intermediate which tautomerises to a hydroxyl substituted aldehyde as shown in the Figure below. On cooling the acidic mixture, the desired product (cone conformation) precipitates from solution. This solid is filtered and suspended in water which is sonicated to remove any acidic residues. Crystals are grown by the slow evaporation of a solution of calixarene in the relevant solvent.
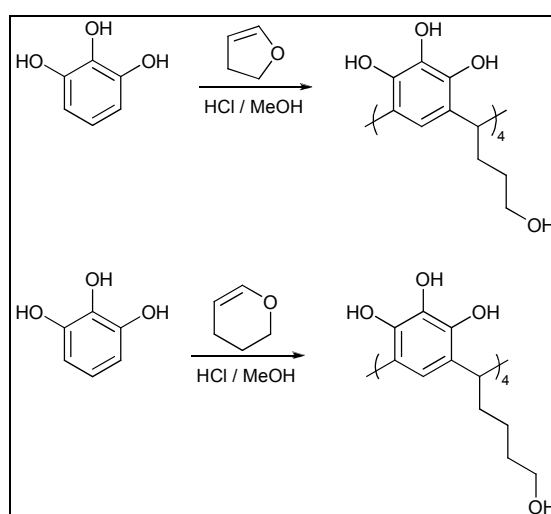
Figure 78 - Synthetic route to hydroxyl substituted calix[4]pyrogallolarenes

3.1 *C*-(3-Propanol)-calix[4]pyrogallolarene acetone clathrate

Two unique crystal structures have been obtained for *C*-(3-propanol)-calix[4]pyrogallolarene acetone clathrate ($C_{40}H_{44}O_{16}\cdot5(CH_3C(O)CH_3)\cdot4(H_2O)$) and ($C_{40}H_{44}O_{16}\cdot(CH_3C(O)CH_3)\cdot3H_2O$). These molecular structures show significant differences in the packing motif. The first structure to be presented is the higher molecular symmetry polymorph. This crystal structure has nine molecules (two calixarene, four acetone and three water molecules) in the asymmetric unit which fill a unit cell by $P2_1/c$ symmetry operation. On inspection of the packing arrangement of the molecules, the calixarenes form a head-to-tail arrangement with the hydroxyl groups of the pendant chains forming hydrogen bonds to the upper rim of the calixarene below (H(9) $\cdots$ O(14) = 1.91 Å (O(11) $\cdots$ O(14) = 2.70(5) Å)

and H(23) ⋯ O(13) = 2.14 Å (O(10) ⋯ O(13) = 2.90(5) Å)). In the cavity which is formed between the cavity of one calixarene molecule and the pendant chains of the calixarene above one acetone molecule is hosted (shown in space-filling representation). The three remaining acetone molecules are *exo* to the cavity of the calixarene as shown in Figure 79.
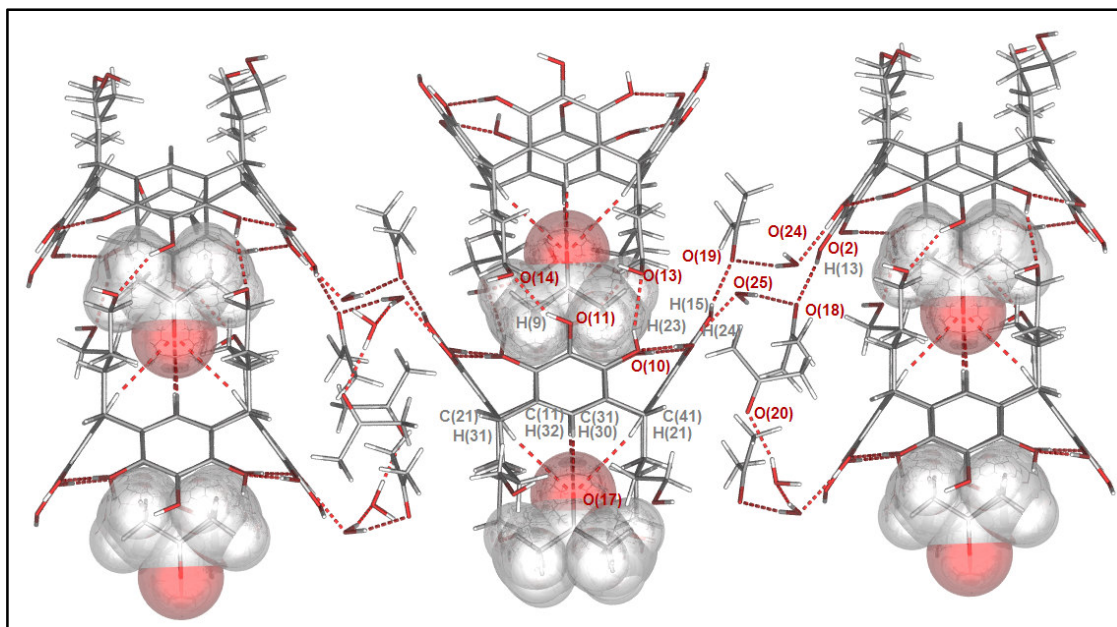
Figure 79 - *C*-(3-Propanol)-calix[4]pyrogallolarene acetonitrile water clathrate

The acetone guest molecule coordinates to the annulus of the calixarene forming hydrogen bonds the mean separation between the hydroxyl oxygen and the lower rim hydrogen atoms (O(17) ⋯ (H(21), H(30), H(31), H(32)) is 2.86 Å (mean separation between O17 and carbon atoms (11) (21) (31) (41)= 3.83 Å). Despite the void which is present below the encapsulated acetone molecule the macrocycle remains undistorted with a distortion factor of 0.98. This forms an alternating sheeting like arrangement with calixarenes aligned in opposite directions. Below the acetone molecule there is a significant void which has formed.

In the second crystal structure there is significantly lower lattice symmetry with five molecules comprising the asymmetric unit (one calixarene, one acetone molecule and three water molecules). This is transposed into a significantly smaller unit cell by $P\bar{1}$ symmetry.

Like the higher symmetry polymorph, there is an infinite alternating sheet architecture formed due to the inversion centre which is present. However, the solvent molecules which lie between the sheets of the higher symmetry sheet is not present in the lower symmetry polymorph. The closer proximity of the sheets allows inter-sheet hydrogen bonding (H(10) ⋯ O(14) = 1.84 Å, O(10) ⋯ O(14) = 2.68(4) Å). This inter sheet bonding forms two sheets which are linked by mutual pendant chain to upper rim hydrogen bonding. This double sheet is bonded by upper rim to upper rim bonding to another sheet – dimer.
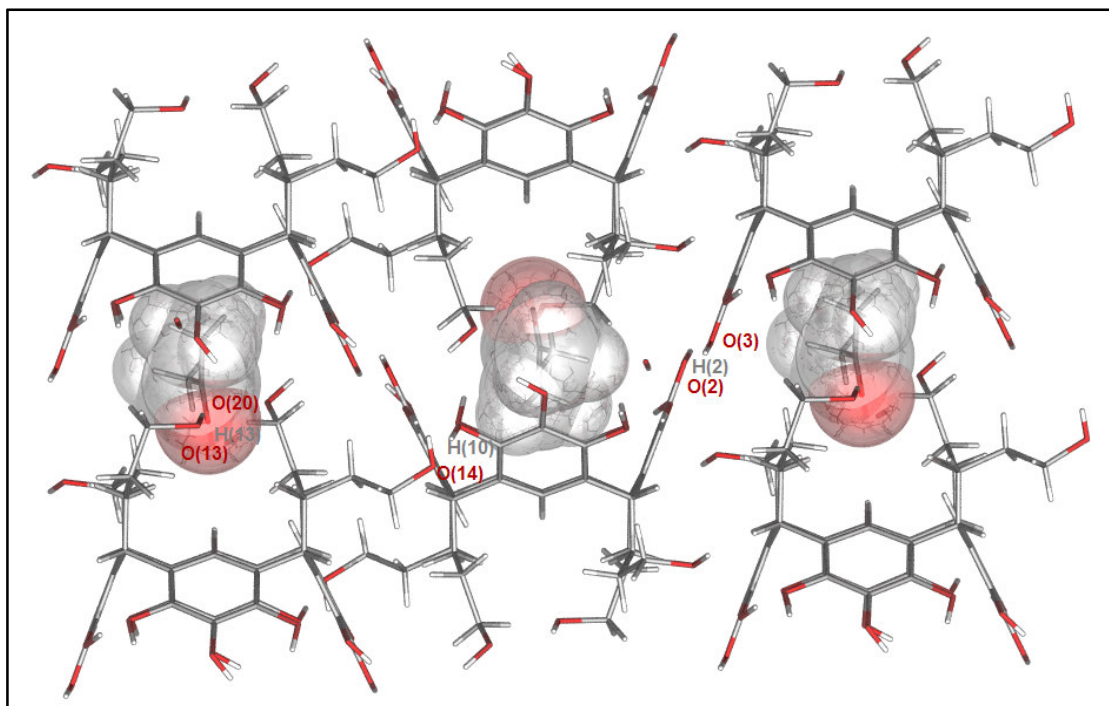
Figure 80 - *C*-(3-Propanol)-calix[4]pyrogallolarene acetonitrile water clathrate

There is also a significant tilting of the acetone molecule (23.8°) relative to the plane of the calixarene (shown in Figure 82 above) whereas the first example is tilted only 1.1° from the plane of the calixarene. The tilted acetonitrile is also twisted by 13.2°. This tilt and twist of the hosted acetone molecule allows formation of a hydrogen bond between to one of the hydroxyl groups (H(13) ⋯ O(20) = 2.03 Å, O(13) ⋯ O(20) = 2.81(12) Å) instead of bonding to the annulus of the calixarene above. This non central alignment of the guest molecule affects the geometry of the macrocycle and causes a decrease in the symmetry of the calixarene and the distortion factor is 0.88.

A tetrahydrofuran clathrate ($C_{40}H_{44}O_{16} \cdot C_4H_8O \cdot 2H_2O$) was formed by slow evaporation of a solution of C3OHPg in THF. Like the acetone clathrates described earlier, the molecule is arranged in a head-to-tail stacking pattern but a higher degree of molecular symmetry is present, with a mirror plane passing through the centre of the calixarene. Three molecular fragments are present in the asymmetric unit; half a calixarene molecule, half a THF, and a water molecule which are subjected to *P*2*/n* symmetry operation which fills the unit cell. Tetrahydrofuran is present within the void created between the lower rim and pendant chains of one calixarene and the upper rim and cavity of one below (shown with transparent van der Waals radii in Figure 81 below).
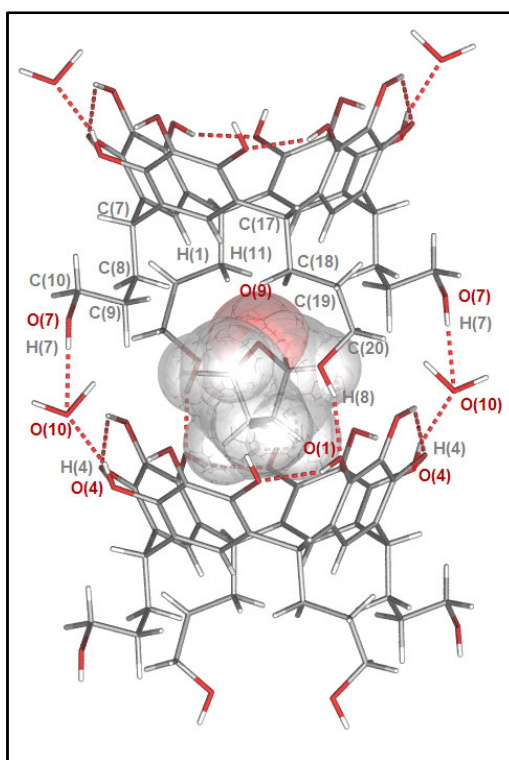
Figure 81 - *C*-(3-Propanol)-calix[4]pyrogallolarene tetrahydrofuran water clathrate

The space between calixarene molecules is gated by two water molecules (O(10)) which form two hydrogen bonds; one to the pendant chain (O10 ⋯ H7 = 1.97 Å (O10 ⋯ O7 = 2.80(6) Å)) and the second to the upper rim of the calixarene (O(10) ⋯ H(4) = 1.87 Å (O(10) ⋯ O(4) = 2.67(5) Å)) below.

A relatively large distance separates the ethereal oxygen of the tetrahydrofuran and the lower rim of the calixarene above (O(9) ⋯ H(11) = 3.69 Å (O(9) ⋯ C(11) = 4.58(18) Å) and O(9) ⋯ H(1) = 3.68 Å (O(9) ⋯ C(1) = 4.75(18) Å)). Therefore, there is no coordination of the guest's oxygen atom to the annulus of the calixarene above unlike the acetone clathrates. This separation may be due in part to the

steric requirement of the two methylene groups which form the ether linkage of THF preventing closer approach of the oxygen, also it may be due to the different electronic structure of the oxygen with the carbonyl oxygen being more polar than the ether which is present in the THF and is therefore less attracted to the slightly positive lower rim. The guest molecule is located centrally in the cavity between two calixarenes. The accommodation of the guest is compensated for by the distortion of one of the pendant chains in the asymmetric unit (and therefore two chains in the complete calixarene molecule) and also distortion of the macrocycle. The Df is 0.91 which is significantly lower than the distortion observed in the acetone clathrate. This distortion can be found to be prevalent in the macrocycle at the methine bridging point (C(17)) bearing the pendant chain which is not distorted outwards (C(18-20)) the angle formed between C(2)-C(17)-C(16) is 111.34° compared to C(6)-C(7)-C(12) = 109.78°.

The water molecule which bridges the gap between calixarene molecules also forms a hydrogen bond to the upper rim of a calixarene chain which is arranged anti-parallel to the original chain (H(10C) ⋯ O(1) = 2.11 Å (O10 ⋯ O1 = 3.14(5) Å)) shown in Figure 82 below.
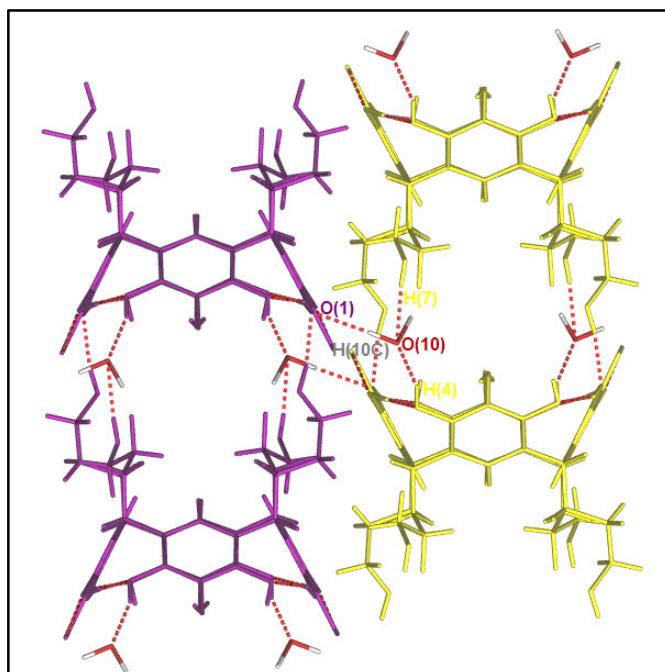
Figure 82 - Anti-parallel arrangement of calixarene chains in *C*-(3-Propanol)-calix[4]pyrogallolarene

tetrahydrofuran clathrate (solvent molecules removed for clarity)

A second unique chain is arranged in an anti-parallel alignment to the original chain and shows a mutual hydrogen bond between the same faces upper rim and pendant chain (H(8) ⋯ O(1) = 1.85 Å, (O8 ⋯ O1 = 2.73(6) Å)) this interaction is highlighted below in Figure 83.
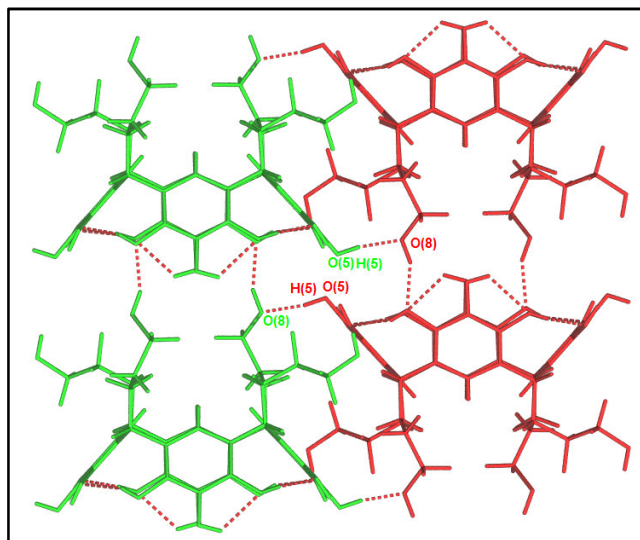
Figure 83 - Hydrogen bonding between anti-parallel calixarene chains in *C*-(3-Propanol)-calix[4]pyrogallolarene tetrahydrofuran water clathrate (solvent molecules removed for clarity)

As the yield of the calixarene synthesis was only 45% of the desired product, the filtrate from initial separation of the precipitate from the reaction mixture was concentrated. This caused small crystals to form; this solution was left to slowly evaporate further to promote growth of crystals which were of suitable quality for single crystal X-ray diffraction studies. On solution the molecular structure reveals the chair conformation. In the asymmetric unit there is a single calixarene molecule and five water molecules.
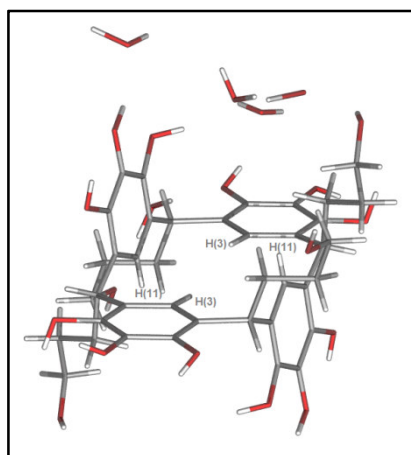
Figure 84 - *C*-(3-Propanol)-calix[4]pyrogallolarene tetra-hydrate chair conformation

The unit cell is in space group $P\bar{1}$ but possesses high molecular symmetry as the molecule has the inversion centre. This crystal structure clearly reveals why two signals for the hydrogen atoms are observed because H(11) and H(3) are clearly in inequivalent molecular environments and the up-field shift of one of the signals may be due to the proximity of the quadrupolar electron cloud of the phenyl rings arranged in the axial positions. This effect is shown in the enlargement of the aromatic region of the ^{1}H NMR spectrum. The peaks at 5.86 and 5.74 ppm are derived from the proton resonance which has split due to the different arrangement of atoms in space.
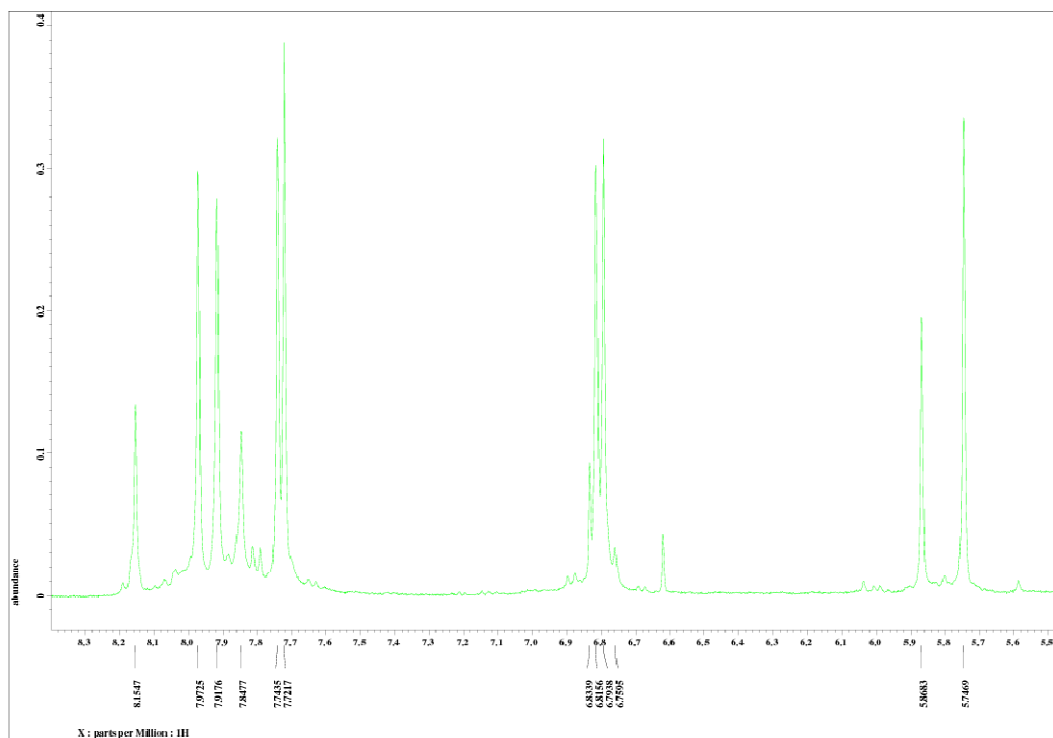
nitrobenzene)-calix[4]pyrogallolarene

3.2   C-(3-Propanol)-calix[4]resorcinarene

C-(3-Propanol)-calix[4]resorcinarene was synthesised solely by traditional methods requiring the use of solvents, as the solvent free method failed to give the desired product. The failure of the green chemistry reaction may be due to the anhydrous reaction conditions because water is required to catalyse the hydrolysis of the alkylated enol equivalent (2,3-dihydropyran). Crystals were grown by dissolution of the product from the reaction in the relevant solvent and allowing the solvent to slowly evaporate.

Two polymorphic structures have been obtained for the acetonitrile clathrate which show similar differences in the arrangement of the guest molecules to that of C-(3-propanol)-calix[4]pyrogallolarene acetone clathrate. Like the structures previously discussed, the calixarene molecule is arranged in a head-to-tail packing motif with the alternating alignment of the calixarenes forming a sheet-like architecture $(C_{40}H_{42}O_{12} \cdot CH_3CN \cdot 2H_2O)$. This is in contrast to the bilayers observed in the C-alkyl-calix[4]arenes.
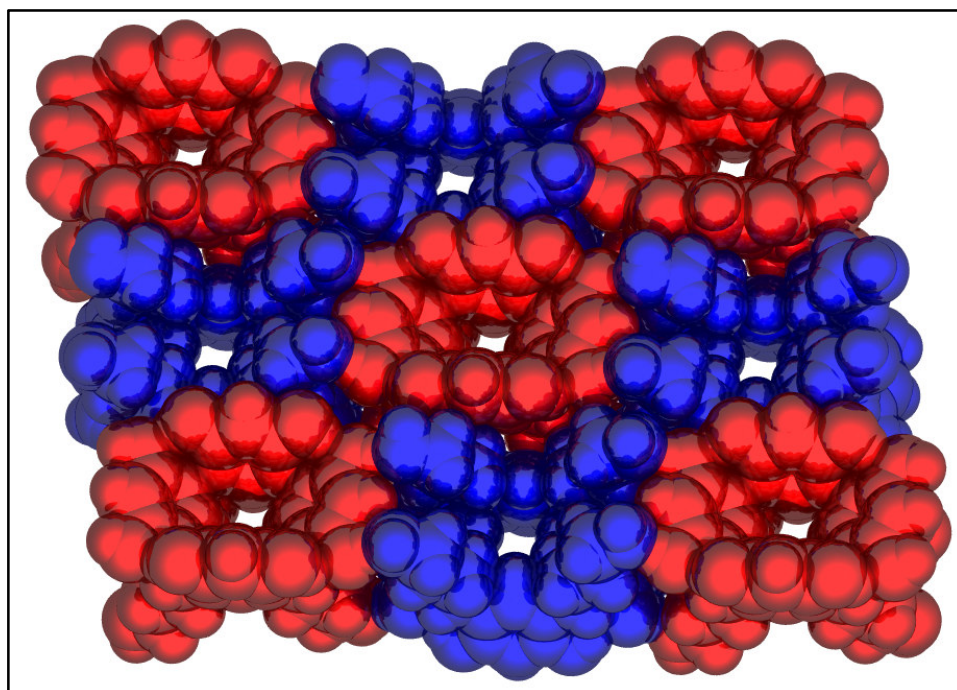
Figure 86 - Sheet of alternating calixarenes in C3OHRs acetonitrile clathrate

Hydrogen bonds are formed within the sheet between the upper rim of the calixarene to the hydroxyl groups of the pendant chain of the calixarene adjacent as shown in Figure 87 below. (H(3) ⋯ O(12) = 1.89 Å (O(3) ⋯ O(12) = 2.72(7) Å), H(4) ⋯ O(11) = 1.80 Å (O(4) ⋯ O(11) = 2.63(9) Å), H(7) ⋯ O(10) = 1.77 Å (O(7) ⋯ O(10) = 2.61(7) Å), H(8) ⋯ O(9) = 1.81 Å (O(8) ⋯ O(9) = 2.64(9) Å)).
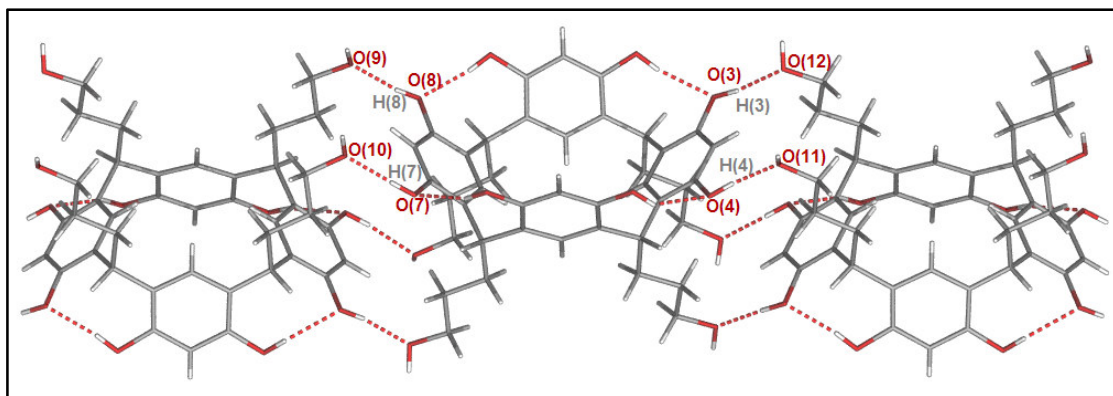
Figure 87 - C-(3-Propanol)-calix[4]resorcinarene acetonitrile water clathrate (solvent molecules removed for clarity)

Between each sheet of calixarenes there are three crystallographically unique solvent molecules (one acetonitrile and two water molecules). Unusually one of the water molecules is located on the interior surface of the cavitand and forms a hydrogen bond to one of the pendant chains (H(9) ⋯ O(14) = 2.12 Å (O(9) ⋯ O(14) = 2.86(14) Å)) of a calixarene in the upper sheet. This hydrogen bond causes a misalignment of the calixarene producing a cubic packing arrangement with the calixarene molecules of each sheet arranged directly above each other. This disruption of the packing of the calixarene molecules affects the orientation of the acetonitrile molecule located within the void formed between the cavity of a calixarene and the pendant chains of a calixarene above. The misalignment of the acetonitrile causes the distance between the annulus and the nitrogen to be too great to form hydrogen bonding interactions. At closest contact (N(1) ⋯ H(21) = 3.15 Å (N(1) ⋯ C(21) = 4.35(10) Å)).

The second structure is a polymorph of the acetonitrile clathrate which has the same ratio of water to the acetonitrile (2:1) shown in the previous structure. A different architecture has been produced which possesses significantly higher molecular and packing symmetry; Only one quarter of the calixarene is crystallographically unique because the structure is in space group $P4_2/ncm$ with the mirror planes passing through the centre of the calixarene.

The higher symmetry polymorph ($C_{40}H_{44}O_{12} \cdot (CH_3CN) \cdot 3(H_2O)$) forms a similar packing motif to the lower symmetry polymorph with a layer arrangement with alternating up-down intra-layer arrangement of the calixarene molecules being shown (as seen in Figure 88). The difference between the structures sheet motifs is the uneven surface of each sheet in the higher symmetry polymorph, the intra-sheet interactions cause an alternating height difference between the constituent calixarene molecules within the sheet. The water molecules which are present in the crystal lattice are *exo* to the cavity of the calixarene, therefore there is no disruption of vertical parallel arrangement of the calixarenes. Hydrogen bonds are formed between the upper rim of the calixarene and the pendant chains of the calixarene above (H(3B) $\cdots$ O(2) = 1.99 Å (O(3) $\cdots$ O(2) = 2.80(4) Å)).
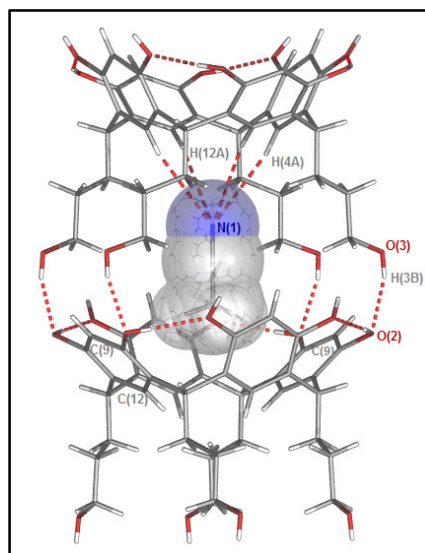
Figure 88 - *C*-(3-Propanol)-calix[4]pyrogallolarene acetonitrile water clathrate (*exo* water molecules removed for clarity)

The phenolic groups which are involved in hydrogen bonding to the pendant chains form a π-π stacking motif and the closest approach is between a centroid generated between C(9) and C(12) and a symmetry generated C(9) (3.70 Å). This distance is within the accepted limits for this type of interaction.[8]

The acetonitrile molecule is completely enclosed in the cavity which is formed between the pendant chains of one calixarene and the cavity of a second calixarene. This is a similar binding motif to that seen in C1Pg and C3OHPg acetonitrile clathrate. However the distance between the nitrogen of the guest molecule and the lower rim of the calixarene is greater than seen in other examples of coordination to the annulus (N(1) ⋯ H(12A) = 3.28 Å (N(1) ⋯ C(12) = 4.19(6) Å), N(1) ⋯ H(4A) = 3.18 Å (N(1) ⋯ C(4) = 4.09(6) Å)). The distance is at the upper limit of a weak hydrogen bond proposed by Jeffrey. [7]

The phenolic hydroxyl groups which are not involved in hydrogen bonding to the calixarene directly above form intra-sheet hydrogen bonds to the adjacent calixarene which is orientated in the opposite direction (H(1B) ⋯ O(3) = 1.85 Å (O(1) ⋯ O(3) = 2.66(4) Å)) as shown in Figure 89 below.
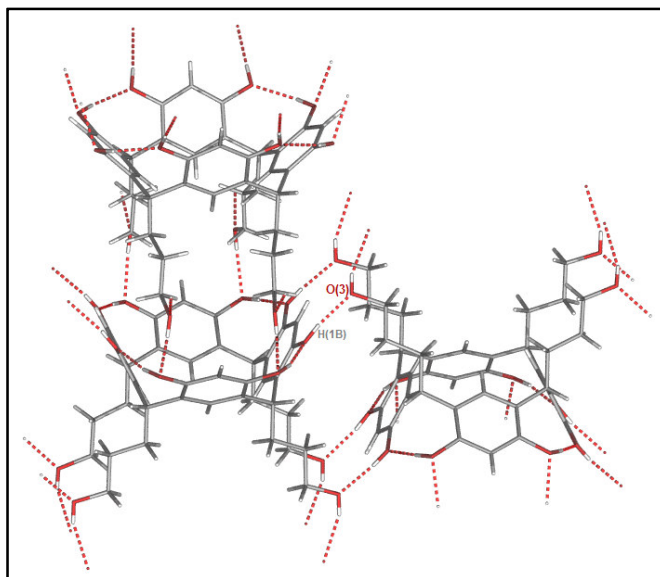
Figure 89 - *C*-(3-Propanol)-calix[4]resorcinarene acetonitrile water clathrate

4   *C*-(4-nitrophenyl)-calix[4]pyrogallolarene

In order to access amino-substituted calixarenes, C-(4-nitrophenyl)-calix[4]pyrogallolarene was synthesised from its corresponding aldehyde with the plan in mind to hydrogenate the resulting product. The synthesis gave the desired product in good yield and purity under standard calixarene synthesis conditions of heating in acidic methanol for 6 days at 60°C.
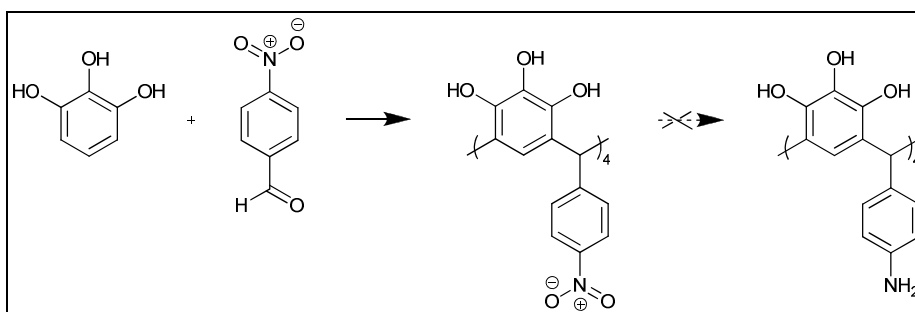
Figure 90 - Synthetic Route to *C*-(4-nitrophenyl)-calix[4]pyrogallolarene

The hydrogenation was unsuccessful in a variety of solvents under atmospheric pressure of hydrogen, however the conditions of the hydrogenation allowed the recrystallisation of the product into crystals suitable for single crystal X-ray diffraction studies. This shows that the prediction of the alpha carbon to the aldehyde was a phenyl group then the chair conformation would dominate, the NMR data also supported this because of the presence of two aryl hydrogen resonances which shows the two conformations.
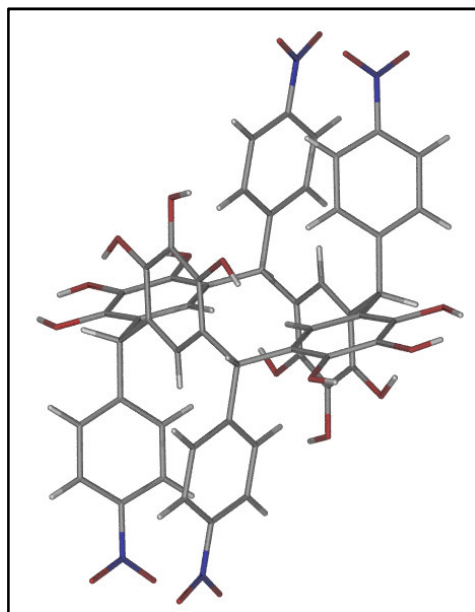
Figure 91 - *C*-(*para*-nitrophenyl)-calix[4]pyrogallolarene

This also shows that aromatic nitro groups could successfully withstand the calixarene synthesis conditions and would be a suitable handle from which to build an amino group. The difficulty in hydrogenation could be due to solubility problems as when the hydrogenation took place in non polar solvents such as toluene significant clumping of the carbon catalyst was observed. When non polar solvents were used then the clumping was not observed. This was speculated to be because the amino groups when formed made the molecule very insoluble in the non-polar solvents and so stuck to the surface of the catalyst making the reaction cease. However when the product was analysed from the polar solvent (methanol) there appeared to be no change.

This success in introducing the nitro functional group into the calixarene system prompted pursuit of an aliphatic nitro-aldehyde, attempts to synthesise this key intermediate however were unsuccessful.

Chapter 6 - Synthesis of halogenated calix[4]pyrogallolarenes

1   Synthesis

Accessing a calixarene with a brominated pendant chain is highly desirable because it allows the further functionalisation of the molecule. This is because bromide is an excellent leaving group and is therefore readily substituted by a variety of nucleophiles.

Taking earlier work on the bromination of the alkene substituted pyrogallolarene into consideration it was found that the approach of functionalising calixarenes was impractical (see section 1.5.1). Therefore this tactic was abandoned in favour of producing an aldehyde precursor bearing a functional group which would both survive the calixarene synthesis conditions and not disrupt the macrocyclisation by hydrogen bonding to the phenolic hydroxyl groups. Halogen functionalised aldehydes were therefore synthesised.

To minimise the number of steps in the synthetic sequence the direct conversion of a bromo-acid to the corresponding aldehyde using 9-BBN was attempted. This failed to give the desired product and intractable mixtures were formed. Therefore the commonly used two step procedure of reducing the acid to the alcohol and then using a mild oxidising agent to produce the corresponding aldehyde was used.
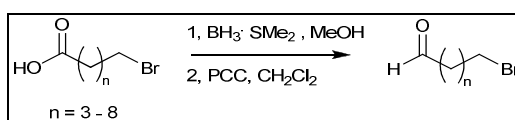
Figure 92 - Synthetic route to 11-Bromoundecanal

The bromo-acids were reacted with borane dimethyl sulphide in freshly distilled tetrahydrofuran. Thin layer chromatography revealed that the starting materials had been consumed after an hour at reflux, after which any residual borane complex was quenched with methanol. The removal of the solvent and the trimethyl borate on a rotary evaporator gave the corresponding bromo alcohol in high yield and purity. These halo-alcohols were oxidised using Corey's reagent (pyridinium chlorochromate) in a dichloromethane solution.[182] The product was separated from the spent oxidising agent by passing the

reaction mixture through a silica plug and eluting it with dichloromethane. The desired bromo-aldehydes was shown to be isolated in high purity by GCMS and NMR analysis.

The bromo aldehyde was reacted with pyrogallol to form the corresponding calixarenes. The solvent free grinding technique was attempted but failed to give the desired product, the NMR of the reactions suggest the reaction produced a mixture of oligomers which were inseparable. When the synthesis was attempted in solution, only 5-bromopentanal, 6-bromohexanal and 11-bromoundecanal gave products which could be isolated from the reaction mixture. When the reaction mixture was cooled in an ice-bath the product was precipitated from the reaction with crystals of sufficient quality to be submitted for X-ray crystallography analysis. Unfortunately the remaining bromo calixarene syntheses failed to yield product.
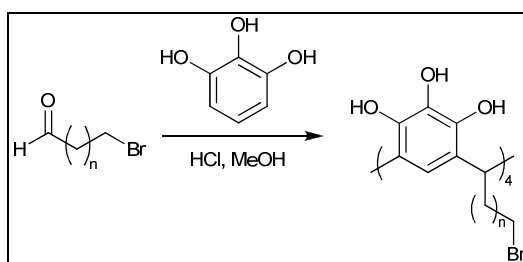
Figure 93 - Synthetic route to *C*-(bromo-alkyl)-calix[4]pyrogallolarenes

Aldehyde	Yield of calixarene %
3-Bromopropanal	0
4-Bromobutanal	0
5-Bromopentanal	49
6-Bromohexanal	43
8-Bromooctanal	0
11-Bromoundecanal	56

Table 4 - Yields of brominated calixarenes

Upon analysis of X-ray data collected on crystals of C4BrPg and C5BrPg the thermal parameters of the terminal atom did not match with those expected for bromine. On close inspection of the mass spectra it showed that there had been a substitution of the bromine atom on the pendant chains for a chlorine atom. As the GCMS and NMR results for the aldehyde synthesis show conclusively that

bromo-aldehydes had been produced, halogen exchange must be taking place during the calixarene synthesis.

As the sole source of chloride in the calixarene synthesis was the hydrochloric acid catalyst, a reaction was performed to see if the presence of pyrogallol was essential for bromine substitution. This was achieved by submitting the aldehyde to the calixarene synthesis reaction conditions in the absence of pyrogallol. The reaction was monitored by gas chromatography-mass spectroscopy (GCMS) analysis which shows halogen exchange taking place *via* an enol-derived cyclic intermediate which is subsequently ring opened to the chloro-aldehyde.
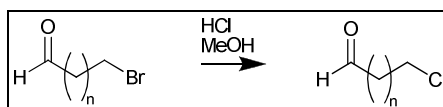
Figure 94 - Halogen exchange in aldehydes

Attempts to repeat the calixarene synthesis with hydrobromic acid as the catalyst failed to yield the desired bromo-calixarene. Three possible reasons for the failure of the reaction under hydrobromic acid catalysis have been considered: The increased strength of the acid catalyst may destroy either the aldehyde or open the calixarene macrocycle and allow oxidation of the pyrogallol rings. Thirdly under the reaction conditions there may have been nucleophilic substitution of the bromide by the phenolic hydroxyl group, producing cross linked polymers in a similar manner to that which is suspected in the bromination of the alkene substituted calixarene.

Crystals of the C4ClPg have been grown from diethyl ether, methanol, ethanol, isopropanol and acetonitrile.

2   *C*-(4-Chlorobutane)-calix[4]pyrogallolarene diethyl ether clathrate

Crystals were grown from a saturated solution of *C*-(4-chlorobutane)-calix[4]pyrogallolarene in diethyl ether which had been sonicated for 30 minutes and left to slowly evaporate. On solution of the diffraction data, the structure which is formed is in space group $P\bar{1}$ with one calixarene and two solvent molecules comprising the asymmetric unit ($C_{44}H_{52}O_{12}Cl_4 \cdot 2(CH_3CH_2OCH_2CH_3)$). The $P\bar{1}$ symmetry operation imparts a head-to-head bilayer packing motif on the calixarenes. There is extensive disorder of the terminal atoms in three of the four pendant chains, in one of the pendant chains (C(41) – C(44)) there is a complete split of the pendant chains at C(41) with the chain being disordered over two positions. In all of the pendant chains there is an extremely close contact with the interdigitating calixarene towards its annulus.
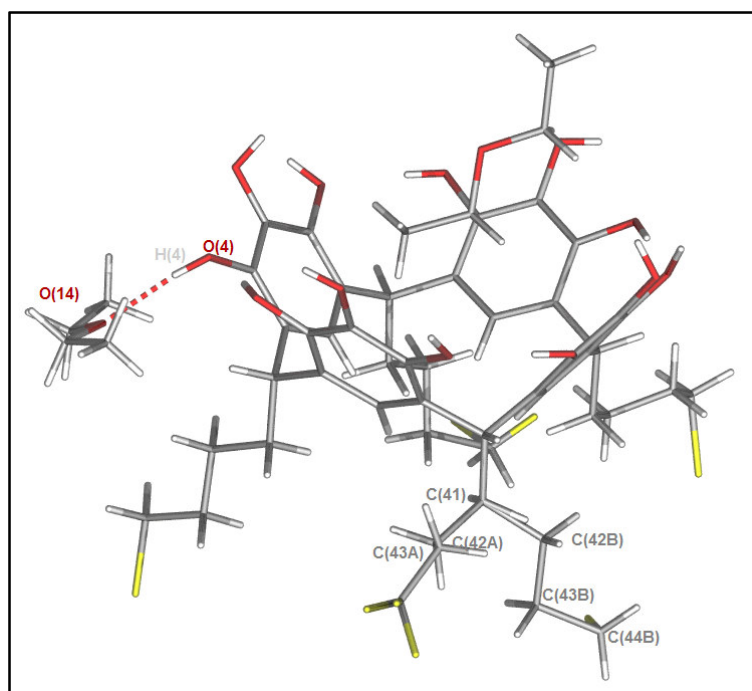
Figure 95 - *C*-(4-Chlorobutane)-calix[4]pyrogallolarene diethyl ether clathrate

One of the ether molecules resides within the cavity of the calixarene in a similar arrangement to that of C1Pg diethyl ether clathrate. However, unlike the former structure, the ethyl group of the guest molecule which is above the upper rim of the calixarene (C(47) & C(48)) does not reside in the cavity of a symmetry generated calixarene. The second ethyl group is therefore *exo* to the calixarene. The

guest molecule is held within the cavity by van der Waals interactions between the ethyl group of the chains and the aromatic rings of the cavity wall. It also held by hydrogen bonding to the next bilayer forming a bond to the upper rim of a calixarene between O(13) and H(1) (O(13) ⋯ H(1) = 1.93 Å (O(13) ⋯ O(1) = 2.71(5) Å)). The second solvent molecule resides exclusively *exo* to any calixarene cavity, but forms a strong hydrogen bond to the upper rim of the calixarene (O(14) ⋯ H(4) = 1.86 Å, (O(14) ⋯ O(4) = 2.69(6) Å)).
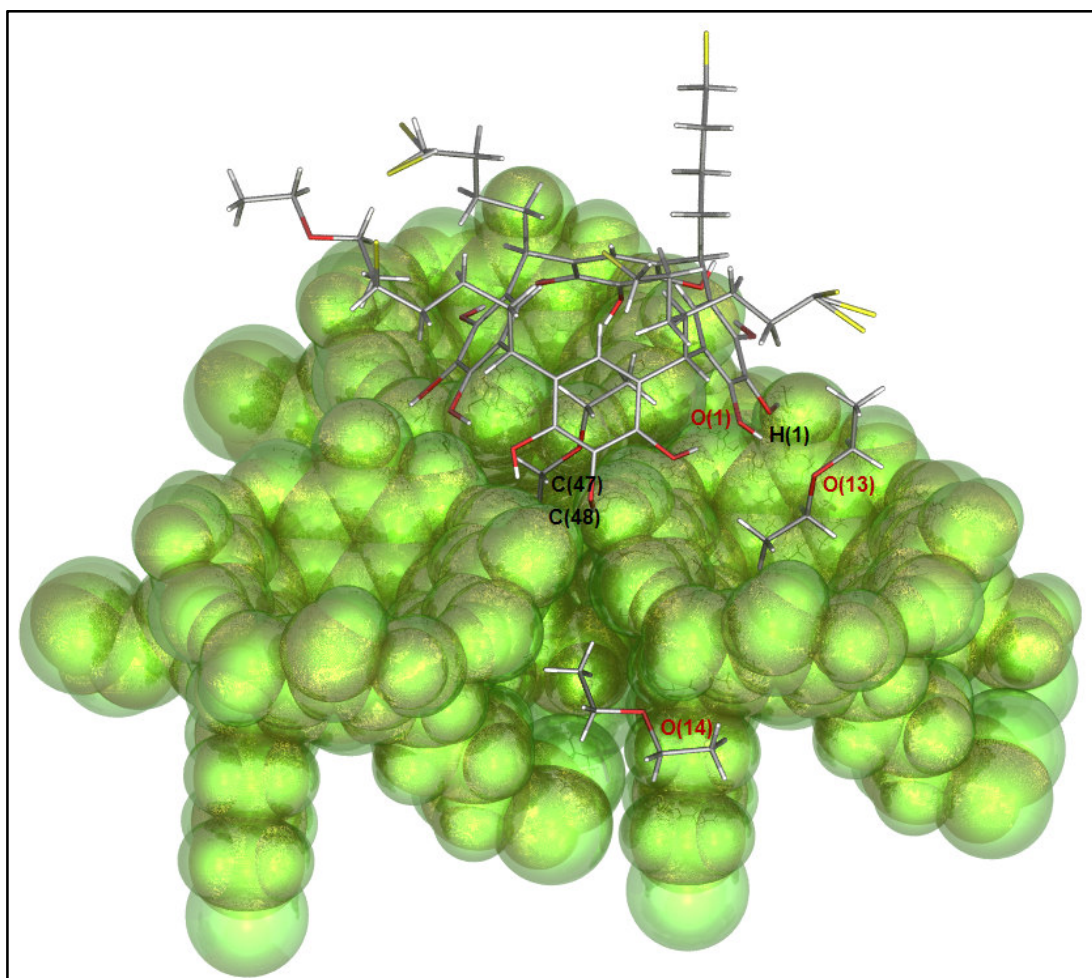
Figure 96 - Bilayer packing motif for C4ClPg diethyl ether clathrate

3   *C*-(4-Chlorobutane)-calix[4]pyrogallolarene propan-2-ol clathrate

Crystals of *C*-(4-chlorobutane)-calix[4]pyrogallolarene 2-propanol clathrate ($C_{44}H_{52}O_{12}Cl_4 \cdot (CH_3CH(OH)CH_3) \cdot 5H_2O$) were grown by slow evaporation of a saturated solution of *C*-(4-chlorobutane)-calix[4]pyrogallolarene in propan-2-ol. The molecular structure generated from the data shows a higher degree of symmetry than the diethyl ether clathrate being in space group $P2_1/c$. The asymmetric unit contains 7 molecules; one calixarene, one propan-2-ol and five water molecules. In addition to the higher symmetry which is present, the molecule has significantly less disorder affecting its pendant chains, with only a single terminal chloride atom (Cl4) being disordered over two positions.
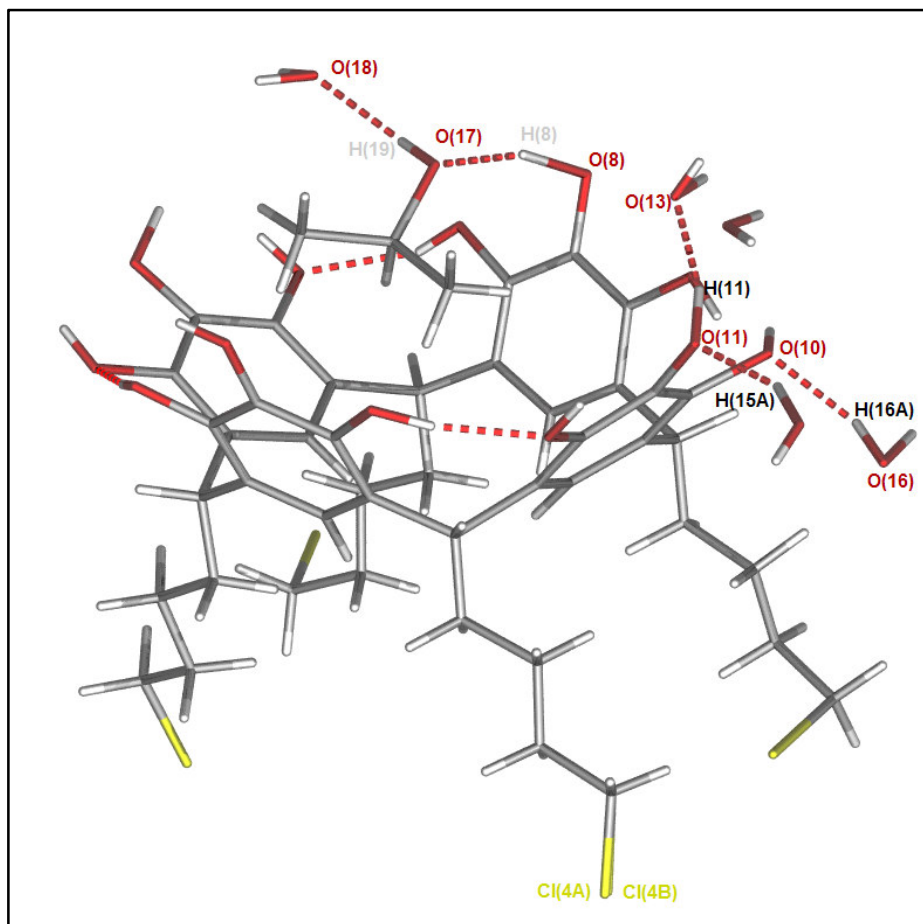
Figure 97 - *C*-(4-chlorobutane)-calix[4]pyrogallolarene 2-propanol water clathrate

Due to its bulky methyl groups and ability to form hydrogen bonds with the upper rim, the 2-propanol guest molecule is tilted to an angle of 85° and forms a hydrogen bond between O(17) and H(8) is 1.76 Å long with the inter-oxygen distance 3.05 Å.

Due to the tilting of the molecule there is a considerable distance between the atom which is furthest within the cavity and a plane created from the average positions of C(1), C(12), C(23), C(34) (H(45A) – plane C(1),C(12),C(23),C(34) = 2.20 Å and C(45) – plane C(1),C(12),C(23),C(34) = 2.98 Å) . This creates a void at the base of the cavity which is larger than observed in other examples reported in this thesis: for example – *C*-methyl-calix[4]pyrogallolarene acetonitrile clathrate has a separation between the plane of the annulus and the closest atom of the guest molecule to be 2.02 Å (H(17B) – C(1)/C(9) plane and C(17) – C(1)/C(9) plane = 2.35 Å).

4   *C*-(4-Chlorobutane)-calix[4]pyrogallolarene ethanol water clathrate

As expected a bilayer packing arrangement is found in the ethanol clathrate with three ethanol, two water and one calixarene molecule comprising the asymmetric unit ($C_{44}H_{52}O_{12}\cdot2(CH_3CH_2OH)\cdot2H_2O$) .
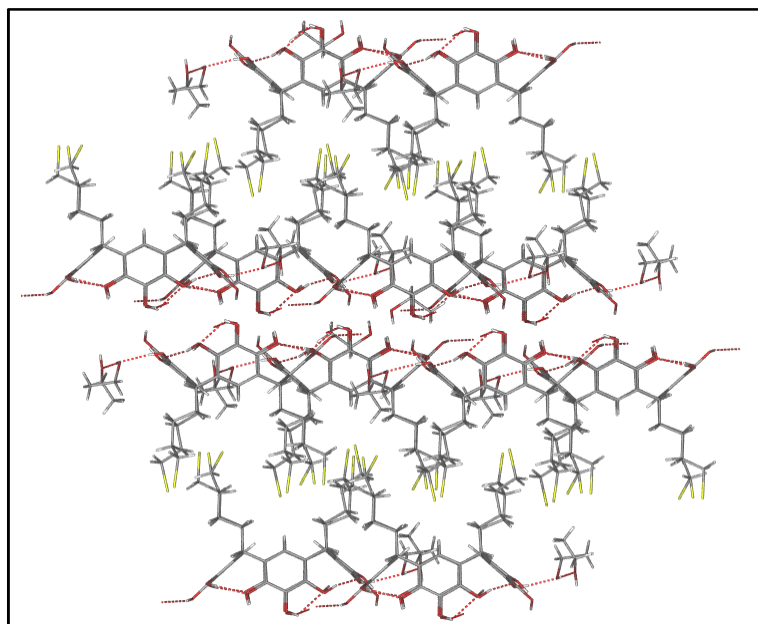
Figure 98 - Packing motif for C-(4-chlorobutane)-calix[4]pyrogallolarene ethanol water clathrate

Two of the ethanol molecules are *exo* to the cavity and fill a void created by the U shaped arrangement of the pendant chains this is highlighted in the cartoon below.
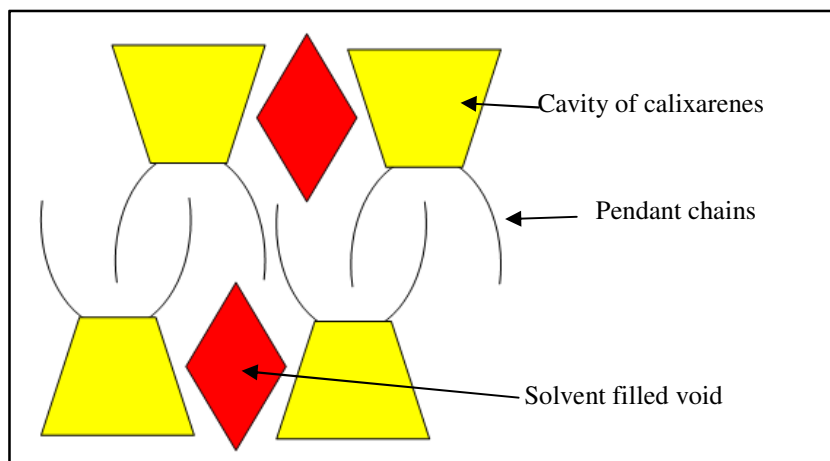
Figure 99 - Packing cartoon of *C*-(4-chlorobutane)-calix[4]pyrogallolarene ethanol water clathrate

The solvent filled void forms a three-molecule (two ethanol and one water molecule) hydrogen bonded linker between the calixarenes: H(1A) ⋯ O(13) = 1.84 Å (O(1) ⋯ O(13) = 2.66(7) Å), H(13) ⋯ O(14) = 1.85 Å (O(13) ⋯ O(14) = 2.68(12) Å), H(14) ⋯ O(16) = 1.94 Å (O(16) ⋯ O(14) = 2.76(13) Å), H(8A) ⋯ O(16) = 1.99 Å (O(8) ⋯ O(16) = 2.76(8) Å).

In previously reported examples of calixarene bilayers where the pendant chains are strongly interdigitated there is distortion of one of the pendant chains in a direction which is parallel to the plane of the bilayer. This allows the voids between calixarene walls to be filled and interdigitation to take place. In C7Pg diethyl ether and ethanol clathrates, this distorted pendant chain forms the base of a solvent filled void. In the molecular structure of C4ClPg the pendant chains are strongly interdigitated but are too short to allow distortion to take place and are therefore all aligned in the same direction. The interdigitation is made possible by the increased polarity of the chloride group allowing interactions with the annulus of the calixarene on the opposite face of the bilayer and also creating a sufficiently polar environment in which the ethanol molecules can reside between the calixarenes.
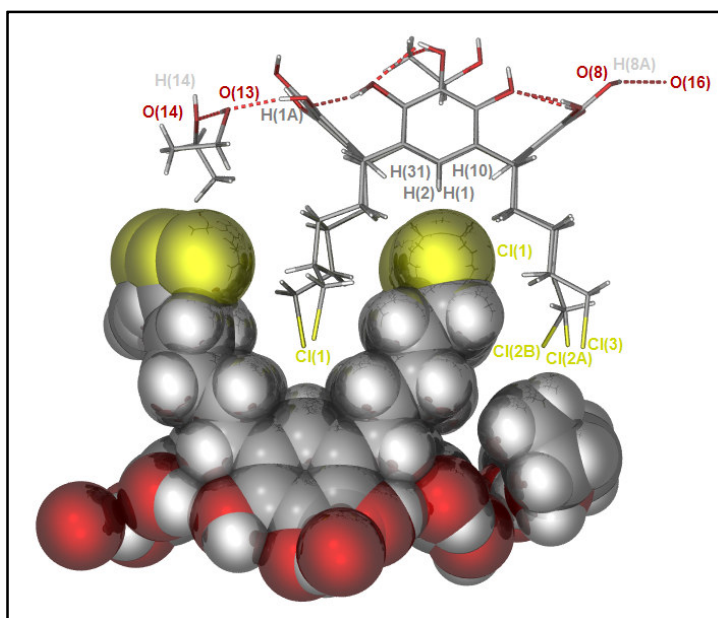
Figure 100 - Interdigitation of pendant chains in *C*-(4-chlorobutane)-calix[4]pyrogallolarene ethanol water clathrate

The mean separation between the calixarene's annulus and the chloride atom is 3.39 Å (Cl(1) ⋯ H(1), H(2), H(10), H(31) and Cl(1) – C(1), C(12), C(23), C(34) = 4.30 Å) this is a larger value than the interactions between the annulus of a calixarene and acetonitrile previously reported, however the significantly larger ionic radius of the chloride is not taken into account. Therefore no void is formed below the annulus.

Only a single inter layer hydrogen bond exists between the hydroxyl group of the endo ethanol molecule and the upper rim of the calixarene in the next layer. (H(10A) ⋯ O(17) = 1.96 Å (O(10) ⋯ O(17) = 2.76(8) Å)).

5 *C*-(5-Chloropentane)-calix[4]pyrogallolarene ethanol clathrate

Crystals of C5ClPg were grown from a saturated solution of ethanol. As expected from data gathered in C-alkyl-calix[4]pyrogallolarenes a bilayer packing motif is formed by the three molecules of the asymmetric unit undergoing the inversion operation of the $P\bar{1}$ space group $C_{48}H_{60}O_{12} \cdot 2(CH_3CH_2OH)$.

In a manner like the previously reported long-chain pyrogallolarene – ethanol clathrates there are two solvent molecules in the asymmetric unit, one of which is bound by the cavity, and the second of which resides externally of the cavity of the calixarene. The *exo* solvent molecule resides within the interstices created by the cubic packing of the calixarene molecules and forms hydrogen bonds to the upper rim of the calixarenes which surround it. H(14) $\cdots$ O(6) = 2.68 Å (O(14) $\cdots$ O(6) = 3.23(4) Å), H(9) $\cdots$ O(14) = 2.17 Å (O(9) $\cdots$ O(14) = 2.77(3) Å).
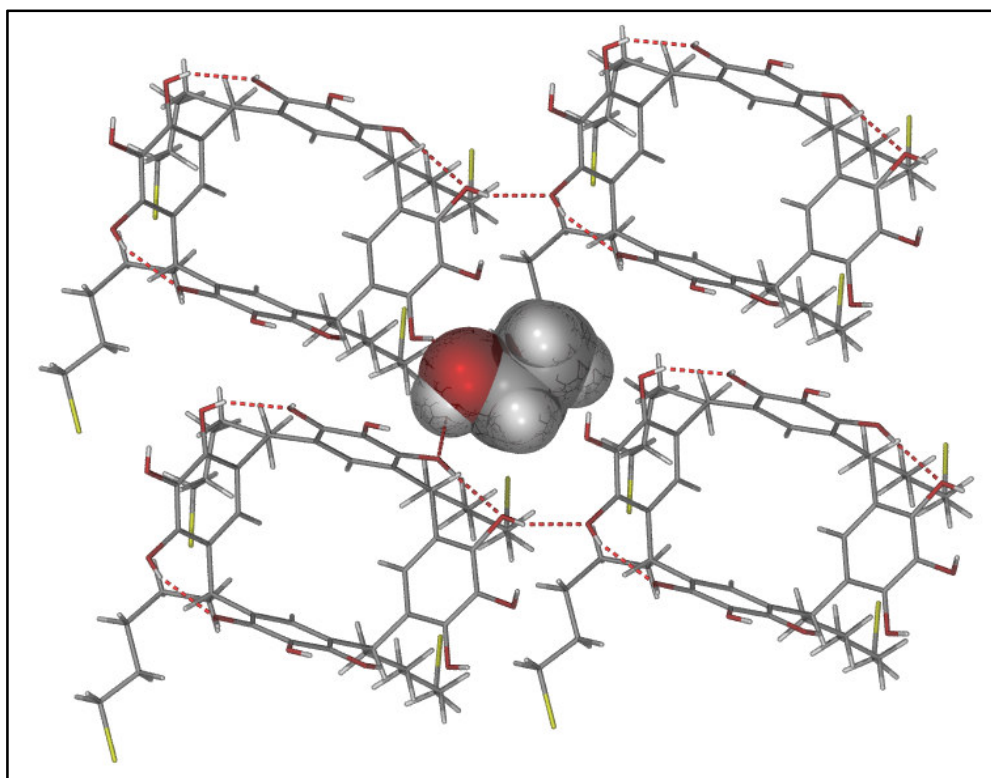
Figure 101 - Location of *exo* ethanol molecule in *C*-(5-Chloropentane)-calix[4]pyrogallolarene ethanol clathrate (*endo* solvent molecules removed for clarity)

Unusually the terminal chloride atoms do not form hydrogen bonds to the annulus of the calixarene forming the opposite face of the same bilayer, and are directed parallel to the plane of the bilayer. This enables very close packing of the bilayer, and the distance between upper rims of opposite faces of the same bilayer is 16.29 Å. (for the unfunctionalised C5Pg MeCN clathrate the inter-upper rim distance is 16.00 Å). Cl(1) forms a van der Waals interaction with its symmetry generated counterpart, Cl(2) and Cl(3) both form hydrogen bonds to the terminal methylene groups of opposite calixarene molecules (Cl(3) ⋯ H(24A) = 2.95 Å (Cl(3) ⋯ C(24) = 3.76(8) Å), Cl(2) ⋯ H(12A) = 3.31 Å (Cl(2) ⋯ C(12) = 3.97(9) Å)). Finally Cl(4) is attached to the pendant chain which is parallel to the plane of the bilayer. This can be seen in Figure 102 below.
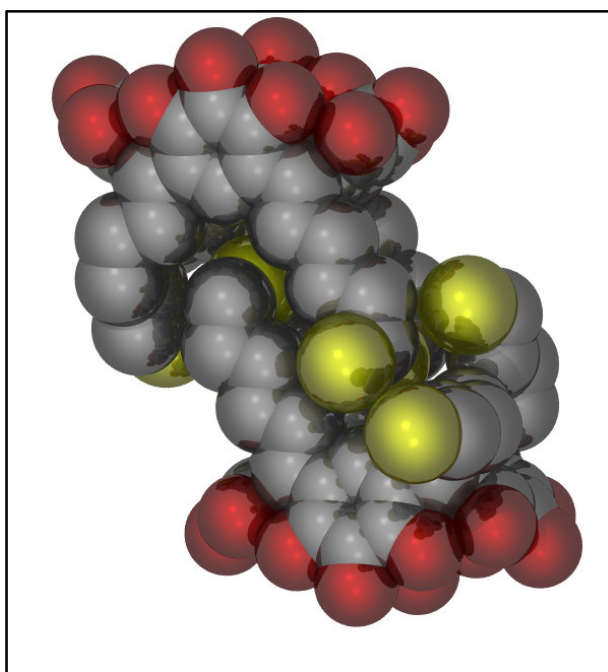
Figure 102 - Detail of interdigitation of pendant chains in *C*-(5-chloropentane)-calix[4]pyrogallolarene ethanol clathrate (hydrogen atoms and solvent molecules removed for clarity)

6 Solid state structures of *C*-(10-bromodecane)-calix[4]pyrogallolarene methanol and ethanol clathrates

C-(10-Bromodecane)-calix[4]pyrogallolarene was successfully synthesised using traditional solvent methods. There was no halogen exchange observed between the calixarenes which may be a result of the increased chain length preventing formation of a cyclic intermediate in the halogen exchange reaction. Two crystal structures were obtained by the slow evaporation from saturated solutions of methanol and ethanol ($C_{68}H_{100}O_{12}Br_4 \cdot 4(CH_3OH)$) and ($C_{68}H_{100}O_{12} \cdot xCH_3CH_2OH$).

Unusually the calixarene system, C10BrPg formed capsular architectures in the solid state when crystals were grown from ethanol and methanol. This is highly unusual because in addition the examples discussed in the previous section showing methanol and ethanol clathrates of *C*-alkyl-calix[4]arenes in bilayer packing motifs there is also wide literature precedent for polar protic solvents to break up the capsular architecture.[106, 115]
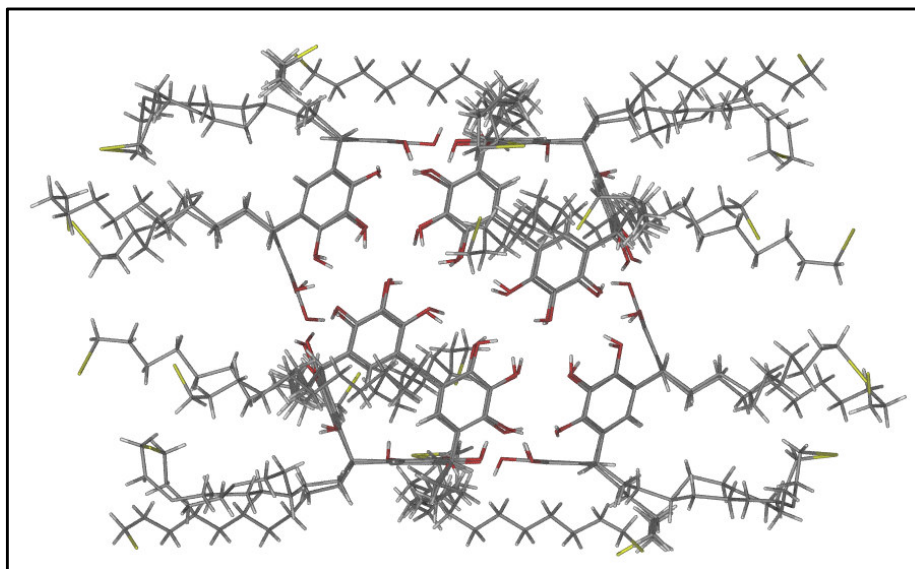
Figure 103 - Nano-capsule formed by *C*-(10-bromodecane)-calix[4]pyrogallolarene ethanol clathrate

In the ethanol clathrate the contents of the capsule could not be conclusively assigned due to extensive disorder, therefore the interior of the capsule was modelled as diffuse electron density. This loss of order in the ethanol sphere may be a result of the slightly more lipophilic and conformationally

flexible nature of the guest than the acetonitrile derived capsule whose guests' location could be determined.

The packing of the nano-spheres is very similar to that of the acetonitrile spheres, with a face to face hexagonal packing arrangement. The external solvent molecules which were observed to form a torroidal arrangement between the stacking faces of the nano-capsules are absent in this structure., This lack of solvent molecules is compensated for by the longer pendant chains which form a lipophilic layer between the capsule, with a high degree of molecular symmetry and a helical arrangement of pendant chains. Each gap between the capsules is filled by six calixarenes donating three out of their four chains to the inter-capsule gap.
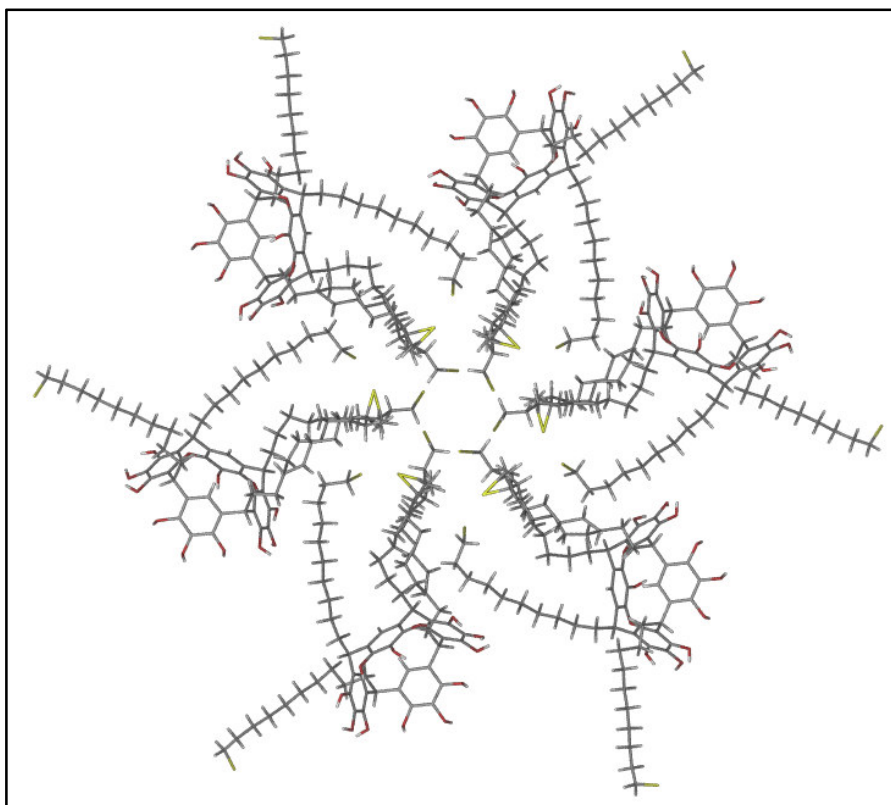
Figure 104 - Inter capsule packing of pendant chains in *C*-(10-bromodecane)-calix[4]pyrogallolarene ethanol clathrate
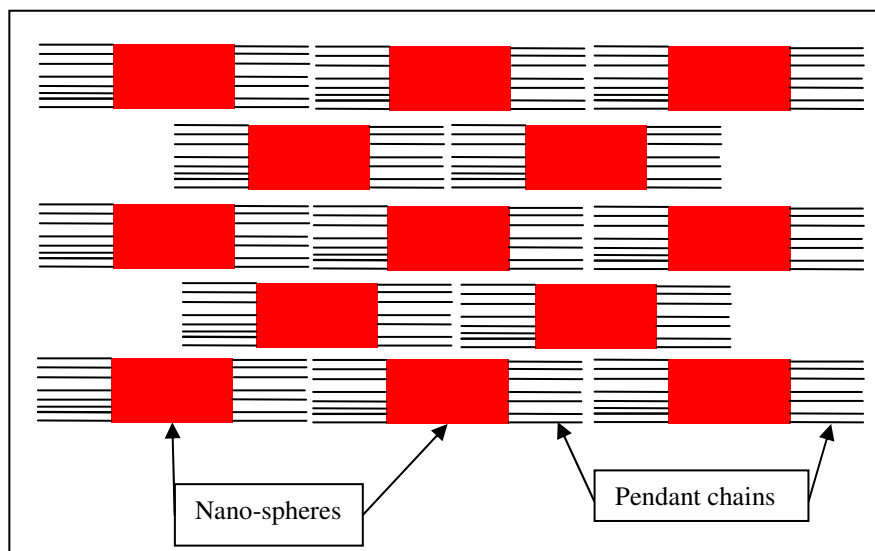
Figure 105 - Cartoon showing packing arrangement of nano-spheres generated by *C*-(10-

bromodecane)-calix[4]pyrogallolarene ethanol clathrate

The methanol nano-spheres have the same arrangement of the pendant chains and therefore show

exactly the same packing arrangement as the ethanol clathrate discussed above. In a significant

difference between the structures, the methanol guest molecules' position can be determined as shown

in Figure 108. This structure shows 24 guest molecules which occupy 65% of the available space.

This is just out of range of the ideal packing coefficient of 55%±9.
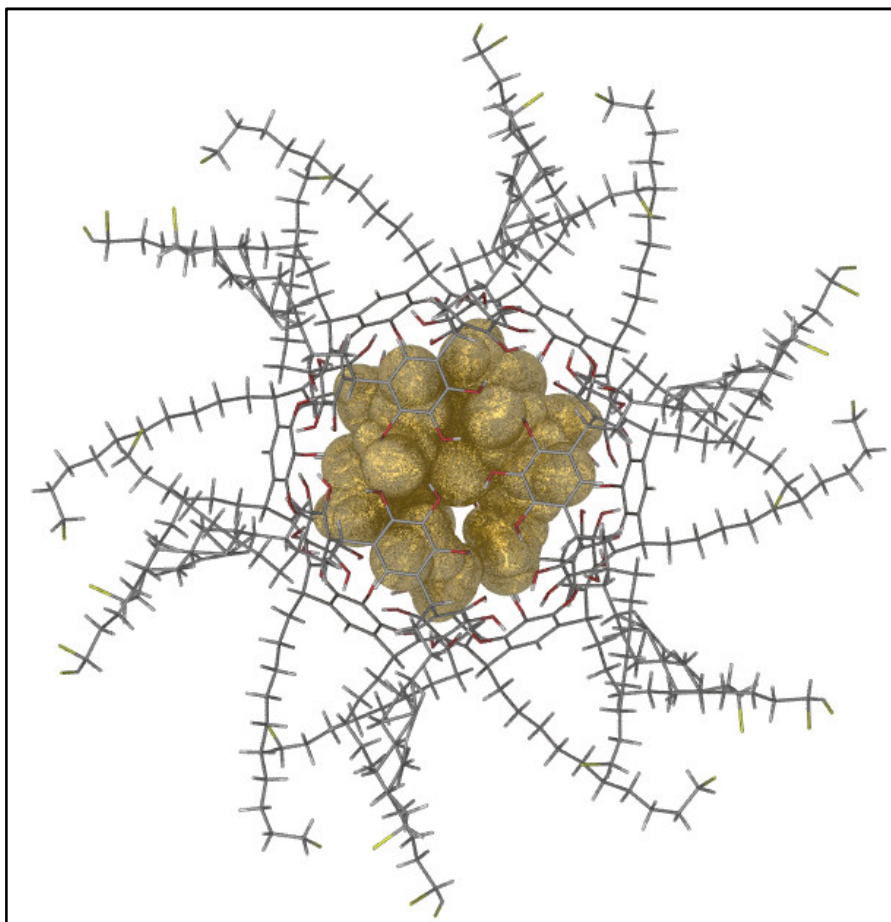
Figure 106 - Nano-capsule formed by *C*-(10-bromodecane)-calix[4]pyrogallolarene methanol clathrate

When compared to the alkene substituted calixarene, the spheres formed from the halogenated derivatives show significant distortion of the macrocycle and therefore capsule due to the more polar guests which have been included into the nano-sphere. This distortion results in a decrease in molecular volume encapsulated (1213 Å^3 for ethanol clathrate and 1209 Å^3 for methanol clathrate) compared to the previously reported nano-spheres (C4Pg MeCN – 1274 Å^3 and C7Pg EtOAc – 1249 Å^3) this is a significant decrease in molecular volume which is encapsulated.

The pendant chains of the brominated calixarene are aligned in bi-directionally, with a trimer of pendant chains with potential hydrogen bonding interactions between the bromine and the methylene hydrogen atoms of the terminal carbon in the chain. The trimers in the methanol sphere interact with another trimer from an adjacent sphere whose chain is perpendicular to the line of the original chain. The remaining pendant chain is aligned in the opposite direction to the trimer and interacts with the annulus of an adjacent sphere, so each sphere interacts with another six spheres *via* the individual

pendant chain. This is perhaps why the shorter alkyl chained halogenated calixarenes cannot form the

nano-sphere in very polar solvents because trimer formation is prevented.
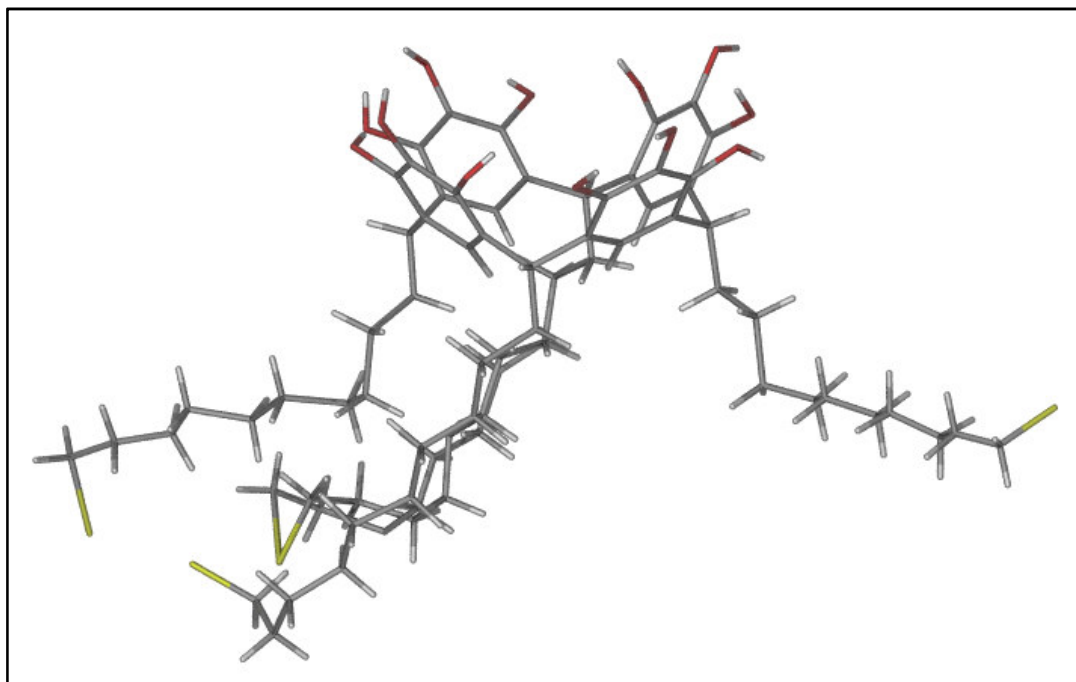
Figure 107 - ASU of *C*-(10-bromodecane)-calix[4]pyrogallolarene ethanol clathrate

7   Behaviour of *C*-(10-bromodecane)-calix[4]pyrogallolarene in solution

Investigation of the behaviour of *C*-(10-bromodecane)-calix[4]pyrogallolarene in solution by DOSY NMR shows that the capsular arrangement is formed in chloroform but is broken down to its constituent monomers in methanol solution.
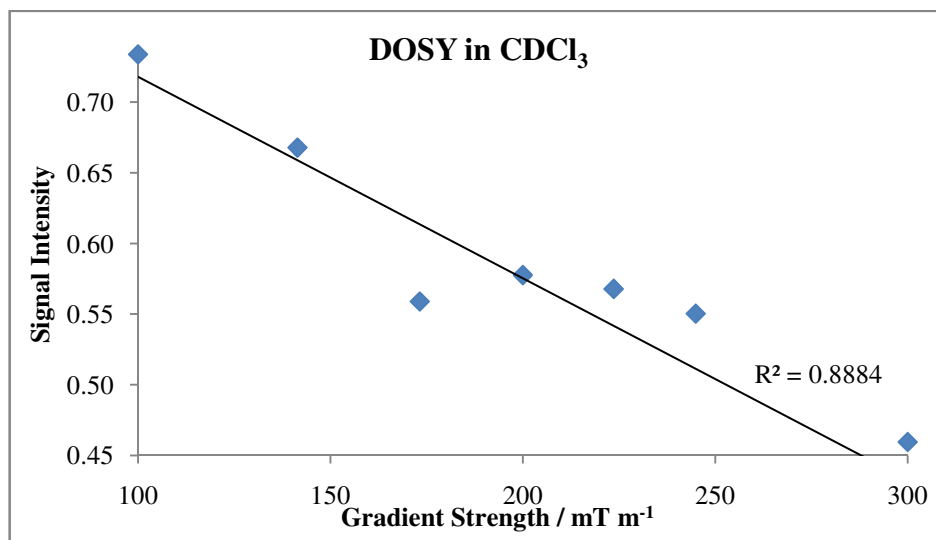
Figure 108 - DOSY NMR data of *C*-(10-bromodecane)-calix[4]pyrogallolarene in CDCl$_3$
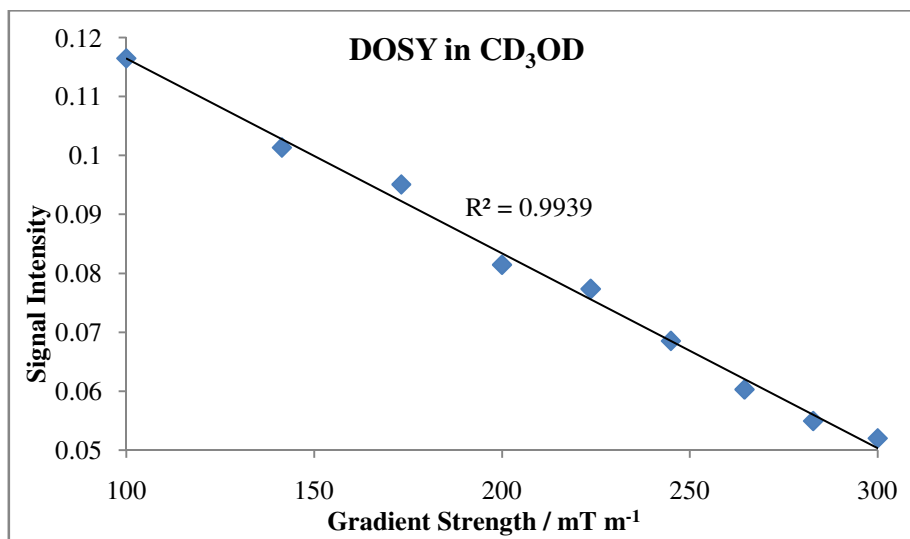
Figure 109 - DOSY NMR data of *C*-(10-bromodecane)-calix[4]pyrogallolarene in CD$_3$OD

In CDCl$_3$, the diffusion coefficient is 2.23×10^{-10} m^{2}s^{-1} therefore the hydrated radius is 17 Å. In CD$_3$OD solution, the diffusion coefficient is 3.66×10^{-10} m^{2}s^{-1} therefore the hydrated radius is 10 Å. In CD$_3$OD

the diffusion coefficient corresponds to that of a monomeric calixarene. This shows that in alcoholic solution the material is in its monomer form but when crystals are grown of the material, the calixarene self assembles into a sphere conformation.

The imperfect correlation between the calculated molecular size of the monomer and the hydrated radius which is derived from the Stokes-Einstein equation is due to the shape of the calixarene. The Stokes Einstein equation is designed for spherical species, while the long alkyl chain of the calixarene gives it a more cylindrical shape. The difference in molecular size is sufficiently large to differentiate between the monomer and the sphere conformation.

The formation of nano-spheres in the solid state by halogenated calixarene derivatives could be due the weak bonds between the trimer of pendant chains which is strong enough to overcome the destructive force of the polar protic solvents. This could be tested by the synthesis of fluorinated derivatives which would show a stronger bond as the electronegativity of the fluoride is significantly higher.

Chapter 7 - Synthesis of cyano substituted calix[4]pyrogallolarenes

1   Introduction

To overcome the problem of denaturation of calixarenes during their functionalisation with basic reagents, the aldehyde used for the calixarene synthesis was substituted with a functional group. This culminated in the synthesis of cyano functionalised calixarenes. It was envisioned that the cyano group would be hydrolysed to the corresponding carboxylic acid during the calixarene synthesis, therefore providing a scaffold from which to bind peptide sequences to the calixarene scaffold.
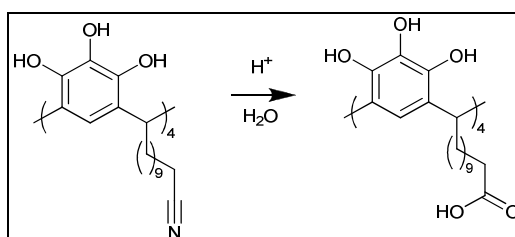
Figure 110 – Cyano-calixarene to carboxyl calixarene

2   Synthesis

The commercially available bromo-carboxylic acid was reduced using borane methyl sulphide complex in THF to yield the corresponding 11-bromoundecanol (step A). A simple nucleophilic substitution of the bromide using sodium cyanide in DMF, gave the cyano alcohol in quantitative yield (Step B). 11-cyanoundecanol was smoothly oxidised to the corresponding aldehyde (step C) using Corey's reagent (pyridinium chlorochromate) in 72% yield over the three steps.
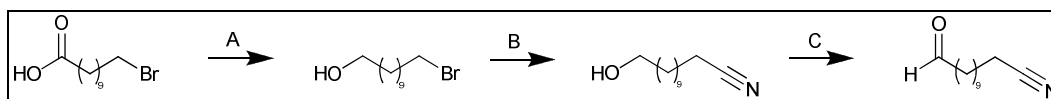
Figure 111 - Synthetic route to 11-cyanoundecanal

The calixarene synthesis was attempted both under conditions developed during the synthesis of the calixarene library (6 days heating at 60°C in acidic ethanol solution) and by green techniques of grinding the aldehyde and pyrogallol together with a pestle and mortar and an automatic pestle and

mortar. The green techniques failed to produce the desired product and only produced a resinous orange material which failed to be recrystallised from any solvent and the NMR failed to show product formation, therefore the reactions were abandoned.
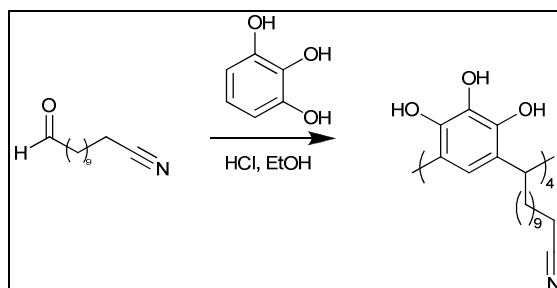
Figure 112 - Synthetic route to *C*-(10-cyanodecane)-calix[4]pyrogallolarene

The standard conditions using a strongly acidic solution of ethanol proved successful but only gave the desired calixarene in 15 % yield. A low yielding step so far down a synthetic sequence is obviously undesirable but investigations have shown it to be unavoidable. There is, however, potential for further refinement of the method which is used in order to improve the yield. The product was isolated by crystallisation from the reaction mixture during cooling in an ice bath after 6 days heating at 60°C, the crystals which grew were suitable for single crystal X-ray diffraction studies.

As there was strong literature precedent for the hydrolysis of nitrile groups in strongly acidic alcohol solutions, it was expected that the nitrile would hydrolyse to the corresponding acid substituted calixarene.[183] The crystalline precipitate which formed on cooling the reaction mixture was analysed by NMR and SC-XRD. Both techniques show hydrolysis had not taken place and the cyano group was preserved during the reaction in both the bulk material and the crystals which formed.
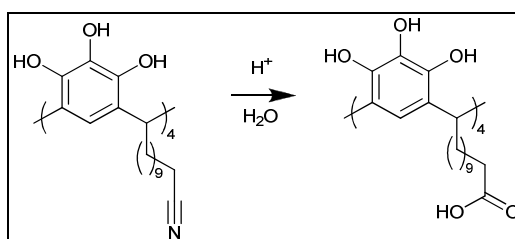
Figure 113 - Proposed route to *C*-carboxyl-calix[4]pyrogallolarene

154

3 Single crystal X-ray diffraction studies

Because the crystals which were analysed were grown from polar protic solvents it was expected that a bilayer packing motif would be formed, however it was found that an unusual capsule packing arrangement was formed.
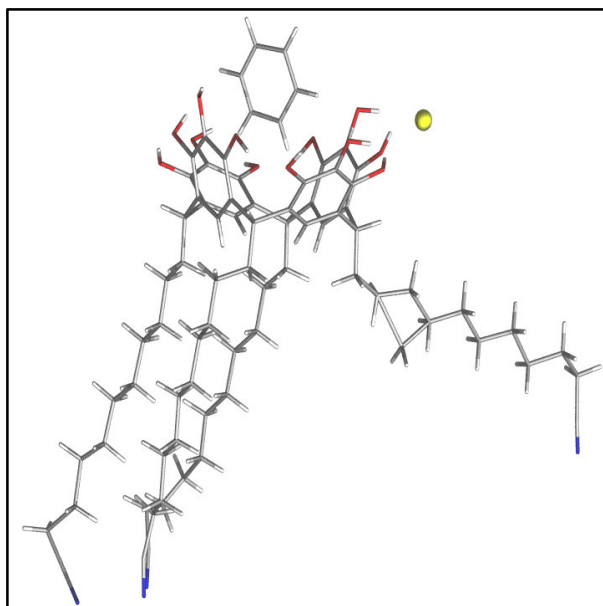
Figure 114 - SCXRD image of *C*-(10-cyanodecane)-calix[4]pyrogallolarene

The cyano-calixarene forms a chloride gated, dimeric capsule, enclosing a single benzene molecule $(2(C_{72}H_{100}N_4O_{12})\cdot(C_6H_6)(2HCl))$. The benzene was an impurity in the reaction solvent. The benzene molecule (molecular volume 77.4 $\mathring{A}^3$) occupies 60% of the available volume within the cavity (130 $\mathring{A}^3$).

The cone of the calixarene is slightly distorted, with a distortion factor (D*f*) = 0.83. The D*f* for unfunctionalised *C*-decyl-calix[4]pyrogallolarene ethanol clathrate = 0.97. This distortion may be attributed to either the presence of a non-spherical guest molecule (benzene) causing contraction of the cavity to maximise host-guest interactions or the presence of the chloride ions which interact with the upper rim.
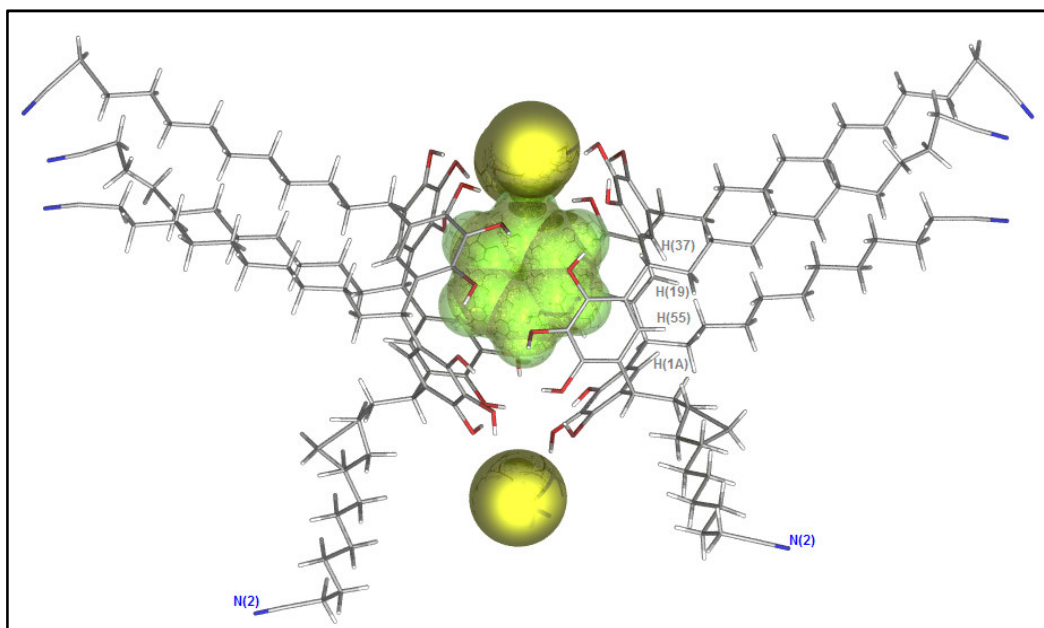
Figure 115 - Dimeric capsule formed by *C*-(10-cyanodecane)-calix[4]pyrogallolarene (Image generated from SCXRD data)

The dimeric capsule is tilted 13.55° from parallel alignment of upper rims, allowing the chloride ions to form an electrostatic interaction with the upper rim (Cl(1) – H(2) = 2.386 Å (Cl(1) – O(2) = 3.168(15) Å)). A monolayer is formed with calixarene molecules alternately rotated through 180°. Uniquely the pendant chains show no interdigitation even though all solid state structures of calixarenes with pendant chains longer than 5 carbons show this type of packing in order to maximise the van der Waals forces between the chains.
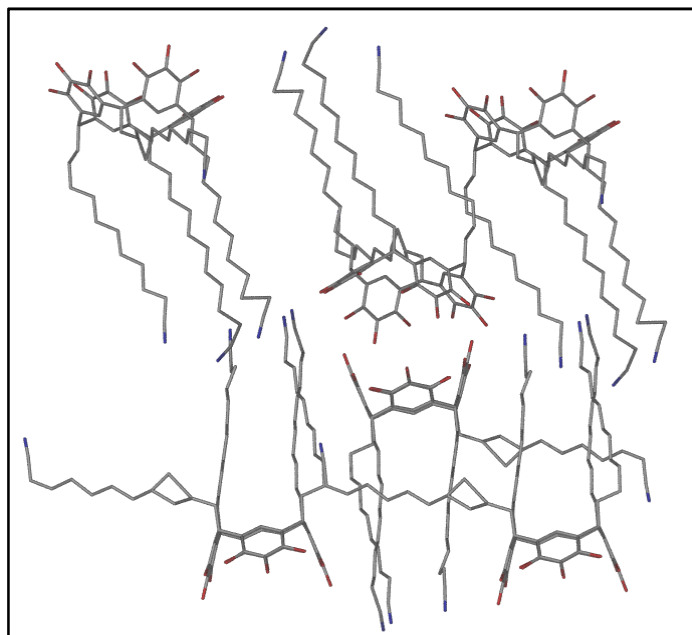
Figure 116 - Alternating monolayer formation of C-(10-cyanodecane)-calix[4]pyrogallolarene hydrochloride benzene clathrate (solvent molecules and hydrogen atoms removed for clarity).

The cyano-calixarene shows a 3:1 split of pendant chains with no interdigitation of the triad of chains but in the isolated chain there is coordination to the annulus of an adjacent calixarene via N(2) as shown in Figure 119. The average distance from cyano nitrogen to hydrogen ions of lower rim is 3.214 Å.
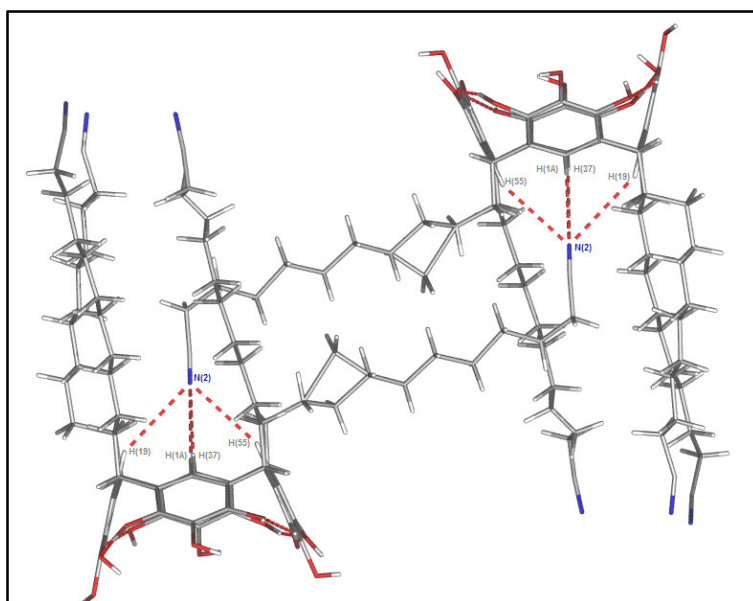
Figure 117 - Coordination of *C*-(10-cyano-decane)-calix[4]pyrogallolarene

Efforts to hydrolyse the cyano group have failed. Subjecting the cyano-calixarene to more vigorous conditions; suspending the solid product in concentrated acid (HCl, HBr, aqueous TFA) and heating, forms a black intractable mixture. This decomposition of the calixarene may be due to hydrolysis of the macrocycle and subsequent oxidation of the phenyl rings.[63]
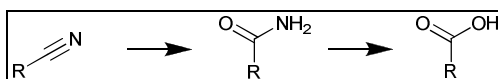
Figure 118 - Hydrolysis of nitrile group

The cyano group also offers the potential to be reduced to the corresponding amine. In the literature it was shown to be very troublesome to hydrogenate a cyano group.[183] This is because the intermediate imine formed, reacts with amines previously produced and results in the production of a mixture of secondary and tertiary amines.
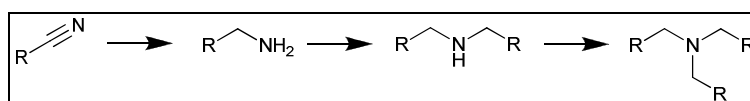
Figure 119 - Reduction of nitrile group

Therefore to avoid this alkylation of the amine groups the reaction can be performed in acetic anhydride or in strongly acidic methanol solution.[183] Both these solutions immediately render the amine un-reactive by acetylation or protonation, under the reaction conditions.
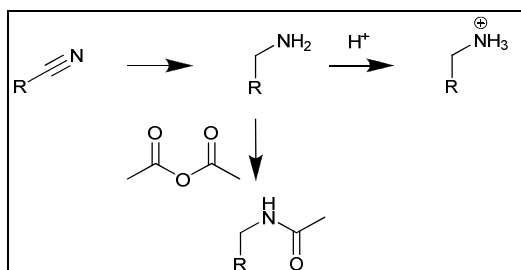
Figure 120 - Protection of amino groups generated from nitrile hydrolysis

Both techniques were attempted using atmospheric hydrogenation apparatus using a palladium on charcoal catalyst (10% metal loading). When the reaction was performed in the strongly acidic conditions did not produce any reduction and starting material was recovered. When the reaction was performed using acetic anhydride as the reaction solvent a new product was found to have formed, which was on further investigation was proved to be a fully acetylated cyano-calixarene. Therefore it can be concluded that under atmospheric pressure which the apparatus available can exert was insufficient for reduction to occur. Reduction of the nitrile group was attempted using $LiAlH_4$, $SnCl_2$ and $BH_3 \cdot SMe_2$ both proving to be unsuccessful with starting materials being isolated after the reaction. This is perhaps due to reagent complexation with the upper rim of the macrocycle in solution, but this theory has not been verified.

4   NMR Studies

The NMR spectrum of the unprotected cyano calixarene is as expected. However when NMR analysis was performed on the acetylated calixarene, the ^{1}H shows no aromatic hydrogen peak and the ^{13}C spectrum showed only a broad peak in the region where the phenyl carbons were expected (100 – 140 ppm) with no resolved peaks which correlate to the phenyl rings. When cooled to –50°C, the solution the broad peak in the ^{13}C spectrum coalesced to well resolved peaks which correspond to the carbon atoms of the phenyl rings.
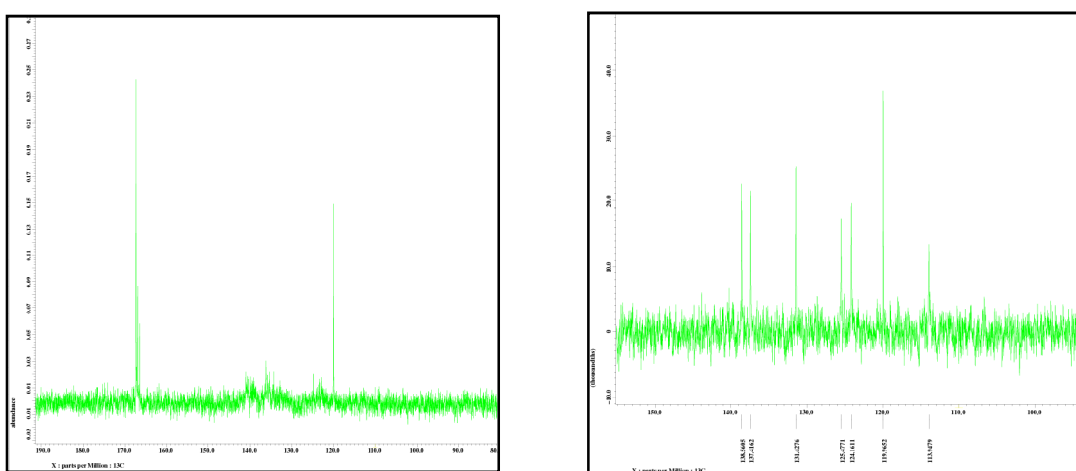
Figure 121 - Resolution of broad peaks in ^{13}C NMR spectra of acetylated cyano-calixarene

This indicates some molecular movement or interconversion was taking place rapidly on an NMR timescale but when it was cooled, the motion was slowed and peaks could be resolved. Taking the work of Höegberg [62] as inspiration this would indicate a conversion between pinched cone conformations.
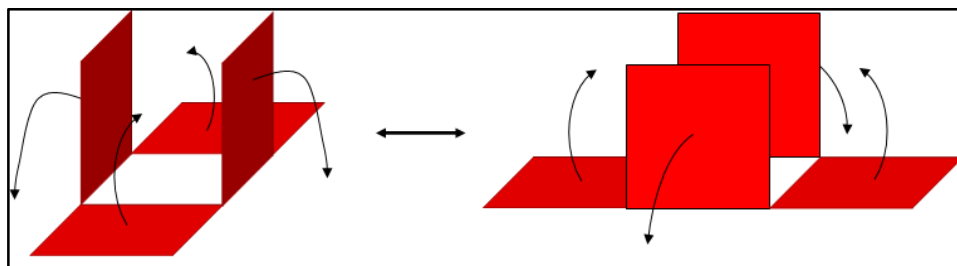
Figure 122 - Interchange between pinched cone conformations in acetylated-cyano-

calix[4]pyrogallolarene

In order to test the capsule forming ability of the pyrogallolarene system, diffusion NMR experiments where carried out on the cyano-calixarene in both chloroform which is known to promote the formation of capsule and methanol where no capsular arrangement of the molecules has been observed.

Diffusion NMR of C10CNPg in CDCl3

$D = 3.024 \times 10^{-10}$ m²/s

$R^2 = 0.923$

X-axis: Magetic Gradient mT/m
Y-axis: Signal Intensity

Diffusion NMR of C10CNPg in CD3OD

$D = 2.964 \times 10^{-10}$ m²/s

$R^2 = 0.9694$

X-axis: Magnetic Gradient mT/m
Y-axis: Signal Intensity
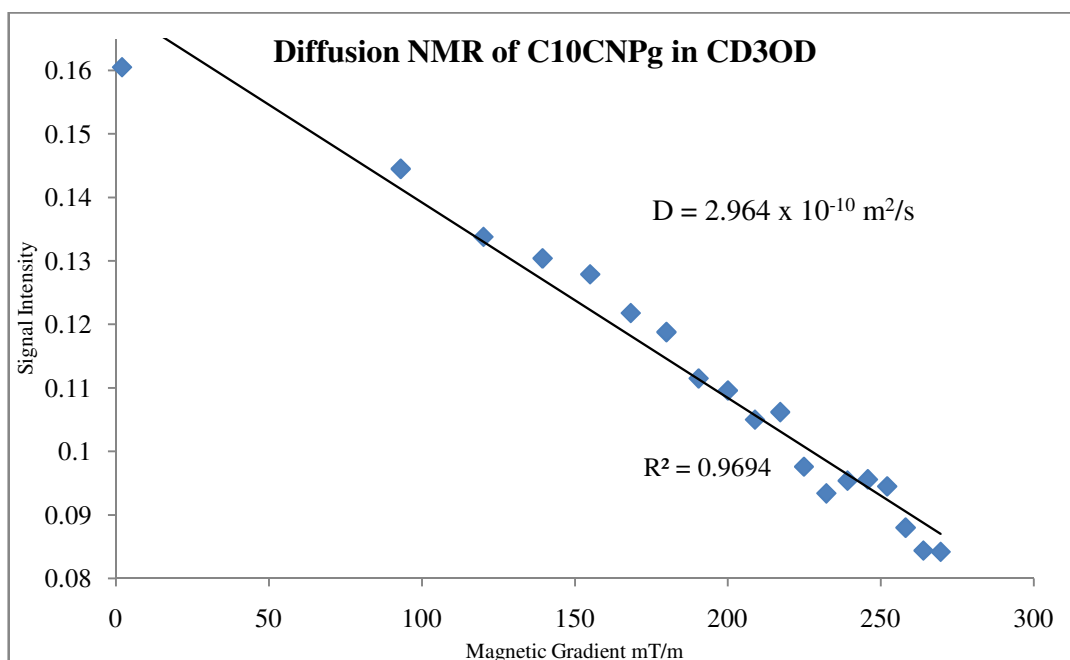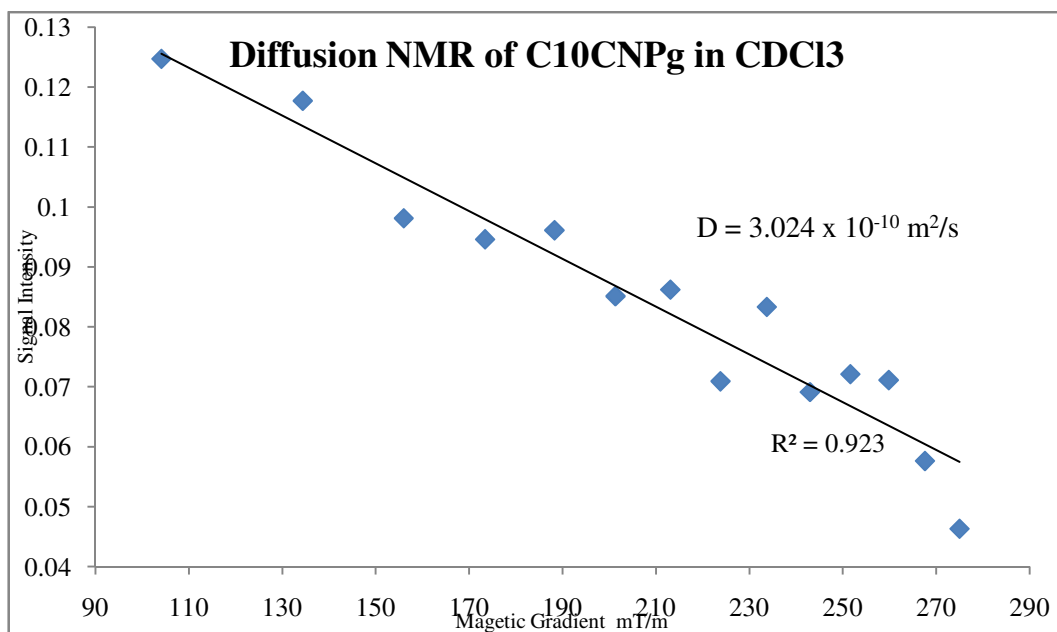
When the Stokes-Einstein equation is applied to this data it shows that even in chloroform, the cyano-calixarene exists as a monomer with a hydrated radius of 12 Å which is not significantly different to

that calculated from the data gathered while in methanol solution (12.4 Å). This shows that in solution the nitrile groups on the pendant chain are sufficiently polar to break up the capsular arrangement of the calixarene nano-sphere.

5   X-ray diffraction studies of acetylated cyano-calixarene

The structure of (undecyl-acetyl)*C*-(10-cyanodecane)-calix[4]pyrogallolarene shows significant differences to the un-protected molecule in both the arrangement of the monomer and the packing motif which it therefore forms. The acetylated molecules are, like their unprotected counterparts arranged in a head-to-head packing motif, however, this is the sole similarity.

The difference in structure is due to the complete acetylation of the upper rim hydroxyl groups and its stereo-electronic effect on the macrocycle. The macrocycle is severely deformed into the pinched cone conformation (distortion factor = 0.674). The strain on the macrocycle also causes deformation of the aromatic rings away from the ideal hexagonal form. The conformation which the macrocycle adopts means that the cavity is no longer available for binding guest molecules and unusually for calixarene molecules there are no solvent molecules entrapped in the crystal lattice. The Figure below is aligned to highlight the pinched cone conformation.
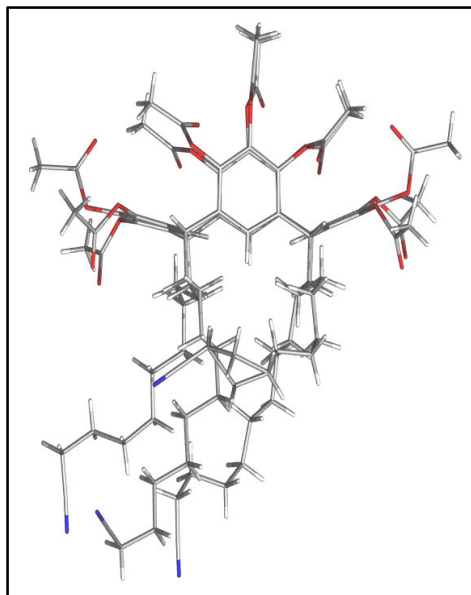
Figure 123 – SC-XRD image of acetylated *C*-(10-cyanodecane)-calix[4]pyrogallolarene

The average distance from cyanide nitrogen to annulus is 2.992 Å which is much closer than unprotected analogue. The acetylation of the hydroxyl groups means that the phenyl rings are slightly more electron deficient than the unprotected cyano as shown in the up-field shift of the peaks. This

electron deficiency allows four hydrogen bonds to form between phenyl hydrogen and nitrile group. This interaction draws adjacent molecules closer, allowing interdigitation of the calixarene's pendant chains.

Even though the ring is more electron deficient when acetylated compared to the acetonitrile solvates (C1Pg MeCN – 2.6 Å) this is a longer hydrogen bond but this could be accounted for by the greater steric encumbrance of the pendant chains which have to become organised. This suggests that it is not only the presence of groups at the terminus of a pendant chain which determine the packing motif but the electron density around the phenyl rings.

In concordance with the structures published by Han *et al.*[58] there are interpenetration of the acetyl groups of the adjacent calixarenes so the acts as a guest to prevent formation of a large unoccupied cavity forming because "nature abhors a vacuum".[184] The dimer is held together with 4 hydrogen bonds between a methyl group of an acetal group and the carbonyl oxygens. In the figure below one monomer is shown in red the other in blue.
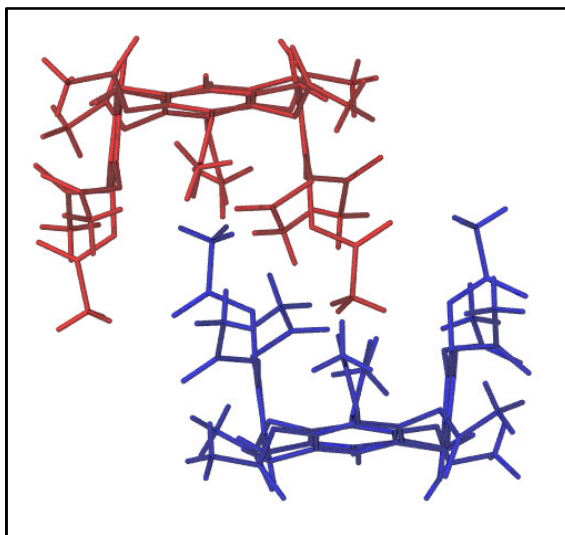
Figure 124 - Dimerisation of acetylated *C*-(10-cyanodecane)-calix[4]pyrogallolarene (pendant chains removed for clarity)

Chapter 8 - Calixarenes as drug delivery

vectors

1   Toxicity of *C*-alkyl-calix[4]pyrogallolarene derivatives

The following section will discuss the investigations undertaken to assess the viability of using calix[4]pyrogallolarene derived systems as drug delivery vectors.

In order to complete preliminary toxicity data the toxicity of a variety of *C*-alkyl-calix[4]pyrogallolarenes was tested. This was to assess the effect on the toxicity of a variety of alkyl chain lengths. The tests were performed by addition of a 10 µg/ml DMSO solution of the calixarene to immature dendritic cells and incubating them together for 168 hours in order to allow the cells to mature. After a week the cell count was assessed and the number of surviving cells was counted. The data as shown in the Figure below shows that the calixarenes do not show significant toxicity on their own towards immature dendritic cells.
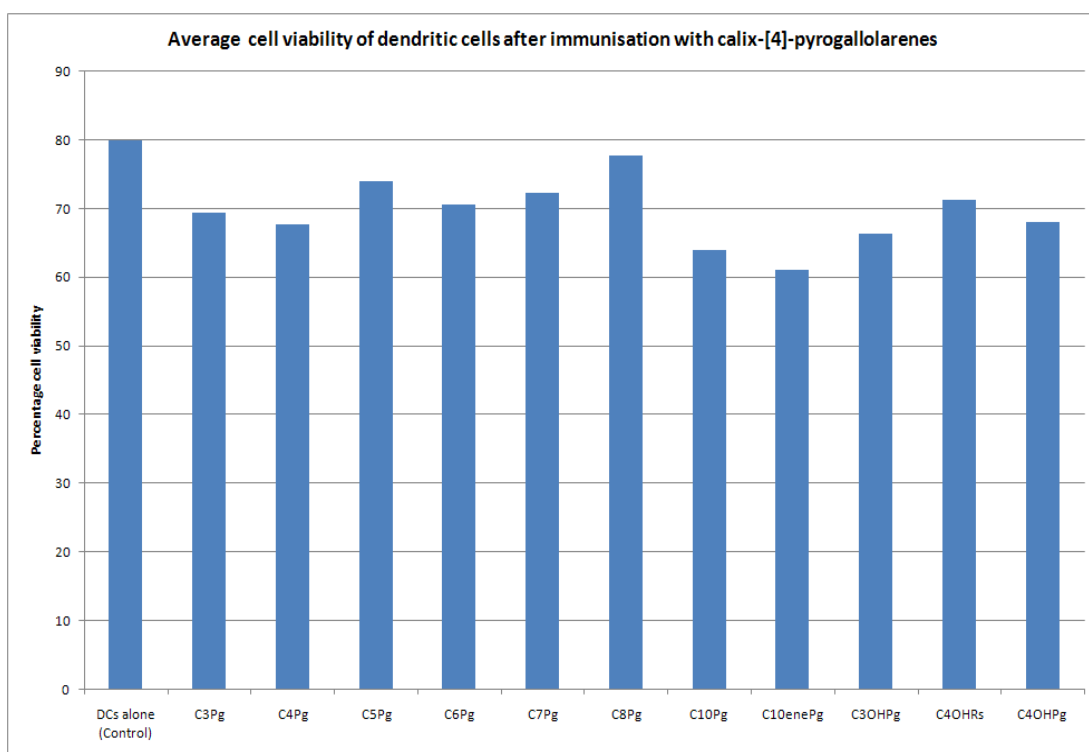
Dendritic cells were used because immature DC cells will uptake a wide variety of materials by phagocytosis. Also more significantly when exposed to a peptide the DC cells mature and present the peptide on the surface of the cell. This peptide sequence is now in an acceptable form to enable the activation of T-cells which will induce an immune response against cells bearing this surface peptide. This will allow the targeting of specific cell types for immunotherapy. Currently no adjuvant for the delivery of short peptide sequences is approved for human use, therefore if the peptide can be immobilised on the surface of a calix[4]pyrogallolarene supramolecular scaffold (in addition to aqueous solubilising groups) a therapy can be developed based on the principles detailed above.

A second round of testing of cytotoxicity was performed once *C*-(10-cyanodecane)-calix[4]pyrogallolarene was synthesised in order to assess the effect of including a highly polar functional group on the pendant chain on the cellular toxicity which the calixarenes present. The assay was shorter in duration due to the peripheral blood mononuclear cells (PBMC) used. While there is significant cell mortality during this assay, when compared to the media-only controls this cannot be attributed to the presence of C10CNPg. Any toxic effect due to the calixarene is rapidly shown (with a significant decrease in cell viability after 5 minutes).
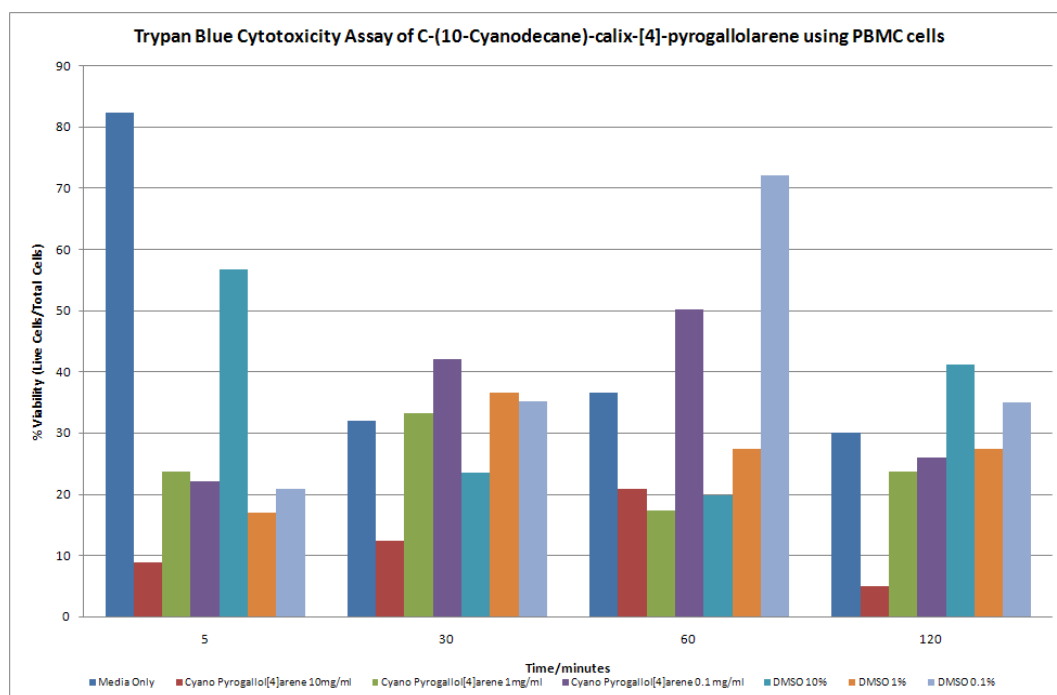
Chapter 9 - Conclusions

Construction of a calix[4]pyrogallolarene containing polar functional groups on its pendant chain is possible by pre-forming the desired functionality onto the aldehyde which is reacted with pyrogallol. Efforts to functionalise the calixarene once formed were complicated by difficulties in protecting the upper rim of the macrocycle and its decomposition.

If the pendant alkyl chains of calix[4]pyrogallolarenes are unconstrained by functionalisation, it is the guest which appears to determine the geometry of the macrocycle. If the chains are functionalised it is the interactions originating from the groups on the chain which takes precedence for the packing motif and any distortion of the macrocycle. Therefore, it may be possible to have sphere-promoting and sphere-dissociating functionality on the pendant chains. The capsule is surprisingly robust when the additional functional groups which promote the formation of a nano-sphere (in the case of the halogen functionalised spheres) are present.

If the pendant chains of the calixarene are sufficiently long (>6 carbon atoms long) the chain can distort and allow solvent molecules to be included within the face of a bilayer, this causes a contraction of the bilayer to allow greater van der Waals interactions to form between the pendant chains.

In a manner similar to that of the induced fit model of enzymes, the macrocycle can distort to accommodate the presence of guest molecules within the cavity. The capsule is generally formed by $R\bar{3}$ symmetry, therefore any change in the conformation of the macrocycle is duplicated around the sphere. This distortion can lead to changes in the supramolecular architecture which is formed. Distortion of the conformation of the calixarene is seen in the nano-spheres which contain highly polar guest molecules (e.g. chloro spheres containing methanol and ethanol and the acetonitrile sphere). Therefore there are guest molecules which are sphere promoting and sphere dissociating.

When the upper rim is unfunctionalised, the hydrogen atoms of the lower rim bear a slight positive charge and therefore electron donors may form hydrogen bonds to the calixarene. These interactions dramatically affect the behaviour of the molecule both in solution and in the solid phase. This is seen in the acetylated cyano calixarene derivatives, where disruption of the hydrogen bonding which keeps

the macrocycle in its cone conformation is eliminated, causing the molecule to become much more conformationally flexible.

The calixarene scaffold shows great potential with initial toxicity data indicating a lack of significant toxicity to the dendritic cells which are the target of the therapy. The obvious target is the synthesis of an amino or carboxyl substituted calixarene which will allow therapeutic peptide sequences to be tagged onto the exterior of the capsule. Further toxicity testing on all derivatives synthesised will aid the understanding of the toxicological profile of this class of molecules.

Chapter 10 - Experimental

1   Instrumentation

Nuclear magnetic resonance (NMR) spectra were recorded on a JEOL ECX 400 (^{1}H: 400 MHz and ^{13}C: 100 MHz) spectrometer in the deuterated solvent stated. All chemical shifts (δ) are quoted in ppm and coupling constants (J) in Hz. Residual signals from the solvents were used as an internal reference. Infrared spectra were recorded on a Perkin-Elmer Spectrum 100 Fourier Transform spectrophotometer with an attenuated total reflectance (ATR) sampling accessory, allowing direct analysis of the sample. Only the characteristic peaks are quoted in cm^{-1}. All reactions involving moisture sensitive reagents were performed under an atmosphere of nitrogen *via* standard vacuum line techniques. Tetrahydrofuran was distilled under an atmosphere of dry nitrogen from potassium. All other solvents were used as supplied (Laboratory, Analytical or HPLC grade), without prior purification. Thin layer chromatography was performed on aluminium sheets coated with 60 F$_{254}$ silica. Sheets were visualised using 1% potassium permanganate. Mass spectra were obtained upon an APCI Platform spectrometer with only molecular ions, fragments from molecular ions and major peaks being reported. Elemental analyses were performed by the microanalysis service of the Inorganic Chemistry Laboratory, London Metropolitan University. Single crystal analysis was performed at Daresbury synchrotron laboratories, Heriot Watt University and by the EPSRC X-ray crystallography service at The University of Southampton. The instruments used respectively were: Bruker-Nonius KappaCCD diffractometers with a rotating anode X-ray generator. One of the instruments has a Bruker Apex II detector. Both diffractometers are fitted with a Cobra cryogenic system.

2 Method for cytotoxicity assay on calixarenes

Cytotoxicity studies were performed using a Trypan blue assay in sterile fume hoods. *C*-(10-cyanodecane)-calix[4]pyrogallolarene was diluted using DMSO to final concentration of 10 mgml^{-1}. 500 ml of RPMI$^®$ media was modified by addition of 1% glutamine and 10% Foetal Calf Serum (FCS). The PBM cells were given an initial wash using the modified media. This was performed by adding the defrosted PBM cells to the modified media. This suspension was centrifuged for 3 minutes at 3Gs. The supernatant was then removed and the pellet re-suspended in modified RPMI media.

The initial cell count was performed by creating a 1 in 10 cell dilution using 450 μl of Trypan blue and 50 μl of the cells. A haemocytometer was cleaned in 70% ethanol, and the cell solution was plated and the cells counted in the four 0.25 mm x 0.25 mm grids. There were 17.5 x10^4 ml^{-1} cells present in the initial sample. As the original volume of the sample was 4 ml, the original sample contained 7x10^6 cells. For the cytotoxicity studies, it was necessary to have 0.5 million cells per well. Each well can contain 1 ml, so 286μl of PBMC cell suspension was added to 14 wells. This was topped up to 1ml using the modified RPMI media, and incubated overnight at 37°C.

Dilutions of *C*-(10-cyanodecane)-calix[4]pyrogallolarene were created using modified RPMI media to give final concentrations of 10, 1, and 0.1 mg ml^{-1}. Serial 1 in 10 dilutions of DMSO were prepared in a similar manner to give 1 in 10, 1 in 100 and 1 in 1000 dilutions for testing. After 24 hours, 100 μl of the supernatant was removed from 12 of the 14 wells. 100 μl of 10 mlml^{-1} C10CNPg was added to two wells, 100 μl of 1 mgml^{-1} of C10CNPg was added to two wells and 100μl of C10CNPg was added to two wells. The DMSO was added to 6 wells in a similar fashion. Two wells were left alone in order to provide a control. The cells were then incubated at 37°C. At 5 minutes, 30 minutes, 1 hour and 2 hours the well was removed from the incubator and 100 μl of each removed into a 1 ml aliquot. The plate was then placed back in the incubator. To each aliquot, 100 μl of Trypan blue was added to provide a 1 in 2 dilution of the cells. Samples were placed on a haemocytometer and the live and dead cells counted in each sample.

3 Synthesis of *C*-methyl-calix[4]pyrogallolarene (C1Pg)
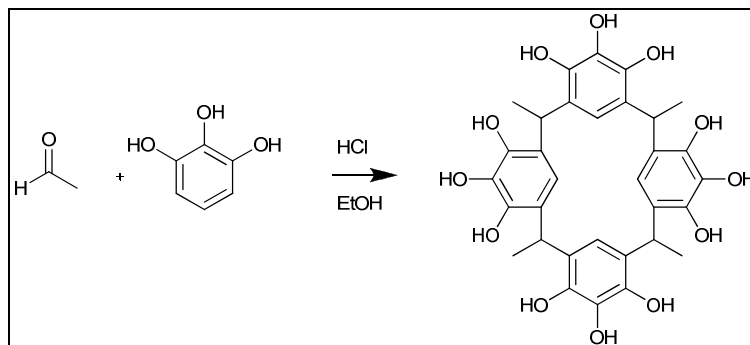
Pyrogallol (10 g, 79 mmol) was dissolved in ethanol (100 ml). Hydrochloric acid (37 % 25 ml) was added and the solution was stirred for 5 minutes. Acetaldehyde (4.40 ml, 79 mmol) in ethanol (20 ml) was added drop-wise to the acidic pyrogallol solution over 1 hour. The reaction mixture was stirred for 24 hours at room temperature then was heated to 60°C for a further 120 hours. The reaction mixture was cooled in an ice bath and a pale yellow precipitate was observed to form from the brown solution. The solid was filtered under vacuum and washed with ice cold ethanol (3 x 10 ml) to yield a buff coloured solid (11.961 g) shown to be product (99% yield).

^{1}H ((CD$_3$)$_2$SO δppm 400 MHz) 6.67 (1 H, s), 4.43 (1 H, t, ^3J = 6.9 Hz), 1.44 (3 H, d, ^3J = 7.32 Hz) ^{13}C {^{1}H}[707070707069] ((CD$_3$)$_2$SO δppm 400 MHz) 140.2, 132.4, 114.4, 28.9, 21.0 IR ν_{max} ATR cm^{-1} 3309, 3158, 2967, 2931, 1609, 1488, 1446, 1316, 1275, 1198, 1094, 1076, 1030.5, 1002, 961, 875, 772, 725, 646. MS *m/z* (ESI+) 609 ([M+H]$^+$, 100%), 626 ([M+H$_2$O]$^+$15), 631 ([M+Na]$^+$20), 646 ([M+K]$^+$ 20), 1217 ([2M+H]$^+$, 25), 1234 ([2M+H$_2$O]$^+$ 15), 1240 ([2M+Na]$^+$ 15), 1255 ([2M+K]$^+$ 15)

Crystal data for *C*-methyl-calix[4]pyrogallolarene diethyl ether clathrate: (C$_{32}$H$_{32}$O$_{12}$·3(CH$_3$CH$_2$OCH$_2$CH$_3$)), *M* = 830.75, colourless block, 0.10 x 0.08 x 0.04 mm^3, monoclinic, space group *C*2/*c* (No. 15), *a* = 27.3835(9), *b* = 21.9504(7), *c* = 17.4697(5) Å, β = 120.1140(10)°, *V* = 9083.4(5) Å^3, *Z* = 8, D_c = 1.215 g/cm^3, F_{000} = 3568, Bruker-Nonius APEX II CCD camera on goniostat, Mo*K*α radiation, λ = 0.71073 Å, *T* = 120(2)K, 2θ$_{max}$ = 55.3°, 53344 reflections collected, 10426 unique (R_{int} = 0.0807). Final *GooF* = 1.125, *R1* = 0.0869, *wR2* = 0.1590, *R* indices based on

6989 reflections with I >2σ (I) (refinement on F^2), 608 parameters, 0 restraints. Lp and absorption corrections applied, $\mu = 0.091$ mm^{-1}.

Crystal data for C-methyl-calix[4]pyrogallolarene acetonitrile clathrate: $(C_{32}H_{32}O_{12}\cdot3(CH_3CN))$, $M = 731.74$, colourless slab, 0.58 x 0.22 x 0.10 mm^3, monoclinic, space group $P2/n$ (No. 13), $a = 12.3862(3)$, $b = 7.2689(2)$, $c = 19.9868(6)$ Å, $\beta = 94.4630(10)°$, $V = 1794.04(9)$ Å^3, $Z = 2$, $D_c = 1.355$ g/cm^3, $F_{000} = 772$, Bruker-Nonius Roper CCD camera on goniostat, Mo$K\alpha$ radiation, $\lambda = 0.71073$ Å, $T = 120(2)$K, $2\theta_{max} = 55.2°$, 19932 reflections collected, 4122 unique ($R_{int} = 0.0525$). Final $GooF = 1.077$, $R1 = 0.0887$, $wR2 = 0.2441$, R indices based on 2866 reflections with I >2σ (I) (refinement on F^2), 111 parameters, 0 restraints. Lp and absorption corrections applied, $\mu = 0.102$ mm^{-1}.

4   Synthesis of C-ethyl-calix[4]pyrogallolarene (C2Pg)
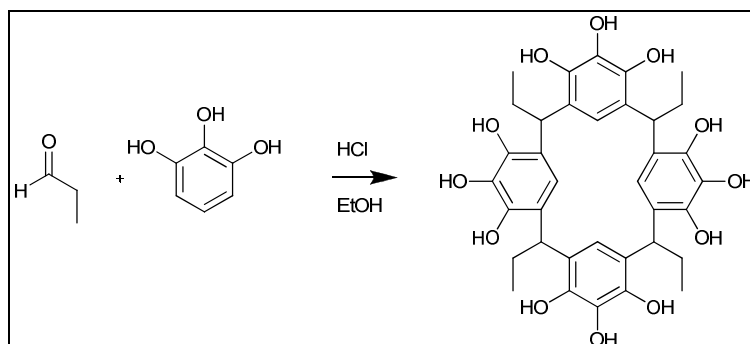
Pyrogallol (10 g, 79 mmol) was dissolved in ethanol (100 ml). Hydrochloric acid (37% 25 ml) was added and the solution was stirred for 5 minutes. Propionaldehyde (5.72 ml, 79 mmol) in ethanol (20 ml) was added drop-wise to the acidic pyrogallol solution over 1 hour. The reaction mixture was stirred for 24 hours at room temperature then was heated to 60°C for a further 120 hours. The reaction mixture was cooled in an ice bath, and the pale purple precipitate which formed was filtered. The solid was washed with ice cold chloroform which decolourised the powder to pale grey. NMR confirms solid as product (4.906 g, 50% yield)

^{1}H ((CD$_3$)$_2$SO δppm 400 MHz) 6.88 (1 H, s), 4.03 (1 H, t, $^3J = 8.48$ Hz), 2.15 (2 H, qn, $^3J = 7.32$), 0.79 (3 H, t, $^3J = 6.88$ Hz). ^{13}C {^{1}H} ((CD$_3$)$_2$SO δppm 100 MHz) 139.6, 132.9, 124.4, 113.6, 36.1,

26.0, 12.8. IR v_{max} ATR cm^{-1} 3220, 2962, 2872, 1607.5, 1500, 1477, 1384, 1322, 1246, 1228, 1209, 1114, 1087, 1057, 1033, 988, 948, 934, 906, 873, 776, 721, 601. MS m/z (ESI) 664 ([M+H]$^{+\cdot}$, 30%), 682 ([M+H$_2$O]$^{+\cdot}$ 40), 687 ([M+Na]$^{+\cdot}$ 35), 703 ([M+K]$^{+\cdot}$ 100), 1329 ([2M+H]$^{+\cdot}$, 5), 1352 ([M+Na]$^{+\cdot}$ 40), 1368 ([M+K]$^{+\cdot}$ 90)

Crystal data for *C*-ethyl-calix[4]pyrogallolarene acetonitrile clathrate: C$_{36}$H$_{40}$O$_{12}$·5(CH$_3$CN), M = 869.97, Colourless Block, 0.28 x 0.24 x 0.18 mm^3, monoclinic, space group *P*2$_1$/*c* (No. 14), a = 11.2014(3), b = 21.3303(4), c = 19.3327(4) Å,β = 92.1080(10)°, V = 4616.02(18) Å^3, Z = 4, D_c = 1.252 g/cm^3, F_{000} = 1848, Bruker-Nonius Roper CCD camera on goniostat, Mo*K*α radiation, λ = 0.71073 Å, T = 120(2)K, 2θ_{max} = 55.1°, 54117 reflections collected, 10598 unique (R_{int} = 0.0791). Final *GooF* = 1.036, *R1* = 0.0617, *wR2* = 0.1418, *R* indices based on 6599 reflections with I >2σ (I) (refinement on F^2), 605 parameters, 0 restraints. Lp and absorption corrections applied, μ = 0.091 mm^{-1}.

5   Synthesis of *C*-ethyl-calix[4]resorcinarene (C2Rs)
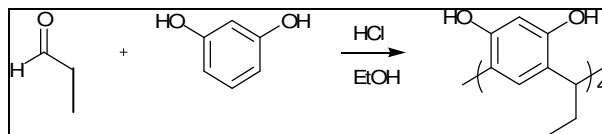
Resorcinarene (10 g, 91 mmol) was dissolved in ethanol (100 ml). Hydrochloric acid (37% 25 ml) was added and the solution was stirred for 5 minutes. Propionaldehyde (6.55 ml, 79 mmol) in ethanol (20 ml) was added drop-wise to the acidic pyrogallol solution over 1 hour. The reaction mixture was stirred for 24 hours at room temperature then was heated to 70°C for a further 144 hours. The reaction mixture was cooled in an ice bath, and the pale purple precipitate which formed was filtered. The solid was washed with ice cold chloroform and dried in a vacuum oven overnight. NMR confirms solid as product (23.08 g, 88% yield)

^{1}H ((CD_3)$_2$SO δppm 400 MHz) 7.21 (s, 1H), 6.14 (s, 1H), 4.07 (t, 1H, ^3J = 7.88 Hz), 2.08 (p, 2H, ^3J = 6.64, 7.32 Hz), 0.77 (q, 3H, ^3J = 6.96 Hz) ^{13}C{^{1}H} ((CD_3)$_2$SO δppm 100 MHz) 151.9, 125.1, 123.3, 100.2, 35.3, 27.9, 12.8

Crystal data for *C*-ethyl-calix[4]resorcinarene: $C_{36}H_{40}O_8$·(CH_3CN)(H_2O), M = 659.81, colourless slab, $0.44 \times 0.33 \times 0.10$ mm^3, monoclinic, space group *P2/n* (No. 13), a = 13.8457(3), b = 7.8652(2), c = 18.3617(5) Å, β = 103.156(2)°, V = 1947.09(8) Å^3, Z = 2, D_c = 1.238 g/cm^3, F_{000} = 772, Bruker-Nonius Roper CCD camera on goniostat, Mo*K*α radiation, λ = 0.71073 Å, T = 120(2)K, $2\theta_{max}$ = 55.0°, 20276 reflections collected, 4477 unique (R_{int} = 0.0457). Final *GooF* = 1.083, *R1* = 0.0931, *wR2* = 0.2454, *R* indices based on 3538 reflections with I >2σ (I) (refinement on F^2), 244 parameters, 0 restraints. Lp and absorption corrections applied, μ = 0.088 mm^{-1}.

6   Synthesis of *C*-propyl-calix[4]pyrogallolarene (C3Pg)
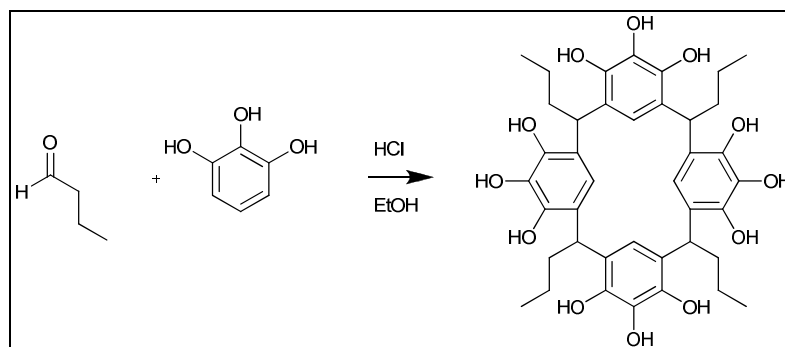
Pyrogallol (10 g, 79 mmol) was dissolved in ethanol (100 ml). Hydrochloric acid (37% 25 ml) was added and the solution was stirred for 5 minutes. Butyraldehyde (7.15 ml, 79 mmol) in ethanol (20 ml) was added drop-wise to the acidic pyrogallol solution over 1 hour. The reaction mixture was stirred for 24 hours at room temperature then was heated to 60°C for a further 120 hours. After 24 hours at 60°C the solution darkened to dark brown. The mixture was cooled in an ice bath and the purple precipitate was filtered. The solid was washed with ice cold toluene which caused decolourisation. Analysis shows the solid to be the desired product (10.389 g, 77% yield).

^{1}H ((CD$_3$)$_2$SO δppm 400 MHz) 6.90 (1 H, s), 4.19 (1H, t, ^3J = 7.76 Hz), 2.14 (2 H, q, ^3J = 7.8 Hz), 1.18, (2 H, m), 0.88 (3 H, t, ^3J = 6.88). ^{13}C{^{1}H} ((CD$_3$)$_2$SO δppm 100 MHz) 139.6, 132.8, 124.5, 113.6, 34.9, 33.4, 20.8, 13.9. IR v_{max} ATR cm^{-1} 3357, 2953, 2927.5, 2867, 1615, 1474, 1465, 1299, 1237, 1196, 1110, 1076.5, 1040, 976, 949, 877, 855, 839, 782, 748, 730, 682, 609, 589. MS *m/z* (ESI) 721 ([M+H]$^+$, 100%), 736 ([M+H$_2$O]$^+$ 70)

Crystal data for *C*-propyl-calix[4]pyrogallolarene ethanol water clathrate: C$_{40}$H$_{48}$O$_{12}$·3C$_2$H$_5$OH·2H$_2$O, *M* = 895.02, colourless plate, 0.46 × 0.20 × 0.03 mm^3, triclinic, space group *P*-1 (No. 2), *a* = 11.5628(5), *b* = 12.2343(5), *c* = 17.2991(9) Å, α = 72.332(2), β = 82.829(2), γ = 86.732(3)°, *V* = 2313.04(18) Å^3, *Z* = 2, *D$_c$* = 1.285 g/cm^3, *F$_{000}$* = 964, Bruker-Nonius Roper CCD camera on goniostat, Mo*K*α radiation, λ = 0.71073 Å, *T* = 120(2)K, 2θ_{max} = 55.2º, 45995 reflections collected, 10590 unique (*R$_{int}$* = 0.0644). Final *GooF* = 1.014, *R1* = 0.0613, *wR2* = 0.1301, *R* indices based on 7213

reflections with I >2σ (I) (refinement on F^2), 829 parameters, 0 restraints. Lp and absorption corrections applied, $\mu = 0.097$ mm^{-1}.

Crystal data for *C*-propyl-calix[4]pyrogallolarene acetone clathrate: $C_{40}H_{48}O_{12}\cdot3(CH_3C(O)CH_3)$, $M = 894.40$, colourless cut block, $0.56 \times 0.44 \times 0.28$ mm^3, monoclinic, space group $P2/c$ (No. 13), $a = 12.0951(3)$, $b = 14.3546(5)$, $c = 15.3913(5)$ Å, $\beta = 109.098(2)°$, $V = 2525.16(14)$ Å^3, $Z = 3$, $D_c = 1.254$ g/cm^3, $F_{000} = 1024$, Bruker-Nonius Roper CCD camera on goniostat, Mo*K*α radiation, λ = 0.71073 Å, $T = 120(2)$K, $2\theta_{max} = 55.1°$, 28932 reflections collected, 5805 unique ($R_{int} = 0.0460$). Final *GooF* = 1.067, *R1* = 0.0545, *wR2* = 0.1448, *R* indices based on 4555 reflections with I >2σ (I) (refinement on F^2), 428 parameters, 0 restraints. Lp and absorption corrections applied, $\mu = 0.092$ mm^{-1}.

Crystal data for *C*-propyl-calix[4]pyrogallolarene diethyl ether water clathrate: $C_{88}H_{116}O_{29}$, $M = 1637.81$, colourless plate, $0.25 \times 0.22 \times 0.04$ mm^3, monoclinic, space group $P2_1/c$ (No. 14), $a = 20.6338(8)$, $b = 11.2266(4)$, $c = 36.0871(15)$ Å, $\beta = 92.6060(10)°$, $V = 8350.8(6)$ Å^3, $Z = 4$, $D_c = 1.303$ g/cm^3, $F_{000} = 3504$, Mo*K*α radiation, λ = 0.71073 Å, $T = 120(2)$K, $2\theta_{max} = 55.0°$, 81565 reflections collected, 18806 unique ($R_{int} = 0.1095$). Final *GooF* = 1.038, *R1* = 0.1180, *wR2* = 0.3195, *R* indices based on 8934 reflections with I >2σ (I) (refinement on F^2), 1082 parameters, 0 restraints. Lp and absorption corrections applied, $\mu = 0.097$ mm^{-1}.

Crystal data for *C*-propyl-calix[4]pyrogallolarene acetonitrile water clathrate: $C_{40}H_{48}O_{12}\cdot C_2H_3N_1\,H_2O$, $M = 794.11$, colourless lath, $0.26 \times 0.12 \times 0.02$ mm^3, triclinic, space group $P1$ (No. 1), $a = 12.3620(5)$, $b = 18.9976(10)$, $c = 20.0390(11)$ Å, $\alpha = 62.434(2)$, $\beta = 76.306(3)$, $\gamma = 88.490(3)°$, $V = 4034.3(3)$ Å^3, $Z = 4$, $D_c = 1.307$ g/cm^3, $F_{000} = 1691$, Bruker-Nonius APEX II CCD camera on goniostat, Mo*K*α radiation, λ = 0.71073 Å, $T = 120(2)$K, $2\theta_{max} = 55.7°$, 59550 reflections collected, 32632 unique ($R_{int} = 0.1164$). Final *GooF* = 1.031, *R1* = 0.1443, *wR2* = 0.2400, *R* indices based on 13301 reflections with I >2σ (I) (refinement on F^2), 2145 parameters, 3 restraints. Lp and absorption corrections applied, $\mu = 0.096$ mm^{-1}. Absolute structure parameter = 3(3) (Flack, H. D. *Acta Cryst*. **1983**, *A39*, 876-881).

# 7   Synthesis of *C*-butyl-calix[4]pyrogallolarene (C4Pg)
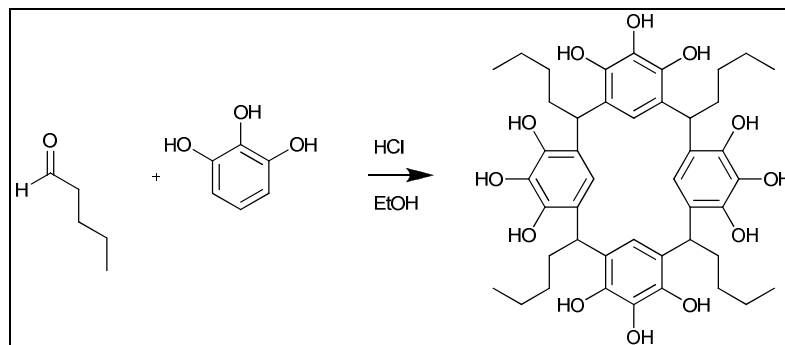
Pyrogallol (10 g, 79 mmol) was dissolved in ethanol (100 ml). Hydrochloric acid (37% 25 ml) was added and the solution was stirred for 5 minutes. Pentanal (8.43 ml, 79 mmol) in ethanol (20 ml) was added drop-wise to the acidic pyrogallol solution over 1 hour. The reaction mixture was stirred for 24 hours at room temperature then was heated to 60°C for a further 120 hours. The reaction mixture was cooled in an ice bath and the resulting grey precipitate was filtered, and washed with ice cold methanol. NMR shows precipitate to be product (7.890 g 51% Yield).

^{1}H ((CD$_3$)$_2$SO δppm 400 MHz) 6.86 (1 H, s), 4.16 (1 H, t, ^{3}J = 7.8 Hz), 2.13 (2 H, m), 1.32 (2 H, m), 1.17 (2 H, m), 0.85 (3 H, t, ^{3}J = 7.76 Hz) ^{13}C{^{1}H} ((CD$_3$)$_2$SO δppm 100 MHz) 139.6, 132.8, 124.5, 113.5, 33.9, 33.1, 22.2. 14.3 IR v_{max} ATR cm^{-1} 3451, 2953, 2926, 2857, 1619, 1495, 1466, 1374, 1276, 1179, 1114, 1067, 1044, 1011, 969, 935, 873, 851, 779, 718, 676, 610, 584. MS *m/z* (ESI) 776 ([M+H]$^{+}$, 95%), 792 ([M+H$_2$O]$^{+\cdot}$ 100)

Crystal data for *C*-butyl-calix[4]pyrogallolarene diethyl ether water clathrate: C$_{48}$H$_{72}$O$_{16}$, *M* = 905.06, colourless plate, $0.20 \times 0.16 \times 0.02$ mm^{3}, monoclinic, space group $P2_1/c$ (No. 14), *a* = 20.6564(9), *b* = 13.1221(6), *c* = 18.2667(7) Å, β = 108.700(2)°, *V* = 4689.9(3) Å^{3}, *Z* = 4, D_c = 1.282 g/cm^{3}, F_{000} = 1952, Bruker-Nonius APEX II CCD camera on goniostat, Mo*K*α radiation, λ = 0.71073 Å, *T* = 120(2)K, $2\theta_{max}$ = 55.3°, 38021 reflections collected, 10627 unique (R_{int} = 0.0702). Final *GooF* = 1.092, *R1* = 0.0999, *wR2* = 0.1653, *R* indices based on 6377 reflections with I >2σ(I) (refinement on F^{2}), 623 parameters, 4 restraints. Lp and absorption corrections applied, μ = 0.095 mm^{-1}.

Crystal data for *C*-butyl-calix[4]pyrogallolarene acetonitrile water clathrate: $C_{48}H_{72}O_{12}$, $C_2H_3N_1$ H_2O, M = 846.11, colourless block, $0.24 \times 0.24 \times 0.1$ mm^3, trigonal, space group $R\overline{3}$ (No. 148), a = b = 35.7719(4), c = 21.3642(6) Å, V = 23675.6(8) Å^3, Z = 21, D_c = 1.246 g/cm^3, F_{000} = 9486, Bruker-Nonius Roper CCD camera on goniostat, Mo*K*α radiation, λ = 0.71073 Å, T = 120(2)K, $2\theta_{max}$ = 55.0º, 69106 reflections collected, 12075 unique (R_{int} = 0.1073). Final *GooF* = 1.503, *R1* = 0.1611, *wR2* = 0.4251, *R* indices based on 6042 reflections with I >2σ (I) (refinement on F^2), 664 parameters, 1 restraint. Lp and absorption corrections applied, μ = 0.089 mm^{-1}.

8   Synthesis of *C*-pentyl-calix[4]pyrogallolarene (C5Pg)
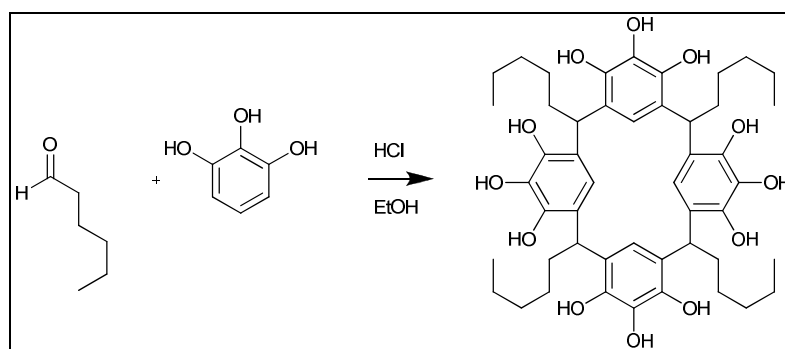
Pyrogallol (10 g, 79 mmol) was dissolved in ethanol (100 ml). Hydrochloric acid (37% 25 ml) was added and the solution was stirred for 5 minutes. Hexanal (9.75 ml, 79 mmol) in ethanol (20 ml) was added drop-wise to the acidic pyrogallol solution over 1 hour. The reaction mixture was stirred for 24 hours at room temperature then was heated to 60°C for a further 120 hours. The dark purple solution was cooled in an ice bath and the purple precipitate which formed was filtered and washed with ice cold methanol to give a pale purple solid which was dried in a vacuum oven. NMR shows solid to be product (8.13 g 49% Yield)

^{1}H ((CD$_3$)$_2$SO δppm 400 MHz) 6.82 (1 H, s), 4.15 (1 H, t, ^3J = 7.7 Hz), 2.11 (2 H, m), 1.30-1.05 (6 H, m), 0.84 (3 H, t, ^3J = 7.14). ^{13}C{^{1}H} ((CD$_3$)$_2$SO δppm 100 MHz)   139.7, 132.9, 124.5, 113.4, 33.9, 33.14, 31.6, 27.7, 22.4, 14.1. IR ν_{max} ATR cm^{-1} 3369, 3187, 2953, 2930, 2860, 1625, 1609, 1473, 1386, 1311, 1274, 1186, 1118, 1085, 1034, 980, 948, 918, 878, 869, 859, 829, 781, 765, 723, 676, 606. MS *m/z* (ESI) 833 ([M + H]$^{+\cdot}$, 40), 413 ([M + 2H]$^{++}$, 100%)

Crystal data for *C*-pentyl-calix[4]pyrogallolarene acetonitrile water clathrate: C$_{50}$H$_{69}$NO$_{13}$, *M* = 892.06, colourless plates, 0.5 × 0.44 × 0.05 mm^3, monoclinic, space group *P*2$_1$/*c* (No. 14), *a* = 18.587(4), *b* = 13.270(3), *c* = 19.692(4) Å, β = 90.31(3)°, *V* = 4857.1(17) Å^3, *Z* = 4, *D*$_c$ = 1.220 g/cm^3, *F*$_{000}$ = 1920, Mo*K*α radiation, λ = 0.71073 Å, *T* = 120(2)K, 2θ_{max} = 55.0°, 47651 reflections collected, 11092 unique (*R*$_{int}$ = 0.0671). Final *GooF* = 1.042, *R1* = 0.0968, *wR2* = 0.2495, *R* indices based on 7618 reflections with I >2σ (I) (refinement on *F*^{2}), 630 parameters, 12 restraints. Lp and absorption corrections applied, μ = 0.087 mm^{-1}

9   Synthesis of *C*-hexyl-calix[4]pyrogallolarene (C6Pg)
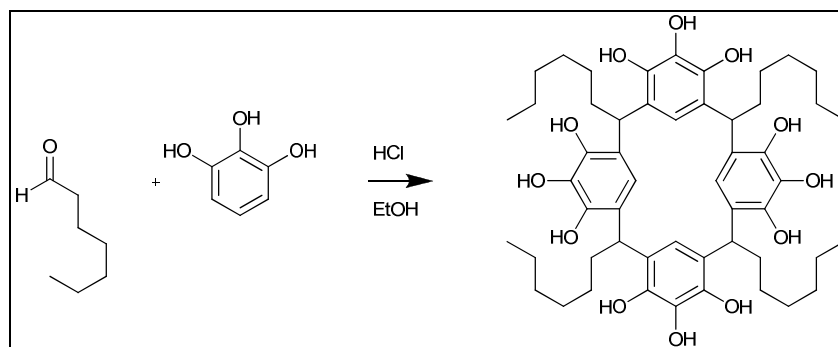
Pyrogallol (10 g, 79 mmol) was dissolved in ethanol (100 ml). Hydrochloric acid (37% 25 ml) was added and the solution was stirred for 5 minutes. Heptanal (11.1 ml, 79 mmol) in ethanol (20 ml) was added drop-wise to the acidic pyrogallol solution over 1 hour. The reaction mixture was stirred for 24 hours at room temperature then was heated to 60°C for a further 120 hours. The reaction was then cooled, and the pale pink precipitate was filtered and washed with ice cold methanol. NMR shows solid (12.598 g) to be product (72% Yield).

^{1}H ((CD$_3$)$_2$SO δppm 400 MHz) 6.78 (1 H, s), 4.20 (1 H, t, ^3J = 7.76 Hz), 2.09 (2 H, m), 1.30-1.10 (8 H, m), 0.85 (3 H, t, ^3J = 7.04 Hz), ^{13}C{^{1}H} ((CD$_3$)$_2$SO δppm 100 MHz) 139.7, 132.7, 124.3, 113.3, 33.7, 33.3, 31.3, 28.7, 27.7, 22.0, 13.7, IR ν_{max} ATR cm^{-1} 3266, 2952, 2926, 2855, 1691, 1611, 1477, 1467, 1314, 1202, 1115, 1078, 1039, 1004, 973, 943, 877, 779, 721, 591, 497. MS *m/z* (ESI) 911 ([M + Na]$^{+\cdot}$, 30), 889 ([M + H]$^{+\cdot}$, 20%), 685 ([M − 1 C$_{11}$H$_{18}$O$_3$ subunit]$^{+\cdot}$, 100), 445 ([M + 2H]$^{++\cdot}$, 20).

Crystal data for *C*-hexyl-calix[4]pyrogallolarene hydrochloride acetonitrile clathrate: C$_{54}$H$_{77}$ClNO$_{13}$, *M* = 983.62, colourless block, 0.24 × 0.20 × 0.10 mm^3, triclinic, space group *P*-1 (No. 2), *a* = 10.6780(4), *b* = 12.4618(5), *c* = 21.1907(10) Å, α = 105.968(2), β = 98.239(2), γ = 95.678(2)°, *V* = 2654.49(19) Å^3, *Z* = 2, D_c = 1.231 g/cm^3, F_{000} = 1058, Bruker-Nonius Roper CCD camera on goniostat, Mo*K*α radiation, λ = 0.71073 Å, *T* = 120(2)K, $2\theta_{max}$ = 55.2°, 55436 reflections collected, 12183 unique (R_{int} = 0.1121). Final *GooF* = 1.035, *R1* = 0.0758, *wR2* = 0.1735, *R* indices based on 6663 reflections with I >2σ(I) (refinement on F^2), 647 parameters, 0 restraints. Lp and absorption corrections applied, μ = 0.135 mm^{-1}.

# 10 Synthesis of *C*-heptyl-calix[4]pyrogallolarene (C7Pg)
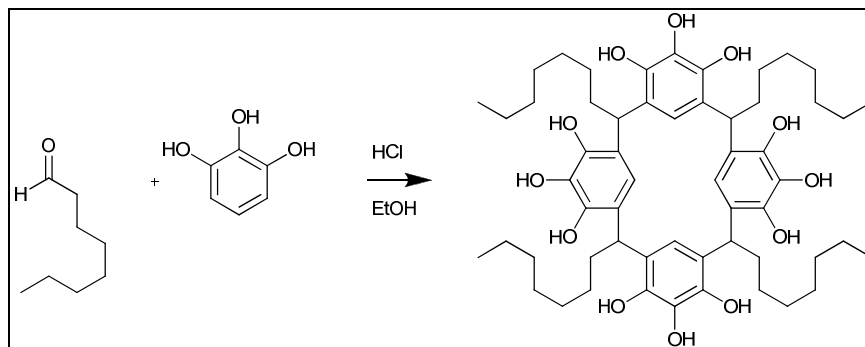
Pyrogallol (10 g, 79 mmol) was dissolved in ethanol (100 ml). Hydrochloric acid (37% 25 ml) was added and the solution was stirred for 5 minutes. Octanal (12.40 ml, 79 mmol) in ethanol (20 ml) was added drop-wise to the acidic pyrogallol solution over 1 hour. The reaction mixture was stirred for 24 hours at room temperature then was heated to 60°C for a further 120 hours. The reaction mixture was cooled in an ice bath and after 1 hour a grey crystalline solid had formed in the solution. The solid was filtered off, and washed with ice cold methanol, and dried *in-vacuo*. Analysis shows the solid (13.199 g) to be the desired product (71% Yield).

^{1}H ((CD$_3$)$_2$SO δppm 400 MHz) 6.72 (1 H, s), 4.13 (1 H, t, ^3J = 7.32 Hz), 2.04, (2 H, m), 1.30-1.05 (10 H, m), 0.82 (3 H, t, ^3J = 7.7 Hz). ^{13}C{^{1}H} ((CD$_3$)$_2$SO δppm 100MHz) 139.8, 133.0, 124.4, 113.2, 34, 33, 31.5, 30, 29.0, 28, 22.2, 14.0. IR ATR cm^{-1} 3269.8, 2922.9, 2853.2, 1612.2, 1479.5, 1465.0, 1378.1, 1314.9, 1240.3, 1200.2, 1115.8, 1086.3, 1035.1, 978.7, 944.5, 870.3, 781.9, 721.7, 614.8, 598.4, 574.9, 499.5 MS *m/z* (ESI) 944 ([M + H]$^{+\cdot}$, 100%), 961 ([M + H$_2$O]$^+$, 80).

Crystal data for *C*-heptyl-calix[4]pyrogallolarene diethyl ether water clathrate: C$_{64}$H$_{100}$O$_{12}$, M = 1092.63, colourless block, 0.44 × 0.17 × 0.12 mm^3, triclinic, space group *P*-1 (No. 2), a = 10.649(2), b = 15.580(3), c = 20.359(4) Å, α = 109.79(3), β = 93.19(3), γ = 98.00(3)°, V = 3128.3(11) Å^3, Z = 2, D_c = 1.178 g/cm^3, F_{000} = 1208, Bruker-Nonius 95mm CCD camera on goniostat, Mo*K*α radiation, λ = 0.71073 Å, T = 120(2)K, $2\theta_{max}$ = 56.1°, 55974 reflections collected, 14352 unique (R_{int} = 0.0697).

Final *GooF* = 1.401, *R1* = 0.1272, *wR2* = 0.3665, *R* indices based on 8252 reflections with I >2σ (I) (refinement on F^2), 720 parameters, 0 restraints. Lp and absorption corrections applied, μ = 0.082 mm^{-1}.

Crystal data for *C*-heptyl-calix[4]pyrogallolarene ethanol water clathrate: $C_{112}H_{196}O_{40}$, *M* = 2180.00, colourless plate, 0.10 × 0.08 × 0.01 mm^3, triclinic, space group *P*-1 (No. 2), *a* = 16.539(2), *b* = 16.629(2), *c* = 23.088(3) Å, α = 73.037(2), β = 81.318(2), γ = 85.089(2)°, *V* = 5998.2(13) Å^3, *Z* = 4, D_c = 1.197 g/cm^3, F_{000} = 2350, Bruker SMART APEX2 CCD diffractometer, synchrotron radiation, λ = 0.6884 Å, *T* = 120(2)K, $2\theta_{max}$ = 42.5°, 33635 reflections collected, 14617 unique (R_{int} = 0.0488). Final *GooF* = 1.040, *R1* = 0.0998, *wR2* = 0.2717, *R* indices based on 8324 reflections with I >2σ (I) (refinement on F^2), 1437 parameters, 21 restraints. Lp and absorption corrections applied, μ = 0.085 mm^{-1}.

Crystal data for *C*-heptyl-calix[4]pyrogallolarene hydrochloride acetonitrile water clathrate: $C_{58}H_{83}ClNO_{13}$, *M* = 1037.70, colourless slab, 0.20 × 0.18 × 0.07 mm^3, triclinic, space group *P*-1 (No. 2), *a* = 10.6185(2), *b* = 12.5157(4), *c* = 22.7434(7) Å, α = 105.9370(10), β = 99.380(2), γ = 95.389(2)°, *V* = 2836.72(14) Å^3, *Z* = 2, D_c = 1.215 g/cm^3, F_{000} = 1118, Bruker-Nonius Roper CCD camera on goniostat, Mo*K*α radiation, λ = 0.71073 Å, *T* = 120(2)K, $2\theta_{max}$ = 55.1°, 52483 reflections collected, 12933 unique (R_{int} = 0.0701). Final *GooF* = 1.030, *R1* = 0.0646, *wR2* = 0.1602, *R* indices based on 8980 reflections with I >2σ (I) (refinement on F^2), 663 parameters, 0 restraints. Lp and absorption corrections applied, μ = 0.130 mm^{-1}.

Crystal data for *C*-heptyl-calix[4]pyrogallolarene ethyl acetate clathrate: $C_{60}H_{88}O_{14}$, *M* = 1033.30, Colourless Block, 0.58 × 0.54 × 0.50 mm^3, trigonal, space group *R*-3 (No. 148), *a* = *b* = 30.059(4), *c* = 36.910(7) Å, *V* = 28883(8) Å^3, *Z* = 18, D_c = 1.069 g/cm^3, F_{000} = 10080, Bruker-Nonius 95mm CCD camera on goniostat, Mo*K*α radiation, λ = 0.71073 Å, *T* = 120(2)K, $2\theta_{max}$ = 55.3°, 87065 reflections collected, 14718 unique (R_{int} = 0.0900). Final *GooF* = 1.866, *R1* = 0.2298, *wR2* = 0.5702, *R* indices based on 5728 reflections with I >2σ (I) (refinement on F^2), 315 parameters, 0 restraints. Lp and absorption corrections applied, μ = 0.075 mm^{-1}.

11 Synthesis of *C*-octyl-calix[4]pyrogallolarene (C8Pg)
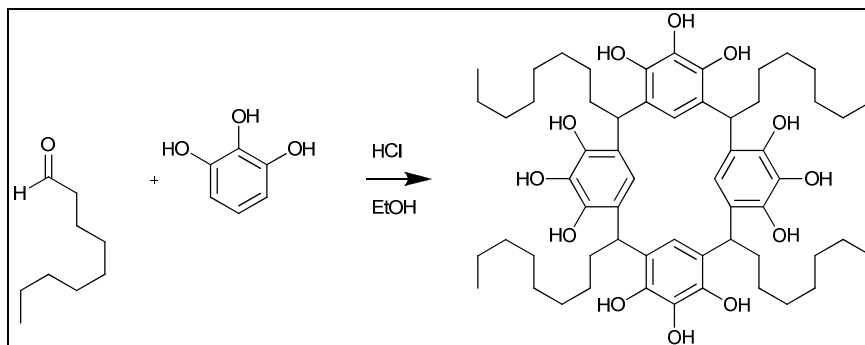
Pyrogallol (10 g, 79 mmol) was dissolved in ethanol (100 ml). Hydrochloric acid (37 %, 25 ml) was added and the solution was stirred for 5 minutes. Nonanal (13.64 ml, 79 mmol) in ethanol (20 ml) was added drop-wise to the acidic pyrogallol solution over 1 hour. The reaction mixture was stirred for 24 hours at room temperature then was heated to 60°C for a further 120 hours. The red solution was cooled in an ice bath for 1 hour and the resulting pink precipitate was filtered, and washed with a little ice cold methanol and dried to yield cream coloured solid which was shown to be product (16.846 g, 85 % Yield).

^{1}H ((CD$_3$)$_2$SO δppm 400 MHz) 6.74 (1 H, s), 4.15 (1 H, t, ^3J = 7.44 Hz), 2.06 (2 H, m), 1.34 – 1.05 (12 H, m), 0.85 (3 H, t), ^{13}C{^{1}H} ((CD$_3$)$_2$SO δppm 100 MHz) 139.7, 132.9, 124.3, 113.1, 33.9, 33.3, 31.4, 29.4, 29.3, 28.9, 28.0, 22.2, 14.0. IR ν_{max} ATR cm^{-1} 3277, 2922, 2853, 1612, 1478.5, 1465, 1377.5, 1312, 1236, 1209, 1116, 1086, 1036, 979, 947, 869, 775, 720.5, 595, 576.0, 500, MS *m/z* (ESI+) 1119 ([M+H]$^+$, 15%), 412.08 (100), 250 (20)

Crystal data for *C*-octyl-calix[4]pyrogallolarene hydrochloride acetonitrile water clathrate: $C_{60}H_{88}O_{12}$·CH$_3$CN·H$_2$O·HCl M = 1106.91, colourless block, 0.58 × 0.24 × 0.12 mm^3, triclinic, space group *P*-1 (No. 2), a = 10.6979(6), b = 12.5868(8), c = 23.5520(17) Å, α = 76.818(3), β = 78.637(3), γ = 84.395(4)°, V = 3022.6(3) Å^3, Z = 2, D_c = 1.216 g/cm^3, F_{000} = 1208, Bruker-Nonius Roper CCD camera on goniostat, Mo*K*α radiation, λ = 0.71073 Å, T = 120(2)K, $2\theta_{max}$ = 55.4º, 55444 reflections collected, 13645 unique (R_{int} = 0.1319). Final *GooF* = 1.005, *R1* = 0.0860, *wR2* = 0.2020, *R* indices

based on 6082 reflections with I >2σ (I) (refinement on F^2), 768 parameters, 66 restraints. Lp and absorption corrections applied, $\mu = 0.126$ mm^{-1}.

12 Synthesis of *C*-decyl-calix[4]pyrogallolarene (C10Pg)
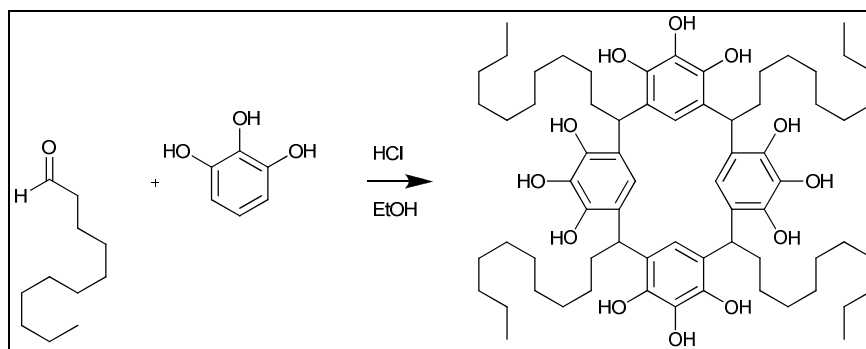
Pyrogallol (10 g, 79 mmol) was dissolved in ethanol (100 ml). Hydrochloric acid (37 % 25 ml) was added and the solution was stirred for 5 minutes. Undecanal (16.37 ml, 79 mmol) in ethanol (20 ml) was added drop-wise to the acidic pyrogallol solution over 1 hour. The reaction mixture was stirred for 24 hours at room temperature then was heated to 60°C for a further 120 hours. The red / orange solution was cooled ad a cream coloured precipitate rapidly formed. The precipitate was filtered and dried in a vacuum oven to yield product (21.827 g, 99 % Yield)

^{1}H ((CD$_3$)$_2$SO δppm 400 MHz) 6.71 (1 H, s), 4.22 (1 H, t, $^3J = 7.8$), 2.04 (2H, m), 1.24 (14 H, m), 0.84 (5 H, m), ^{13}C{^{1}H} ((CD$_3$)$_2$SO δppm 100 MHz) 139.7, 132.6, 124.0, 112.9, 33.6, 33.3, 31.0, 29.0, 28.9, 28.8, 28.7, 28.4, 27.6, 21.8, 13.5. IR v_{max} ATR cm^{-1} 3540, 3505, 3310, 2955, 2919, 2851, 1613, 1466, 1378, 1307.5, 1237, 1119, 1082.5, 1045, 973, 948, 878, 781, 721, 682, 608, 585, 496, 425, 413, MS m/z (ESI+) 1013 ([M+H]$^{+\cdot}$,20%), 790 (5), 526 (70), 388 (100)

13 Synthesis of *C*-(dec-10-ene)-calix[4]pyrogallolarene (C10enePg)
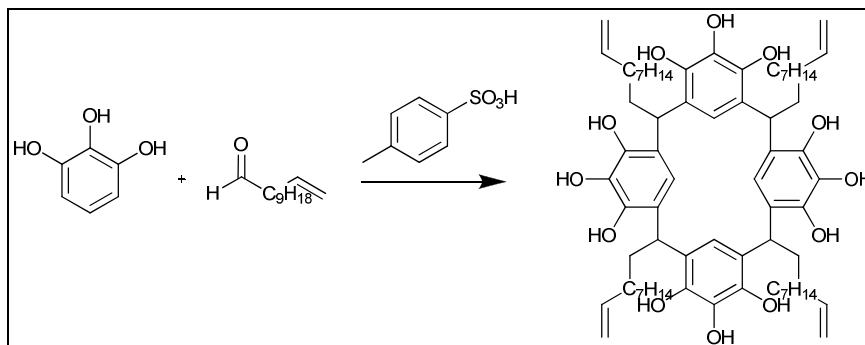
Pyrogallol (1 g, 8 mmol) and *p*-toluene sulfonic acid (2 mg 0.01 mmol) were ground together to a fine powder with a mortar and pestle. Undecyleneic aldehyde (1.68 ml, 8 mmol) was added and the mixture was ground together. After 10 minutes of grinding the mixture had become viscous and thickened. This mixture was left to stand for an hour whereupon it hardened and became brittle. Recrystallisation of this solid from acetonitrile gave a white solid which was shown by NMR and MS to be the desired product (2.01 g, 1.8 mmol, 88% yield).

[1]H ((CDCl$_3$ δppm 400 MHz) 6.76 (s, 1H), 5.75 (m, 1H), 4.87 (m, 2H), 4.29 (s, 1H), 2.14 (s, 2H), 1.98 (m, 2H) 1.30 (m, 12H), [13]C{[1]H} ((CD$_3$)$_2$SO δppm 100 MHz) 139.1, 138.4, 137.3, 131.3, 125.3, 124.0, 114.1, 33.9, 30.0, 29.8, 29.7, 29.6, 29.3, 29.1, 28.3, IR v_{max} ATR cm^{-1} 3451, 2923, 2852, 1638, 1505, 1466, 1276, 907, 720 391, MS *m/z* (ESI) 1127 ([M+Na]$^{+\cdot}$, 100%)

Crystal data for *C*-(dec-10-ene)-calix[4]pyrogallolarene ethyl acetate clathrate: C$_{430}$H$_{624}$O$_{84}$, *M* = 7128.63, colourless block, $0.37 \times 0.23 \times 0.10$ mm^3, trigonal, space group *R*-3 (No. 148), *a* = *b* = 37.216(5), *c* = 26.038(5) Å, *V* = 31232(9) Å^3, *Z* = 3, *D*$_c$ = 1.166 g/cm^3, *F*$_{000}$ = 11826, Mo*K*α radiation, λ = 0.71073 Å, *T* = 120(2)K, $2\theta_{max}$ = 46.6°, 88333 reflections collected, 10033 unique (*R*$_{int}$ = 0.0696). Final *GooF* = 1.674, *R1* = 0.1247, *wR2* = 0.3531, *R* indices based on 5809 reflections with I >2σ (I) (refinement on *F*^{2}), 786 parameters, 11 restraints. Lp and absorption corrections applied, μ = 0.081 mm^{-1}.

# 14 Synthesis of *C*-Propanol-calix[4]pyrogallolarene (C3OH Pg)
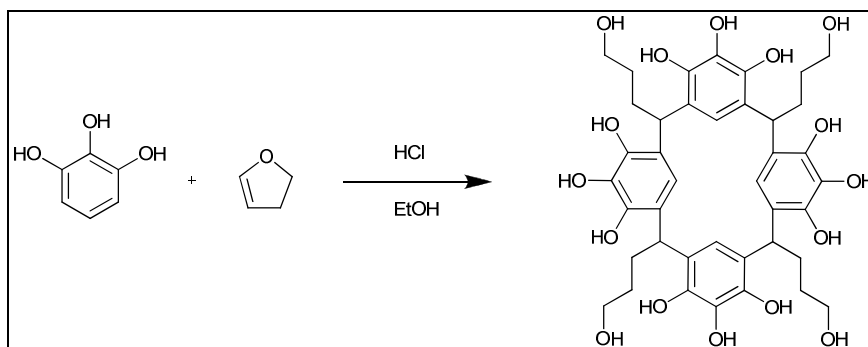
Pyrogallol (10 g, 79mmol) was dissolved in methanol (60ml). Hydrochloric acid (15 ml 37%) was added and the mixture stirred for 5 minutes. 2,3-Dihydropyran (6 ml 79 mmol) was added drop-wise to the acidic pyrogallol solution and the mixture was stirred for 1 hour at room temperature. The reaction mixture was heated to 30°C for 12 hours after which the temperature was increased to 50°C and the reaction was stirred for a further 144 hours. The reaction was cooled in an ice bath, the colourless precipitate which formed was filtered off. The solid was suspended in water and sonicated for 30 minutes. The solid was filtered and dried in a vacuum oven. Analysis shows solid to be product (7.649 g 49% Yield).

^{1}H ((CD$_3$)$_2$SO δppm 400 MHz) 6.87 (1 H, s), 4.13 (1 H, t, ^{3}J = 7.8 Hz), 3.42 (2 H, t, ^{3}J = 6.4 Hz), 2.15 (2 H, m), 1.33 (2 H, m), ^{13}C{^{1}H} ((CD$_3$)$_2$SO δppm 100 MHz) 139.6, 132.9, 124.5, 113.5, 60.7, 33.6, 31.3, 29.2, MS *m/z* (ESI) 807 [M+Na]$^{+}$, 100%), IR v_{max} ATR cm^{-1} 3194, 2946, 1637, 1466, 1297, 1092, 1047, 970, 867, 676, 493

Crystal data for *C*-(3-hydroxypropane)-calix[4]pyrogallolarene acetone water clathrate: C$_{43}$H$_{56}$O$_{20}$, *M* = 892.94, colourless Blade, 0.50 × 0.20 × 0.05 mm^3, triclinic, space group *P*-1 (No. 2), *a* = 10.4216(3), *b* = 10.8206(4), *c* = 11.8989(5) Å, α = 91.955(2), β = 104.612(2), γ = 116.399(2)°, *V* = 1146.33(7) Å^3, *Z* = 1, *D*$_c$ = 1.398 g/cm^3, *F*$_{000}$ = 516, Bruker-Nonius 95mm CCD camera on goniostat, Mo*K*α radiation, λ = 0.71073 Å, *T* = 120(2)K, 2θ_{max} = 55.5°, 23346 reflections collected, 5293 unique (*R*$_{int}$ = 0.0470). Final *GooF* = 1.061, *R1* = 0.0536, *wR2* = 0.1416, *R* indices based on 3766

reflections with I >2σ (I) (refinement on F^2), 435 parameters, 0 restraints. Lp and absorption corrections applied, $\mu = 0.118$ mm^{-1}.

Crystal data for *C*-(3-hydroxypropane)-calix[4]pyrogallolarene tetrahydrofuran water clathrate: $C_{44}H_{60}O_{19}$, $M = 892.92$, Colourless Block, $0.14 \times 0.07 \times 0.03$ mm^3, monoclinic, space group *P2/n* (No. 13), $a = 13.9100(4)$, $b = 9.6399(2)$, $c = 16.1474(4)$ Å, $\beta = 90.4790(10)°$, $V = 2165.15(9)$ Å^3, $Z = 2$, $D_c = 1.370$ g/cm^3, $F_{000} = 952$, Bruker-Nonius 95mm CCD camera on goniostat, Mo*K*α radiation, $\lambda = 0.71073$ Å, $T = 120(2)$K, $2\theta_{max} = 55.0°$, 31057 reflections collected, 4969 unique ($R_{int} = 0.0500$). Final *GooF* = 1.066, *R1* = 0.0627, *wR2* = 0.1699, *R* indices based on 4149 reflections with I >2σ (I) (refinement on F^2), 386 parameters, 0 restraints. Lp and absorption corrections applied, $\mu = 0.107$ mm^{-1}.

Crystal data for *C*-(3-hydroxypropane)-calix[4]pyrogallolarene acetone water clathrate: $C_{55}H_{86}O_{25}$, $M = 1147.24$, Colourless Needle, $0.168 \times 0.014 \times 0.015$ mm^3, monoclinic, space group *P2$_1$/c* (No. 14), $a = 15.051(2)$, $b = 16.979(2)$, $c = 27.627(3)$ Å, $\beta = 122.481(5)°$, $V = 5955.7(12)$ Å^3, $Z = 4$, $D_c = 1.279$ g/cm^3, $F_{000} = 2464$, Bruker SMART APEX2 CCD diffractometer, synchrotron radiation, $\lambda = 0.6941$ Å, $T = 120(2)$K, $2\theta_{max} = 54.3°$, 51684 reflections collected, 13142 unique ($R_{int} = 0.0364$). Final *GooF* = 1.029, *R1* = 0.0413, *wR2* = 0.1028, *R* indices based on 9860 reflections with I >2σ (I) (refinement on F^2), 919 parameters, 0 restraints. Lp and absorption corrections applied, $\mu = 0.101$ mm^{-1}.

15 Synthesis of *C*-Propanol-Calix[4]resorcinarene (C3OH Rs)
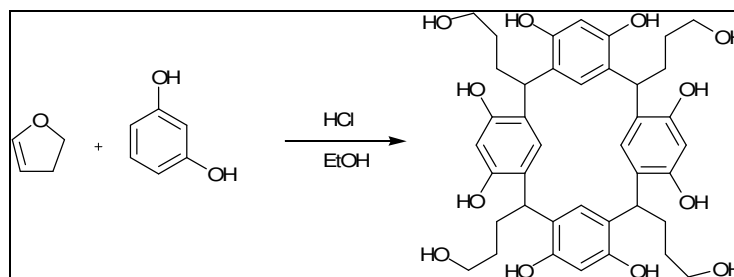
Resorcinol (5 g 45 mmol) was dissolved in methanol (200 ml). Hydrochloric acid (37% 50 ml) was added and the solution was stirred for 5 minutes at room temperature. 2,3-Dihydropyran (3.18 g, 45 mmol) in methanol (50 ml) was added drop-wise to the acidic resorcinol solution over 1 hour. The reaction mixture was stirred for 1 hour at room temperature under an atmosphere of nitrogen. The reaction was then heated to 60°C for 144 hours. The reaction was then cooled in an ice bath and the resulting precipitate was filtered. The off-white solid was suspended in water and sonicated for 15 minutes. The white solid was filtered once more and dried in a vacuum oven overnight. NMR shows solid (5.29 g) to be product (65 % Yield).

^{1}H NMR(CD$_3$OD / D$_2$O δppm 400 MHz) 7.23 (s, 1H), 6.23 (s, 1H), 4.25 (t, 1H, ^3J = 7.71 Hz), 3.60 (t, 2H, ^3J = 6.75 Hz), 2.23 (m, 2H), 1.48 (m, 2H), ^{13}C{^{1}H} NMR (CD$_3$OD / D$_2$O δppm 100 MHz) 152.6, 141.4, 125.4, 103.9, 62.8, 35.9, 31.9, 30.7, IR ATR cm^{-1} 3159, 2934, 1616, 1498, 1441, 1366, 1285, 1223, 1157, 1021, 845, 518, MS *m/z* (ESI+) 743 [M+Na]$^{+}$ (100%)

Crystal data for *C*-(Propan-3-ol)-calix[4]resorcinarene acetonitrile water clathrate: C$_{168}$H$_{204}$N$_4$O$_{56}$, *M* = 3175.35, Orange Plate, 0.58 × 0.50 × 0.10 mm^3, monoclinic, space group *P*2$_1$/*c* (No. 14), *a* = 13.379(3), *b* = 19.146(4), *c* = 18.112(7) Å, β = 119.50(2)°, *V* = 4038(2) Å^3, *Z* = 1, *D*$_c$ = 1.306 g/cm^3, *F*$_{000}$ = 1688, Bruker-Nonius 95mm CCD camera on goniostat, Mo*K*α radiation, λ = 0.71073 Å, *T* = 120(2)K, 2θ_{max} = 55.1°, 50561 reflections collected, 9277 unique (*R*$_{int}$ = 0.0465). Final *GooF* = 1.075, *R1* = 0.0954, *wR2* = 0.2464, *R* indices based on 6613 reflections with I >2σ (I) (refinement on *F*^{2}), 532 parameters, 0 restraints. Lp and absorption corrections applied, μ = 0.098 mm^{-1}.

Crystal data for C-(Propan-3-ol)-calix[4]resorcinarene acetonitrile water clathrate: $C_{42}H_{51}NO_{15}$, M = 811.88, light yellow slab, $0.40 \times 0.32 \times 0.14$ mm^3, tetragonal, space group $P4_2/ncm$ (No. 138), $a = b =$ 15.48520(10), c = 17.4646(3) Å, V = 4187.86(8) Å^3, Z = 4, D_c = 1.294 g/cm^3, F_{000} = 1744, Bruker-Nonius 95mm CCD camera on goniostat, MoKα radiation, λ = 0.71073 Å, T = 120(2)K, $2\theta_{max}$ = 55.0º, 34174 reflections collected, 2533 unique (R_{int} = 0.0442). Final *GooF* = 1.210, *R1* = 0.0890, *wR2* = 0.2194, R indices based on 2305 reflections with I >2sigma(I) (refinement on F^2), 152 parameters, 0 restraints. Lp and absorption corrections applied, μ = 0.098 mm^{-1}.

16 Synthesis of C-*p*Nitrobenzene-calix[4]pyrogallolarene (C-*p*NO2C6H4 Pg)
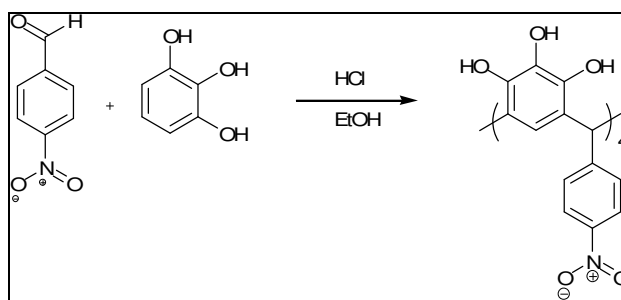
Pyrogallol (10 g, 79 mmol) was dissolved in ethanol (100 ml), hydrochloric acid (37% 25 ml) was added and the solution was stirred for 5 minutes at room temperature. *p*-Nitrobenzaldehyde (11.9 g 79 mmol) in ethanol (20 ml) was added drop-wise over 1 hour to the acidic pyrogallol solution. The mixture was stirred at room temperature for 1 hour the heated to 60°C for 120 hours. The mixture was then cooled and the resulting precipitate was filtered off and the solid (14.29 g) was washed with ice cold methanol. Analysis shows solid to be the desired product (70% yield)

[1]H ((CD$_3$)$_2$SO δppm 400 MHz) 7.76 (d, 2H, J^3 = 8.72 Hz), 6.84 (d, 2H, ^3J = 8.28 Hz), 5.83 (s, 1H), 5.77 (s, 1H), 1.22 (s, 1H), [13]C{[1]H} ((CD$_3$)$_2$SO δppm 100 MHz) 152.8, 144.7, 142.8, 142.4, 131.9, 129.9, 122.2, 121.0, 119.9, 48.6, IR v_{max} ATR cm^{-1} 3435, 2926, 1624, 1603, 1518, 1462, 1350, 1287, 1077, 1013, 859, 818, 700, 563 MS *m/z* (ESI+) 1037 [M+H]$^+$ (25%), 1059 [M+Na]$^+$ (100), 1122 [M+K]$^{+\cdot}$

Crystal data for *C*-(4-nitrophenyl)-calix[4]pyrogallolarene ethyl methyl ketone water clathrate: $C_{38}H_{42}N_2O_{17}$, *M* = 798.74, brown-green block, $0.10 \times 0.10 \times 0.04$ mm^3, triclinic, space group *P*-1 (No. 2), *a* = 10.909(4), *b* = 14.075(5), *c* = 14.615(5) Å, α = 91.686(4), β = 106.942(4), γ = 102.816(4)°, *V* = 2082.5(13) Å^3, *Z* = 2, D_c = 1.274 g/cm^3, F_{000} = 840, Bruker SMART APEX2 CCD diffractometer, synchrotron radiation, λ = 0.7977 Å, *T* = 120(2)K, $2\theta_{max}$ = 47.1°, 15321 reflections collected, 7279 unique (R_{int} = 0.0375). Final *GooF* = 1.811, *R1* = 0.1580, *wR2* = 0.4365, *R* indices based on 4325 reflections with I >2σ (I) (refinement on F^2), 425 parameters, 0 restraints. Lp and absorption corrections applied, μ = 0.101 mm^{-1}.

17 Synthesis of 3-Bromopropanol
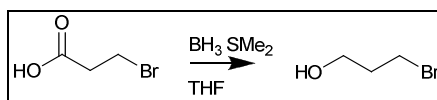
In a flame-dried, 3 necked round bottomed flask; 3-bromopropionic acid (20 g, 131 mmol) was dissolved in freshly distilled THF (250 ml). Borane-methyl sulphide complex (12.6 ml, 131 mmol) in THF (200 ml) was added drop-wise. When half the borane solution was added, the reaction was heated to reflux. Once at reflux the remaining borane was added drop-wise. The reaction mixture was stirred for 2 hours at reflux, then cooled to room temperature. The reaction was slowly poured into ice cold methanol (400 ml), once the addition was complete, the solution was allowed to warm to room temperature and was then stirred for 1 hour. The solvent was removed by rotary evaporation, and the resulting yellow oil (18 g 129 mmol) shown to be product. (99 % Yield)

^{1}H (CDCl$_3$ δppm, 400 MHz) 3.71 (*t*, 2H, ^3J = 6.46 Hz), 3.42 (*t*, 2H, ^3J = 6.36 Hz), 2.021 (*q*, 2H, ^3J = 6.12 Hz), ^{13}C{^{1}H} (CDCl$_3$, δppm, 100 MHz) 54.9, 38.8, 30.2, IR ν_{max} ATR cm^{-1} 3328, 2949, 2882, 1726, 1254, 1082, 910, 646, 563, MS *m/z* (ESI) 137 [M+H]$^+$ (5%), 120 [M – OH + H]$^+$ (100), 58 [M – Br + H] $^+$ (90)

18 Synthesis of 3-Bromopropanal
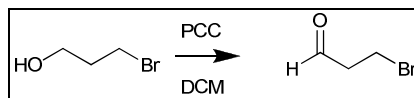
To a rapidly stirring solution of 3-bromopropanol (10 g, 72 mmol) in dichloromethane (300 ml), pyridinium chlorochromate was added (18.56 g, 86 mmol). The pale yellow solution immediately darkened to a deep brown colour, and the solution was heated to reflux for 3 hours. The reaction was monitored by thin layer chromatography (3:7 ethyl acetate / 40 – 60ºC petroleum ether on silica) and once the starting materials had been consumed after 3 hours at reflux, the black solution was cooled and was passed through a silica plug which was then washed with further portions of dichloromethane to ensure complete recovery of product. The solvent was then removed by rotary evaporation to yield a yellow oil (7.45 g, 54 mmol), which on analysis was shown to be the desired product. (76 % yield)

^{1}H (CDCl$_3$ δppm, 400 MHz) 9.77 (*s*, 1H), 3.43 (*t*, 2H, ^3J = 6.5 Hz), 2.64 (*t*, 2H, ^3J = 6.7 Hz), ^{13}C{^{1}H} (CDCl$_3$, δppm, 100 MHz) 202.0, 32.91, 42.2, IR ν_{max} ATR cm^{-1} 2925, 2857, 1727, 1421, 1259, 1122, 1072, 921, MS *m/z* (ESI) 137 [M+H]$^+$, (20%), 57 [M – Br]$^+$(100)

19 Synthesis of 4-Bromobutanol
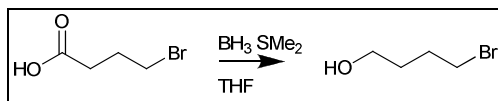
In a flame dried, 3 necked round bottomed flask; 4-bromobutyric acid (5 g, 30 mmol) was dissolved in freshly distilled THF (200 ml). Borane-methyl sulphide complex (2.9 ml, 30 mmol) in THF (200 ml) was added drop-wise to the solution. When half the borane solution was added, the reaction was heated to reflux. Once at reflux the remaining borane was added drop-wise. The reaction mixture was stirred for 1½ hours at reflux and then cooled to room temperature. The reaction was slowly poured into ice cold methanol (400 ml), once the addition was complete, the solution was allowed to warm to room temperature and was then stirred for a further hour. The solvent was removed by rotary evaporation, and the resulting yellow oil (4.362 g) shown to be product. (95 % Yield)

^{1}H (CDCl$_3$ δppm, 400 MHz) 3.55 (*t*, 2H, ^3J = 6.43 Hz), 3.38 (*t*, 2H, ^3J = 6.65 Hz), 1.86 (*qn*, 2H, ^3J = 7.85, 6.96 Hz), 1.62 (*qn*, 2H, ^3J = 8.10, 6.46), ^{13}C{^{1}H} (CDCl$_3$, δppm, 100 MHz) 60.9, 33.4, 30.6, 28.9, IR v_{max} ATR cm^{-1} 3331, 2944, 1630, 1035, 392, MS *m/z* (ESI) 151 [M+H]$^{+\cdot}$, (5%), 134 [M - OH]$^{+\cdot}$ (25), 55 [M - OH & - Br]$^{+\cdot}$ (100)

20 Synthesis of 4-Bromobutanal
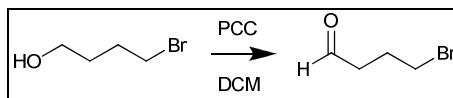
To a rapidly stirring solution of 4-bromobutanol (3 g, 20 mmol) in dichloromethane (100 ml), pyridinium chlorochromate was added (5.06 g, 12 mmol). The pale yellow solution immediately darkened to a deep brown colour, and the solution was heated to reflux for 3 hours. The reaction was monitored by thin layer chromatography (3:7 ethyl acetate / 40 – 60ºC petroleum ether on silica) and once the starting materials had been consumed, the black solution was cooled and was passed through a silica plug which was then washed with further portions of dichloromethane to ensure complete recovery of product. The solvent was then removed by rotary evaporation to yield a yellow oil (2.72 g, 18 mmol), which on analysis by gas chromatography – mass spectrometry was shown to be the desired product. (92 % yield)

^{1}H (CDCl$_3$ δppm, 400 MHz) 9.75 (s,1H), 2.62 (t, 2H, ^3J = 7.39 Hz), 2.44 (t, 2H, ^3J = 7.17 Hz), 2.12 (qn, 2H, ^3J = 6.74, 6.52 Hz), ^{13}C{^{1}H} (CDCl$_3$, δppm, 100 MHz) 200.8, 53.4, 42.1, 32.7, 24.9, IR v_{max} ATR cm^{-1} 2927, 2860, 1720, 1459, 1440, 1400, 1259, 1174, 735, 635, MS m/z (ESI) 151 [M+H]$^+$, (20%), 71 [M – Br]$^+$(100)

21 Synthesis of 5-Bromopentanol
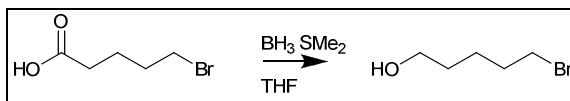
In a flame dried, 3 neck round bottomed flask, 5-bromopenanoic acid (20 g, 110 mmol) was dissolved in freshly distilled THF (200 ml). Borane-dimethyl sulfide complex (10.6 ml, 110 mmol) in THF (200 ml) was added drop-wise. When half the borane solution was added, the reaction was heated to reflux. Once at reflux the remaining borane was added drop-wise to the refluxing solution. The reaction mixture was stirred for 2 hours at reflux, and then cooled to room temperature. The reaction was slowly poured into ice cold methanol (400 ml), once the addition was complete, the solution was allowed to warm to room temperature and was then stirred for 1 hour. The solvent was removed by rotary evaporation, and the resulting yellow oil (18.119 g, 108 mmol) upon analysis was shown to be the desired product. (99 % Yield)

^{1}H (CDCl$_3$ δppm, 400 MHz) 3.57 (t, 2H, ^3J = 6.22 Hz), 3.36 (t, 2H, ^3J = 6.51 Hz), 1.83 (qn, 2H, ^3J = 6.73, 7.65 Hz), 1.56 - 1.42 (m, 4H), ^{13}C{^{1}H} (CDCl$_3$, δppm, 100 MHz) 62.2, 33.7, 32.2, 31.5, 24.3, IR v_{max} ATR cm^{-1} 3333, 2937, 2864, 1732, 1455, 1431, 1246, 1044, 733, 641, 559, MS m/z (ESI) 167 [M+H]$^{+\cdot}$, (40%), 87 [M – Br]$^{+\cdot}$(100)

22 Synthesis of 5-Bromopentanal
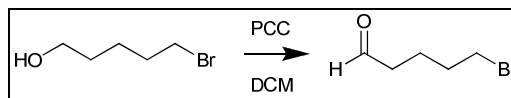
To a rapidly stirring solution of 5-bromopentanol (10 g, 60 mmol) in dichloromethane (400 ml), pyridinium chlorochromate was added (25.8 g, 120 mmol). The pale yellow solution immediately darkened to a deep brown colour, and the solution was heated to reflux for 3 hours. The reaction was monitored by thin layer chromatography (3:7 ethyl acetate / 40 – 60ºC petroleum ether on silica) and once the starting materials had been consumed, the black solution was cooled and was passed through a silica plug which was then washed with further portions of dichloromethane to ensure complete recovery of product. The solvent was then removed by rotary evaporation to yield a yellow oil (9.432 g), which on analysis was shown to be the desired product. (95 % yield)

^{1}H (CDCl$_3$ δppm, 400 MHz) 9.71 (*s*, 1H), 3.36 (*t*, 2H, ^3J = 6.63 Hz), 2.43 (*t*, 2H, ^3J = 7.29 Hz), 1.87 - 1.68 (*m*, 4H), ^{13}C{^{1}H} (CDCl$_3$, δppm, 100 MHz) 201.7, 42.6, 33.0, 31.7, 20.4, IR v_{max} ATR cm^{-1} 2940, 2726, 1722, 1433, 1253, 1122, 1061, 751, 560, MS *m/z* (ESI) 164 [M+H]$^{+}$, (20%), 159 [M – CHO]$^{+}$(100)

23 Synthesis of 6-Bromohexanol
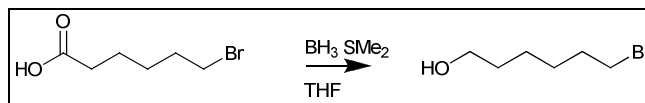
In a flame dried, 3 neck round bottomed flask, 6-bromohexanoic acid (10 g, 51 mmol) was dissolved in freshly distilled THF (200 ml). Borane-dimethyl sulfide complex (4.9 ml, 51 mmol) in THF (200 ml) was added drop-wise. When half the borane solution was added, the reaction was heated to reflux. Once at reflux the remaining borane was added drop-wise to the refluxing solution. The reaction mixture was stirred for 2 hours at reflux, then cooled to room temperature. The reaction was slowly poured into ice cold methanol (200 ml), once the addition was complete, the solution was allowed to warm to room temperature and was then stirred for 2 hours. The solvent was removed by rotary evaporation, and the resulting yellow oil (9.2 g, 50 mmol) shown to be product. (99 % Yield)

^{1}H (CDCl$_3$ δppm, 400 MHz) 3.52 (t, 2H, ^3J = 6.82 Hz), 3.35 (t, 2H, ^3J = 6.82 Hz), 1.79 (qn, 2H, ^3J = 6.89, 6.95), 1.52 - 1.25 (m, 6H), ^{13}C{^{1}H} (CDCl$_3$, δppm, 100 MHz) 61.9, 33.6, 32.4, 31.9, 27.6, 24.6, IR ν_{max} ATR cm^{-1} 3347, 2933, 2858, 1721, 1459, 1436, 1258, 1051, 1031, 727, 642, 559, 383, MS m/z (ESI) 181 [M+H]$^{+\cdot}$, (20%), 101 [M – Br]$^{+\cdot}$(100)

24 Synthesis of 6-Bromohexanal
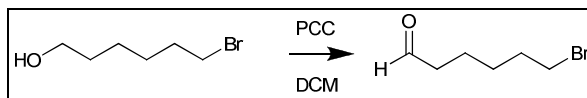
To a rapidly stirring solution of 6-bromohexanol (5 g, 28 mmol) in dichloromethane (150 ml), pyridinium chlorochromate was added (11.9 g, 55 mmol). The pale yellow solution immediately darkened to a deep brown colour, and the solution was heated to reflux for 3 hours. The reaction was monitored by thin layer chromatography (3:7 ethyl acetate / 40 – 60°C petroleum ether on silica) and once the starting materials had been consumed, the black solution was cooled and was passed through a silica plug which was then washed with further portions of dichloromethane to ensure complete recovery of product. The solvent was then removed by rotary evaporation to yield a colourless oil (3.647 g, 20 mmol), which on analysis was shown to be the desired product (74 % yield).

^{1}H (CDCl$_3$ δppm, 400 MHz) 9.72 (s, 1H), 3.37 (t, 2H, ^3J = 6.81 Hz), 2.42 (t, 2H, ^3J = 7.11 Hz), 1.84 (qn, 2H, ^3J = 6.78, 7.04), 1.61 (qn, 2H, ^3J = 7.32, 7.32), 1.47 - 1.39 (m, 2H), ^{13}C\{^{1}H\} (CDCl$_3$, δppm, 100 MHz) 202.2, 53.4, 33.4, 32.3, 27.5, 21.0, IR ν_{max} ATR cm^{-1} 2938, 2864, 2723, 1722, 1459, 1437, 1410, 1265, 1197, 735, 640, 559, MS m/z (ESI) 179 [M+H]$^+$, (5%), 150 [M – CHO] $^+$(100)

25 Synthesis of 8-Bromooctanol
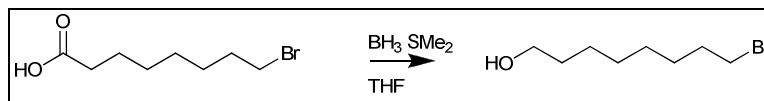
In a flame dried, 3 neck round bottomed flask, 8-bromooctanoic acid (5 g, 22 mmol) was dissolved in freshly distilled THF (100 ml). Borane-dimethyl sulfide complex (2.15 ml, 22 mmol) in THF (20 ml) was added drop-wise. When half the borane solution was added, the reaction was heated to reflux. Once at reflux the remaining borane was added drop-wise to the refluxing solution. The reaction mixture was stirred for 2 hours at reflux, then cooled to room temperature. The reaction was slowly poured into ice cold methanol (200 ml), once the addition was complete, the solution was allowed to warm to room temperature and was then stirred for 2 hours. The solvent was removed by rotary evaporation, and the resulting yellow oil (4.72 g, mmol) shown to be product. (99 % Yield)

^{1}H (CDCl$_3$ δppm, 400 MHz) 3.28 (*m*, 2H), 3.11 (*m*, 2H), 1.52 (*qn*, 2H, ^3J = 7.18, 7.62 Hz), 1.23 - 0.95 (*m*, 10H), ^{13}C{^{1}H} (CDCl$_3$, δppm, 100 MHz) 62.0, 33.5, 32.2, 29.0, 28.5, 27.8, 25.4, IR v_{max} ATR cm$^-$^{1} 3339, 2928, 2855, 1723, 1462, 1272, 1126, 1054, 723, 643, 561, MS *m/z* (ESI) 209 [M+H]$^{+\cdot}$, (2%), 129 [M – Br]$^{+\cdot}$(100)

26 Synthesis of 8-Bromooctanal
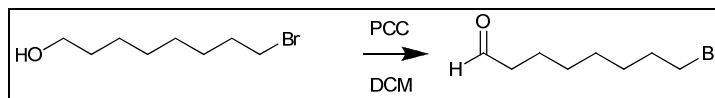
To a rapidly stirring solution of 6-bromohexanol (4 g, 19 mmol) in dichloromethane (150 ml), pyridinium chlorochromate was added (8.23 g, 38 mmol). The pale yellow solution immediately darkened to a deep brown colour, and the solution was heated to reflux for 3 hours. The reaction was monitored by thin layer chromatography (3:7 ethyl acetate / 40 – 60ºC petroleum ether on silica) and once the starting materials had been consumed, the black solution was cooled and was passed through a silica plug which was then washed with further portions of dichloromethane to ensure complete recovery of product. The solvent was then removed by rotary evaporation to yield a colourless oil (1.2 g, 6 mmol), which on analysis was shown to be the desired product (32 % yield).

^{1}H (CDCl$_3$ δppm 400 MHz) 9.72 (s, 1H), 3.36 (t, 2H, ^3J = 6.8 Hz), 2.38 (m, 2H), 1.81 (m, 2H), 1.60 (m, 2H), 1.41 (m, 2H), 1.29 (m, 4H), ^{13}C{^{1}H} (CDCl$_3$ δppm 100 MHz) 202.6, 43.7, 33.8, 32.6, 28.8, 28.4, 27.8, 21.8, IR v_{max} ATR cm^{-1} 2930, 2857, 1707, 1461, 1269, 1122, 1072, 941, 737, 644, 561, MS *m/z* (ESI) 207 [M+H]$^{+\cdot}$, (25%), 178 [M – CHO] $^+$(100)

27 Synthesis of 11-Bromoundecanol
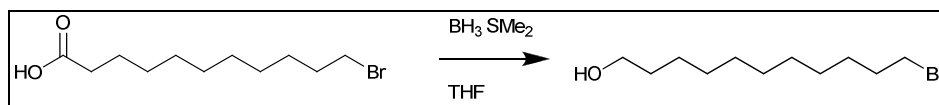
In a flame dried, 3 neck round bottomed flask, 11-Bromoundecanoic acid (10 g, 38 mmol) was dissolved in freshly distilled THF (150 ml). Borane-dimethyl sulfide complex (3.8 ml, mmol) in THF (50 ml) was added drop-wise. When half the borane solution was added, the reaction was heated to reflux. Once at reflux the remaining borane was added drop-wise to the refluxing solution. The reaction mixture was stirred for 2 hours at reflux, then cooled to room temperature. The reaction was slowly poured into ice cold methanol (200 ml), once the addition was complete, the solution was allowed to warm to room temperature and was then stirred for 1 hour. The solvent was removed by rotary evaporation, and the resulting yellow oil (9.261 g, 36 mmol) crystallised on standing. Shown to be product. (98 % Yield)

^{1}H (CDCl$_3$ δppm, 400 MHz) 3.60 (*t*, 2H, ^3J = 6.85 Hz), 3.38 (*t*, 2H, ^3J = 7.01 Hz), 1.82 (*qn*, 2H, ^3J = 6.85, 6.63 Hz), 1.53 (*qn*, 2H, ^3J = 6.41, 6.85 Hz) 1.39 - 1.17 (*m*, 14H), ^{13}C{^{1}H} (CDCl$_3$, δppm, 100 MHz) 63.11, 34.2, 32.9, 32.8, 29.6, 29.6, 29.4 (two concurrent resonances), 28.8, 28.2, 25.8, IR ν_{max} ATR cm^{-1} 3427, 2917, 2892, 2850, 1466, 1345, 1302, 1266, 1240, 1209, 1187, 1057, 1050, 1034, 1001, 982, 972, 723, 644, 594, 519, 492, MS *m/z* (ESI+) 250 [M + H]$^+$ (100%)

28 Synthesis of 11-Cyanoundecanol
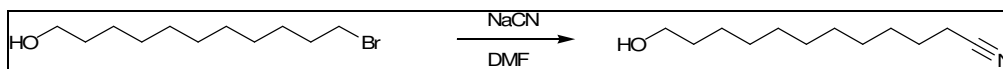
To a solution of 11-bromoundecanol (20 g, 79 mmol) in N,N'-dimethylformamide (500 ml) sodium cyanide (3.9 g, 79 mmol) was added. The mixture was stirred under nitrogen at 60°C for 3 hours after which, TLC analysis (3 : 7 ethyl acetate / 40- 60°C petroleum ether) shows the starting material (Rf = 0.30) has been consumed. The solvent was removed by distillation under reduced pressure. The solid residue was suspended in diethyl ether which was then washed three times with water and then once with brine. The layers were separated and the organic solvent was dried over anhydrous magnesium sulphate then removed on a rotary evaporator to yield a yellow oil (11.18 g, 71 % yield) which solidified on cooling. NMR and GCMS analysis shows oil to be pure product.

^{1}H ((CDCl$_3$ δppm 400 MHz) 3.53 (2H, t, ^3J = 6.72 Hz), 2.27 (2H, t, ^3J = 6.9 Hz), 1.57 (m, 2H), 1.47 (m, 2H), 1.35 (m, 2H), 1.21 (m, 12H), ^{13}C{^{1}H} (CDCl$_3$ δppm 100 MHz) 162.7, 119.9, 62.8, 32.7, 29.5,29.4, 29.3, 28.8, 28.7, 25.8, 25.4, 17.1, IR v_{max} ATR cm^{-1} 3440, 2923, 2853, 2247, 1732, 1466, 1350, 1052, 722, 581, MS m/z (ESI+) 198 [M+H]$^+$, (90%), 180 [M – OH + H]$^+$ (100)

29 Synthesis of 11-Cyanoundecanal
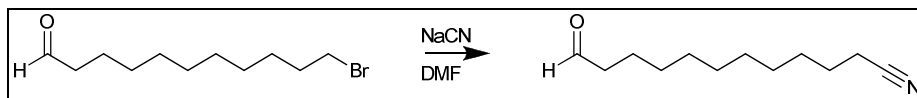
To a rapidly stirring solution of 11-cyanoundecanol (5 g, 25 mmol) in dichloromethane (50 ml), pyridinium chlorochromate (11.02 g, 50 mmol) was added. The mixture was heated to reflux for 2 hours after which TLC analysis (3 : 7 ethyl acetate / 40- 60°C petroleum ether) showed complete consumption of the starting material (R*f* 0.68). The reaction mixture was passed through a plug of silica gel which was eluted with dichloromethane. The collected solvent was removed using a rotary evaporator to yield a yellow oil (3.48 g, 77 % yield) which was shown by NMR and GCMS analysis to be pure product.

^{1}H ((CD$_3$)$_2$SO δppm 400 MHz) 9.69 (s, 1H, H*a*), 2.35 (t, ^3J = 7.43 Hz, 2H, H*k*), 2.27 (t, ^3J = 7.20 Hz, 2H, H*b*), 1.56 (m, 4H, H*i,j*), 1.37 (m, 2H, H*c*), 1.22 (m, 10H, H*d-h*), ^{13}C{^{1}H} (CDCl$_3$ δppm 100 MHz) 202.9 (C*a*), 119.9 (C*l*), 43.9 (C*k*), 29.3, 29.3, 29.2, 29.1, 28.7, 28.6, 25.4, 22.0, 17.1 (C*b-j*), IR v_{max} ATR cm^{-1} 2926, 2855, 2720, 2246, 1723, 1465, 1430, 736, 526, MS (ESI+) 194 (M$^{+\cdot}$), 167 (M – CN)

30 Synthesis of *C*-(4-chlorobutane)-calix[4]pyrogallolarene
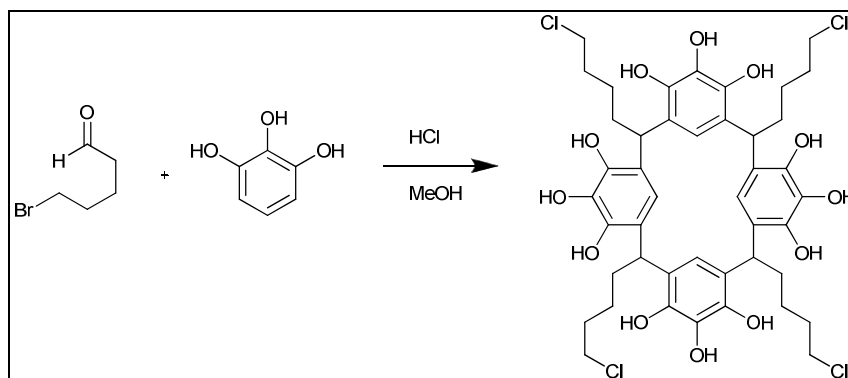
Pyrogallol (2.53 g, 20 mmol) was dissolved in ethanol (100 ml) and hydrochloric acid (25 ml, 283 mmol) was added. The solution was stirred at room temperature for 10 minutes, after which, 5-bromopentanal (5 g, 20 mmol) in ethanol (20 ml) was added drop-wise over 20 minutes. The solution was stirred for 1 hour at room temperature and then heated to 50ºC for 144 hours. The reaction mixture was allowed to cool to room temperature and the crystalline precipitate was filtered (3.525 g, 49% Yield). NMR shows precipitate to be product. Crystals suitable for single x-ray crystallography formed over 24 hours in the mother liquors of the filtration.

^{1}H ((CD$_3$)$_2$SO δppm 400 MHz) 6.86 (*s*, 1H), 4.16 (*t*, 1H, ^3J = 7.61 Hz), 3.60 (*t*, 2H, ^3J = 6.76 Hz), 2.16 (*m*, 2H), 1.76 (*m*, 2H), 1.29 (*m*, 2H), ^{13}C{^{1}H} ((CD$_3$)$_2$SO δppm 400 MHz) 39.7, 132.9, 124.3, 113.4, 56.0, 45.5, 32.2, 25.3, 18.6, IR ν_{max} ATR cm^{-1} 3205, 2934, 2866, 1622, 1475, 1387, 1306, 1094, 1033, 978, 720, MS m/z (ESI+) 915 ([M+H]$^{+}$, 90%), 937 [M + Na]$^+$ (10), 959 [M + C$_2$H$_5$OH + H]$^+$ (30)

Crystal data for *C*-(4-chlorobutane)-calix[4]pyrogallolarene diethylether clathrate: C$_{52}$H$_{73}$Cl$_5$O$_{15}$, *M* = 1115.35, colourless plate, 0.48 × 0.36 × 0.08 mm^3, triclinic, space group *P*-1 (No. 2), *a* = 13.0897(4), *b* = 13.2617(4), *c* = 18.3750(5) Å, α = 78.5860(10), β = 76.8360(10), γ = 64.842(2)°, *V* = 2792.75(14) Å^3, *Z* = 2, *D*$_c$ = 1.326 g/cm^3, *F*$_{000}$ = 1180, Bruker-Nonius Roper CCD camera on goniostat, Mo*K*α radiation, λ = 0.71073 Å, *T* = 120(2)K, 2θ_{max} = 55.3°, 58121 reflections collected, 12821 unique (*R*$_{int}$ = 0.0427). Final *GooF* = 1.025, *R1* = 0.0940, *wR2* = 0.2468, *R* indices based on 10086 reflections

with I $>2\sigma$ (I) (refinement on F^2), 719 parameters, 4 restraints. Lp and absorption corrections applied, $\mu = 0.324$ mm^{-1}.

Crystal data for C-(4-chlorobutane)-calix[4]pyrogallolarene 2-propanol clathrate: $C_{188}H_{276}Cl_{16}O_{72}$, M = 4255.29, colourless plate, $0.55 \times 0.42 \times 0.06$ mm^3, monoclinic, space group $P2_1/c$ (No. 14), a = 18.2796(4), b = 13.2600(5), c = 20.7196(7) Å, β = 94.955(2)°, V = 5003.4(3) Å^3, Z = 1, D_c = 1.412 g/cm^3, F_{000} = 2252, Bruker-Nonius APEX II CCD camera on goniostat, Mo$K\alpha$ radiation, λ = 0.71073 Å, T = 120(2)K, $2\theta_{max}$ = 62.5°, 45253 reflections collected, 11412 unique (R_{int} = 0.0931). Final $GooF$ = 1.097, $R1$ = 0.1113, $wR2$ = 0.2098, R indices based on 7043 reflections with I $>2\sigma$ (I) (refinement on F^2), 697 parameters, 1 restraint. Lp and absorption corrections applied, $\mu = 0.310$ mm^{-1}.

Crystal data for C-(4-chlorobutane)-calix[4]pyrogallolarene ethanol water clathrate: $C_{48}H_{68}Cl_4O_{16}$, M = 900.45, colourless plate, $0.10 \times 0.08 \times 0.03$ mm^3, triclinic, space group P-1 (No. 2), a = 11.5783(5), b = 12.3650(3), c = 18.5273(7) Å, α = 97.505(2), β = 91.704(2), γ = 94.074(2)°, V = 2621.06(16) Å^3, Z = 2, D_c = 1.375 g/cm^3, F_{000} = 1148, Bruker-Nonius APEX II CCD camera on goniostat, Mo$K\alpha$ radiation, λ = 0.71073 Å, T = 120(2)K, $2\theta_{max}$ = 55.3°, 41446 reflections collected, 11959 unique (R_{int} = 0.0895). Final $GooF$ = 1.058, $R1$ = 0.1243, $wR2$ = 0.2160, R indices based on 6193 reflections with I $>2\sigma$ (I) (refinement on F^2), 667 parameters, 6 restraints. Lp and absorption corrections applied, $\mu = 0.296$ mm^{-1}.

31 Synthesis of *C*-(5-chloropentane)-calix[4]pyrogallolarene
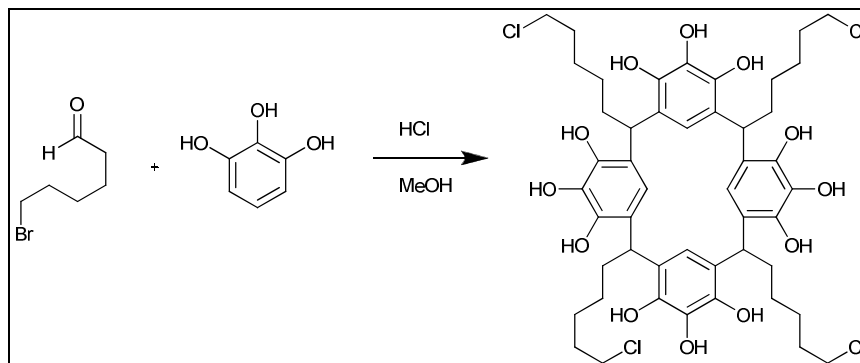
Pyrogallol (2.53 g, 20 mmol) was dissolved in ethanol (100 ml) and hydrochloric acid (25 ml, 283 mmol) was added. The solution was stirred at room temperature for 10 minutes, after which, 6-bromohexanal (5 g, 20 mmol) in ethanol (20 ml) was added drop-wise. The solution was stirred for 1 hour at room temperature and then heated to 50ºC for 144 hours. The reaction mixture was allowed to cool to room temperature and the crystalline precipitate was filtered (43% Yield). NMR shows precipitate to be product. Crystals suitable for single X-ray crystallography formed over 24 hours in the mother liquors of the filtration.

^{1}H ((CD$_3$)$_2$SO δppm 400 MHz) 6.86 (*s*, 1H), 4.36 (*t*, 1H, ^3J = 6.74 Hz), 3.55 (*t*, 2H, ^3J = 7.35 Hz), 2.25 (*m*, 2H), 1.79 (*qn*, 2H, ^3J = 6.52, 6.52 Hz), 1.58 (*m*, 2H), 1.36 (*m*, 2H), ^{13}C{^{1}H} ((CD$_3$)$_2$SO δppm 400 MHz) 137.4, 131.4, 125.3, 113.6, 58.4, 34.0, 32.6, 27.5, 26.9, 18.4, IR ν_{max} ATR cm^{-1} 3286, 2928, 2855, 1612, 1474, 1307, 1098, 977, 720, MS m/z (ESI+) 970 [M+H]$^+$, (90%), 991 [M + Na]$^+$ (15), 1015 [M + C$_2$H$_5$OH + H]$^+$ (10)

Crystal data for *C*-(5-chloropentane)-calix[4]pyrogallolarene ethanol clathrate: C$_{52}$H$_{72}$Cl$_4$O$_{14}$, *M* = 1062.90, Colourless Slab, 0.2 × 0.18 × 0.06 mm^3, triclinic, space group *P*-1 (No. 2), *a* = 10.3726(2), *b* = 13.2310(2), *c* = 19.4494(4) Å, α = 87.0790(10), β = 80.4320(10), γ = 88.1340(10)°, *V* = 2627.90(8) Å^3, *Z* = 2, *D*$_c$ = 1.343 g/cm^3, *F*$_{000}$ = 1128, Bruker-Nonius Roper CCD camera on goniostat, MoKα radiation, λ = 0.71073 Å, *T* = 120(2)K, $2\theta_{max}$ = 55.1°, 54792 reflections collected, 12082 unique (R$_{int}$ = 0.0477). Final *GooF* = 1.005, *R1* = 0.0693, *wR2* = 0.1805, *R* indices based on 9149 reflections with

I >2σ (I) (refinement on F^2), 681 parameters, 0 restraints. Lp and absorption corrections applied, μ = 0.290 mm^{-1}.

32 Synthesis of *C*-(10-Bromodecane)-calix[4]pyrogallolarene
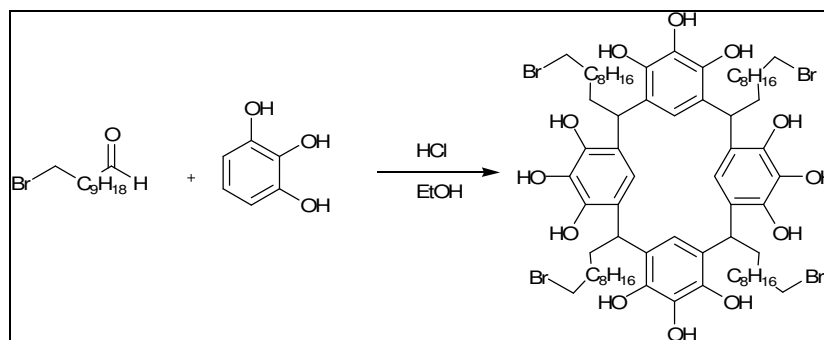
Pyrogallol (2.53 g, 20 mmol) was dissolved in ethanol (100 ml) and hydrochloric acid (25 ml) was added. The solution was stirred at room temperature for 10 minutes, after which, 11-bromoundecanal (5 g, 20 mmol) in ethanol (20 ml) was added drop-wise. The solution was stirred for 1 hour at room temperature and then heated to 50ºC for 144 hours. The reaction mixture was allowed to cool to room temperature and the crystalline precipitate was filtered to yield a colourless solid which upon analysis was shown to be the desired product (3.525 g, 56 % yield). Crystals suitable for single X-ray crystallography formed over 24 hours in the mother liquors of the filtration and were submitted to the EPSRC X-ray crystallography analysis service.

^{1}H (CDCl$_3$ δppm 400 MHz) 8.70 (s, 1H), 7.40 (s, 1H), 6.81 (s, 1H), 6.76 (s, 1H), 6.76 (s, 1H), 3.46 (t, 1H ^3J = 6.60 Hz), 3.31 (t, 2H, ^3J = 6.82 Hz), 1.78 (p, 2H, ^3J = 7.21 Hz), 1.70 (p, 2H, ^3J = 7.12 Hz), 1.47 – 1.23 (m, 14H), ^{13}C{^{1}H} ((CD$_3$)$_2$SO δppm 400 MHz) 131.5, 127.6, 125.6, 123.9, 45.1, 34.0, 32.8, 32.6, 29.7, 29.5, 28.9, 28.9, 28.8, 28.2, IR ν_{max} ATR cm^{-1} 3454, 3263, 2923, 2852, 1634, 1508, 1479, 1338, 1280, 1239, 1083, 978, 932, 778, 721, 681, 640, 544, 390, MS *m/z* (ES+) 1347 (M+ -Br, 20%), 554 (50), 392 (100)

Crystal data for C-(10-bromodecane)-calix[4]pyrogallolarene ethanol clathrate: $C_{204}H_{294}Br_{12}O_{36}$, $M =$ 4281.31, Colourless Rhombus, $0.2 \times 0.18 \times 0.14$ mm^3, trigonal, space group R-3 (No. 148), $a = b =$ 37.2327(5), $c = 27.2555(8)$ Å, $V = 32721.5(11)$ Å^3, $Z = 6$, $D_c = 1.304$ g/cm^3, $F_{000} = 13356$, MoKα radiation, $\lambda = 0.71073$ Å, $T = 273(2)$K, $2\theta_{max} = 55.0º$, 67280 reflections collected, 16584 unique (R_{int} = 0.0804). Final $GooF = 1.650$, $R1 = 0.2319$, $wR2 = 0.5224$, R indices based on 6400 reflections with I $>2\sigma$ (I) (refinement on F^2), 778 parameters, 3 restraints. Lp and absorption corrections applied, $\mu =$ 2.268 mm^{-1}.

Crystal data for C-(10-Bromodecane)-calix[4]pyrogallolarene methanol clathrate: $C_{424}H_{654}Br_{24}O_{92}$, M = 9141.31, colourless block, $0.4 \times 0.33 \times 0.08$ mm^3, trigonal, space group R-3 (No. 148), $a = b =$ 37.2447(6), $c = 27.2736(8)$ Å, $V = 32764.4(12)$ Å^3, $Z = 3$, $D_c = 1.390$ g/cm^3, $F_{000} = 14322$, Bruker-Nonius Roper CCD camera on goniostat, MoKα radiation, $\lambda = 0.71073$ Å, $T = 120(2)$K, $2\theta_{max} =$ 55.0º, 74104 reflections collected, 16693 unique ($R_{int} = 0.0961$). Final $GooF = 1.872$, $R1 = 0.2385$, $wR2 = 0.5355$, R indices based on 7500 reflections with I $>2\sigma$ (I) (refinement on F^2), 815 parameters, 99 restraints. Lp and absorption corrections applied, $\mu = 2.273$ mm^{-1}.

## 33 Synthesis of *C*-(10-cyanodecane)-calix[4]pyrogallolarene
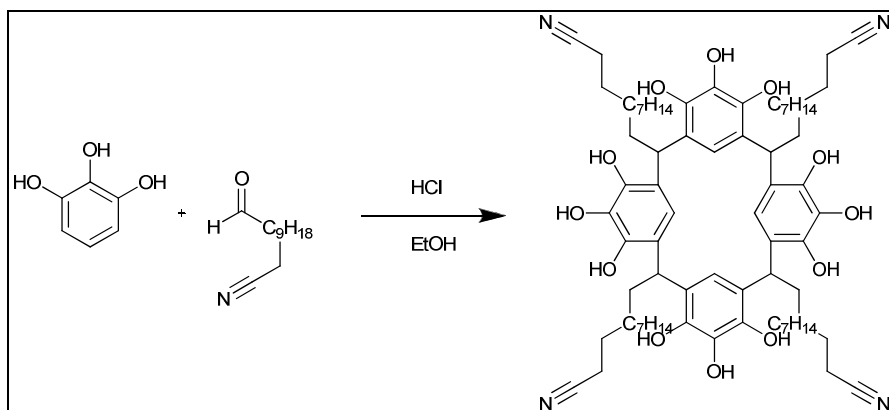
Pyrogallol (0.905 g, 7 mmol) was dissolved in ethanol (20 ml) and hydrochloric acid was added (37 % 5 ml). The solution was placed under nitrogen and stirred for 20 minutes at room temperature. 11-Cyanoundecanal (1.4 g, 7 mmol) in ethanol (20 ml) was added over 6 minutes to the acidic pyrogallol solution. The solution was stirred at room temperature for 10 minutes and then heated to 50°C for 6 days. After this time the solution was concentrated to approximately half its volume and then cooled in an ice bath. After *c.*2 hours crystals formed which were filtered and upon analysis were shown to be the desired product (0.65 g, 0.5 mmol, 30% yield)

^{1}H ((CD$_3$)$_2$SO δppm 400 MHz) 7.07 (*s*, 1H), 2.41 (*m*, 2H), 2.25 (*m*, 2H), 1.59 (*m*, 1H), 1.283 (*m*, 16H), ^{13}C{^{1}H} (CDCl$_3$ δppm 100 MHz) 40.9, 134.4, 126.2, 121.3, 114.2, 35.2, 34.6, 30.8, 30.7, 30.7, 30.5, 30.0, 29.8, 29.2, 26.5, 17.3. MS *m/z* (ESI) 1213 ([M+H]$^+$, 10%), 1235 ([M+Na]$^+$, 100), IR v_{max} ATR cm^{-1} 3313.8, 2920, 2851, 2251, 1719, 1609, 1537, 1468, 1294, 1110, 978, 931, 778, 721, 595

Crystal data for *C*-(10-cyanodecane)-calix[4]pyrogallolarene: C$_{149}$H$_{204}$N$_8$O$_{24}$Cl$_2$, *M* = 2559.0, colourless cut block, $0.35 \times 0.40 \times 0.3$ mm^3, monoclinic, space group *C*2/*c* (No. 15), *a* = 34.066(7), *b* = 12.568(3), *c* = 34.785(7) Å, β = 107.05(3)°, *V* = 14238(5) Å^3, *Z* = 4, *D*$_c$ = 1.195 g/cm^3, *F*$_{000}$ = 5520, Bruker-Nonius Roper CCD camera on goniostat, MoKα radiation, λ = 0.71073 Å, *T* = 173(2)K, 2θ_{max} = 46.6°, 37452 reflections collected, 10197 unique (R$_{int}$ = 0.0450). Final *GooF* = 1.537, *R1* = 0.1179, *wR2* = 0.3479, *R* indices based on 6414 reflections with I >2σ (I) (refinement on *F*^{2}), 839 parameters, 132 restraints. Lp and absorption corrections applied, μ = 0.116 mm^{-1}.

34 Synthesis of dodecyl-acetate-*C*-(10-Cyanodecane)-calix[4]pyrogallolarene
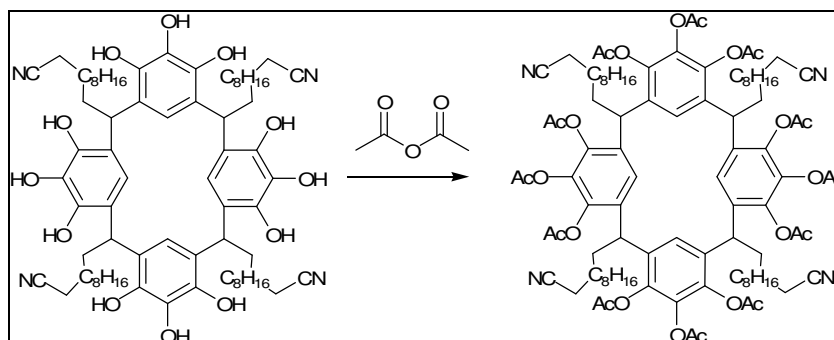
C-(10-cyanodecane)-calix[4]pyrogallolarene (0.1 g, 82 µmol) was suspended in freshly distilled acetic anhydride. The suspension was placed under a stream of nitrogen and stirred for 8 hours at room temperature until the solid starting material had dissolved into the solvent. The residual solvent was removed under vacuum to yield an off-white powder (0.12 g 85% yield) which upon analysis was shown to be the desired product. Crystals suitable for single crystal X-ray diffraction studies were grown by allowing the reaction mixture to slowly evaporate.

^{1}H ((CD$_3$)$_2$SO δppm 400 MHz) 7.29 (broad singlet, 1H), 4.08 (t, 2H, J^3 = 7.7 Hz), 2.29 (t, 2H, ^3J = 7.01 Hz), 2.14 (m, 2H), 1.60 (p, 2H, ^3J = 7.57 Hz), 1.37 (m, 2H), 1.21 (m, 14H), ^{13}C{^{1}H} ((CD$_3$)$_2$SO δppm 100 MHz) 167.4, 167.0, 166.5, 120.0, 37.1, 34.4, 29.6, 29.5, 29.4, 29.3, 28.8, 28.7, 27.9, 25.4, 22.2, 20.0, 17.1, IR v_{max} ATR cm^{-1} 2926, 2855, 1771, 1728, 1440, 1370, 1203, 1165, 1072, 1029, 899, 868, 588, 523

Crystal data for *C*-(10-Cyanodecyl)-calix[4]pyrogallolarene dodecyl-acetal: C$_{96}$H$_{122}$N$_4$O$_{24}$, M = 1715.98, colourless block, $0.20 \times 0.10 \times 0.08$ mm^3, triclinic, space group $P\bar{1}$ (No. 2), a = 12.521(6), b = 17.207(9), c = 24.217(12) Å, α = 96.828(6), β = 101.104(6), γ = 110.673(6)°, V = 4690(4) Å^3, Z = 2, D_c = 1.215 g/cm^3, F_{000} = 1836, Bruker SMART APEX2 CCD diffractometer, synchrotron radiation, λ = 0.6941 Å, T = 120(2)K, $2\theta_{max}$ = 40.6°, 22765 reflections collected, 9743 unique (R$_{int}$ = 0.0950). Final *GooF* = 0.959, *R1* = 0.0739, *wR2* = 0.1702, *R* indices based on 4635 reflections with I >2σ (I) (refinement on F^2), 1137 parameters, 0 restraints. Lp and absorption corrections applied, μ = 0.087 mm^{-1}.

35 Synthesis of supramolecular complex of *C*-(heptyl) calix[4]pyrogallolarene methanol solvate and 4-phenyl-terpyridine hydrochloride
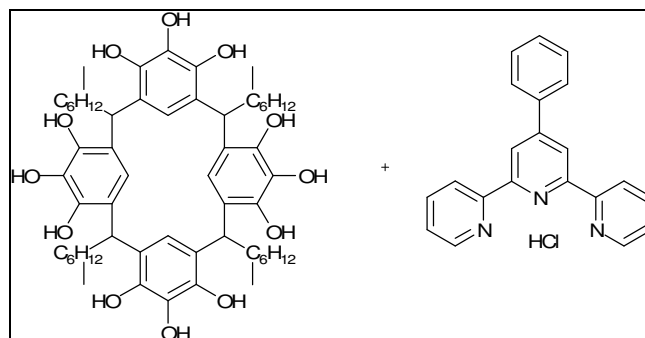
C-(Heptyl) calix[4]pyrogallolarene (0.2 g, 0.21 mmol) which was tae directly from the calixarene synthesis reaction without further purification was dissolved in methanol (20 ml) and 4-phenyl terpyridine was added (0.065 g, 0.21 mmol). The solution was sonicated for 30 minutes and then left to slowly evaporate. After 10 days the volume of solvent had reduced significantly (~10 mL) and crystals suitable for single crystal X-ray diffraction studies formed.

Crystal data for *C*-Heptyl-calix[4]pyrogallolarene 4-phenyl-tripyridine methanol solvate: $C_{59}H_{103}N_3O_{14}Cl$, M = 1113.89, colourless plate, $0.20 \times 0.08 \times 0.01$ mm^3, triclinic, space group *P*-1 (No. 2), a = 12.845(3), b = 13.052(3), c = 23.136(7) Å, α = 77.57(4), β = 80.22(4), γ = 71.71(3)°, V = 3574.6(16) Å^3, Z = 2, D_c = 1.035 g/cm^3, F_{000} = 1455, Bruker SMART APEX2 CCD diffractometer, synchrotron radiation, λ = 0.6941 Å, T = 120(2)K, $2\theta_{max}$ = 45.5°, 10241 reflections collected, 10241 unique (R_{int} = 0.0000). Final *GooF* = 1.064, *R1* = 0.0950, *wR2* = 0.2606, *R* indices based on 6197 reflections with I >2σ (I) (refinement on F^2), 902 parameters, 1 restraint. Lp and absorption corrections applied, μ = 0.121 mm^{-1}.

References

1. F. Corbellini, R. M. A. Knegtel, P. D. J. Grootenhuis, M. Crego-Calama and D. N. Reinhoudt, *Chemistry-a European Journal*, 2004, **11**, 298-307.
2. J. L. Atwood, L. J. Barbour and A. Jerga, *Science*, 2002, **296**, 2367-2369.
3. A. Wei, *Chemical Communications*, 2006, 1581-1591.
4. Rebek J, *Chemical Communications*, 2000, 637-643.
5. J. M. Lehn, in *The Nobel Prize for Chemistry Lecture*, The Nobel Foundation, Stockholm, Sweden, 1987.
6. E. Jabri, M. B. Carr, R. P. Hausinger and P. A. Karplus, *Science*, 1995, **268**, 998-1004.
7. G. A. Jeffrey, *An Introduction to Hydrogen Bonding*, Oxford University Press, 1997.
8. J. W. Steed and J. L. Atwood, *Supramolecular Chemistry*, John Wiley & Sons, Ltd, 2000.
9. D. A. Dougherty, *Science*, 1996, **271**, 163-168.
10. K. Muller-Dethlefs and P. Hobza, *Chemical Reviews*, 2000, **100**, 143-167.
11. J. C. Ma and D. A. Dougherty, *Chemical Reviews*, 1997, **97**, 1303-1324.
12. T. J. Shepodd, M. A. Petti and D. A. Dougherty, *Journal of the American Chemical Society*, 1986, **108**, 6085-6087.
13. M. A. Petti, T. J. Shepodd, R. E. Barrans and D. A. Dougherty, *Journal of the American Chemical Society*, 1988, **110**, 6825-6840.
14. T. J. Shepodd, M. A. Petti and D. A. Dougherty, *Journal of the American Chemical Society*, 1988, **110**, 1983-1985.
15. J. L. Sussman, M. Harel, F. Frolow, C. Oefner, A. Goldman, L. Toker and I. Silman, *Science*, 1991, **253**, 872-879.
16. M. H. Ledu, P. Marchot, P. E. Bougis and J. C. Fontecillacamps, *Journal of Biological Chemistry*, 1992, **267**, 22122-22130.
17. C. Cerveansky, A. Engstrom and E. Karlsson, *European Journal of Biochemistry*, 1995, **229**, 270-275.
18. J. M. Lehn, *Supramolecular Chemistry: Concepts and Perspectives*, VCH, 1995.
19. P. A. Tipler, Mosca, Gene, *Physics for Scientists and Engineers*, W.H. Freeman & Company, 2004.
20. P. J. Collings, Hird, M., *Introduction to Liquid Crystals: Chemistry and Physics*, Taylor & Francis, 1997.
21. M. Kranenburg, M. Vlaar and B. Smit, *Biophysical Journal*, 2004, **87**, 1596-1605.
22. M. Orsi, D. Y. Haubertin, W. E. Sanderson and J. W. Essex, *Journal of Physical Chemistry B*, 2008, **112**, 802-815.
23. J. T. Mohr, G. W. Gribble, S. S. Lin, R. G. Eckenhoff and R. S. Cantor, *Journal of Medicinal Chemistry*, 2005, **48**, 4172-4176.
24. G. Pabst, S. Danner, S. Karmakar, G. Deutsch and V. A. Raghunathan, *Biophysical Journal*, 2007, **93**, 513-525.
25. P. F. A. Maderson, *Nature*, 1964, **203**, 780-781.
26. R. Ruibal and V. Ernst, *Journal of Morphology*, 1965, **117**, 271-&.
27. K. Autumn, Y. A. Liang, S. T. Hsieh, W. Zesch, W. P. Chan, T. W. Kenny, R. Fearing and R. J. Full, *Nature*, 2000, **405**, 681-685.
28. T. W. Kim and B. Bhushan, *Journal of the Royal Society Interface*, 2008, **5**, 319-327.
29. K. J. Laidler, J. H. Meiser and B. C. Sanctuary, *Physical Chemistry*, Houghton Mifflin Company, 2003.
30. M. P. Schramm and J. Rebek, *Chemistry-a European Journal*, 2006, **12**, 5924-5933.
31. L. Trembleau and J. Rebek, Jr., *Science*, 2003, **301**, 1219-1220.
32. Paul D. Beer, Philip A. Gale and D. K. Smith, *Supramolecular Chemistry*, Oxford University Press, 1999.
33. J. A. Thoma and D. E. Koshland, *Journal of the American Chemical Society*, 1960, **82**, 3329-3333.
34. M. F. Perutz, *Nature*, 1990, **348**, 583-584.
35. P. Kumar and M. Clark, *Clinical Medicine*, Elsevier Saunders, 2005.
36. M. F. Perutz, *Trends in Biochemical Sciences*, 1989, **14**, 42-44.
37. M. F. Perutz, *Nature*, 1970, **228**, 726-734.

38.   S. J. Lippard and J. M. Berg, *Principles of Bioinorganic Chemistry*, University Science Books, US, 1994.

39.   W. Kaim and B. Schwederski, *Bioinorganic Chemistry: Inorganic Elements in the Chemistry of Life. An Introduction and Guide*, John Wiley and Sons Ltd, 1999.

40.   R. M. Winslow, M. L. Swenberg, R. L. Berger, R. I. Shrager, M. Luzzana, M. Samaja and L. Rossi-Bernardi, *Journal of Biological Chemistry*, 1977, **252**, 2331-2337.

41.   B. Giardina, D. Mosca and M. C. De Rosa, *Acta Physiologica Scandinavica*, 2004, **182**, 229-244.

42.   C. D. Gutsche, *Calixarenes Revisited (Monographs in Supramolecular Chemistry)*, The Royal Society of Chemistry 1998.

43.   C. D. Gutsche, *Calixarenes: An Introduction (Monographs in Supramolecular Chemistry)*, Royal Society of Chemistry, 2008.

44.   P. J. Cragg, M. C. Allen and J. W. Steed, *Chemical Communications*, 1999, 553-554.

45.   J. M. Harrowfield, M. I. Ogden, W. R. Richmond and A. H. White, *Journal of the Chemical Society-Chemical Communications*, 1991, 1159-1161.

46.   J. T. Lenthall and J. W. Steed, *Coordination Chemistry Reviews*, 2007, **251**, 1747-1760.

47.   A. Ahman and M. Nissinen, *Chemical Communications*, 2006, 1209-1211.

48.   T. Suzuki, K. Nakashima and S. Shinkai, *Chemistry Letters*, 1994, 699-702.

49.   J. L. Atwood, G. A. Koutsantonis and C. L. Raston, *Nature*, 1994, **368**, 229-231.

50.   L. J. Hubble and C. L. Raston, *Chemistry-a European Journal*, 2007, **13**, 6755-6760.

51.   T. Haino, M. Yanase, C. Fukunaga and Y. Fukazawa, *Tetrahedron*, 2006, **62**, 2025-2035.

52.   S. Kunsagi-Mate, K. Szabo, I. Bitter, G. Nagy and L. Kollar, *Tetrahedron Letters*, 2004, **45**, 1387-1390.

53.   J. W. Steed, P. C. Junk, J. L. Atwood, M. J. Barnes, C. L. Raston and R. S. Burkhalter, *Journal of the American Chemical Society*, 1994, **116**, 10346-10347.

54.   C. L. D. Gibb and B. C. Gibb, *Journal of the American Chemical Society*, 2004, **126**, 11408-11409.

55.   D. J. Cram, H. J. Choi, J. A. Bryant and C. B. Knobler, *Journal of the American Chemical Society*, 1992, **114**, 7748-7765.

56.   G. W. V. Cave, M. C. Ferrarelli and J. L. Atwood, *Chemical Communications*, 2005, 2787-2789.

57.   L. Abis, E. Dalcanale, A. Du Vosel and S. Spera, *Journal of Organic Chemistry*, 1988, **53**, 5475-5479.

58.   J. Han, X. Song, L. Liu and C. Yan, *Journal of Inclusion Phenomena and Macrocyclic Chemistry*, 2007, **59**, 257-263.

59.   J. L. Atwood and Steed. J. W, *Organic Nanostructures*, Wiley-VCH, 2008.

60.   P. O. Brown, G. D. Enright and J. A. Ripmeester, *CrystEngComm*, 2006, **8**, 381-383.

61.   J. B. Niederl and H. J. Vogel, *Journal of the American Chemical Society*, 1940, **62**, 2512-2514.

62.   A. G. S. Hoegberg, *Journal of the American Chemical Society*, 1980, **102**, 6046-6050.

63.   A. G. S. Hoegberg, *Journal of Organic Chemistry*, 1980, **45**, 4498-4500.

64.   K. Fairfull-Smith, P. M. J. Redon, J. W. Haycock and N. H. Williams, *Tetrahedron Letters*, 2007, **48**, 1317-1319.

65.   I. Stoll, A. Mix, A. B. Rozhenko, B. Neumann, H.-G. Stammler and J. Mattay, *Tetrahedron*, 2008, **64**, 3813-3825.

66.   A. Ahman, M. Luostarinen, C. A. Schalley, M. Nissinen and K. Rissanen, *European Journal of Organic Chemistry*, 2005, 2793-2801.

67.   G. W. V. Cave, J. Antesberger, L. J. Barbour, R. M. McKinlay and J. L. Atwood, *Angewandte Chemie-International Edition*, 2004, **43**, 5263-5266.

68.   P. Lidstrom, *Microwave Assisted Organic Synthesis*, CRC Press Inc., 2004.

69.   M. Hedidi, S. M. Hamdi, T. Mazari, B. Boutemeur, C. Rabia, F. Chemat and M. Hamdi, *Tetrahedron*, 2006, **62**, 5652-5655.

70.   C. Yan, W. Chen, J. Chen, T. Jiang and Y. Yao, *Tetrahedron*, 2007, **63**, 9614-9620.

71.   A. G. M. Barrett, C. Braddock, J. P. Henschke and E. R. Walker, *Journal of the Chemical Society; Perkin Transitions 1*, 1999, 873 - 878.

72.   B. A. Roberts, G. W. V. Cave, C. L. Raston and J. L. Scott, *Green Chemistry*, 2001, **3**, 280 - 284.

73.   J. Antesberger, G. W. V. Cave, M. C. Ferrarelli, M. W. Heaven, C. L. Raston and J. L. Atwood, *Chemical Communications*, 2005, 892-894.

74.	Y. Aoyama, Y. Tanaka, H. Toi and H. Ogoshi, *Journal of the American Chemical Society*, 1988, **110**, 634-635.
75.	L. R. MacGillivray and J. L. Atwood, *Nature*, 1997, **389**, 469-472.
76.	J. Kang and J. Rebek, *Nature*, 1997, **385**, 50-52.
77.	T. Gerkensmeier, W. Iwanek, C. Agena, R. Frohlich, S. Kotila, C. Nather and J. Mattay, *European Journal of Organic Chemistry*, 1999, 2257-2262.
78.	L. Avram and Y. Cohen, *Journal of the American Chemical Society*, 2004, **126**, 11556-11563.
79.	A. J. Dalgarno S. J., McKinlay R. J., Atwood J. L., *Chemistry - A European Journal*, 2007, **13**, 8248-8255.
80.	L. Avram and Y. Cohen, *Organic Letters*, 2002, **4**, 4365-4368.
81.	G. W. V. Cave, S. J. Dalgarno, J. Antesberger, M. C. Ferrarelli, R. M. McKinlay and J. L. Atwood, *Supramolecular Chemistry*, 2008, **20**, 157-159.
82.	S. J. Dalgarno, K. M. Claudio-Bosque, J. E. Warren, T. E. Glass and J. L. Atwood, *Chemical Communications*, 2008, 1410-1412.
83.	J. L. Atwood and N. Given, WO2003033649-A; US2003073872-A1; WO2003033649-A2; AU2002340007-A1; AU2002340007-A8; US7014868-B2.
84.	G. W. V. C. Brett A. Roberts, Colin L. Raston and Janet L. Scott, *Green Chemistry*, 2001, **3**, 280 - 284.
85.	X. J. Liu, Y. Liu, G. Li and R. Warmuth, *Angewandte Chemie-International Edition*, 2006, **45**, 901-904.
86.	X. Liu, Y. Liu and R. Warmuth, *Supramolecular Chemistry*, 2008, **20**, 41-50.
87.	G. W. Orr, L. J. Barbour and J. L. Atwood, *Science*, 1999, **285**, 1049-1052.
88.	J. L. Atwood, F. Hamada, K. D. Robinson, G. W. Orr and R. L. Vincent, *Nature*, 1991, **349**, 683-684.
89.	J. L. Atwood, Barbour, L. J., Hardie, M. J., Raston, C. L, *Coordination Chemistry Reviews*, 2001, **222**, 3-32.
90.	S. J. Dalgarno, N. P. Power, J. E. Warren and J. L. Atwood, *Chemical Communications*, 2008, 1539-1541.
91.	N. P. Power, S. J. Dalgarno and J. L. Atwood, *New Journal of Chemistry*, 2007, **31**, 17-20.
92.	B. M. O'Leary, T. Szabo, N. Svenstrup, C. A. Schalley, A. Lutzen, M. Schafer and J. Rebek, *Journal of the American Chemical Society*, 2001, **123**, 11519-11533.
93.	R. M. McKinlay, G. W. V. Cave and J. L. Atwood, *Proceedings of the National Academy of Sciences*, 2005, **102**, 5944-5948.
94.	R. M. McKinlay, P. K. Thallapally and J. L. Atwood, *Chemical Communications*, 2006, 2956-2958.
95.	O. Ugono, J. P. Moran and K. T. Holman, *Chemical Communications*, 2008, 1404-1406.
96.	L. R. MacGillivray, K. T. Holman and J. L. Atwood, *Crystal Engineering*, 1998, **1**, 87-96.
97.	G. W. V. Cave, M. J. Hardie, B. A. Roberts and C. L. Raston, *European Journal of Organic Chemistry*, 2001, 3227-3231.
98.	K. Kobayashi, T. Shirasaka, E. Horn, N. Furukawa, K. Yamaguchi and S. Sakamoto, *Chemical Communications*, 2000, 41-42.
99.	J. L. Atwood and G. W. Gokel, *Nature*, 1991, **354**, 354-355.
100.	J. C. Sherman and D. J. Cram, *Journal of the American Chemical Society*, 1989, **111**, 4527-4528.
101.	S. Mecozzi and J. Rebek, *Chemistry-a European Journal*, 1998, **4**, 1016-1022.
102.	M. Zurcher, T. Gottschalk, S. Meyer, D. Bur and F. Diederich, *Chemmedchem*, 2008, **3**, 237-240.
103.	L. Avram and Y. Cohen, *Journal of the American Chemical Society*, 2002, **124**, 15148-15149.
104.	L. Avram and Y. Cohen, *Journal of the American Chemical Society*, 2003, **125**, 16180-16181.
105.	L. Avram and Y. Cohen, *Organic Letters*, 2003, **5**, 1099-1102.
106.	L. Avram and Y. Cohen, *Organic Letters*, 2003, **5**, 3329-3332.
107.	L. Avram and Y. Cohen, *Journal of the American Chemical Society*, 2005, **127**, 5714-5719.
108.	Y. Cohen, L. Avram and L. Frish, *Angewandte Chemie-International Edition*, 2005, **44**, 520-554.
109.	L. Avram and Y. Cohen, *Organic Letters*, 2006, **8**, 219-222.
110.	K. Murayama and K. Aoki, *Chemical Communications*, 1998, 607-608.
111.	L. Avram and Y. Cohen, *Organic Letters*, 2008, **10**, 1505-1508.

112.   T. Amaya and J. Rebek, *Journal of the American Chemical Society*, 2004, **126**, 14149-14156.
113.   J. L. Atwood, L. J. Barbour and A. Jerga, *Proceedings of the National Academy of Sciences of the United States of America*, 2002, **99**, 4837-4841.
114.   E. S. Barrett, T. J. Dale and J. R. Jr, *Chemical Communications*, 2007, 4224-4226.
115.   E. S. Barrett, T. J. Dale and J. Rebek, *Journal of the American Chemical Society*, 2008, **130**, 2344 -2350.
116.   D. Ajami, M. P. Schramm, A. Volonterio and J. J. Rebek, *Angewandte Chemie International Edition*, 2007, **46**, 242-244.
117.   C. A. Schalley, T. Martin, U. Obst and J. Rebek, *Journal of the American Chemical Society*, 1999, **121**, 2133-2138.
118.   C. A. Schalley, R. K. Castellano, M. S. Brody, D. M. Rudkevich, G. Siuzdak and J. Rebek, *Journal of the American Chemical Society*, 1999, **121**, 4568-4579.
119.   N. K. Beyeh, M. Kogej, A. Ahman, K. Rissanen and C. A. Schalley, *Angewandte Chemie-International Edition*, 2006, **45**, 5214-5218.
120.   R. Porter, *The Greatest Benefit to Mankind: A Medical History of Humanity from Antiquity to the Present*, HarperCollins, 1999.
121.   W. Sneader, *Drug Discovery: A History*, John Wiley & Sons Inc., 2005.
122.   N. C. Lloyd, H. W. Morgan, B. K. Nicholson and R. S. Ronimus, *Angewandte Chemie-International Edition*, 2005, **44**, 941-944.
123.   G. L. Patrick, *An Introduction to Medicinal Chemistry*, Oxford University Press, 2001.
124.   Gisvold, *Textbook of Organic Medicinal and Pharmaceutical Chemistry*, Lippincott Williams & Wilkins, 1998.
125.   D. Schuster, C. Laggner and T. Langer, *Current Pharmaceutical Design*, 2005, **11**, 3545-3559.
126.   J. F. Pritchard, M. Jurima-Romet, M. L. J. Reimer, E. Mortimer, B. Rolfe and M. N. Cayen, *Nature Reviews Drug Discovery*, 2003, **2**, 542-553.
127.   J. G. Lombardino and J. A. Lowe, *Nature Reviews Drug Discovery*, 2004, **3**, 853-862.
128.   K. H. Bleicher, H. J. Bohm, K. Muller and A. I. Alanine, *Nature Reviews Drug Discovery*, 2003, **2**, 369-378.
129.   J. A. Kramer, J. E. Sagartz and D. L. Morris, *Nature Reviews Drug Discovery*, 2007, **6**, 636-649.
130.   H. J. Smith, *Smith and Williams' Introduction to the Principles of Drug Design and Action*, CRC Press, Taylor & Francis Group, 2006.
131.   P. M. Webber, *Nature Reviews Drug Discovery*, 2003, **2**, 823-830.
132.   B. Wang, *Drug Delivery : Principles and Applications*, John Wiley & Sons, 2005.
133.   R. A. Prentis, Y. Lis and S. R. Walker, *British Journal of Clinical Pharmacology*, 1988, **25**, 387-396.
134.   R. Lobenberg and G. L. Amidon, *European Journal of Pharmaceutics and Biopharmaceutics*, 2000, **50**, 3-12.
135.   M. M. D. H. P. Rang, J. M. Ritter, P. K. Moore, *Pharmacology*, Elsevier, 2003.
136.   A. Fahr and X. Liu, *Expert Opinion on Drug Delivery*, 2007, **4**, 403-416.
137.   A. K. Singla, A. Garg and D. Aggarwal, *International Journal of Pharmaceutics*, 2002, **235**, 179-192.
138.   F. A. Holmes, R. S. Walters, R. L. Theriault, A. D. Forman, L. K. Newton, M. N. Raber, A. U. Buzdar, D. K. Frye and G. N. Hortobagyi, *Journal of the National Cancer Institute*, 1991, **83**, 1797-1805.
139.   N. K. Ibrahim, N. Desai, S. Legha, P. Soon-Shiong, R. L. Theriault, E. Rivera, B. Esmaeli, S. E. Ring, A. Bedikian, G. N. Hortobagyi and J. A. Ellerhorst, *Clinical Cancer Research*, 2002, **8**, 1038-1044.
140.   W. Bouquet, W. Ceelen, B. Fritzinger, P. Pattyn, M. Peeters, J. P. Remon and C. Vervaet, *European Journal of Pharmaceutics and Biopharmaceutics*, 2007, **66**, 391-397.
141.   W. J. Gradishar, S. Tjulandin, N. Davidson, H. Shaw, N. Desai, P. Bhar, M. Hawkins and J. O'Shaughnessy, *Journal of Clinical Oncology*, 2005, **23**, 7794-7803.
142.   G. Gregoriadis, *New England Journal of Medicine*, 1976, **295**, 704-710.
143.   G. Gregoriadis, *New England Journal of Medicine*, 1976, **295**, 765-770.
144.   R. Langer, *Science*, 1990, **249**, 1527-1533.
145.   W. C. Zamboni, *Oncologist*, 2008, **13**, 248-260.
146.   D. N. Waterhouse, T. D. Madden, P. R. Cullis, M. B. Bally, L. D. Mayer and M. S. Webb, in *Liposomes, Part E*, 2005, pp. 40-57.
147.   S. K. Sahoo, F. Dilnawaz and S. Krishnakumar, *Drug Discovery Today*, 2008, **13**, 144-151.

148. S. Wagner, O. Peters, C. Fels, G. Janssen, A.-K. Liebeskind, A. Sauerbrey, M. Suttorp, P. Hau and J. Wolff, *Journal of Neuro-Oncology*, 2008, **86**, 175-181.
149. D. D. Lasic, *Nature*, 1996, **380**, 561-562.
150. D. A. Gewirtz, *Biochemical Pharmacology*, 1999, **57**, 727-741.
151. The British Medical Association and The Royal Pharmaceutical Soceity of Great Britain, *The British National Formulary*, The British Medical Association, 2003.
152. in *Oxford Concise Medical Dictionary*, ed. E. A. Martin, Oxford University Press, 2003.
153. M. Sharpe, S. E. Easthope, G. M. Keating and H. M. Lamb, *Drugs*, 2002, **62**, 2089.
154. D. D. Lasic, F. J. Martin, A. Gabizon, S. K. Huang and D. Papahadjopoulos, *Biochimica et Biophysica Acta (BBA) - Biomembranes*, 1991, **1070**, 187-192.
155. H. Maeda, J. Wu, T. Sawa, Y. Matsumura and K. Hori, *Journal of Controlled Release*, 2000, **65**, 271-284.
156. D. Duchene, D. Wouessidjewe and G. Ponchel, *Journal of Controlled Release*, 1999, **62**, 263-268.
157. T. Loftsson, S. B. Vogensen, M. E. Brewster and F. Konradsdottir, *Journal of Pharmaceutical Sciences*, 2007, **96**, 2532-2546.
158. T. Loftsson and D. Duchene, *International Journal of Pharmaceutics*, 2007, **329**, 1-11.
159. T. Loftssona and T. Järvinen, *Advanced Drug Delivery Reviews*, 1999, **36**, 59-79.
160. R. A. Rajewski and V. J. Stella, *Journal of Pharmaceutical Sciences*, 1996, **85**, 1142-1169.
161. D. A. Stevens, *Pharmacotherapy*, 1999, **19**, 603-611.
162. C. Hammond, *The Basics of Crystallography and Diffraction*, Oxford University Press, 1997.
163. C. Giacovazzo, Monaco, H. L., Viterbo, D., Scordari, F., Gilli, G., Zanotti, G., Catti, M., *Fundamentals of Crystallography*, Oxford University Press, 1992.
164. D. E. Sands, *Introduction to Crystallography*, Dover, 1993.
165. W. Clegg, *Crystal Structure Determination*, Oxford University Press, 1999.
166. L. Avram and Y. Cohen, *Journal of Organic Chemistry*, 2002, **67**, 2639-2644.
167. B. C. Gibb, R. G. Chapman and J. C. Sherman, *Journal of Organic Chemistry*, 1996, **61**, 1505-1509.
168. K. Miyazaki, S. Arai, T. Iwamoto, M. Takasaki and A. Tomoda, *Tohoku Journal of Experimental Medicine*, 2004, **203**, 319-330.
169. L. J. Barbour, 1997.
170. Sheldrick, 1990.
171. Sheldrick, 1997.
172. , EPSRC-CCDb.
173. L. J. Barbour, 2003.
174. G. W. V. Cave and C. L. Raston, *Chemical Communications*, 2000, 2199-2200.
175. M. T. Messina, P. Metrangolo, S. Pappalardo, M. E. Parisi, T. Pilati and G. Resnati, *Chemistry-a European Journal*, 2000, **6**, 3495-3500.
176. P. J. Nichols, C. L. Raston and J. W. Steed, *Chemical Communications*, 2001, 1062-1063.
177. C. Schiel, G. A. Hembury, V. V. Borovkov, M. Klaes, C. Agena, T. Wada, S. Grimme, Y. Inoue and J. Mattay, *Journal of Organic Chemistry*, 2006, **71**, 976-982.
178. A. Ahman, M. Luostarinen, K. Rissanen and M. Nissinen, *New Journal of Chemistry*, 2007, **31**, 169-177.
179. T. W. Greene and P. G. M. Wuts, *Protective Groups in Organic Synthesis*, John Wiley & Sons, 1999.
180. G. Parmiani, C. Castelli, L. Rivoltini, C. Casati, G. A. Tully, L. Novellino, A. Patuzzo, D. Tosi, A. Anichini and M. Santinami, *Seminars in Cancer Biology*, 2003, **13**, 391-400.
181. R. Nairn and M. Helbert, *Immunology for Medical Students*, Mosby, 2003.
182. E. J. Corey and J. W. Suggs, *Tetrahedron Letters*, 1975, **16**, 2647-2650.
183. S. Patai, Rappoport, Z., *Supplement C: The Chemistry of Triple-Bonded Functional Groups*, Wiley, Chichester, 1983.
184. J. Gribbin, *Science: A history 1543 - 2001*, Allen Lane The Penguin Press, 2002.

Appendix

Please see attached CD-ROM for crystallographic data for the species reported in this thesis.

Below is a list of 'Class A' errors generated by the online IUCR basic .CIF checking package (http://journals.iucr.org/services/cif/checking/checkbasic.html) with a list of explanations of the errors which are generated. These errors arise as a result of the unique nature of the crystallographic system studied in this thesis.

C1PgEt2O

```
PLAT432_ALERT_2_A
Short Inter X...Y Contact  C36A   ..  C43B   ..      2.82 Ang.
PLAT773_ALERT_2_A
Suspect C-C Bond in CIF:   C44A   --  C43B   ..      1.95 Ang.
PLAT223_ALERT_4_A
Large Solvent/Anion  H    Ueq(max)/Ueq(min) ...      5.56 Ratio
```

The short inter-hydrogen distance and the large solvent H errors are due to the disordered nature of the solvent molecule which is *exo* to the cavity of the calixarene interacting with the ordered solvent molecule which resides within the cavity of the calixarene.

C1PgMeCN

```
PLAT414_ALERT_2_A
Short Intra D-H..H-X       H2     ..  H7     ..      1.78 Ang.
```

The electron density pattern suggests that hydrogen 2 forms a hydrogen bond to oxygen 3, bringing it into close contact with hydrogen 7 which is the bound to methine carbon of the macrocycle as a consequence of intramolecular hydrogen bonding. It has only been modelled in the highest electron density position, however it is acknowledged that there is a dynamic interchange of position between the two sites.

C2RsMeCN

No category A alerts were produced for this dataset.

C2PgMeCN

```
PLAT222_ALERT_3_A
Large Non-Solvent   H    Ueq(max)/Ueq(min) ...      5.35 Ratio
```

This error is due to the solvent molecule exo to the cavity being disordered over two positions, despite successfully modelling it as a disordered entity the error persists.

C3OHPgAcetone1

```
SHFSU01_ALERT_2_A
The absolute value of parameter shift to su ratio > 0.20
Absolute value of the parameter shift to su ratio given   2.679
Additional refinement cycles may be required.
```

Despite repeated cycles of refinement, the R_1 remained unchanged at 0.0411 and the structure was stable.

C3OHPgAcetone2

```
PLAT306_ALERT_2_A
Isolated Oxygen Atom (H-atoms Missing ?) .......      O17
PLAT306_ALERT_2_A
Isolated Oxygen Atom (H-atoms Missing ?) .......      O18
```

This error is due to the lack of hydrogen atoms on a water molecule which have been located in the structure. Xseed does not currently support placement of hydrogen atoms on water molecules.

C3OHRsMeCNlowsymm

```
PLAT306_ALERT_2_A
Isolated Oxygen Atom (H-atoms Missing ?) .......      O13
PLAT306_ALERT_2_A
Isolated Oxygen Atom (H-atoms Missing ?) .......      O14
```

This error is due to the lack of hydrogen atoms on two water molecules which have been located in the structure. Xseed does not currently support geometrical location of hydrogen atoms on water molecules.

C3OHPgChairConf

```
SHFSU01_ALERT_2_A
The absolute value of parameter shift to su ratio > 0.20
Absolute value of the parameter shift to su ratio given   3.411
Additional refinement cycles may be required.
PLAT080_ALERT_2_A
Maximum Shift/Error ...........................      3.41
PLAT222_ALERT_3_A
Large Non-Solvent    H    Ueq(max)/Ueq(min) ...      8.70 Ratio
```

This structure has a network of five water molecules within the asymmetric unit which have been assigned hydrogen atoms empirically rather than the usual protocol of geometrical addition, which may be the cause of the PLAT080 error. Despite repeated cycles of refinement, the R_1 remained unchanged at 0.0536 and the structure was stable.

C3RsMeCNHighSymm

SHFSU01_ALERT_2_A
The absolute value of parameter shift to su ratio > 0.20
Absolute value of the parameter shift to su ratio given   0.449
Additional refinement cycles may be required.
PLAT080_ALERT_2_A
Maximum Shift/Error 0.45
PLAT306_ALERT_2_A
Isolated Oxygen Atom (H-atoms Missing ?) O4
PLAT306_ALERT_2_A
Isolated Oxygen Atom (H-atoms Missing ?) O5

The PLAT306 error is due to the lack of hydrogen atoms on two water molecules which have been located in the structure. Xseed does not currently support placement of hydrogen atoms on water molecules. The absolute parameter shift is due to the formation of a channel of solvent molecules exo to the cavity of the calixarene molecules, therefore the exact atomic positions could not be determined and were therefore modelled as oxygen atoms.

C3OHPgTHF

PLAT222_ALERT_3_A
Large Non-Solvent   H   Ueq(max)/Ueq(min) ...   6.75 Ratio

The source of the error above is the free water molecule whose hydrogen atoms were located empirically and not geometrically.

C3PgAcetone

No class A errors were generated for this dataset

C3PgEt2O

SHFSU01_ALERT_2_A
The absolute value of parameter shift to su ratio > 0.20
Absolute value of the parameter shift to su ratio given   4.997
Additional refinement cycles may be required.
PLAT080_ALERT_2_A
Maximum Shift/Error 5.00
PLAT215_ALERT_3_A
Disordered C50B   has ADP max/min Ratio 6.10
PLAT220_ALERT_2_A
Large Non-Solvent   C   Ueq(max)/Ueq(min) ...   4.76 Ratio
PLAT220_ALERT_2_A
Large Non-Solvent   O   Ueq(max)/Ueq(min) ...   10.00 Ratio
PLAT220_ALERT_2_A
Large Non-Solvent   C   Ueq(max)/Ueq(min) ...   9.55 Ratio
PLAT222_ALERT_3_A
Large Non-Solvent   H   Ueq(max)/Ueq(min) ...   5.93 Ratio
PLAT222_ALERT_3_A
Large Non-Solvent   H   Ueq(max)/Ueq(min) ...   10.00 Ratio
PLAT413_ALERT_2_A
Short Inter XH3 .. XHn   H20C .. H50B   ..   1.74 Ang.
PLAT432_ALERT_2_A
Short Inter X...Y Contact O27   .. C85   ..   2.20 Ang.
PLAT432_ALERT_2_A
Short Inter X...Y Contact O29   .. C84B   ..   2.07 Ang.
PLAT432_ALERT_2_A
Short Inter X...Y Contact O29   .. C84   ..   2.40 Ang.
PLAT432_ALERT_2_A
Short Inter X...Y Contact C20A .. C50A   ..   2.79 Ang.
PLAT221_ALERT_4_A
Large Solvent/Anion C   Ueq(max)/Ueq(min) ...   10.00 Ratio
PLAT223_ALERT_4_A
Large Solvent/Anion H   Ueq(max)/Ueq(min) ...   10.00 Ratio
PLAT780_ALERT_1_A
Coordinates do not Form a Properly Connected Set   ?

SHFSU01 is due to the isotropic refinement applied to the two solvent molecules causing oscillation within the structure. The disorder of the pendant chains contributes errors PLAT220, PLAT222 and PLAT432. The interdigitation of the two sets of disordered chains gives rise to the close contacts which produce the errors. The close contact between O27 and C85 is a result of a water molecule (O27) which is hydrogen bonded to the upper rim of a calixarene molecule coming into close contact with the methyl group of a diethyl ether molecule housed in the cavity of a calixarene.

C3PgEtOH

PLAT222_ALERT_3_A
Large Non-Solvent   H   Ueq(max)/Ueq(min) ...   10.00 Ratio

The presence of this error is due to the inclusion of a water molecule into the crystal lattice. The hydrogen atoms were placed onto the oxygen by empirical methods as the geometrical placing of hydrogen atoms onto an isolated oxygen is not currently supported by Xseed.

C3PgMeCN

PLAT220_ALERT_2_A
Large Non-Solvent   C   Ueq(max)/Ueq(min) ...   7.82 Ratio
PLAT222_ALERT_3_A
Large Non-Solvent   H   Ueq(max)/Ueq(min) ...   9.13 Ratio

This large Ueq is due to the formation of a small void by the interdigitation of the pendant chains, allowing some conformational flexibility of the terminal methyl group.

C4ClPgEtOH

PLAT220_ALERT_2_A
Large Non-Solvent   C   Ueq(max)/Ueq(min) ...   10.00 Ratio
PLAT222_ALERT_3_A
Large Non-Solvent   H   Ueq(max)/Ueq(min) ...   10.00 Ratio
PLAT241_ALERT_2_A
Check High   Ueq as Compared to Neighbors for   C22
PLAT242_ALERT_2_A
Check Low   Ueq as Compared to Neighbors for   Cl2A
PLAT242_ALERT_2_A
Check Low   Ueq as Compared to Neighbors for   Cl2B
PLAT242_ALERT_2_A
Check Low   Ueq as Compared to Neighbors for   C21
PLAT306_ALERT_2_A
Isolated Oxygen Atom (H-atoms Missing ?) O15
PLAT306_ALERT_2_A
Isolated Oxygen Atom (H-atoms Missing ?) O16
PLAT224_ALERT_1_A
Ueq(Rep) and Ueq(Calc) differ by -0.010 Ang**2 .   C22

The errors generated from C22 and Cl12A and Cl12B are due to the disordering of the terminal chlorine atom over two positions. The isolated oxygen atom are due to lack of hydrogen atoms on two water molecules which have been located in the structure. Xseed does not currently support geometrical placement of hydrogen atoms on water molecules.

C4ClPgEt$_2$O

PLAT215_ALERT_3_A
Disordered C22B   has ADP max/min Ratio 15.60
PLAT220_ALERT_2_A
Large Non-Solvent   C   Ueq(max)/Ueq(min) ...   10.00 Ratio
PLAT220_ALERT_2_A
Large Non-Solvent Cl   Ueq(max)/Ueq(min) ...   6.21 Ratio
PLAT222_ALERT_3_A
Large Non-Solvent   H   Ueq(max)/Ueq(min) ...   10.00 Ratio
PLAT242_ALERT_2_A
Check Low   Ueq as Compared to Neighbors for   Cl2B
PLAT242_ALERT_2_A
Check Low   Ueq as Compared to Neighbors for   C22A
PLAT242_ALERT_2_A
Check Low   Ueq as Compared to Neighbors for   Cl4A
PLAT245_ALERT_2_A
U(iso) H22B   Smaller than U(eq) C22B   by ...   0.29 AngSq
PLAT306_ALERT_2_A
Isolated Oxygen Atom (H-atoms Missing ?) O15

The PLAT215, 220, 222, 242, 245 errors are generated by disorder of a pendant chain which forms the base of a solvent filled void within the crystal lattice. This void is bounded on three sides by the aryl rings of adjacent calixarene molecules which have low conformational flexibility, however the base of this void is completed by a pendant chain which has conformational flexibility which has been modelled. The PLAT306 error is due to the presence of a water molecule within the asymmetric unit. Currently Xseed does not support placement of hydrogen atoms in geometrical positions on isolated oxygen atoms.

C4ClPg*i*PrOH

PLAT306_ALERT_2_A
Isolated Oxygen Atom (H-atoms Missing ?) O13
PLAT306_ALERT_2_A
Isolated Oxygen Atom (H-atoms Missing ?) O14
PLAT306_ALERT_2_A
Isolated Oxygen Atom (H-atoms Missing ?) O15
PLAT306_ALERT_2_A
Isolated Oxygen Atom (H-atoms Missing ?) O16
PLAT306_ALERT_2_A
Isolated Oxygen Atom (H-atoms Missing ?) O18
PLAT414_ALERT_2_A
Short Intra D-H..H-X   H1   .. H40   ..   1.72 Ang.
PLAT414_ALERT_2_A
Short Intra D-H..H-X   H7   .. H18   ..   1.76 Ang.
PLAT414_ALERT_2_A
Short Intra D-H..H-X   H9   .. H29   ..   1.59 Ang

The PLAT306 error is due to the presence of five water molecules within the asymmetric unit. Currently Xseed does not support placement of hydrogen atoms in geometrical positions on isolated oxygen atoms. The PLAT414 error is due to the arrangement of hydrogen atoms of the upper rim into a intra-molecular hydrogen bonded motif. These hydrogen atoms come into close contact with the methine carbon. It is acknowledged that this is a dynamic system and at room temperature rotation of these bonds will be possible.

C4PgEt$_2$O

No class A errors were generated for this dataset

C4PgMeCN

```
RFACR01_ALERT_3_A
The value of the weighted R factor is > 0.45
Weighted R factor given   0.472
SHFSU01_ALERT_2_A
The absolute value of parameter shift to su ratio > 0.20
Absolute value of the parameter shift to su ratio given   5.261
Additional refinement cycles may be required.
PLAT080_ALERT_2_A
Maximum Shift/Error ...........................    5.26
PLAT084_ALERT_2_A
High R2 Value .................................    0.47
PLAT220_ALERT_2_A
Large Non-Solvent    C    Ueq(max)/Ueq(min) ...    7.09 Ratio
PLAT222_ALERT_3_A
Large Non-Solvent    H    Ueq(max)/Ueq(min) ...    8.83 Ratio
PLAT242_ALERT_2_A
Check Low       Ueq as Compared to Neighbors for     C10
PLAT306_ALERT_2_A
Isolated Oxygen Atom (H-atoms Missing ?) .......     O15
PLAT430_ALERT_2_A
Short Inter D...A Contact  O15    .. O15    ..    2.00 Ang.
PLAT430_ALERT_2_A
Short Inter D...A Contact  O15    .. O15    ..    2.00 Ang.
PLAT430_ALERT_2_A
Short Inter D...A Contact  O15    .. N4     ..    2.54 Ang.
PLAT432_ALERT_2_A
Short Inter X...Y Contact  N4     .. C51    ..    2.55 Ang.
PLAT432_ALERT_2_A
Short Inter X...Y Contact  N5     .. C54    ..    2.70 Ang.
PLAT432_ALERT_2_A
Short Inter X...Y Contact  C51    .. C52    ..    1.89 Ang.
PLAT773_ALERT_2_A
Suspect C-C Bond in CIF:   C51    -- C52    ..    1.90 Ang.
```

This crystal structure is a calixarene molecule arranged by $R\bar{3}$ symmetry to form a nano-sphere. The large unit cell combined with the intrinsic difficulty in assigning the electron density within the nano capsule lead to a high R1 and R2 factor. The contents of the nano sphere are tentatively assigned as 18 acetonitrile molecules, which account for the close contacts seen in the .CIF check. The isolated oxygen atom is an extra-capsular water molecule. Xseed does not allow geometrical assignment of hydrogen atoms in water molecules.

C5ClPgEtOH

PLAT222_ALERT_3_A
Large Non-Solvent   H   Ueq(max)/Ueq(min) ...   6.67 Ratio

This error is due to the empirical location of the hydroxyl hydrogen atoms around the upper rim of the calixarene molecule. There is an intramolecular hydrogen bonding network around each calixarene molecule which would cause this error as they are slightly disordered.

C5PgMeCN

PLAT220_ALERT_2_A
Large Non-Solvent   C   Ueq(max)/Ueq(min) ...   10.00 Ratio
PLAT222_ALERT_3_A
Large Non-Solvent   H   Ueq(max)/Ueq(min) ...   10.00 Ratio
PLAT242_ALERT_2_A
Check Low   Ueq as Compared to Neighbors for   C23

This is a false alarm generated by the .CIF checking engine, The carbon atom which has been flagged as erroneously assigned is the penultimate atom of a pendant chain which forms an interdigitated bilayer. The atom in question has larger than usual thermal ellipsoid parameters, which indicate some degree of freedom of positional location within the crystal lattice. On packing the structure around the atom in question a small void is apparent which would support the theory of conformational freedom of the terminal two atoms of the pendant chain.

C6PgMeCN

PLAT220_ALERT_2_A
Large Non-Solvent   C   Ueq(max)/Ueq(min) ...   4.66 Ratio
PLAT222_ALERT_3_A
Large Non-Solvent   H   Ueq(max)/Ueq(min) ...   5.50 Ratio

This large Ueq is due to the formation of a small void by the interdigitation of the pendant chains, allowing some conformational flexibility of the terminal methyl group.

C7PgEt$_2$O

PLAT220_ALERT_2_A Large Non-Solvent   C   Ueq(max)/Ueq(min) ...
9.68 Ratio
PLAT222_ALERT_3_A Large Non-Solvent   H   Ueq(max)/Ueq(min) ...
10.00 Ratio
PLAT241_ALERT_2_A Check High   Ueq as Compared to Neighbors for
C52
PLAT306_ALERT_2_A Isolated Oxygen Atom (H-atoms Missing ?) ....
O10

The possible cause of the PLAT220 and PLAT 222 errors is the presence of a small void below the pendant chain bearing C55 which may allow a small amount of conformational flexibility causing disorder within the structure. The PLAT306 error is due to the lack of hydrogen atoms on two water molecules which have been located in the structure. Xseed does not currently support placement of hydrogen atoms on water molecules.

<u>C7PgEtOAc</u>

RFACR01_ALERT_3_A
The value of the weighted R factor is > 0.45
Weighted R factor given   0.465
SHFSU01_ALERT_2_A
The absolute value of parameter shift to su ratio > 0.20
Absolute value of the parameter shift to su ratio given   0.958
Additional refinement cycles may be required.
PLAT080_ALERT_2_A
Maximum Shift/Error 0.96
PLAT084_ALERT_2_A
High R2 Value 0.46
PLAT220_ALERT_2_A
Large Non-Solvent   C   Ueq(max)/Ueq(min) ...   10.00 Ratio
PLAT222_ALERT_3_A
Large Non-Solvent   H   Ueq(max)/Ueq(min) ...   10.00 Ratio
PLAT241_ALERT_2_A
Check High   Ueq as Compared to Neighbors for   C12
PLAT241_ALERT_2_A
Check High   Ueq as Compared to Neighbors for   C27
PLAT241_ALERT_2_A
Check High   Ueq as Compared to Neighbors for   C55
PLAT242_ALERT_2_A
Check Low   Ueq as Compared to Neighbors for   C13
PLAT413_ALERT_2_A
Short Inter XH3 .. XHn   H14C   .. H42A   ..   1.83 Ang.
PLAT413_ALERT_2_A
Short Inter XH3 .. XHn   H14C   .. H42C   ..   1.57 Ang.
PLAT432_ALERT_2_A
Short Inter X...Y Contact C14   .. C42   ..   2.87 Ang.
PLAT601_ALERT_2_A
Structure Contains Solvent Accessible VOIDS of .   1205.00 A**3
PLAT224_ALERT_1_A
Ueq(Rep) and Ueq(Calc) differ by 0.010 Ang**2 .   C14
PLAT234_ALERT_4_A
Large Hirshfeld Difference C13   -- C14   ..   0.37 Ang.

This crystal structure is a calixarene molecule arranged by $R\overline{3}$ symmetry to form a nano-sphere. The large unit cell combined with the intrinsic difficulty in assigning the electron density within the nano capsule lead to a high R2 factor. Despite repeated cycles of refinement the R1 remained at 0.158.

The contents of the nano sphere are assigned as diffuse electron density and are modelled by the SQUEEZE programme. It has been shown in the literature that 6 ethyl acetate molecules may occupy the internal volume of the nano-sphere. The errors which refer to C14 (and corresponding hydrogen atoms) are due to the presence of a small void within the crystal lattice allowing the terminal methyl group of a pendant chain to be conformationally flexible, therefore enlarging the thermal parameters of this terminal group.

<u>C7PgMeCN</u>

```
PLAT220_ALERT_2_A
Large Non-Solvent   C   Ueq(max)/Ueq(min) ...      5.06 Ratio
PLAT222_ALERT_3_A
Large Non-Solvent   H   Ueq(max)/Ueq(min) ...      5.81 Ratio
PLAT306_ALERT_2_A
Isolated Oxygen Atom (H-atoms Missing ?) .......    O16
```

The errors which refer to C73 (and corresponding hydrogen atoms) are due to the presence of a small void within the crystal lattice which is formed by the interdigitation of the pendant chains. This void allows the terminal methyl group of the affected pendant chain to be conformationally flexible, therefore enlarging the thermal parameters of this terminal group.

The PLAT306 error is due to the lack of hydrogen atoms on two water molecules which have been located in the structure. Xseed does not currently support placement of hydrogen atoms on water molecules

```
PLAT306_ALERT_2_A
```

C7PgEtOH

```
THETM01_ALERT_3_A
The value of sine(theta_max)/wavelength is less than 0.550
Calculated sin(theta_max)/wavelength =    0.5263
PLAT220_ALERT_2_A
Large Non-Solvent    C    Ueq(max)/Ueq(min) ...      6.22 Ratio
PLAT220_ALERT_2_A
Large Non-Solvent    C    Ueq(max)/Ueq(min) ...     10.00 Ratio
PLAT222_ALERT_3_A
Large Non-Solvent    H    Ueq(max)/Ueq(min) ...      5.45 Ratio
PLAT222_ALERT_3_A
Large Non-Solvent    H    Ueq(max)/Ueq(min) ...     10.00 Ratio
PLAT241_ALERT_2_A
Check High     Ueq as Compared to Neighbors for      C52
PLAT241_ALERT_2_A
Check High     Ueq as Compared to Neighbors for      C79
PLAT241_ALERT_2_A
Check High     Ueq as Compared to Neighbors for      C82
PLAT241_ALERT_2_A
Check High     Ueq as Compared to Neighbors for      C96
PLAT241_ALERT_2_A
Check High     Ueq as Compared to Neighbors for      C111
PLAT242_ALERT_2_A
Check Low      Ueq as Compared to Neighbors for      C51
PLAT242_ALERT_2_A
Check Low      Ueq as Compared to Neighbors for      C53
PLAT242_ALERT_2_A
Check Low      Ueq as Compared to Neighbors for      C78
PLAT242_ALERT_2_A
Check Low      Ueq as Compared to Neighbors for      C81
PLAT242_ALERT_2_A
Check Low      Ueq as Compared to Neighbors for      C83
PLAT242_ALERT_2_A
Check Low      Ueq as Compared to Neighbors for      C97
PLAT242_ALERT_2_A
Check Low      Ueq as Compared to Neighbors for      C110
PLAT306_ALERT_2_A
Isolated Oxygen Atom (H-atoms Missing ?) .......      O26
PLAT306_ALERT_2_A
Isolated Oxygen Atom (H-atoms Missing ?) .......      O30
PLAT412_ALERT_2_A
Short Intra XH3 .. XHn    H11D   .. H12C    ..      1.69 Ang.
PLAT415_ALERT_2_A
Short Inter D-H..H-X      H13    .. H84A    ..      1.80 Ang.
```

This dataset was collected by the EPSRC crystallography service at Daresbury synchrotron because despite repeated attempts to crystallise the material, only small crystal dimensions and low diffraction angles could be achieved. This accounts for the THETM01 error.

The PLAT220, 222, 241, 242, 412 and 415 are due to the molecules forming an interdigitated bilayer. This bilayer arrangement allows a small degree of conformational flexibility within the crystal lattice and therefore accounts for the large thermal parameters observed for the atoms highlighted above.

The PLAT306 error is due to the lack of hydrogen atoms on two water molecules which have been located in the structure. Xseed does not currently support placement of hydrogen atoms on water molecules

C7PgTerpy

SHFSU01_ALERT_2_A
The absolute value of parameter shift to su ratio > 0.20
Absolute value of the parameter shift to su ratio given   1.207
Additional refinement cycles may be required.
PLAT213_ALERT_2_A
Atom C26   has ADP max/min Ratio ....   5.30 prola
PLAT220_ALERT_2_A
Large Non-Solvent   C   Ueq(max)/Ueq(min) ...   10.00 Ratio
PLAT222_ALERT_3_A
Large Non-Solvent   H   Ueq(max)/Ueq(min) ...   10.00 Ratio
PLAT241_ALERT_2_A
Check High   Ueq as Compared to Neighbors for   C12
PLAT241_ALERT_2_A
Check High   Ueq as Compared to Neighbors for   C25
PLAT241_ALERT_2_A
Check High   Ueq as Compared to Neighbors for   C26
PLAT242_ALERT_2_A
Check Low   Ueq as Compared to Neighbors for   C11
PLAT242_ALERT_2_A
Check Low   Ueq as Compared to Neighbors for   C24
PLAT242_ALERT_2_A
Check Low   Ueq as Compared to Neighbors for   C27
PLAT353_ALERT_3_A
Long   N-H Bond (0.87A)   N1   -   H80   ...   1.21 Ang.
PLAT410_ALERT_2_A
Short Intra H...H Contact H58   .. H73   ..   1.79 Ang.
PLAT410_ALERT_2_A
Short Intra H...H Contact H60   .. H63   ..   1.58 Ang.
PLAT413_ALERT_2_A
Short Inter XH3 .. XHn   H24A   .. H28C   ..   1.17 Ang.
PLAT413_ALERT_2_A
Short Inter XH3 .. XHn   H60   .. H79C   ..   1.81 Ang.
PLAT413_ALERT_2_A
Short Inter XH3 .. XHn   H63   .. H79A   ..   1.59 Ang.
PLAT413_ALERT_2_A
Short Inter XH3 .. XHn   H77   .. H79C   ..   1.61 Ang.
PLAT413_ALERT_2_A
Short Inter XH3 .. XHn   H78B   .. H79A   ..   1.83 Ang.
PLAT415_ALERT_2_A
Short Inter D-H..H-X   H4   .. H79B   ..   1.48 Ang.
PLAT432_ALERT_2_A
Short Inter X...Y Contact O5   .. C79   ..   2.42 Ang.
PLAT432_ALERT_2_A
Short Inter X...Y Contact C63   .. C79   ..   2.66 Ang.
PLAT224_ALERT_1_A
Ueq(Rep) and Ueq(Calc) differ by -0.010 Ang**2 .   C28
PLAT234_ALERT_4_A
Large Hirshfeld Difference C12   -- C13   ..   0.31 Ang.

The crystal produced were very small plates which due to their size were only suitable for examination at a synchrotron radiation source.

Errors PLAT241 and 242 are due to disorder within the pendant chains which form an interdigitated bilayer and therefore have some degree of conformational flexibility. The errors PLAT360, PLAT410 and PLAT 413 are due to the two methanol molecules which are present within the crystal lattice. Refinement of these molecules was confined to isotropic refinement only as including them in the isotropic refinement model introduced instability into the model. With this compensation in place for the solvent molecules, despite repeated cycles of refinement, the R_1 remained unchanged at 0.111 and the structure was stable.

<u>C8PgMeCN</u>

<u>SHFSU01_ALERT_2_A</u>
The absolute value of parameter shift to su ratio > 0.20
Absolute value of the parameter shift to su ratio given   4.892
Additional refinement cycles may be required.
<u>PLAT080_ALERT_2_A</u>
Maximum Shift/Error 4.89
<u>PLAT220_ALERT_2_A</u>
Large Non-Solvent   C   Ueq(max)/Ueq(min) ...   9.46 Ratio
<u>PLAT222_ALERT_3_A</u>
Large Non-Solvent   H   Ueq(max)/Ueq(min) ...   10.00 Ratio
<u>PLAT241_ALERT_2_A</u>
Check High   Ueq as Compared to Neighbors for   C30
<u>PLAT242_ALERT_2_A</u>
Check Low   Ueq as Compared to Neighbors for   C29A
<u>PLAT390_ALERT_3_A</u>
Deviating Methyl C30   X-C-H Bond Angle ......   137.00 Deg.
<u>PLAT390_ALERT_3_A</u>
Deviating Methyl C30   X-C-H Bond Angle ......   64.00 Deg.
<u>PLAT410_ALERT_2_A</u>
Short Intra H...H Contact H58A   .. H60E   ..   1.61 Ang.
<u>PLAT410_ALERT_2_A</u>
Short Intra H...H Contact H58B   .. H60E   ..   1.45 Ang.
<u>PLAT411_ALERT_2_A</u>
Short Inter H...H Contact H13   .. H60D   ..   1.61 Ang.
<u>PLAT411_ALERT_2_A</u>
Short Inter H...H Contact H14   .. H60D   ..   1.76 Ang.

Two of the pendant chains within the calixarene show significant disorder which has been modelled. The half occupancy model which has been written is the source of the PLAT220, 222, 241, 242, 290, 410 and 411. This disorder is due to the increasing length of the pendant chains allowing greater conformational variability within the bilayer which has formed, thereby introducing disorder into the crystal. Despite repeated cycles of refinement, the R_1 remained unchanged at 0.0859 and the structure was stable when the disorder was modelled.

C10BrPgEtOH

RFACG01_ALERT_3_A
The value of the R factor is > 0.20
R factor given   0.229
RFACR01_ALERT_3_A
The value of the weighted R factor is > 0.45
Weighted R factor given   0.548
PLAT082_ALERT_2_A
High R1 Value 0.23
PLAT084_ALERT_2_A
High R2 Value 0.55
PLAT215_ALERT_3_A
Disordered C16B   has ADP max/min Ratio 7.70
PLAT220_ALERT_2_A
Large Non-Solvent   C   Ueq(max)/Ueq(min) ...   10.00 Ratio
PLAT222_ALERT_3_A
Large Non-Solvent   H   Ueq(max)/Ueq(min) ...   10.00 Ratio
PLAT241_ALERT_2_A
Check High   Ueq as Compared to Neighbors for   Br1
PLAT241_ALERT_2_A
Check High   Ueq as Compared to Neighbors for   C62
PLAT241_ALERT_2_A
Check High   Ueq as Compared to Neighbors for   C67
PLAT242_ALERT_2_A
Check Low   Ueq as Compared to Neighbors for   C16A
PLAT242_ALERT_2_A
Check Low   Ueq as Compared to Neighbors for   C17A
PLAT242_ALERT_2_A
Check Low   Ueq as Compared to Neighbors for   C17B
PLAT242_ALERT_2_A
Check Low   Ueq as Compared to Neighbors for   C51
PLAT242_ALERT_2_A
Check Low   Ueq as Compared to Neighbors for   C61
PLAT242_ALERT_2_A
Check Low   Ueq as Compared to Neighbors for   C63
PLAT242_ALERT_2_A
Check Low   Ueq as Compared to Neighbors for   C66
PLAT242_ALERT_2_A
Check Low   Ueq as Compared to Neighbors for   C68
PLAT245_ALERT_2_A
U(iso) H16A   Smaller than U(eq) C16B   by ...   0.32 AngSq
PLAT601_ALERT_2_A
Structure Contains Solvent Accessible VOIDS of .   1178.00 A**3

This structure shows a spherical arrangement of the calixarene molecules, the SQUEEZE program was applied to model the disordered contents of the sphere as diffuse electron density. This un-assignable electron density is the cause of the high R1 and R2 values. PLAT215, 220, 242, 241, 245 errors are due to the disorder of two pendant chains, and despite modelling the disorder, the errors persisted.

C10BrPgMeOH

RFACG01_ALERT_3_A
The value of the R factor is > 0.20
R factor given   0.242
RFACR01_ALERT_3_A
The value of the weighted R factor is > 0.45
Weighted R factor given   0.574
SHFSU01_ALERT_2_A
The absolute value of parameter shift to su ratio > 0.20
Absolute value of the parameter shift to su ratio given   2.004
Additional refinement cycles may be required.
PLAT080_ALERT_2_A
Maximum Shift/Error 2.00
PLAT082_ALERT_2_A
High R1 Value 0.24
PLAT084_ALERT_2_A
High R2 Value 0.57
PLAT213_ALERT_2_A
Atom O1   has ADP max/min Ratio ....   6.40 prola
PLAT213_ALERT_2_A
Atom O2   has ADP max/min Ratio ....   6.20 prola
PLAT213_ALERT_2_A
Atom O5   has ADP max/min Ratio ....   5.80 oblat
PLAT213_ALERT_2_A
Atom O11   has ADP max/min Ratio ....   7.50 prola
PLAT213_ALERT_2_A
Atom C11   has ADP max/min Ratio ....   6.10 prola
PLAT213_ALERT_2_A
Atom C49   has ADP max/min Ratio ....   5.40 prola
PLAT213_ALERT_2_A
Atom C58   has ADP max/min Ratio ....   6.00 prola
PLAT220_ALERT_2_A
Large Non-Solvent   C   Ueq(max)/Ueq(min) ...   10.00 Ratio
PLAT222_ALERT_3_A
Large Non-Solvent   H   Ueq(max)/Ueq(min) ...   10.00 Ratio
PLAT241_ALERT_2_A
Check High   Ueq as Compared to Neighbors for   C11
PLAT241_ALERT_2_A
Check High   Ueq as Compared to Neighbors for   C17
PLAT241_ALERT_2_A
Check High   Ueq as Compared to Neighbors for   C29
PLAT241_ALERT_2_A
Check High   Ueq as Compared to Neighbors for   C32
PLAT241_ALERT_2_A
Check High   Ueq as Compared to Neighbors for   C49
PLAT241_ALERT_2_A
Check High   Ueq as Compared to Neighbors for   C51
PLAT242_ALERT_2_A
Check Low   Ueq as Compared to Neighbors for   C10
PLAT242_ALERT_2_A
Check Low   Ueq as Compared to Neighbors for   C16
PLAT242_ALERT_2_A
Check Low   Ueq as Compared to Neighbors for   C28A
PLAT242_ALERT_2_A
Check Low   Ueq as Compared to Neighbors for   C31A
PLAT242_ALERT_2_A
Check Low   Ueq as Compared to Neighbors for   C34
PLAT242_ALERT_2_A
Check Low   Ueq as Compared to Neighbors for   C48

PLAT242_ALERT_2_A
Check Low   Ueq as Compared to Neighbors for   C50
PLAT242_ALERT_2_A
Check Low   Ueq as Compared to Neighbors for   C68
PLAT410_ALERT_2_A
Short Intra H...H Contact H31B   .. H33B   ..   1.72 Ang.
PLAT413_ALERT_2_A
Short Inter XH3 .. XHn   H69B   .. H71B   ..   1.73 Ang.
PLAT413_ALERT_2_A
Short Inter XH3 .. XHn   H69C   .. H71A   ..   1.55 Ang.
PLAT432_ALERT_2_A
Short Inter X...Y Contact O14   .. C69   ..   2.70 Ang.
PLAT432_ALERT_2_A
Short Inter X...Y Contact C69   .. C71   ..   2.71 Ang.
PLAT234_ALERT_4_A
Large Hirshfeld Difference C32   -- C33   ..   0.41 Ang.

This structure shows a spherical arrangement of the calixarene molecules, the SQUEEZE program was applied to model the disordered contents of the sphere as diffuse electron density. This unassignable electron density is the cause of the high R1 and R2 values. PLAT213, 220, 234, 241, 242, 245, 410, 413, 432 errors are due to the disorder of two pendant chains, and despite modelling the disorder, the errors persisted.

C10CNPg Benzene

SHFSU01_ALERT_2_A
The absolute value of parameter shift to su ratio > 0.20
Absolute value of the parameter shift to su ratio given   6.839
Additional refinement cycles may be required.
PLAT080_ALERT_2_A
Maximum Shift/Error 6.84
PLAT213_ALERT_2_A
Atom C52   has ADP max/min Ratio ....   7.00 prola
PLAT215_ALERT_3_A
Disordered C64B   has ADP max/min Ratio 8.60
PLAT220_ALERT_2_A
Large Non-Solvent   C   Ueq(max)/Ueq(min) ...   10.00 Ratio
PLAT220_ALERT_2_A
Large Non-Solvent   N   Ueq(max)/Ueq(min) ...   8.95 Ratio
PLAT222_ALERT_3_A
Large Non-Solvent   H   Ueq(max)/Ueq(min) ...   10.00 Ratio
PLAT241_ALERT_2_A
Check High   Ueq as Compared to Neighbors for   C17
PLAT241_ALERT_2_A
Check High   Ueq as Compared to Neighbors for   C35
PLAT241_ALERT_2_A
Check High   Ueq as Compared to Neighbors for   C50
PLAT241_ALERT_2_A
Check High   Ueq as Compared to Neighbors for   C52
PLAT241_ALERT_2_A
Check High   Ueq as Compared to Neighbors for   C65
PLAT241_ALERT_2_A
Check High   Ueq as Compared to Neighbors for   C68
PLAT242_ALERT_2_A
Check Low   Ueq as Compared to Neighbors for   C16
PLAT242_ALERT_2_A
Check Low   Ueq as Compared to Neighbors for   C18
PLAT242_ALERT_2_A
Check Low   Ueq as Compared to Neighbors for   C34
PLAT242_ALERT_2_A
Check Low   Ueq as Compared to Neighbors for   C36
PLAT242_ALERT_2_A
Check Low   Ueq as Compared to Neighbors for   C49
PLAT242_ALERT_2_A
Check Low   Ueq as Compared to Neighbors for   C51
PLAT242_ALERT_2_A
Check Low   Ueq as Compared to Neighbors for   C53
PLAT242_ALERT_2_A
Check Low   Ueq as Compared to Neighbors for   C54
PLAT242_ALERT_2_A
Check Low   Ueq as Compared to Neighbors for   C63
PLAT242_ALERT_2_A
Check Low   Ueq as Compared to Neighbors for   C64A
PLAT242_ALERT_2_A
Check Low   Ueq as Compared to Neighbors for   C66
PLAT242_ALERT_2_A
Check Low   Ueq as Compared to Neighbors for   C69
PLAT245_ALERT_2_A
U(iso) H63A   Smaller than U(eq) C64B   by ...   0.37 AngSq
PLAT331_ALERT_2_A
Small Average Phenyl C-C Dist. C100   -C101_a   1.34 Ang.
PLAT773_ALERT_2_A
Suspect C-C Bond in CIF: C64B   --   C65   ..   1.76 Ang.

```
PLAT224_ALERT_1_A
Ueq(Rep) and Ueq(Calc) differ by -0.010 Ang**2 .          N1
PLAT224_ALERT_1_A
Ueq(Rep) and Ueq(Calc) differ by -0.010 Ang**2 .          C17
PLAT224_ALERT_1_A
Ueq(Rep) and Ueq(Calc) differ by -0.010 Ang**2 .          C18
PLAT234_ALERT_4_A
Large Hirshfeld Difference N4     -- C18     ..       0.55  Ang.
PLAT234_ALERT_4_A
Large Hirshfeld Difference C67    -- C68     ..       0.36  Ang.
```

The errors generated are due to disorder of two pendant chains within the molecule. Despite modelling of the disorder the error persisted. This is the first dataset collected for this molecule, due to the future importance of this molecule as an intermediate in the synthesis of a therapeutic delivery system further investigations into the structural behaviour of substituted calixarene molecules. The disorder of pendant chains may be due to the interactions between the pendant chains preventing interdigitation, this would allow greater conformational flexibility of the chains and therefore disorder within the crystal lattice.

C10CNPgAcetylated

```
THETM01_ALERT_3_A
The value of sine(theta_max)/wavelength is less than 0.550
Calculated sin(theta_max)/wavelength =    0.4998
PLAT220_ALERT_2_A
Large Non-Solvent   C    Ueq(max)/Ueq(min) ...        5.00 Ratio
PLAT242_ALERT_2_A
Check Low      Ueq as Compared to Neighbors for       C16A
PLAT242_ALERT_2_A
Check Low      Ueq as Compared to Neighbors for        C18
```

Despite repeated attempts to crystallize the material, the crystals which grew were only suitable for synchrotron radiation due to their small size. The PLAT220 and 242 errors are due to the disorder of the penultimate carbon atom of one of the pendant chains. Despite modelling the disorder the error persists.

C10enePgEtOAc

PLAT213_ALERT_2_A
Atom C51   has ADP max/min Ratio ....   8.10 prola
PLAT220_ALERT_2_A
Large Non-Solvent   C   Ueq(max)/Ueq(min) ...   10.00 Ratio
PLAT220_ALERT_2_A
Large Non-Solvent   C   Ueq(max)/Ueq(min) ...   10.00 Ratio
PLAT222_ALERT_3_A
Large Non-Solvent   H   Ueq(max)/Ueq(min) ...   10.00 Ratio
PLAT241_ALERT_2_A
Check High   Ueq as Compared to Neighbors for   C44
PLAT241_ALERT_2_A
Check High   Ueq as Compared to Neighbors for   C47
PLAT241_ALERT_2_A
Check High   Ueq as Compared to Neighbors for   C49
PLAT241_ALERT_2_A
Check High   Ueq as Compared to Neighbors for   O13
PLAT241_ALERT_2_A
Check High   Ueq as Compared to Neighbors for   C70
PLAT241_ALERT_2_A
Check High   Ueq as Compared to Neighbors for   C71
PLAT242_ALERT_2_A
Check Low   Ueq as Compared to Neighbors for   C32
PLAT242_ALERT_2_A
Check Low   Ueq as Compared to Neighbors for   C33
PLAT242_ALERT_2_A
Check Low   Ueq as Compared to Neighbors for   C46
PLAT242_ALERT_2_A
Check Low   Ueq as Compared to Neighbors for   C48
PLAT242_ALERT_2_A
Check Low   Ueq as Compared to Neighbors for   C50
PLAT242_ALERT_2_A
Check Low   Ueq as Compared to Neighbors for   O14
PLAT242_ALERT_2_A
Check Low   Ueq as Compared to Neighbors for   C69
PLAT306_ALERT_2_A
Isolated Oxygen Atom (H-atoms Missing ?) O15
PLAT780_ALERT_1_A
Coordinates do not Form a Properly Connected Set   ?

This structure shows a spherical arrangement of the calixarene molecules. The PLAT213, 220, 222, 241 and 242 errors are due to a disordered pendant chain which, despite modelling the errors persisted. The PLAT306 is due to the presence of a water molecule within the crystal lattice. Xseed does not currently support geometric placement of hydrogen atoms on isolated oxygen atoms.

C*p*NO$_2$C$_6$H$_4$Pg

```
PLAT306_ALERT_2_A
Isolated Oxygen Atom (H-atoms Missing ?) .......        O14
PLAT306_ALERT_2_A
Isolated Oxygen Atom (H-atoms Missing ?) .......        O15
PLAT412_ALERT_2_A
Short Intra XH3 .. XHn     H31B   ..  H34C    ..    1.61 Ang.
PLAT415_ALERT_2_A
Short Inter D-H..H-X       H3A    ..  H34A    ..    1.67 Ang.
PLAT415_ALERT_2_A
Short Inter D-H..H-X       H3A    ..  H34B    ..    1.63 Ang.
PLAT430_ALERT_2_A
Short Inter D...A Contact  O14    ..  O14     ..    1.94 Ang.
PLAT432_ALERT_2_A
Short Inter X...Y Contact  O3     ..  C34     ..    2.69 Ang.
PLAT432_ALERT_2_A
Short Inter X...Y Contact  O4     ..  C27     ..    2.65 Ang.
PLAT432_ALERT_2_A
Short Inter X...Y Contact  O6     ..  C38     ..    2.66 Ang.
```

Despite multiple attempts to crystallize C*p*NO$_2$C$_6$H$_4$Pg from a number of different solvents under varying conditions, crystals only grew from a saturated solution of methyl ethyl ketone exposed to the atmosphere and allowed to slowly evaporate. The small crystal size and low quality required synchrotron radiation to collect an adequate dataset. These factors required the use of the SQUEEZE program to model extensively disordered solvent molecules *exo* to the cavity of the calixarene. The PLAT306 error is due to XSEED currently not supporting the geometrical placement of hydrogen atoms on isolated oxygen atoms. PLAT415, 430, 432 are due to the extensive disorder of the solvent molecules *exo* to the cavity of the calixarene.

Phenanthrene

This structure produced no class A or B alerts.